

# **Exploring the Role of Cellular Metabolism in Anticancer Drug Resistance**

**a Metabolomics Approach**

Esther Zaal

ISBN 978-90-393-7001-8

Coverdesign by Mathijs van der Linden

Lay out by wenz iD || Wendy Schoneveld

Printed by Proefschriftmaken || [Proefschriftmaken.nl](http://Proefschriftmaken.nl)

The research presented in this thesis was performed in the Biomolecular Mass Spectrometry and Proteomics Group, Bijvoet Center for Biomolecular Research, at the University of Utrecht, The Netherlands

# **Exploring the Role of Cellular Metabolism in Anticancer Drug Resistance**

**a Metabolomics Approach**

**De rol van stofwisseling in geneesmiddelresistentie bij kanker  
een metabolomics studie**

(met een samenvatting in het Nederlands)

**Proefschrift**

ter verkrijging van de graad van doctor aan  
de Universiteit Utrecht op gezag van de rector magnificus,  
prof. dr. H.R.B.M. Kummeling,  
ingevolge het besluit van het college voor promoties  
in het openbaar te verdedigen op  
maandag 11 juni 2018 des middags te 12.45 uur

door

**Esther Angelita Zaal**

geboren op 11 juni 1988 te Made en Drimmelen

Promotoren: Prof. dr. C.R. Berkers  
Prof. dr. A.J.R. Heck





# Contents

**Introduction** 9

**Chapter 1** The interplay between cellular metabolism and drug resistance in cancer 13

---

I

## **Identification of metabolic vulnerabilities in proteasome inhibitor resistance**

**Chapter 2** Bortezomib resistance in multiple myeloma is associated with increased serine synthesis 42

**Chapter 3** Mitochondrial respiration as a target in bortezomib-resistant multiple myeloma cells 77

---

II

## **Metabolomics in multi-omics approaches to study responses to anticancer therapy**

**Chapter 4** Lapatinib resistance in breast cancer cells is accompanied by phosphorylation-mediated reprogramming of glycolysis 109

**Chapter 5** Multi-OMIC profiling of survival and metabolic signaling networks in cells subjected to photodynamic therapy 135



---

## **Metabolism beyond cancer**

<b>Chapter 6</b>	Metabolic regulation of proteasome activity	173
------------------	---	-----



---

## **Synopsis and Perspective**

<b>Chapter 7</b>	Summarizing discussion	195
	Nederlandse samenvatting	207
	Acknowledgements	213
	About the author	
	List of publications	220
	Curriculum Vitae	223



---

# Introduction



---

## Feeding the beast

Cancer cells are hungry. Not only do they eat more than normal cells, but they also process their nutrients differently. Although this has been known since the 1920's, recent advances have shown that metabolic alterations may be more than just an epiphenomenon. In fact, a rewired metabolism is essential for the development and growth of cancer cells as they become addicted to specific metabolic pathways to survive in a hostile environment. Having to survive under highly variable circumstances, cancer cells have evolved to be extremely flexible with their nutrients. As a consequence of this inherent metabolic flexibility, they are able to quickly rewire in response to chemotherapeutic drugs.

In this thesis, I focus on this re-wiring of metabolic pathways when cancer cells are attacked by anticancer drugs. Having changed their diets when they became cancer, these cells again change their metabolism to become resistant to anticancer drugs. But this metabolic flexibility comes with a cost. Their addiction to specific nutrients and metabolic pathways (which are less important to normal cells) makes them vulnerable to interferences with these nutrients and processes. This can be as simple as dietary restriction or as complex as chemical inhibition of enzymatic reactions. Understanding how metabolism is altered in drug-resistant cancer can thus lead to novel therapeutic strategies to overcome resistance.

## Metabolomics

Finding metabolic vulnerabilities is easier said than done. Cellular metabolism is an extremely complex network of interconnected chemical reactions transforming nutrients into cellular end-products. A human cell manages an estimated 16,000 different endogenous metabolites and countless more exogenous metabolites. Together, these small-molecule nutrients, intermediates, by-products and end-products are called the 'metabolome'. This metabolome is characterized by high molecular diversity, structural heterogeneity and large concentration differences. The study of the metabolome – 'metabolomics' – therefore requires highly specific and sensitive analytical techniques.

Mass spectrometry (MS) is one of the central instruments in the large-scale quantification of metabolites. Recent advances in high-resolution MS allow for the identification and quantification of metabolites with high sensitivity and accuracy. In the work described in this thesis, MS was coupled to liquid chromatography (LC) to identify and quantify both intra- and extracellular metabolites. This approach results in information about up- and downregulation of metabolites in different conditions.

Although up- and downregulated metabolites can be indicative of metabolic adaptation, the complexity of the metabolic roadmap precludes definitive conclusions

about the causes and directions of these adaptations. To overcome this problem, substrates (nutrients) with stable isotopic atoms are used to follow nutrients through the network of pathways. Because high resolution MS makes it possible to identify a mass shift after the incorporation of the isotopic label, the fate of heavy labeled atoms can be traced over time through the complex roadmap of the metabolome.

In analyzing metabolic adaptations, it is important to recognize that the metabolome is inherently intertwined with the proteome (the sum of proteins, the cellular machinery), the genome (the sum of genes, the cellular blueprint) and the transcriptome (the sum of genetic transcriptions, the active cellular program). Metabolomic findings can therefore be put in a better perspective when combined with proteomic, genomic and/or transcriptomic analyses.

### **Outline of the thesis**

The work presented in this thesis is focused on the role of cellular metabolism in drug-resistant cancers. For this, I applied MS-based metabolomics and metabolic flux analyses to study how cellular metabolism is altered when cells become resistant to drug treatment.

In chapter 1, I introduce the important aspects of cancer metabolism in general, with a special focus in metabolic pathways in central carbon metabolism. In addition, I review the current knowledge on how metabolic alterations are linked to anticancer drug resistance.

In chapters 2 and 3, I present work in search of metabolic vulnerabilities in bortezomib-resistant cells. I combine MS-based metabolomics, metabolic flux studies and targeted proteomics to map the differences in metabolism in bortezomib-sensitive and resistant cells.

The second part of this thesis shows how metabolomics can contribute to a better understanding of metabolic rewiring when combined with other -omics technologies. In chapter 4, I used metabolomics in combination with (phosphor)proteomics to study differences in lapatinib-sensitive and -resistant breast cancer cells. In chapter 5, transcriptomics, proteomics and metabolomics were combined to study the effect of photodynamic therapy.

In the third part of this thesis, I demonstrate that metabolism influences drug response beyond cancer. Specifically, in chapter 6, I show that metabolism influences the effect of proteasome activating compounds, which illustrates the value of metabolomics in understanding drug action.

Finally, the summarizing discussion represents a synthesis of my work together with a discussion of the implications and limitations of the research presented in this thesis.





---

# Chapter 1

## The interplay between cellular metabolism and drug resistance in cancer

Esther A. Zaal<sup>1</sup>, Celia R. Berkers<sup>1</sup>

<sup>1</sup> Biomolecular Mass Spectrometry and Proteomics, Bijvoet Center for Biomolecular Research, Utrecht University, Utrecht, The Netherlands

## INTRODUCTION

Metabolic alterations have been shown to be involved in resistance towards anticancer agents. This makes cancer metabolism a promising field to find novel strategies to overcome drug resistance, which will be the focus of this chapter.

Increased knowledge about the molecular mechanisms of cancer has led to the development of novel therapeutic compounds that specifically target cancer cells. Even though these targeted agents increase progression-free survival, this does not always translate in overall survival benefits due to rapid development of resistance [1]. Although adaptive resistance can be targeted to improve drug efficacy, new adaptive resistance is often rapidly developing, underlining the heterogeneity and adaptivity of cancer cells [2]. Therefore, understanding how resistance can be prevented, targeted and predicted becomes increasingly important to improve cancer therapy.

In the last decade, it has become apparent that alterations in cellular metabolism are a hallmark of cancer cells [3]. Many signalling pathways that are affected by genetic mutations in cancer influence metabolism [4]. Cancer cells can become addicted to specific metabolic pathways, which had led to the development of drugs that target these metabolic vulnerabilities [5, 6].

In this chapter, I will first introduce the important aspects of metabolic transformation in cancer in general, which is essential knowledge for the following parts of the chapter, as well as the rest of this thesis. In the second part, I will review how these metabolic alterations interfere with sensitivity to different anticancer therapeutics. Finally, I will discuss how these metabolic alterations can be targeted to overcome drug resistance in cancer.

## METABOLIC TRANSFORMATION IN CANCER

### **Changes in metabolism are essential to sustain cancer cell growth and proliferation**

Changes in metabolism are one of the emerging hallmarks of cancer cells [3]. Alterations in cellular metabolism sustain rapid production of adenosine triphosphate (ATP) and increased biosynthesis of macromolecules, including nucleotides, lipids and amino acids, and also help maintain cellular redox state [4, 7]. As such, changes in metabolism are essential to provide the needs for rapid cell growth and proliferation (Fig. 1).

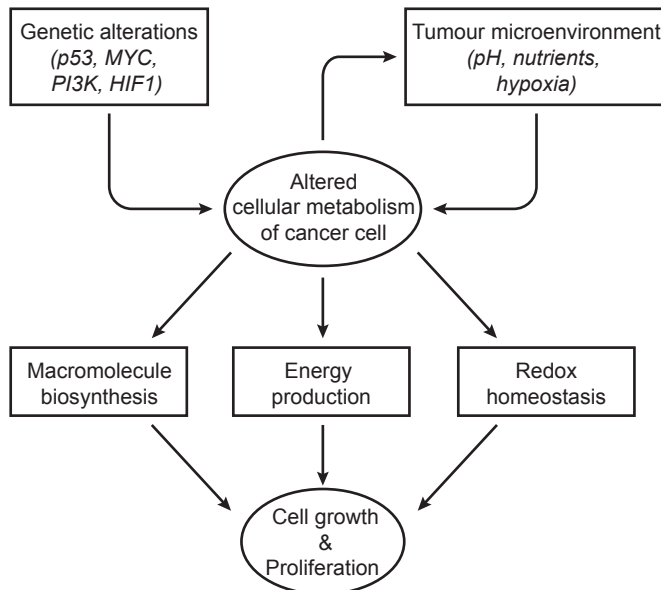


**Figure 1. Metabolic alterations in cancer cells are essential to sustain cancer cell growth and proliferation.** Alterations in cellular metabolism in cancer cells are a result of intrinsic (genetic) factors and external factors. Genetic alterations in cancer cells result in loss of tumor suppressors (e.g. p53) or activation of oncoproteins (e.g. PI3K), which affect signaling pathways that control metabolism. In addition, metabolism is influenced by environmental conditions such as hypoxia, pH, and availability of nutrients, as well as the presence of other cells. The resulted altered metabolism provides energy in the form of adenosine triphosphate (ATP), building blocks for biosynthesis of macromolecules and aids in redox homeostasis, which are essential for rapid cell growth and proliferation. PI3K = phosphoinositide 3-kinase, HIF1 = hypoxia-inducible factor 1.

Both intrinsic and extrinsic mechanisms contribute to the characteristic metabolic alterations in cancer cells. Many different oncogenic as well as tumor suppressor signalling pathways influence metabolism, such as hypoxia-inducible factor 1 (HIF1), p53 and MYC. In addition, cancer metabolism is influenced by the tumour microenvironment, for example the interaction with surrounding cells and the variation in availability of nutrients and oxygen (Fig. 1) [8]. Many of these mechanisms affect pathways involved in central carbon metabolism, such as glycolysis and the tricarboxylic acid (TCA) cycle, as described in more detail below. How these different mechanisms affect metabolism has been extensively reviewed by others and is beyond the scope of this review [4, 8–15].

### **Switching from oxidative phosphorylation to glycolysis for energy production**

Glycolysis is the main pathway that is responsible for the breakdown of glucose to pyruvate involving several steps (Fig. 2). Glycolysis results in the production of a limited amount of energy in the form of ATP and of reducing equivalents in the form

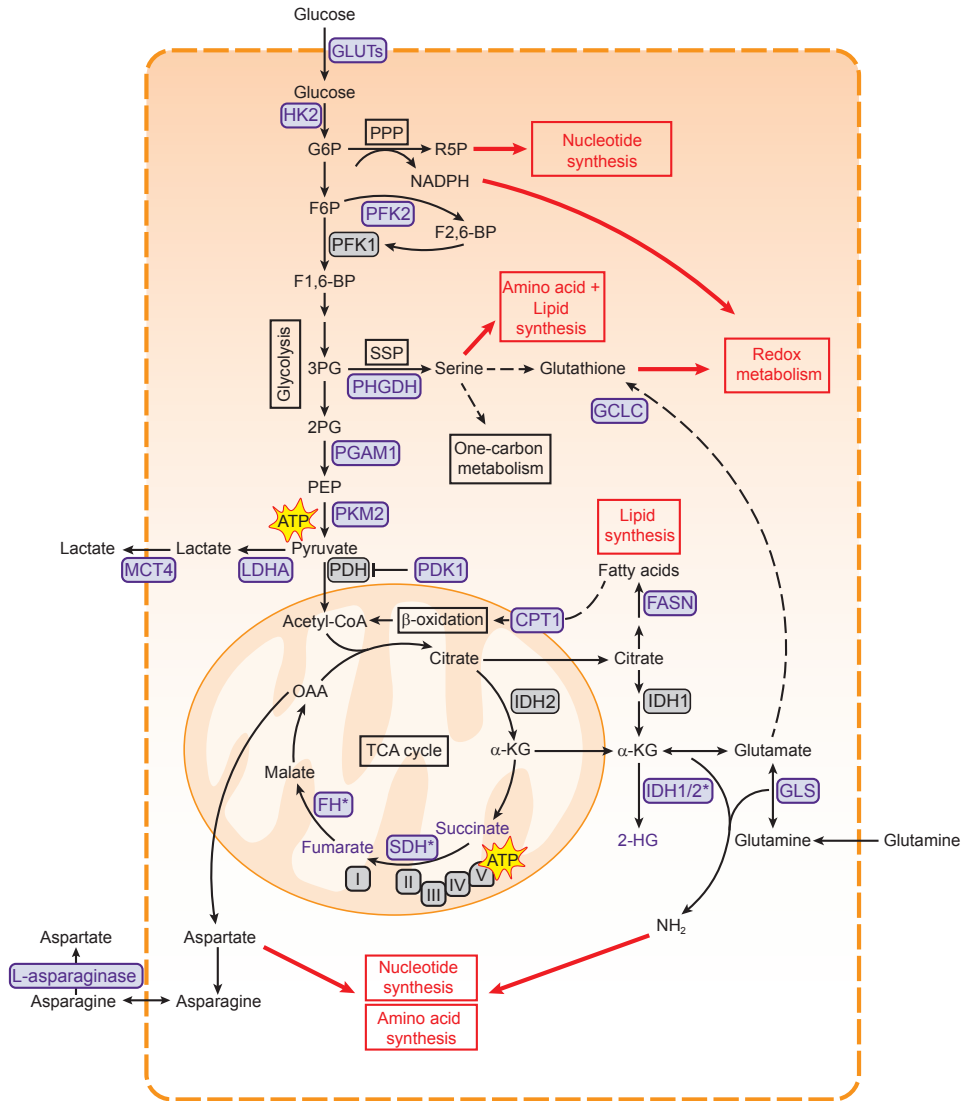


**Figure 2. Metabolic pathways associated with cancer.**

Pathways involved in central carbon metabolism are presented. Metabolic enzymes that are often upregulated in cancer and serve as potential therapeutic targets are shown in purple. These metabolic pathways are involved in the synthesis of building blocks for macromolecules and redox homeostasis (shown in red boxes). 2PG = 2-phosphoglycerate; 3PG = 3-phosphoglycerate; ATP = adenosine triphosphate; CPT1 = carnitine palmitoyltransferase I; F1,6-BP = fructose-1,6-bisphosphate; F2,6-BP = fructose-2,6-bisphosphate; F6P = fructose- 6-phosphate; FASN = fatty acid synthase; FH = fumarase; G6P = glucose-6-phosphate; GCLC = glutamate-cysteine ligase; GLS = glutaminase; GLUT = glucose transporter type; HK2 = hexokinase 2; I = complex I; IDH = isocitrate dehydrogenase; II = complex II; III = complex III; IV = complex IV; LDHA = lactate dehydrogenase A; MCT4 = monocarboxylate transporter 4; OAA = oxaloacetate; PDH = pyruvate dehydrogenase complex; PDK1 = pyruvate dehydrogenase kinase 1; PEP = phosphoenol pyruvate; PFK1 = phosphofructokinase 1; PFK2 = phosphofructokinase 2; PGAM1 = phosphoglycerate mutase 1; PHGDH= 3-phosphoglycerate dehydrogenase; PKM2 = pyruvate kinase M2; PPP = pentose phosphate pathway; R5P = ribose 5-phosphate; SDH = succinate dehydrogenase; SSP = serine synthesis pathway; TCA = tricarboxylic acid cycle; V = complex V.

of NADH. Pyruvate can subsequently be fed into the mitochondrial TCA cycle, where it is condensed with oxaloacetate (OAA) to produce citrate. A series of subsequent reactions supply reducing equivalents in the form of NADH and FADH<sub>2</sub>, which can be oxidized in the electron transport chain (ETC) complexes to ultimately produce ATP in a process called oxidative phosphorylation (OXPHOS) [16, 17] (Fig. 2). While ATP production via OXPHOS is more efficient, the majority of cancer cells generate most of their ATP through glycolysis, even in the presence of oxygen [18]. This phenomenon, known as aerobic glycolysis or “the Warburg effect”, is characterized by an increased rate of glycolysis, whereby pyruvate is converted to lactate and subsequently secreted by the cell instead of being funnelled into the TCA cycle.

In order to maintain these high glycolytic rates, cancer cells have a higher demand for extracellular glucose as compared to healthy cells, which is often sustained by overexpression of glucose transporters (GLUTs) [19, 20]. In addition, glycolytic cancers often show higher levels of monocarboxylate transporter 4 (MCT4), which is responsible for lactate export and thereby maintaining intracellular pH and continued glycolysis [21, 22]. Likewise, several metabolic enzymes that catalyse the chemical reactions involved in glycolysis are overexpressed in different cancers. Interestingly, cancer cells seem to rely more on specific isoforms of glycolytic enzymes, making these promising targets to specifically inhibit glycolysis in cancer cells [6]. For example, the M2 isoform of pyruvate kinase (PKM2) is preferentially expressed over other isoforms in most cancer cells [23]. PKM2 catalyses the final step in glycolysis, and cancer cells are thought to regulate its activity to either increase glycolytic rates or divert glycolytic intermediates to biosynthetic pathways [24]. Cancers can also be more dependent on isoforms of hexokinase (HK2) [25, 26], and lactate dehydrogenase (LDHA) [27] or overexpress phosphoglycerate mutase 1 (PGAM1) [28, 29]. Finally, enzymes that serve as regulators of glycolysis are highly expressed in cancer, including pyruvate dehydrogenase kinase 1 (PDK1) [30] and phosphofructokinase 2 (PFK2) [31, 32], allowing cancer cells to easily adapt glucose metabolism to meet their needs.

There still is debate about why cancer cells prefer the less efficient glycolysis over OXPHOS for ATP production. Initially, Warburg hypothesized that cancer cells increased glycolytic activity because of impaired mitochondrial function [18]. Indeed, several cancers are associated with mutations in TCA cycle enzymes, supporting this hypothesis [33] (Fig. 2). Fumarate hydratase (FH) and succinate dehydrogenase (SDH) are tumour suppressors. Loss-of-function mutations in these genes are associated with tumorigenesis (reviewed in [34]) and result in the accumulation of succinate and fumarate, respectively, both of which function as oncometabolites [35, 36]. Mutations in isocitrate dehydrogenase 1 (IDH1) and

IDH2 are present in many cancers [37, 38] and result in the production of the oncometabolite 2-hydroxyglutarate [39]. How these oncometabolites promote cancer is not completely clear, but a common feature is stabilization of HIF1, which is a known regulator of glycolytic activity. Hence, the presence of these mutations provides a link between the Warburg effect and TCA cycle defects [40].

Later work showed that cancer cells prefer glycolysis also when mitochondrial function is intact [41, 42], suggesting that glycolysis confers other advantages to cancer cells. Likely, the increased glycolytic rates help cancer cells to fulfil the increased needs for biosynthesis of macromolecules and redox homeostasis by diverting glycolytic intermediates to key biosynthetic pathways [7] (described in more detail below). In addition, the production and secretion of lactate could aid tumor cells in creating an extracellular milieu that favours tumor growth, as lactate secretion results in an acidic tumor environment, which promotes migration and invasion [43, 44].

### **Diverting glycolytic resources towards the production of building blocks for macromolecules**

Several glycolytic intermediates can branch off to biosynthetic pathways to generate nucleotides, amino acids and fatty acids. One of these pathways is the pentose phosphate pathway (PPP), which both sustains the biosynthesis of macromolecules and maintains redox homeostasis [45–47]. The PPP produces ribose-5-phosphate, which is needed for nucleotide synthesis, and regenerates NADPH, which provides reducing power for both glutathione (GSH) and thioredoxin that capture reactive oxygen species (ROS) produced during rapid cell proliferation. Glucose-6-phosphate dehydrogenase (G6PD), whose activity reflects PPP activity, is upregulated in numerous cancer cells, underlining the importance of PPP in cancer metabolism [47, 48].

In addition, glucose is used for the synthesis of several non-essential amino acids, as 3-phosphoglycerate is a precursor for the biosynthesis of serine and downstream metabolites through the serine synthesis pathway (SSP). The SSP has emerged as a key pathway in cancer metabolism. Serine is needed to synthesize reduced GSH and phospholipids and also plays a major role in the one-carbon cycle, which sustains both the biosynthesis of nucleotides and NADPH regeneration [49, 50]. In line with this role, the SSP is often highly active in cancer cells and 3-phosphoglycerate dehydrogenase (PHGDH), the first and rate-limiting enzyme in this pathway, is frequently upregulated in different cancers [51, 52].

Both glycolytic flux through SSP and PPP are regulated by PKM2 [53–56] and PGAM1 [57]. Cancer cells thus employ various strategies to divert glycolytic

metabolites into biosynthetic pathways, underscoring the importance of glycolytic regulators in cancer metabolism [7].

### **Turning glutamine into an important carbon source**

Intermediates of the TCA cycle can also serve as building blocks for the biosynthesis of lipids and nucleotides (Fig. 2). Because TCA intermediates leave the TCA cycle for biosynthetic pathways, a new supply of carbons is needed to maintain TCA cycle activity, a process called anaplerosis. One of the most important anaplerotic pathways in cancer is glutaminolysis, in which glutamine is used to replenish the TCA cycle. Next to glucose, glutamine is the most consumed metabolite in proliferating cells in cell culture [58, 59] and it has been shown that many tumor cells are more dependent on glutamine as compared to healthy cells [60, 61]. However, a range of other metabolites has also been described to fuel the TCA cycle in cancer, including fatty acids (through  $\beta$ -oxidation) [62], lactate [63], acetate [64], and branched chain amino acids (BCAA) [65], illustrating the complexity of cancer metabolism.

After glutamine enters the cell, it is converted to glutamate by glutaminase (GLS). Glutamate in turn can be further converted to  $\alpha$ -ketoglutarate that can subsequently enter the TCA cycle (Fig. 2). As TCA cycle intermediates fuel pathways that have complementary functions to those diverting from glycolysis, the TCA cycle is as important as glycolysis for cancer cell anabolism. For example, glutamine is used for the production of the amino acids glutamate, aspartate and proline and for protein-, fatty acid and nucleotide synthesis as well as redox homeostasis [66, 67].

Both aspartate and proline, synthesized from glutamine, can be limiting for proliferation in cancer cells [68–70]. In addition, glutathione cysteine ligase (GCLC), which converts glutamate to GSH, is highly expressed in several cancers [71, 72]. Citrate can be used for fatty acid synthesis via fatty acid synthase (FASN), which has shown to be important in cancer cells (reviewed in [73]). Fatty acids are not only important components of membranes, but are also energy-rich compounds that can be degraded to provide ATP via  $\beta$ -oxidation [74]. Carnitine palmitoyl transferase 1 (CPT1) conjugates fatty acids with carnitine to translocate them to mitochondria, where  $\beta$ -oxidation takes place (Fig. 2). CPT1C, an atypical isoform of CPT1, is highly expressed in cancers and promotes  $\beta$ -oxidation and ATP production [62]. These examples underscore the importance of glutamine and downstream pathways in cancer growth.

## LINKING METABOLISM TO ANTICANCER DRUG RESISTANCE

Resistance to therapeutic agents, either intrinsic or acquired, is currently a major problem in the treatment of cancers and occurs in virtually every type of anti-cancer therapy [75, 76]. Acquired drug resistance can be the result of mutations causing decreased drug binding, increased activity of the drug target or due to the upregulation of multi-drug resistance transporters (Fig. 3). Acquired resistance can also be the result of various adaptive responses that occur downstream of the drug target and that help cancer cells withstand the effects of the drug (Fig. 3). (reviewed in [1, 76, 77]. Examples of such mechanisms are the upregulation of cellular pro-survival pathways, including the activation of DNA repair mechanisms [78], the upregulation of anti-apoptotic proteins [79, 80], and the upregulation of autophagy [81]. Another mechanism of resistance, that is frequently observed with kinase inhibitor therapy, is the so-called ‘oncogenic bypass’, in which the target pathway is activated through an alternative kinase, even when the primary kinase remains inhibited [82–85].

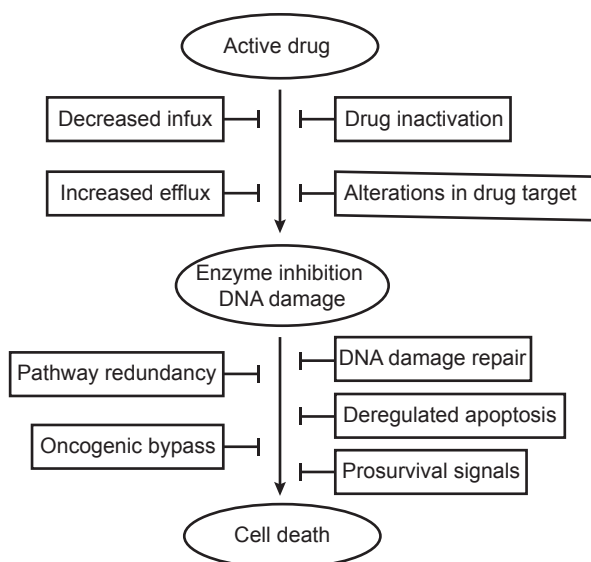


**Figure 3. General mechanisms of drug resistance.**

Drug resistance in cancer can be a result of adaptation mechanisms upstream or downstream of the drug target. Drug binding can be prevented by lowering intracellular drug concentrations (i.e. increased breakdown / efflux, decreased uptake) or mutations in the drug target. After drug binding, several mechanisms can occur that counteract the effect of the drug, including DNA damage repair and activation of pro-survival signals, as well as pathway redundancy and oncogenic bypass.



A number of recent studies now also show the influence of metabolism on drug response in several cancers, identifying metabolic rewiring as a novel and important mechanism of adaptive resistance. An overview of these studies is given in Table 1. Studies focusing on multiple myeloma (proteasome inhibitors), breast cancer (EGFR inhibitors), lung cancer / ovarian cancer (cisplatin) and melanoma (BRAF inhibitors) are discussed in detail below (Fig. 4).

### **Metabolism-mediated resistance to proteasome inhibitors in multiple myeloma**

Proteasome inhibitors are a cornerstone in the treatment of multiple myeloma [86, 87], with bortezomib being the first clinically available proteasome inhibitor. Proteasome inhibition results in a disbalance between production and degradation of proteins and eventually causes apoptosis in malignant cells via multiple pathways, including overproduction of ROS [88–90]. Although bortezomib therapy prolongs survival, some patients show intrinsic resistance to therapy, while others develop resistance during treatment [80, 90, 91]. Bortezomib resistance is associated with mutations in the proteasomal bortezomib-binding pocket and upregulation of the proteasomal machinery, both of which lower the efficacy of the drug [92–97].

However, intracellular concentrations of bortezomib seems to correlate with proteasome inhibition, but not with cytotoxicity [98], suggesting that other mechanisms must be involved in proteasome inhibition resistance. Indeed, recent studies suggest that downstream regulatory mechanisms are also important in bortezomib resistance, such as the unfolded protein response and vesicular exocytosis of ubiquitinated proteins [88, 99–102].

Several studies describe a role for metabolism in mediating sensitivity towards bortezomib (see Table 1, Fig. 4a) [103–108]. In particular, enzymes involved in the TCA cycle and the anti-oxidant response are upregulated in bortezomib resistance, as also described in chapters 2 and 3 of this thesis. Bortezomib-resistant cells, for example, have higher mitochondrial function and different expression of mitochondrial genes, including superoxide dismutase 2 (SOD2) which is important for mitochondrial ROS cleaning [109]. Proteomic screening of bortezomib-resistant and -sensitive cell lines showed that resistant cells have increased levels of proteins involved in mitochondrial function and enzymes involved in the generation of reducing equivalents [107]. Higher levels of mitochondrial biomarkers were also found in primary plasma cells from multiple myeloma patients that responded poorly to bortezomib [106]. The latter study also showed that mitochondrial respiration is increased in proteasome inhibitor resistant cell lines, with glutamine being the primary carbon source for the TCA cycle. Although these studies predict that inhibition of the TCA cycle would be toxic to bortezomib-resistant cells, dichloroacetate (DCA), which inhibits PDK1 and thereby

**Tabel 1.** Overview of metabolic alterations associated with drug resistance in cancer

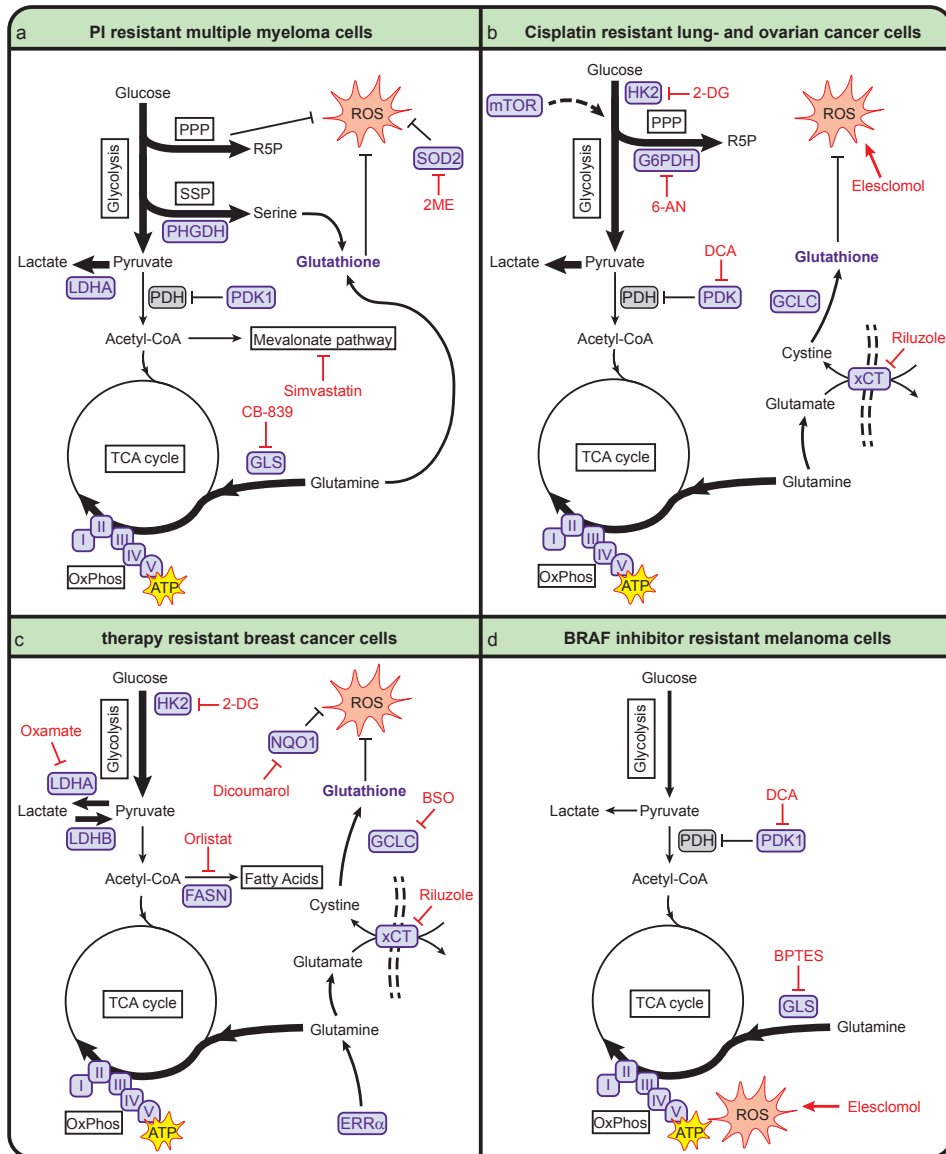
Cancer type	Pathways associated with resistance	Therapy	Target in resistance (proposed therapy)	Ref
<b>Multiple Myeloma</b>				
	Glycolysis	Bortezomib	LDHA, PDK1	[110, 112, 161]
	Mitochondrial energy metabolism	Bortezomib, Carfilzomib	SOD2 (2ME),	[106, 107, 109, 111]
	Redox metabolism	Bortezomib	-	[104, 107, 108]
	Glutaminolysis	Bortezomib, Carfilzomib	GLS (CB-839)	[106]
	Mevalonate pathway	Bortezomib	HMG-CoA (simvastatin)	[103]
	Serine synthesis	Bortezomib	PHGDH	[108]
<b>Lung cancer</b>				
	Mitochondrial energy metabolism	Cisplatin	-	[144]
	Glutaminolysis	Cisplatin	xCT antiporter (riluzole)	[119, 144]
	Redox metabolism	Cisplatin	ASS, TRX1 (Elesclomol), GCLC	[114, 115, 118, 162]
	Glycolysis	Cisplatin, paclitaxel	HK2 (2DG), mTOR, PDK2 (DCA)	[119, 121, 163]
<b>Ovarian cancer</b>				
	Glycolysis	Cisplatin	-	[117]
	Pentose phosphate pathway	Cisplatin	G6PDH (6-AN)	[117]
	Redox metabolism	Cisplatin	GSH	[117]
<b>Breast cancer</b>				
	Fatty acid synthase	Adriamycin	FASN (Orlistat)	[149]
	Redox metabolism	Adriamycin, Tamoxifen	xCT antiporter, GCLC (BSO)	[71, 128, 164]
	Glycolysis	Lapatinib, Paclitaxel, Trastuzumab, Tamoxifen	HK (2-deoxyglucose) LDHA (oxamate)	[46, 122-125]
	Mitochondrial energy metabolism	Lapatinib, Tamoxifen	ERRa, NQO1	[126-128]
<b>Melanoma</b>				
	Mitochondrial energy metabolism	BRAF inhibitor	ETC (esclomol)	[130-133]
	Glutaminolysis	BRAF inhibitor	GLS (BPTES)	[131]
	Arginine metabolism	BRAF inhibitor	ASS1 (arginine starvation)	[155]
	Glycolysis	BRAF inhibitor (Vemurafenib)	PDK1 (DCA)	[133, 134]

Table 1. *Continued*

Cancer type	Pathways associated with resistance	Therapy	Target in resistance (proposed therapy)	Ref
<b>Leukemia</b>				
	Glycolysis	Daunorubicin	-	[165]
	Mitochondrial energy metabolism	Imatinib	-	[166]
<b>Hepatocellular carcinoma</b>				
	Glutaminolysis	Sorefanib	GLS1 (BPTES), PPAR $\delta$	[140]
<b>Squamous cell carcinoma</b>				
	Glycolysis	Cisplatin, radiation therapy	PKM2	[151, 167]
	Redox metabolism	Cisplatin, radiation therapy		[151, 167]
	Nucleotide metabolism	Gemcitabine	(metformin)	[168]
	Fatty acid synthesis	Radiation therapy	FASN (orlistat)	[151]
<b>Colon Cancer</b>				
	Glycolysis	Multiple chemotherapeutic agents		[169]
<b>Pancreatic cancer</b>				
	Fatty acid synthesis	Gemcitabine	FASN (orlistat)	[150, 170]
	Glutaminolysis	Gemcitabine		[171]
	Redox metabolism	Gemcitabine	xCT antiporter	[139]

promotes pyruvate entry in to the TCA cycle, increases sensitivity of multiple myeloma cells to bortezomib both in vitro and in myeloma-bearing mice [105, 110]. Since high intracellular glutathione levels protect cells from bortezomib-induced apoptosis [104], it is likely that DCA enhances the toxicity of bortezomib due to increased ROS levels that result from increased mitochondrial respiration. In line with this, the combination of SOD2 inhibition and bortezomib also induces cell death in bortezomib-resistant multiple myeloma cells via mitochondrial ROS overproduction [111].

In addition to SOD2, other antioxidant-related pathways are also upregulated in bortezomib-resistant cells, such as the PPP and SSP [108]. Furthermore, the presence of serine in the culture media influences the effect of bortezomib and high levels of PHGDH were found in a panel of bortezomib-resistant cells, demonstrating the importance of serine metabolism in bortezomib resistance (see chapter 2) [108].



**Figure 4. Metabolic pathways involved in anticancer drug resistance.**

Pathways involved in different drug-resistant cancer are presented. Metabolic enzymes that are associated with drug resistance are shown in purple. Metabolic inhibitors that can be used to target drug-resistant cancers are depicted in red. 2-DG = 2-deoxyglucose; 2ME = 2-methoxyestradiol; 6-AN = 6-aminonicotinamide; ATP = adenosine triphosphate; BPTES = bis-(2-(5-phenylacetamido-1,3,4-thiadiazol-2-yl)ethyl) sulfide; BSO = buthionine sulphoximine; FASN = fatty acid synthase; G6PDH = glucose-6-phosphate dehydrogenase; GCLC = glutamate-cysteine ligase; GLS = glutaminase; HK2 = hexokinase 2; I = complex I; II = complex II; III = complex III; IV = complex IV; LDHA = lactate dehydrogenase A; LDHB = lactate dehydrogenase B; mTOR = mammalian target of rapamycin; NQO1 = NAD(P)H quinone dehydrogenase; PDH = pyruvate dehydrogenase complex; PDK1 = pyruvate dehydrogenase kinase 1; PHGDH = 3-phosphoglycerate dehydrogenase; PPP = pentose phosphate pathway; R5P = ribose 5-phosphate; ROS = reactive oxygen species; SOD2 = superoxide dismutase 2; SSP = serine synthesis pathway; TCA = tricarboxylic acid cycle; V = complex V; xCT = glutamate/cysteine xCT antiporter.

Finally, several studies show that bortezomib resistance is accompanied with higher glycolytic activity [107, 110, 112]. Soriano et al. showed that proteasome-resistant cells display higher levels of glycolytic enzymes and higher glycolytic rates than parental cell lines [107]. Higher glycolytic activity has also been found to lower bortezomib sensitivity under hypoxic conditions, while inhibition of LDHA enhanced sensitivity of bortezomib under these conditions [112]. In addition, LDHA expression correlated to poor prognosis in multiple myeloma patients [110]. Together, these studies suggest that glycolytic inhibition could be a novel strategy to overcome bortezomib resistance.

### **Metabolic rewiring in lung and ovarian cancer in response to cisplatin treatment**

Cisplatin is a widely used chemotherapeutic agent in several types of cancer, including lung cancer and ovarian cancer. Its anticancer effect lies in the ability of cisplatin to interact with reducing equivalents (e.g. GSH) and DNA, resulting in increased ROS and DNA damage, which eventually leads to apoptosis [113]. Many mechanisms involved in cisplatin resistance have been described [113], and a number of studies suggest that metabolic rewiring of cisplatin-resistant cells is involved in redox buffering in both lung cancer and ovarian cancer cells (Table 1, Fig. 4b) [114–118]. Cisplatin-resistant lung cancer cells have higher levels of ROS, in part due to low levels of intracellular thioredoxin [114], and also display higher levels of GSH and GCLC [79, 115], likely to counteract the high ROS levels induced by cisplatin. Catanzaro et al. showed that cisplatin-resistant ovarian cancer cells have higher levels of GSH and G6PD, the rate limiting enzyme of the PPP and that PPP inhibition with 6-aminonicotinamide (6-AN) increases cisplatin cytotoxicity in these resistant cells [117]. In line with this, several studies show that cisplatin-resistant cells are vulnerable for ROS inducing agents. Cisplatin-resistant lung cancer cells have been reported to be more sensitive to elesclomol, an agent that is known to increase ROS [116]. In addition, the xCT-cysteine/glutamate pump that provides cells with cystine for GSH synthesis, is upregulated in these cisplatin-resistant cells, and they are sensitive to the xCT-cysteine/glutamate pump inhibitor riluzole as compared to their parental counterpart [116]. Also, inhibition of GSH biosynthesis with buthionine sulfoximine (BSO) enhances the effect of cisplatin in breast cancer cells [71]. Together, these studies suggest that interfering with redox metabolism can improve cisplatin response.

In addition, cisplatin-resistant cells have an altered energy metabolism compared to sensitive cells, but the findings on glycolysis and oxidative phosphorylation in lung and ovarian cancers are opposing. Cisplatin-resistant ovarian cancer cells were found to have higher rates of glycolysis and reduced mitochondrial activity compared to their cisplatin-sensitive counterparts. This leads to a higher sensitivity

of resistant cells to glucose starvation or to treatment with 2 deoxyglucose (2-DG), a competitive inhibitor of HK [117]. Cisplatin-resistant lung cancer cells, on the other hand, have lower rates of glycolysis and rely on oxidative phosphorylation instead [116, 119]. Cisplatin-resistant lung cancer cells have lower levels of HK1 and HK2 [119], in accordance with the observation that cisplatin treatment itself lowers HK expression [120]. Cisplatin resistant lung cancer cells also display lower levels of LDHA as compared to sensitive parental cell lines as well as lower glucose uptake and lactate production [116], all of which is indicative of lower glycolytic activity. In line with lower glycolysis rates, cisplatin-resistant lung cancer cells are not sensitive to glucose starvation in comparison with parental cells under normal growth conditions. However, under hypoxic conditions, these cells are more vulnerable for 2-DG treatment. As cells depend on glycolysis for energy in the absence of oxygen, the lower levels of HK in cisplatin-resistant cells likely makes them more vulnerable for 2-DG under these conditions [119]. The lower glycolytic activity in cisplatin-resistant lung cancer cells is accompanied by higher rates of oxidative phosphorylation and mitochondrial activity [114, 116, 119], as well as a higher dependence on glutamine. [116]. In addition to glutamine,  $\beta$ -oxidation of fatty acids seem to fuel the TCA-cycle in cisplatin-resistant lung cancer cells [114, 119].

The metabolic reprogramming in lung cancer cells seems to some extent specific for cisplatin. Paclitaxel-resistant lung cancer cells show higher expression of PDK2 as compared to their parental cells [121]. As a result, these resistant cells are more dependent on glycolysis than OXPHOS and could be sensitised to paclitaxel through PDK2 inhibition.

### **Metabolic alterations involved in drug-resistant breast cancers**

Increased glycolysis is a common feature of drug-resistant breast cancer cells, irrespective of the type of chemotherapeutic agent used (Table 1, Fig. 4c). For example, several studies have found that resistance to lapatinib, an EGFR/ErbB2 tyrosine kinase inhibitor that is widely used in ErbB2 overexpressing breast cancer, is associated with increased glycolysis [122, 123]. Lapatinib-resistant SKBR3 breast cancer cells show increased expression of genes associated with glucose deprivation compared to sensitive cells, which correlates to poor outcome in patients. These genes include glucose transporters and enzymes involved in glycolysis, as well as alternative pathways for energy production, such as  $\beta$ -oxidation [122]. Overexpression of glycolytic genes was also found in a multi-omic approach involving (phospho)proteomics and metabolomics on lapatinib-resistant BT474 breast cancer cells (see chapter 4) [123]. As a result, resistant cells have higher activity of glycolysis and are more sensitive towards glycolytic inhibition. Increased glycolytic activity,

mediated by heat shock factor 1 and LDHA contributes to trastuzumab resistance in ErbB2-positive breast cancer cells and inhibition of glycolysis with 2-DG and the LDH inhibitor oxamate resensitizes resistant cells to trastuzumab [124].

Finally, downregulation of LDHA by knockdown or combining oxamate with paclitaxel shows a synergistic effect on promoting apoptosis in paclitaxel-resistant breast cancer cells [125]. Interestingly, Park et al. (2016) showed that the nuclear receptor estrogen-related receptor alpha (ERR $\alpha$ ) regulates a metabolic switch to allow breast cancer cells to use lactate as a substrate for mitochondrial respiration in the absence of glucose. The ability to bypass glycolysis makes these cells less vulnerable for PI3K/mTOR inhibitors in the presence of lactate and ERR $\alpha$  antagonists are able to restore drug efficacy [126]. This finding underscores the importance of nutrient availability and metabolic alterations in the effectiveness of drugs. The importance of ERR $\alpha$  in regulating metabolism is further emphasized by Deblois et al. (2016), who showed that lapatinib-resistant breast cancer cells restore ERR $\alpha$  levels through reactivation of mTOR signaling, resulting in increased glutamine metabolism and anti-oxidant capacity [127]. Moreover, in a HER2-induced mammary tumour mouse model, targeting ERR $\alpha$  counteracts the metabolic alterations associated with lapatinib resistance and overcomes resistance to this drug [127]. Targeting ERR $\alpha$  is therefore emerging as a strategy to increase the sensitivity of drug-resistant breast cancer cells in the context of metabolism.

A second aspect that is observed in drug-resistant breast cancer cells is increased levels of OXPHOS, coupled to higher levels of oxidative stress. For example, tamoxifen-resistant MCF-7 breast cancer cells display increased mitochondrial metabolism and ATP production [128]. The biguanides metformin and phenformin, which inhibit ETC, selectively kill breast cancer stem cells which were resistant to standard chemotherapy [129], underscoring the importance of OXPHOS activity in the response to drugs. This higher mitochondrial activity may also explain the observation that tamoxifen-resistant breast cancer cells display lower levels of GSH [128], as these cells probably experience higher levels of oxidative stress in. In line with this, tamoxifen-resistant cells have higher expression of NADPH dehydrogenase 1 (NQO1) and GCLC, both involved in the defence against oxidative stress. Moreover, transduction of these genes into MCF-7 cells results in a tamoxifen-resistant phenotype and NQO1 mRNA levels associate with disease progression in patients that received endocrine therapy [128]. Together, these results suggest that an increased anti-oxidant defence mechanism drives tamoxifen resistance. Finally, increased GSH synthesis in PI3K/Akt driven breast cancer is required for resistance to oxidative stress and inhibition of GSH biosynthesis synergizes with cisplatin to induce regression of in PI3K/Akt driven breast cancer [71].

### **Metabolic contributions to BRAF inhibitor resistance in melanoma**

The majority of cutaneous melanomas harbour activating mutations in the protein kinase BRAF, which makes inhibitors that target mutant BRAF promising agents to treat melanoma patients. In terms of metabolism, melanomas that express mutant BRAF and that developed resistance against BRAF inhibitors display increased activity of mitochondrial oxidative metabolism, increased dependency on mitochondria for survival and higher levels of ROS (Table 1, Fig. 4d) [130–133]. Treatment of mutant BRAF melanoma cells with the BRAF inhibitor vemurafenib results in increased mitochondrial respiration. Inhibition of mitochondrial respiration enhances vemurafenib-induced cell death, suggesting that increased mitochondrial activity serves as a defence mechanism against the drug. At the same time, increased levels of ROS that accompany the increased respiration renders these cells more vulnerable for further oxidative stress, induced by exogenous agents such as elesclomol [130]. Baenke et al. showed that increased dependency on mitochondrial respiration is associated with a metabolic switch that makes cells more dependent on glutamine rather than glucose. Hence, resistant BRAF mutant melanoma cells are more sensitive to the GLS inhibitor BPTES, which reduces ATP levels in resistant cells but not in parental cells. Moreover, BPTES enhances the anti-tumour activity of BRAF inhibitors, underscoring the importance of glutamine in mediating BRAF inhibitor resistance [131].

A second metabolic switch in BRAF inhibitor-resistant melanoma cells was found on the level of PDK [133, 134]. PDK inhibition results in more pyruvate influx into the TCA cycle, which increases ROS and thereby reduced viability of BRAF inhibitor resistant cells [133]. The susceptibility to higher rates of oxidative stress was also observed in other tumour types that harboured a mutation in BRAF, as mutant BRAF colorectal cancer cells are prone to cell death after exposure to the oxidized form of vitamin C, which causes oxidative stress via GSH depletion [135].

## **TARGETING DRUG RESISTANCE THROUGH THE MANIPULATION OF METABOLISM**

Metabolic rewiring is an established hallmark of cancer and many studies have shown that cancer cells have an increased consumption of glucose and glutamine to satisfy their needs for energy, biosynthesis and redox balance. From the studies discussed above, it becomes apparent that metabolic alterations are often linked to anticancer drug resistance and may consequently be targeted to overcome drug resistance or to enhance the efficacy of current anti-cancer therapy. Among the



different drug-resistant cancers described, pathways involved in redox and energy metabolism are frequently altered (Table 1, Fig. 4), making them very promising pathways to target in drug-resistant cancers.

### **Targeting the redox balance**

Resistance in many tumor types is accompanied with increased activity of pathways involved in redox balance. A majority of anticancer agents induce apoptosis by increasing oxidative stress [104, 118, 136–140] and it is likely that drug-resistant cells in general increase their anti-oxidant capacity to counteract the effect of drug treatment, albeit via different pathways. The fact that many resistant cells show an increased anti-oxidant capacity likely renders them cross-resistant to other oxidative stress inducing agents. Interfering with pathways involved in redox balance could therefore be a novel strategy to overcome (multidrug) resistance towards anticancer drugs that induce oxidative stress. But although an increased anti-oxidant capacity seems to be a common characteristic of drug-resistant cells, metabolic profiles are altered in drug-specific manners. For example, some drug resistant cells rely more on NADPH production via the PPP [108, 117, 140], while others have higher activity of GSH synthesis [71, 115, 128]. The fact that several different pathways are involved suggests not only that a tailored approach may be needed to overcome resistance to specific drugs, but also that these redundant pathways may protect cancer cells to a large extent from inhibition of one specific pathway.

### **Exploiting energy metabolism**

Many studies show an association between drug resistant cells and the Warburg effect, suggesting that a high glycolytic rate helps cancer cells to survive anticancer treatment [112, 125, 133, 134, 141]. Higher glycolytic rates may lower drug efficacy through the increased secretion of lactate into the extracellular space, as it has been postulated that an acidic extracellular pH contributes to drug resistance because some drugs are not stable under acidic conditions [142, 143]. High glycolytic rates in drug-resistant cells are often accompanied with higher expression of glycolytic regulators such as PDK1 and LDHA, making these enzymes interesting targets for drug-resistant cancers.

Other resistant tumours rely more on mitochondrial activity fueled by glutamine rather than glucose [106, 131, 144]. Interfering with glutamine metabolism, via either inhibition of glutaminolysis or glutamine uptake, could be a strategy for drug-resistant tumors that rely on glutamine for energy production [145, 146]. In addition, as glutamine is mainly used for mitochondrial energy production, inhibition of ETC with biguanides holds great promise in cancer therapy and drug resistance [145, 147]

Whether the cells rely more on glycolysis or OXPHOS could be a result of multiple processes, such as the origin of the tumour and its genetic state. In addition, the location of the tumor can influence the metabolic state, because of differences in availability of oxygen and nutrients.

### **Beyond central carbon metabolism**

The majority of studies on metabolism-mediated drug resistance so far focused on pathways such as glycolysis and the TCA cycle and the role of the main carbon sources glutamine and glucose. But fatty acids and branched chain amino acids can also provide energy, and are also linked to tumorigenesis [74, 148]. Interesting opportunities to target drug resistance may therefore also be found beyond glycolysis and the TCA cycle.

FASN correlates with poor prognosis in various types of cancer and also interferes with drug efficacy [74]. FASN overexpression causes resistance to the anticancer drugs adriamycin and mitoxantrone in breast cancer cells [149], gemcitabine-resistant pancreatic cells [150] and radiotherapy resistant head and neck squamous cell carcinomas [151]. Orlistat, a FASN inhibitor, increases the sensitivity to all drugs, suggesting that FASN can be a new target in drug resistant cancers.

Amino acid metabolism may also yield promising targets to treat drug-resistant tumors. Cancer cells can be dependent on specific amino acids, such as serine [52, 152], proline [70, 153], aspartate [68, 69] and arginine [154]. Although the role of amino acid metabolism in drug resistance is largely unexplored, studies suggest that amino acid availability could be important in drug response and the development of drug resistance. For example, BRAF inhibitor resistant melanoma cells are more sensitive to arginine deprivation as compared to parental cells [155].

Finally, serine synthesis is associated with bortezomib resistance in multiple myeloma and serine starvation enhanced the cytotoxic effect of bortezomib (see chapter 2) [108]. These studies not only underscore the complexity of cancer metabolism, but also suggest that the exploration of amino acid metabolism may be a promising avenue to identify novel targets to overcome drug resistance.

## **CONCLUSION**

It is clear that understanding cancer metabolism can improve cancer therapy, as exemplified by the widespread use of 18-fluorodeoxyglucose, a glucose analogue that exploits the Warburg effect in PET imaging for cancer diagnosis, treatment and prognosis [156]. The potential of metabolic inhibitors in cancer is illustrated by the use

of antimetabolites, such as 5-fluorouracil and methotrexate, which have been used for decades to treat cancers [157], even though their anticancer effects were only coupled to metabolic interference much later [6]. Another example of a successful metabolic drug is the use of L-asparaginase, which is used in the treatment of acute lymphoblastic leukaemia [158].

The recent surge in knowledge in the field of cancer metabolism has sparked increased interest to exploit the altered metabolism of cancer cells to find novel targets for therapy. As a result, compounds have been developed that specifically target the unique metabolism of cancers. Several of these are now being tested in clinical trials [5, 6, 113, 159]. For many chemotherapeutic agents, combinational treatments are used to increase drug efficacy [77, 160].

Here, I discussed specific metabolic programs and adaptations that exist in drug-resistant tumors. I explained how these adaptations depend both on the drug and the origin of the tumor and how they contribute to drug resistance. From these studies, it becomes apparent that a better understanding of the altered metabolism in different drug resistant cancers is essential to improve cancer therapy. Such understanding will provide insights into the molecular mechanisms of resistance and may ultimately lead to novel metabolic targets that can be used for (combinational) therapy to increase the efficacy of current drugs. This knowledge may also lead to prognostic biomarkers for drug response, which may advance current therapy by predicting drug response based on the metabolic state of a tumor and thereby contribute towards more efficacious personalized medicine.

## REFERENCES

1. Groenendijk FH, Bernards RE. Drug resistance to targeted therapies: D e j a vu all over again. *Mol Oncol*. 2014;8:1067–83.
2. Swanton C. Intratumor heterogeneity: evolution through space and time. *Cancer Res*. 2012;72:4875–82.
3. Hanahan D, Weinberg RA. Hallmarks of cancer: The next generation. *Cell*. 2011;144:646–74.
4. Cairns RA, Harris IS, Mak TW. Regulation of cancer cell metabolism. *Nat Rev Cancer*. 2011;11:85–95.
5. Tennant DA, Durán R V., Gottlieb E. Targeting metabolic transformation for cancer therapy. *Nat Rev Cancer*. 2010;10:267–77.
6. Vander Heiden MG. Targeting cancer metabolism: A therapeutic window opens. *Nat Rev Drug Discov*. 2011;10:671–84.
7. Vander Heiden MG, Cantley LC, Thompson CB. Understanding the Warburg effect: the metabolic requirements of cell proliferation. *Science*. 2009;324:1029–33.
8. Lyssiotis CA, Kimmelman AC. Metabolic Interactions in the Tumor Microenvironment. *Trends Cell Biol*. 2017;27:863–75.
9. Berkers CR, Maddocks ODK, Cheung EC, Mor I, Vousden KH. Metabolic regulation by p53 family members. *Cell Metab*. 2013;18:617–33.
10. Stine ZE, Walton ZE, Altman BJ, Hsieh AL, Dang C V. MYC, Metabolism, and Cancer. *Cancer Discov*. 2015;5:1024–39.
11. Herzig S, Shaw RJ. AMPK: guardian of metabolism and mitochondrial homeostasis. *Nat Rev Mol Cell Biol*. 2017.
12. Lien EC, Lyssiotis CA, Cantley LC. Metabolic Reprogramming by the PI3K-Akt-mTOR Pathway in Cancer. In: Cramer T, A. Schmitt C, editors. *Metabolism in Cancer*. Cham: Springer International Publishing; 2016. p. 39–72.
13. Semenza GL. HIF-1: upstream and downstream of cancer metabolism. *Curr Opin Genet Dev*. 2010;20:51–6.
14. Kawada K, Toda K, Sakai Y. Targeting metabolic reprogramming in KRAS-driven cancers. *Int J Clin Oncol*. 2017;22:651–9.
15. Plas DR, Thompson CB. Akt-dependent transformation: there is more to growth than just surviving. *Oncogene*. 2005;24:7435–42.
16. Nicholls DG, Budd SL. Mitochondria and neuronal survival. *Physiol Rev*. 2000;80:315–60.
17. Pavlova NN, Thompson CB. The Emerging Hallmarks of Cancer Metabolism. *Cell Metab*. 2016;23:27–47.
18. Warburg O. On the Origin of Cancer Cells. *Science* (80- ). 1956;123:309–14.
19. Yamamoto T, Seino Y, Fukumoto H, Koh G, Yano H, Inagaki N, et al. Over-expression of facilitative glucose transporter genes in human cancer. *Biochem Biophys Res Commun*. 1990;170:223–30.
20. Macheda ML, Rogers S, Best JD. Molecular and cellular regulation of glucose transporter (GLUT) proteins in cancer. *J Cell Physiol*. 2005;202:654–62.
21. Lee JY, Lee I, Chang WJ, Ahn SM, Lim SH, Kim HS, et al. MCT4 as a potential therapeutic target for metastatic gastric cancer with peritoneal carcinomatosis. *Oncotarget*. 2016;7:43492–503.
22. Baek GH, Tse YF, Hu Z, Cox D, Buboltz N, McCue P, et al. MCT4 Defines a Glycolytic Subtype of Pancreatic Cancer with Poor Prognosis and Unique Metabolic Dependencies. *Cell Rep*. 2014;9:2233–49.
23. Mazurek S. Pyruvate kinase type M2: a key regulator of the metabolic budget system in tumor cells. *Int J Biochem Cell Biol*. 2011;43:969–80.
24. Liu VM, Vander Heiden MG. The Role of Pyruvate Kinase M2 in Cancer Metabolism. *Brain Pathol*. 2015;25:781–3.
25. Shinohara Y, Yamamoto K, Kogure K, Ichihara J, Terada H. Steady state transcript levels of the type II hexokinase and type 1 glucose transporter in human tumor cell lines. *Cancer Lett*. 1994;82:27–32.
26. Wolf A, Agnihotri S, Micallef J, Mukherjee J, Sabha N, Cairns R, et al. Hexokinase 2 is a key mediator of aerobic glycolysis and promotes tumor growth in human glioblastoma multiforme. *J Exp Med*. 2011;208:313–26.
27. Fantin VR, St-Pierre J, Leder P. Attenuation of LDH-A expression uncovers a link between glycolysis, mitochondrial physiology, and tumor maintenance. *Cancer Cell*. 2006;9:425–34.

28. Ren F, Wu H, Lei Y, Zhang H, Liu R, Zhao Y, et al. Quantitative proteomics identification of phosphoglycerate mutase 1 as a novel therapeutic target in hepatocellular carcinoma. *Mol Cancer*. 2010;9:81.
29. Chaneton B, Gottlieb E. PGAMgnam Style: A Glycolytic Switch Controls Biosynthesis. *Cancer Cell*. 2012;22:565–6.
30. Kim J, Tchernyshyov I, Semenza GL, Dang C V. HIF-1-mediated expression of pyruvate dehydrogenase kinase: a metabolic switch required for cellular adaptation to hypoxia. *Cell Metab*. 2006;3:177–85.
31. Atsumi T, Chesney J, Metz C, Leng L, Donnelly S, Makita Z, et al. High expression of inducible 6-phosphofructo-2-kinase/fructose-2,6-bisphosphatase (iPFK-2; PFKFB3) in human cancers. *Cancer Res*. 2002;62:5881–7.
32. Yalcin A, Telang S, Clem B, Chesney J. Regulation of glucose metabolism by 6-phosphofructo-2-kinase/fructose-2,6-bisphosphatases in cancer. *Exp Mol Pathol*. 2009;86:174–9.
33. Anderson NM, Mucka P, Kern JG, Feng H. The emerging role and targetability of the TCA cycle in cancer metabolism. *Protein Cell*. 2017;;1–22.
34. King A, Selak MA, Gottlieb E. Succinate dehydrogenase and fumarate hydratase: Linking mitochondrial dysfunction and cancer. *Oncogene*. 2006;25:4675–82.
35. Selak MA, Armour SM, MacKenzie ED, Boulahbel H, Watson DG, Mansfield KD, et al. Succinate links TCA cycle dysfunction to oncogenesis by inhibiting HIF- $\alpha$  prolyl hydroxylase. *Cancer Cell*. 2005;7:77–85.
36. Sciacovelli M, Frezza C. Oncometabolites: Unconventional triggers of oncogenic signalling cascades. *Free Radic Biol Med*. 2016;100:175–81.
37. Parsons DW, Jones S, Zhang X, Lin JC, Leary RJ, Angenendt P, et al. An integrated genomic analysis of human glioblastoma multiforme. *Science*. 2008;321:1807–12.
38. Yan H, Parsons DW, Jin G, McLendon R, Rasheed BA, Yuan W, et al. IDH1 and IDH2 mutations in gliomas. *N Engl J Med*. 2009;360:765–73.
39. Dang L, White DW, Gross S, Bennett BD, Bittinger MA, Driggers EM, et al. Cancer-associated IDH1 mutations produce 2-hydroxyglutarate. *Nature*. 2009;462:739–44.
40. Yang M, Soga T, Pollard PJ. Oncometabolites: Linking altered metabolism with cancer. *J Clin Invest*. 2013;123:3652–8.
41. DeBerardinis RJ, Chandel NS. Fundamentals of cancer metabolism. *Sci Adv*. 2016;2:e1600200.
42. Frezza C, Gottlieb E. Mitochondria in cancer: Not just innocent bystanders. *Semin Cancer Biol*. 2009;19:4–11.
43. Fischer K, Hoffmann P, Voelkl S, Meidenbauer N, Ammer J, Edinger M, et al. Inhibitory Effect of Tumor Cell-Derived Lactic Acid on Human T Cells. *Blood*. 2015;109:3812–20.
44. Goetze K, Walenta S, Ksiazkiewicz M, Kunz-Schughart LA, Mueller-Klieser W. Lactate enhances motility of tumor cells and inhibits monocyte migration and cytokine release. *Int J Oncol*. 2011;39:453–63.
45. Benito A, Polat IH, Noé V, Ciudad CJ, Marin S, Cascante M. Glucose-6-phosphate dehydrogenase and transketolase modulate breast cancer cell metabolic reprogramming and correlate with poor patient outcome. *Oncotarget*. 2017;8:106693–706.
46. Ambrosio MR, D'Esposito V, Costa V, Liguoro D, Collina F, Cantile M, et al. Glucose impairs tamoxifen responsiveness modulating connective tissue growth factor in breast cancer cells. *Oncotarget*. 2017;8:109000–17.
47. Patra KC, Hay N. The pentose phosphate pathway and cancer. *Trends Biochem Sci*. 2014;39:347–54.
48. Kowalik MA, Columbano A, Perra A. Emerging Role of the Pentose Phosphate Pathway in Hepatocellular Carcinoma. *Front Oncol*. 2017;7 May:87.
49. Maddocks ODK, Labuschagne CF, Adams PD, Vousden KH. Serine Metabolism Supports the Methionine Cycle and DNA/RNA Methylation through De Novo ATP Synthesis in Cancer Cells. *Mol Cell*. 2016;61:210–21.
50. Labuschagne CF, van den Broek NJF, Mackay GM, Vousden KH, Maddocks ODK. Serine, but not glycine, supports one-carbon metabolism and proliferation of cancer cells. *Cell Rep*. 2014;7:1248–58.
51. Locasale JW, Grassian AR, Melman T, Lyssiotis CA, Mattaini KR, Bass AJ, et al. Phosphoglycerate dehydrogenase diverts glycolytic flux and contributes to oncogenesis. *Nat Genet*. 2011;43:869–74.
52. Possemato R, Marks KM, Shaul YD, Pacold ME, Kim D, Birsoy K, et al. Functional genomics reveal that the serine synthesis

- pathway is essential in breast cancer. *Nature*. 2011;476:346–50.
53. Chaneton B, Hillmann P, Zheng L, Martin ACL, Maddocks ODK, Chokkathukalam A, et al. Serine is a natural ligand and allosteric activator of pyruvate kinase M2. *Nature*. 2012;491:458–62.
  54. Ye J, Mancuso A, Tong X, Ward PS, Fan J, Rabinowitz JD, et al. Pyruvate kinase M2 promotes de novo serine synthesis to sustain mTORC1 activity and cell proliferation. *Proc Natl Acad Sci U S A*. 2012;109:6904–9.
  55. Anastasiou D, Yu Y, Israelsen WJ, Jiang J-K, Boxer MB, Hong BS, et al. Pyruvate kinase M2 activators promote tetramer formation and suppress tumorigenesis. *Nat Chem Biol*. 2012;8:839–47.
  56. Kuehne A, Emmert H, Soehle J, Winnefeld M, Fischer F, Wenck H, et al. Acute Activation of Oxidative Pentose Phosphate Pathway as First-Line Response to Oxidative Stress in Human Skin Cells. *Mol Cell*. 2015;59:359–71.
  57. Hitosugi T, Zhou L, Elf S, Fan J, Kang H-B, Seo JH, et al. Phosphoglycerate mutase 1 coordinates glycolysis and biosynthesis to promote tumor growth. *Cancer Cell*. 2012;22:585–600.
  58. Eagle H. Nutrition needs of mammalian cells in tissue culture. *Science*. 1955;122:501–14.
  59. Reitzer LJ, Wice BM, Kennell D. Evidence that glutamine, not sugar, is the major energy source for cultured HeLa cells. *J Biol Chem*. 1979;254:2669–76.
  60. Wise DR, DeBerardinis RJ, Mancuso A, Sayed N, Zhang X-Y, Pfeiffer HK, et al. Myc regulates a transcriptional program that stimulates mitochondrial glutaminolysis and leads to glutamine addiction. *Proc Natl Acad Sci U S A*. 2008;105:18782–7.
  61. Gao P, Tchernyshyov I, Chang T-C, Lee Y-S, Kita K, Ochi T, et al. c-Myc suppression of miR-23a/b enhances mitochondrial glutaminase expression and glutamine metabolism. *Nature*. 2009;458:762–5.
  62. Zaugg K, Yao Y, Reilly PT, Kannan K, Kiarash R, Mason J, et al. Carnitine palmitoyltransferase 1C promotes cell survival and tumor growth under conditions of metabolic stress. *Genes Dev*. 2011;25:1041–51.
  63. Hui S, Ghergurovich JM, Morscher RJ, Jang C, Teng X, Lu W, et al. Glucose feeds the TCA cycle via circulating lactate. *Nature*. 2017;551:115–8.
  64. Mashimo T, Pichumani K, Vemireddy V, Hatanpaa KJ, Singh DK, Sirasanagandla S, et al. Acetate is a bioenergetic substrate for human glioblastoma and brain metastases. *Cell*. 2014;159:1603–14.
  65. Green CR, Wallace M, Divakaruni AS, Phillips SA, Murphy AN, Ciaraldi TP, et al. Branched-chain amino acid catabolism fuels adipocyte differentiation and lipogenesis. *Nat Chem Biol*. 2016;12:15–21.
  66. Hosios AM, Hecht VC, Danai L V., Johnson MO, Rathmell JC, Steinhauser ML, et al. Amino Acids Rather than Glucose Account for the Majority of Cell Mass in Proliferating Mammalian Cells. *Dev Cell*. 2016;36:540–9.
  67. DeBerardinis RJ, Mancuso A, Daikhin E, Nissim I, Yudkoff M, Wehrli S, et al. Beyond aerobic glycolysis: transformed cells can engage in glutamine metabolism that exceeds the requirement for protein and nucleotide synthesis. *Proc Natl Acad Sci U S A*. 2007;104:19345–50.
  68. Birsoy K, Wang T, Chen WW, Freinkman E, Abu-Remaileh M, Sabatini DM. An Essential Role of the Mitochondrial Electron Transport Chain in Cell Proliferation Is to Enable Aspartate Synthesis. *Cell*. 2015;162:540–51.
  69. Sullivan LB, Gui DY, Hosios AM, Bush LN, Freinkman E, Vander Heiden MG. Supporting Aspartate Biosynthesis Is an Essential Function of Respiration in Proliferating Cells. *Cell*. 2015;162:552–63.
  70. Loayza-Puch F, Rooijers K, Buil LCM, Zijlstra J, Oude Vrielink JF, Lopes R, et al. Tumour-specific proline vulnerability uncovered by differential ribosome codon reading. *Nature*. 2016;530:490–4.
  71. Lien EC, Lyssiotis CA, Juvekar A, Hu H, Asara JM, Cantley LC, et al. Glutathione biosynthesis is a metabolic vulnerability in PI(3)K/Akt-driven breast cancer. *Nat Cell Biol*. 2016;18.
  72. Beatty A, Fink LS, Singh T, Strigun A, Peter E, Ferrer CM, et al. Metabolite profiling reveals the glutathione biosynthetic pathway as a therapeutic target in triple negative breast cancer. *Mol Cancer Ther*. 2017;5500:molcanther.0407.2017.
  73. Röhrig F, Schulze A. The multifaceted roles of fatty acid synthesis in cancer. *Nat Rev Cancer*. 2016;16:732–49.
  74. Carracedo A, Cantley LC, Pandolfi PP. Cancer metabolism: fatty acid oxidation in the limelight. *Nat Rev Cancer*. 2013;13:227–32.

75. Longley DB, Johnston PG. Molecular mechanisms of drug resistance. *J Pathol.* 2005;205:275–92.
76. Holohan C, Van Schaeybroeck S, Longley DB, Johnston PG. Cancer drug resistance: an evolving paradigm. *Nat Rev Cancer.* 2013;13:714–26.
77. Housman G, Byler S, Heerboth S, Lapinska K, Longacre M, Snyder N, et al. Drug resistance in cancer: An overview. *Cancers (Basel).* 2014;6:1769–92.
78. Kirschner K, Melton DW. Multiple roles of the ERCC1-XPF endonuclease in DNA repair and resistance to anticancer drugs. *Anticancer Res.* 2010;30:3223–32.
79. Jain A, Jahagirdar D, Nilendu P, Sharma NK. Molecular approaches to potentiate cisplatin responsiveness in carcinoma therapeutics. *Expert Rev Anticancer Ther.* 2017;17:815–25.
80. McConkey DJ, Zhu K. Mechanisms of proteasome inhibitor action and resistance in cancer. *Drug Resist Updat.* 2008;11:164–79.
81. Hu Y-L, DeLay M, Jahangiri A, Molinaro AM, Rose SD, Carbonell WS, et al. Hypoxia-induced autophagy promotes tumor cell survival and adaptation to antiangiogenic treatment in glioblastoma. *Cancer Res.* 2012;72:1773–83.
82. Engelman JA, Zejnullahu K, Mitsudomi T, Song Y, Hyland C, Park JO, et al. MET Amplification Leads to Gefitinib Resistance in Lung Cancer by Activating ERBB3 Signaling. *Science (80- ).* 2007;316:1039–43.
83. Nazarian R, Shi H, Wang Q, Kong X, Koya RC, Lee H, et al. Melanomas acquire resistance to B-RAF(V600E) inhibition by RTK or N-RAS upregulation. *Nature.* 2010;468:973–7.
84. Wagle N, Emery C, Berger MF, Davis MJ, Sawyer A, Pochanard P, et al. Dissecting therapeutic resistance to RAF inhibition in melanoma by tumor genomic profiling. *J Clin Oncol.* 2011;29:3085–96.
85. Johannessen CM, Boehm JS, Kim SY, Thomas SR, Wardwell L, Johnson LA, et al. COT drives resistance to RAF inhibition through MAP kinase pathway reactivation. *Nature.* 2010;468:968–72.
86. Moreau P, Richardson PG, Cavo M, Orłowski RZ, San Miguel JF, Palumbo A, et al. Proteasome inhibitors in multiple myeloma: 10 years later. *Blood.* 2012;120:947–59.
87. Anderson KC. The 39th David A. Karnofsky Lecture: bench-to bedside translation of targeted therapies in multiple myeloma. *J Clin Oncol.* 2012;30:445–52.
88. Obeng EA, Carlson LM, Gutman DM, Harrington WJ, Lee KP, Boise LH. Proteasome inhibitors induce a terminal unfolded protein response in multiple myeloma cells. *Blood.* 2006;107:4907–16.
89. Lipchick BC, Fink EE, Nikiforov MA. Oxidative stress and proteasome inhibitors in multiple myeloma. *Pharmacol Res.* 2016;105:210–5.
90. Niewerth D, Jansen G, Assaraf YG, Zweegman S, Kaspers GJL, Cloos J. Molecular basis of resistance to proteasome inhibitors in hematological malignancies. *Drug Resist Updat.* 2015;18:18–35.
91. Orłowski RZ, Kuhn DJ. Proteasome inhibitors in cancer therapy: Lessons from the first decade. *Clin Cancer Res.* 2008;14:1649–57.
92. Oerlemans R, Franke NE, Assaraf YG, Cloos J, van Zantwijk I, Berkers CR, et al. Molecular basis of bortezomib resistance: proteasome subunit beta5 (PSMB5) gene mutation and overexpression of PSMB5 protein. *Blood.* 2008;112:2489–99.
93. Franke NE, Niewerth D, Assaraf YG, van Meerloo J, Vojtekova K, van Zantwijk CH, et al. Impaired bortezomib binding to mutant  $\beta 5$  subunit of the proteasome is the underlying basis for bortezomib resistance in leukemia cells. *Leukemia.* 2012;26:757–68.
94. de Wilt LHAM, Jansen G, Assaraf YG, van Meerloo J, Cloos J, Schimmer AD, et al. Proteasome-based mechanisms of intrinsic and acquired bortezomib resistance in non-small cell lung cancer. *Biochem Pharmacol.* 2012;83:207–17.
95. Rückrich T, Kraus M, Gogel J, Beck A, Ovaa H, Verdoes M, et al. Characterization of the ubiquitin-proteasome system in bortezomib-adapted cells. *Leukemia.* 2009;23:1098–105.
96. Balsas P, Galán-Malo P, Marzo I, Naval J. Bortezomib resistance in a myeloma cell line is associated to PSM $\beta 5$  overexpression and polyploidy. *Leuk Res.* 2012;36:212–8.
97. Niewerth D, Kaspers GJL, Jansen G, van Meerloo J, Zweegman S, Jenkins G, et al. Proteasome subunit expression analysis and chemosensitivity in relapsed paediatric acute leukaemia patients receiving bortezomib-containing chemotherapy. *J Hematol Oncol.* 2016;9:82.
98. Dettmer S, Theile D, Schäfer J, Seckinger A, Burhenne J, Weiss J. Proteasome inhibition correlates with intracellular bortezomib



- concentrations but not with antiproliferative effects after bolus treatment in myeloma cell lines. *Naunyn Schmiedebergs Arch Pharmacol.* 2016;389:1091–101.
99. Ling SCW, Lau EKK, Al-Shabeeb A, Nikolic A, Catalano A, Iland H, et al. Response of myeloma to the proteasome inhibitor bortezomib is correlated with the unfolded protein response regulator XBP-1. *Haematologica.* 2012;97:64–72.
  100. Leung-Hagesteijn C, Erdmann N, Cheung G, Keats JJ, Stewart a. K, Reece DE, et al. Xbp1s-negative tumor B cells and pre-plasmablasts mediate therapeutic proteasome inhibitor resistance in multiple myeloma. *Cancer Cell.* 2013;24:289–304.
  101. Driessen C, Kraus M, Joerger M, Rosing H, Bader J, Hitz F, et al. Treatment with the HIV protease inhibitor nelfinavir triggers the unfolded protein response and may overcome proteasome inhibitor resistance of multiple myeloma in combination with bortezomib: a phase I trial (SAKK 65/08). *Haematologica.* 2016;101:346–55.
  102. Franke NE, Kaspers GL, Assaraf YG, van Meerloo J, Niewerth D, Kessler FL, et al. Exocytosis of polyubiquitinated proteins in bortezomib-resistant leukemia cells: a role for MARCKS in acquired resistance to proteasome inhibitors. *Oncotarget.* 2016;7:74779–96.
  103. Fuchs D, Berges C, Opelz G, Daniel V, Naujokat C. HMG-CoA reductase inhibitor simvastatin overcomes bortezomib-induced apoptosis resistance by disrupting a geranylgeranyl pyrophosphate-dependent survival pathway. *Biochem Biophys Res Commun.* 2008;374:309–14.
  104. Du Z-X, Zhang H-Y, Meng X, Guan Y, Wang H-Q. Role of oxidative stress and intracellular glutathione in the sensitivity to apoptosis induced by proteasome inhibitor in thyroid cancer cells. *BMC Cancer.* 2009;9:56.
  105. Sanchez WY, McGee SL, Connor T, Mottram B, Wilkinson A, Whitehead JP, et al. Dichloroacetate inhibits aerobic glycolysis in multiple myeloma cells and increases sensitivity to bortezomib. *Br J Cancer.* 2013;108:1624–33.
  106. Thompson RM, Dytfeld D, Reyes L, Robinson RM, Smith B, Manevich Y, et al. Glutaminase inhibitor CB-839 synergizes with carfilzomib in resistant multiple myeloma cells. *Oncotarget.* 2017;8:35863–76.
  107. Soriano GP, Besse L, Li N, Kraus M, Besse A, Meeuwenoord N, et al. Proteasome inhibitor-adapted myeloma cells are largely independent from proteasome activity and show complex proteomic changes, in particular in redox and energy metabolism. *Leukemia.* 2016;30:2198–207.
  108. Zaal EA, Wu W, Jansen G, Zweegman S, Cloos J, Berkers CR. Bortezomib resistance in multiple myeloma is associated with increased serine synthesis. *Cancer Metab.* 2017;5:7.
  109. Song IS, Kim HK, Lee SR, Jeong SH, Kim N, Ko KS, et al. Mitochondrial modulation decreases the bortezomib-resistance in multiple myeloma cells. *Int J cancer.* 2013;133:1357–67.
  110. Fujiwara S, Kawano Y, Yuki H, Okuno Y, Nosaka K, Mitsuya H, et al. PDK1 inhibition is a novel therapeutic target in multiple myeloma. *Br J Cancer.* 2013;108:170–8.
  111. Song I-S, Jeong YJ, Jeong SH, Heo HJ, Kim HK, Lee SR, et al. Combination treatment with 2-methoxyestradiol overcomes bortezomib resistance of multiple myeloma cells. *Exp Mol Med.* 2013;45:e50.
  112. Maiso P, Huynh D, Moschetta M, Sacco A, Aljawai Y, Mishima Y, et al. Metabolic signature identifies novel targets for drug resistance in multiple myeloma. *Cancer Res.* 2015;75:2071–82.
  113. Galluzzi L, Kepp O, Vander Heiden MG, Kroemer G. Metabolic targets for cancer therapy. *Nat Rev Drug Discov.* 2013;12:829–46.
  114. Wangpaichitr M, Sullivan EJ, Theodoropoulos G, Wu C, You M, Feun LG, et al. The relationship of thioredoxin-1 and cisplatin resistance: its impact on ROS and oxidative metabolism in lung cancer cells. *Mol Cancer Ther.* 2012;11:604–15.
  115. Galluzzi L, Senovilla L, Vitale I, Michels J, Martins I, Kepp O, et al. Molecular mechanisms of cisplatin resistance. *Oncogene.* 2012;31:1869–83.
  116. Wangpaichitr M, Wu C, Li YY, Nguyen DJM, Kandemir H, Shah S, et al. Exploiting ROS and metabolic differences to kill cisplatin resistant lung cancer. *Oncotarget.* 2017;8:49275–92.
  117. Catanzaro D, Gaude E, Orso G, Giordano C, Guzzo G, Rasola A, et al. Inhibition of glucose-6-phosphate dehydrogenase sensitizes cisplatin-resistant cells to death. *Oncotarget.* 2015;6:30102–14.



118. Marullo R, Werner E, Degtyareva N, Moore B, Altavilla G, Ramalingam SS, et al. Cisplatin induces a mitochondrial-ROS response that contributes to cytotoxicity depending on mitochondrial redox status and bioenergetic functions. *PLoS One*. 2013;8:e81162.
119. Sullivan EJ, Kurtoglu M, Brennenman R, Liu H, Lampidis TJ. Targeting cisplatin-resistant human tumor cells with metabolic inhibitors. *Cancer Chemother Pharmacol*. 2014;73:417–27.
120. Leyton J, Latigo JR, Perumal M, Dhaliwal H, He Q, Aboagye EO. Early detection of tumor response to chemotherapy by 3'-deoxy-3'-[18F]fluorothymidine positron emission tomography: the effect of cisplatin on a fibrosarcoma tumor model in vivo. *Cancer Res*. 2005;65:4202–10.
121. Sun H, Zhu A, Zhou X, Wang F. Suppression of pyruvate dehydrogenase kinase-2 re-sensitizes paclitaxel-resistant human lung cancer cells to paclitaxel. *Oncotarget*. 2017;5:1–9.
122. Komurov K, Tseng J-T, Muller M, Seviour EG, Moss TJ, Yang L, et al. The glucose-deprivation network counteracts lapatinib-induced toxicity in resistant ErbB2-positive breast cancer cells. *Mol Syst Biol*. 2012;8:596.
123. Ruprecht B, Zaal EA, Zecha J, Wu W, Berkers CR, Kuster B, et al. Lapatinib Resistance in Breast Cancer Cells Is Accompanied by Phosphorylation-Mediated Reprogramming of Glycolysis. *Cancer Res*. 2017;77:1842–53.
124. Zhao Y, Liu H, Liu Z, Ding Y, Ledoux SP, Wilson GL, et al. Overcoming trastuzumab resistance in breast cancer by targeting dysregulated glucose metabolism. *Cancer Res*. 2011;71:4585–97.
125. Zhou M, Zhao Y, Ding Y, Liu H, Liu Z, Fodstad O, et al. Warburg effect in chemosensitivity: targeting lactate dehydrogenase-A re-sensitizes taxol-resistant cancer cells to taxol. *Mol Cancer*. 2010;9:33.
126. Park S, Chang C, Safi R, Liu X, Baldi R, Jasper JS, et al. ERR $\alpha$ -Regulated Lactate Metabolism Contributes to Resistance to Targeted Therapies in Breast Cancer. *Cell Rep*. 2016;15:323–35.
127. Deblois G, Smith HW, Tam IS, Gravel S-P, Caron M, Savage P, et al. ERR $\alpha$  mediates metabolic adaptations driving lapatinib resistance in breast cancer. *Nat Commun*. 2016;7:12156.
128. Fiorillo M, Sotgia F, Sisci D, Cappello AR, Lisanti MP. Mitochondrial “power” drives tamoxifen resistance: NQO1 and GCLC are new therapeutic targets in breast cancer. *Oncotarget*. 2017;8:20309–27.
129. Janzer A, German NJ, Gonzalez-Herrera KN, Asara JM, Haigis MC, Struhl K. Metformin and phenformin deplete tricarboxylic acid cycle and glycolytic intermediates during cell transformation and NTPs in cancer stem cells. *Proc Natl Acad Sci U S A*. 2014;111:10574–9.
130. Corazao-Rozas P, Guerreschi P, Jendoubi M, André F, Jonneaux A, Scalbert C, et al. Mitochondrial oxidative stress is the Achilles' heel of melanoma cells resistant to BRAF-mutant inhibitor. *Oncotarget*. 2013;4:1986–98.
131. Baenke F, Chaneton B, Smith M, Van Den Broek N, Hogan K, Tang H, et al. Resistance to BRAF inhibitors induces glutamine dependency in melanoma cells. *Mol Oncol*. 2016;10:73–84.
132. Zhang G, Frederick DT, Wu L, Wei Z, Krepler C, Srinivasan S, et al. Targeting mitochondrial biogenesis to overcome drug resistance to MAPK inhibitors. *J Clin Invest*. 2016;126:1834–56.
133. Cesi G, Walbreccq G, Zimmer A, Kreis S, Haan C. ROS production induced by BRAF inhibitor treatment rewires metabolic processes affecting cell growth of melanoma cells. *Mol Cancer*. 2017;16:102.
134. Kaplon J, Zheng L, Meissl K, Chaneton B, Selivanov V a, Mackay G, et al. A key role for mitochondrial gatekeeper pyruvate dehydrogenase in oncogene-induced senescence TL - 498. *Nature*. 2013;498 VN-:109–12.
135. Yun J, Mullarky E, Lu C, Bosch KN, Kavalier A, Rivera K, et al. Vitamin C selectively kills KRAS and BRAF mutant colorectal cancer cells by targeting GAPDH. *Science*. 2015;350:1391–6.
136. Aird KM, Allensworth JL, Batinic-Haberle I, Lyerly HK, Dewhirst MW, Devi GR. ErbB1/2 tyrosine kinase inhibitor mediates oxidative stress-induced apoptosis in inflammatory breast cancer cells. *Breast Cancer Res Treat*. 2012;132:109–19.
137. Teppo H-R, Soini Y, Karihtala P. Reactive Oxygen Species-Mediated Mechanisms of Action of Targeted Cancer Therapy. *Oxid Med Cell Longev*. 2017;2017:1–11.

138. Conklin KA. Chemotherapy-associated oxidative stress: impact on chemotherapeutic effectiveness. *Integr Cancer Ther.* 2004;3:294–300.
139. Lo M, Ling V, Wang YZ, Gout PW. The x-cystine/glutamate antiporter: a mediator of pancreatic cancer growth with a role in drug resistance. *Br J Cancer.* 2008;99:464–72.
140. Kim M-J, Choi Y-K, Park SY, Jang SY, Lee JY, Ham HJ, et al. PPAR $\delta$  Reprograms Glutamine Metabolism in Sorafenib-Resistant HCC. *Mol Cancer Res.* 2017;15:1230–42.
141. Sullivan LB, Gui DY, Vander Heiden MG. Altered metabolite levels in cancer: implications for tumour biology and cancer therapy. *Nat Rev Cancer.* 2016;16:680–93.
142. Wojtkowiak JW, Verduzco D, Schramm KJ, Gillies RJ. Drug resistance and cellular adaptation to tumor acidic pH microenvironment. *Mol Pharm.* 2011;8:2032–8.
143. Vukovic V, Tannock IF. Influence of low pH on cytotoxicity of paclitaxel, mitoxantrone and topotecan. *Br J Cancer.* 1997;75:1167–72.
144. Wangpaichitr M, Wu C, Li YY, Nguyen DJM, Kandemir H, Shah S, et al. Exploiting ROS and metabolic differences to kill cisplatin resistant lung cancer. *Oncotarget.* 2017;1.
145. Wise DR, Thompson CB. Glutamine addiction: a new therapeutic target in cancer. *Trends Biochem Sci.* 2010;35:427–33.
146. Smith B, Schafer XL, Ambeskovic A, Spencer CM, Land H, Munger J. Addiction to Coupling of the Warburg Effect with Glutamine Catabolism in Cancer Cells. *Cell Rep.* 2016;17:821–36.
147. Bridges HR, Jones AJY, Pollak MN, Hirst J. Effects of metformin and other biguanides on oxidative phosphorylation in mitochondria. *Biochem J.* 2014;462:475–87.
148. Mayers JR, Torrence ME, Danai L V, Papagiannakopoulos T, Davidson SM, Bauer MR, et al. Tissue of origin dictates branched-chain amino acid metabolism in mutant Kras-driven cancers. *Science.* 2016;353:1161–5.
149. Liu H, Liu Y, Zhang J-T. A new mechanism of drug resistance in breast cancer cells: fatty acid synthase overexpression-mediated palmitate overproduction. *Mol Cancer Ther.* 2008;7:263–70.
150. Yang Y, Liu H, Li Z, Zhao Z, Yip-Schneider M, Fan Q, et al. Role of fatty acid synthase in gemcitabine and radiation resistance of pancreatic cancers. *Int J Biochem Mol Biol.* 2011;2:89–98.
151. Mims J, Bansal N, Bharadwaj MS, Chen X, Molina AJ, Tsang AW, et al. Energy Metabolism in a Matched Model of Radiation Resistance for Head and Neck Squamous Cell Cancer. *Radiat Res.* 2015;183:291–304.
152. Maddocks ODK, Berkers CR, Mason SM, Zheng L, Blyth K, Gottlieb E, et al. Serine starvation induces stress and p53-dependent metabolic remodelling in cancer cells. *Nature.* 2013;493:542–6.
153. Krishnan N, Dickman MB, Becker DF. Proline modulates the intracellular redox environment and protects mammalian cells against oxidative stress. *Free Radic Biol Med.* 2008;44:671–81.
154. Kremer JC, Prudner BC, Lange SES, Bean GR, Schultze MB, Brashears CB, et al. Arginine Deprivation Inhibits the Warburg Effect and Upregulates Glutamine Anaplerosis and Serine Biosynthesis in ASS1-Deficient Cancers. *Cell Rep.* 2017;18:991–1004.
155. Li Y-Y, Wu C, Chen S-M, Shah SS, Wangpaichitr M, Feun LG, et al. BRAF inhibitor resistance enhances vulnerability to arginine deprivation in melanoma. *Oncotarget.* 2016;7:17665–80.
156. Farwell MD, Pryma DA, Mankoff DA. PET/CT imaging in cancer: current applications and future directions. *Cancer.* 2014;120:3433–45.
157. Farber S, Diamond LK. Temporary remissions in acute leukemia in children produced by folic acid antagonist, 4-aminopteroyl-glutamic acid. *N Engl J Med.* 1948;238:787–93.
158. Masetti R, Pession A. First-line treatment of acute lymphoblastic leukemia with pegasparginase. *Biologics.* 2009;3:359–68.
159. Martinez-Outschoorn UE, Peiris-Pagés M, Pestell RG, Sotgia F, Lisanti MP. Cancer metabolism: a therapeutic perspective. *Nat Rev Clin Oncol.* 2017;14:11–31.
160. Kapoor P, Ramakrishnan V, Rajkumar SV. Bortezomib combination therapy in multiple myeloma. *Semin Hematol.* 2012;49:228–42.
161. Sanchez WY, McGee SL, Connor T, Mottram B, Wilkinson A, Whitehead JP, et al. Dichloroacetate inhibits aerobic glycolysis in multiple myeloma cells and increases sensitivity to bortezomib. *Br J Cancer.* 2013;108:1624–33.
162. Wangpaichitr M, Wu C, You M, Maher JC, Dinh V, Feun LG, et al. N',N'

- Dimethyl-N',N'-bis(phenylcarbonothioyl) Propanedihydrazide (Elesclomol) Selectively Kills Cisplatin Resistant Lung Cancer Cells through Reactive Oxygen Species (ROS). *Cancers* (Basel). 2009;1:23–38.
163. Wu C, Wangpaichitr M, Feun L, Kuo MT, Robles C, Lampidis T, et al. Overcoming cisplatin resistance by mTOR inhibitor in lung cancer. *Mol Cancer*. 2005;4:25.
164. Ge C, Cao B, Feng D, Zhou F, Zhang J, Yang N, et al. The down-regulation of SLC7A11 enhances ROS induced P-gp over-expression and drug resistance in MCF-7 breast cancer cells. *Sci Rep*. 2017;7:3791.
165. Stäubert C, Bhuiyan H, Lindahl A, Broom OJ, Zhu Y, Islam S, et al. Rewired metabolism in drug-resistant leukemia cells: a metabolic switch hallmarked by reduced dependence on exogenous glutamine. *J Biol Chem*. 2015;290:8348–59.
166. Kuntz EM, Baquero P, Michie AM, Dunn K, Tardito S, Holyoake TL, et al. Targeting mitochondrial oxidative phosphorylation eradicates therapy-resistant chronic myeloid leukemia stem cells. *Nat Med*. 2017;23:1234–40.
167. Fukuda S, Miyata H, Miyazaki Y, Makino T, Takahashi T, Kurokawa Y, et al. Pyruvate Kinase M2 Modulates Esophageal Squamous Cell Carcinoma Chemotherapy Response by Regulating the Pentose Phosphate Pathway. *Ann Surg Oncol*. 2015;22:1461–8.
168. Mynhardt C, Damelin LH, Jivan R, Peres J, Prince S, Veale RB, et al. Metformin-induced alterations in nucleotide metabolism cause 5-fluorouracil resistance but gemcitabine susceptibility in oesophageal squamous cell carcinoma. *J Cell Biochem*. 2017; July:1–11.
169. Zhou Y, Tozzi F, Chen J, Fan F, Xia L, Wang J, et al. Intracellular ATP levels are a pivotal determinant of chemoresistance in colon cancer cells. *Cancer Res*. 2012;72:304–14.
170. Tadros S, Shukla SK, King RJ, Gunda V, Vernucci E, Abrego J, et al. De Novo Lipid Synthesis Facilitates Gemcitabine Resistance through Endoplasmic Reticulum Stress in Pancreatic Cancer. *Cancer Res*. 2017;77:5503–17.
171. Chen R, Lai LA, Sullivan Y, Wong M, Wang L, Riddell J, et al. Disrupting glutamine metabolic pathways to sensitize gemcitabine-resistant pancreatic cancer. *Sci Rep*. 2017;7:7950.



---

**Part I**

**Identification of metabolic  
vulnerabilities in  
proteasome inhibitor  
resistance**



---

# Part I

# Chapter 2

## **Bortezomib resistance in multiple myeloma is associated with increased serine synthesis**

Esther A. Zaal<sup>1</sup>, Wei Wu<sup>1</sup>, Gerrit Jansen<sup>2</sup>, Sonja Zweegman<sup>3</sup>, Jacqueline Cloos,<sup>3,4</sup>  
Celia R. Berkers<sup>1</sup>

<sup>1</sup> Biomolecular Mass Spectrometry and Proteomics, Bijvoet Center for Biomolecular Research, Utrecht University, Utrecht, The Netherlands

<sup>2</sup> Amsterdam Rheumatology and Immunology Center – Location VUmc, VU University Medical Center, Amsterdam, The Netherlands

<sup>3</sup> Department of Hematology and <sup>4</sup> Pediatric Oncology/Hematology, VU University Medical Center, Amsterdam, The Netherlands

## ABSTRACT

The proteasome inhibitor bortezomib (BTZ) is successfully applied in the treatment of multiple myeloma, but its efficacy is restricted by the wide-spread occurrence of resistance. Metabolic alterations play an important role in cancer development and aid in the cellular adaptation to pharmacologically changed environments. Metabolic changes could therefore play an essential role in the development of drug resistance. However, specific metabolic pathways that can be targeted to improve bortezomib therapy remain unidentified.

We elucidated the metabolic mechanisms underlying bortezomib resistance by using mass spectrometry-based metabolomics and proteomics on BTZ-sensitive and BTZ-resistant multiple myeloma cell lines as well as in a set of CD138+ cells obtained from multiple myeloma patients.

Our findings demonstrate that a rewired glucose metabolism sustains bortezomib resistance. Mechanistically, this results in higher activity of both the pentose phosphate pathway and serine synthesis pathway, ultimately leading to an increased anti-oxidant capacity of BTZ-resistant cells. Moreover, our results link both serine synthesis pathway activity and expression of 3-phosphoglycerate dehydrogenase (PHGDH), which catalyses the rate-limiting step of serine synthesis, to bortezomib resistance across different BTZ-resistant multiple myeloma cell lines. Consistently, serine starvation enhanced the cytotoxicity of bortezomib, underscoring the importance of serine metabolism in the response to BTZ. Importantly, in CD138+ cells of clinically bortezomib refractory multiple myeloma patients, PHGDH expression was also markedly increased.

Our findings indicate that interfering with serine metabolism can be a novel strategy to improve bortezomib therapy and identify PHGDH as a potential biomarker for BTZ resistance.



## INTRODUCTION

The proteasome inhibitor bortezomib (BTZ) is widely used in the treatment of multiple myeloma (MM) [1, 2]. The proteasome is a large intracellular protease complex, composed of a 20S core particle and two 19S regulatory particles. The 20S core particle consists of two outer rings of  $\alpha$ -subunits and two inner rings of  $\beta$ -subunits. Three of these  $\beta$ -subunits, termed  $\beta 1$ ,  $\beta 2$  and  $\beta 5$  are catalytically active [3]. They can be replaced by the three interferon inducible subunits  $\beta 1i$ ,  $\beta 2i$  and  $\beta 5i$  to form immunoproteasomes. BTZ acts by inhibiting primarily the  $\beta 5/\beta 5i$  subunits and to a lesser extent the  $\beta 1/\beta 1i$  subunits [4]. The resulting imbalance between production and degradation of proteins leads to the accumulation of (regulatory) proteins, causing endoplasmic reticulum stress and activation of the unfolded protein response. Proteasome inhibition eventually causes apoptosis in malignant cells via multiple pathways, including overproduction of reactive oxygen species [5–7].

Despite good clinical results of initial treatment, many patients eventually relapse from BTZ therapy [7–9]. Resistance is associated with mutations in the binding pocket of the  $\beta 5$  subunit (*PSMB5*), resulting in impaired binding of the drug [10–12], upregulation of the proteasomal machinery, and a change in the ratio of (immuno) proteasomal subunits [13–15]. However, how relevant *PSMB5* mutations are in relapsed patients remains unclear [16] and more recent studies suggest that other mechanisms are involved in BTZ resistance, such as the unfolded protein response and vesicular exocytosis of ubiquitinated proteins [5, 17–20].

Targeting metabolism is emerging as a promising strategy for cancer therapy [21–23]. Metabolic alterations have been linked to resistance to chemotherapeutic agents [24–27] and may also play a role in the (lack of) response to BTZ. In particular, higher glycolytic activity has been found to lower BTZ sensitivity under hypoxic conditions [28] and BTZ resistant cells were found to have proteomic changes in redox and energy metabolism [29]. However, specific metabolic targets that can serve to augment responses to BTZ therapy remain unidentified.

In this study we aimed to identify altered metabolic pathways in BTZ-resistant MM cells that drive resistance. By using mass spectrometry and tracer-based metabolomics combined with proteomics, we show that BTZ-resistant cells adapt their glucose metabolism. Mechanistically, this metabolic rewiring results in higher activity of both the pentose phosphate pathway (PPP) and serine synthesis pathway (SSP) and ultimately leads to an increased anti-oxidant capacity of BTZ-resistant cells. We also demonstrate that serine starvation enhances the effect of BTZ and that 3-phosphoglycerate dehydrogenase (PHGDH), which catalyzes the rate limiting step in the SSP, is upregulated across different BTZ resistant MM cells. Our results

indicate that serine metabolism is associated with BTZ resistance and that interfering with this pathway can be a novel strategy to improve BTZ therapy.

## RESULTS

### **Bortezomib resistance in MM cells is not solely driven by adaptation of the proteasome itself**

To study BTZ resistance, we compared human BTZ-sensitive RPMI-8226 wild-type (WT) MM cells with two BTZ-resistant cell lines (BTZ/7 and BTZ/100), which grow in the presence of 7 nM and 100 nM BTZ, respectively [11]. Cell viability assays showed the 48-hour  $IC_{50}$  values of BTZ to be  $7.3 \pm 2.4$  nM,  $25.3 \pm 6.6$  nM and  $231.9 \pm 73$  nM in the WT, BTZ/7 and BTZ/100 cell lines, respectively (Fig. 1a), in line with previous reports [11, 30]. Comparable  $IC_{50}$  values were found by analysing the cell growth of these cell lines, and also cell death assays using propidium iodide showed similar trends (Supplemental Fig. S1a). BTZ-resistant cells displayed cross-resistance towards the proteasome inhibitor carfilzomib (CFZ), but not to the chemotherapeutic drugs methotrexate (folate antagonist) and melphalan (alkylating agent) (Supplemental Fig. S1b). This suggests that the adaptations are related to proteasome inhibitor resistance rather than multidrug resistance, as also previously described for THP-1 cells [10].

Next, we evaluated the proteasome activity in these cells with and without BTZ treatment using the cell-permeable fluorescent proteasome activity probe  $Me_4BodipyFL-Ahx_3L_3VS$ . In this assay, the fluorescence intensity directly correlates to the proteasome (subunit) activity, which can be visualized using SDS-PAGE [31]. Without BTZ treatment, both BTZ/7 and BTZ/100 cells showed reduced activity of the  $\beta 2i$  subunit, a relative upregulation of the  $\beta 2$  activity and a lower total proteasome activity compared to WT cells (Fig. 1b), consistent with published reports [11, 30, 32]. BTZ treatment decreased total proteasome activity in a dose dependent manner with 50% proteasome inhibition at  $107.5 \pm 56$  nM for the BTZ/100 cells and  $10.3 \pm 4.1$  nM and  $15.1 \pm 0.9$  nM in the WT and BTZ/7 cells, respectively (Fig. 1c, Supplemental Fig. S1c). Whereas the onset of  $\beta 2$  inhibition was shifted towards higher BTZ concentrations in the BTZ/100 cells, only small differences were observed in the onset of  $\beta 1/5$  inhibition between sensitive and resistant cell lines (Supplemental Fig. S1c). These results suggest that upregulation of  $\beta 2$  activity is one of the main proteasomal driving forces of BTZ resistance in RPMI-8226 cells. However, in contrast to WT cells, both resistant cell lines still show survival at 50% proteasome inhibition, in line with earlier results [29]. This indicates that in order to survive BTZ treatment, BTZ/7 and

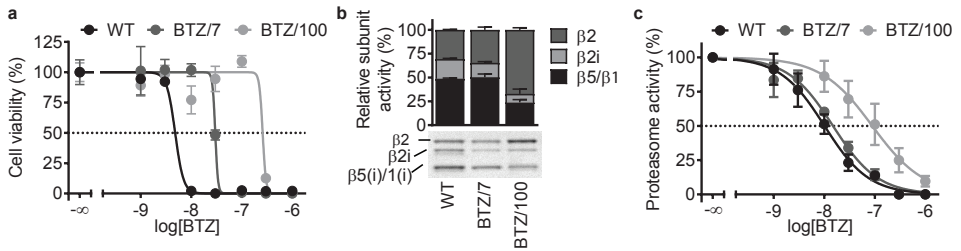


**Figure 1. Bortezomib resistance is not solely driven by adaptations of the proteasome.**

**a** Cell viability of RPMI-8226 wild type (WT) and bortezomib-resistant (BTZ/7 and BTZ/100) cells after a 48-hour treatment with increasing concentrations of bortezomib. Results represent % cell viability  $\pm$  SD compared to non-treated controls of a representative experiment ( $n=3$ ). **b** In gel fluorescence measurements of a representative experiment showing proteasome activity profiles of RPMI-8226 WT, BTZ/7 and BTZ/100 cells after a 1-hour incubation with proteasome activity probe Me<sub>4</sub>BodipyFL-Ahx<sub>3</sub>L<sub>3</sub>VS (lower panel). Quantification of gel images, with subunit activity plotted as of total proteasome activity. Results represent averages of 3 independent experiments (upper panel). **c** Total proteasome activity of RPMI-8226 WT, BTZ/7 and BTZ/100 cells after a 2-hour incubation with increasing concentrations of bortezomib, compared to non-treated controls. Results represent quantification of gel images obtained by a 1-hour incubation with Me<sub>4</sub>BodipyFL-Ahx<sub>3</sub>L<sub>3</sub>VS. Results represent averages of 3 independent experiments. BTZ = bortezomib.

BTZ/100 cells not only change the proteasome itself, but also adapt to survive under conditions of continuous proteasome inhibition.

### Bortezomib-resistant cells have an enhanced pentose phosphate pathway activity

Because metabolic alterations are increasingly recognized as a driving force in drug resistance, we next investigated whether such metabolic changes drive adaptation to continuous proteasome inhibition in BTZ-resistant MM cells. BTZ sensitivity has been linked to higher glycolytic activity under hypoxic conditions [28]. However, many metabolic pathways branch off from glycolysis, including the tricarboxylic acid (TCA) cycle, pentose phosphate pathway (PPP) and nucleotide synthesis pathway. Hence, to get a more comprehensive insight into the altered glucose metabolism in BTZ resistant cells, we first mapped the glucose metabolism in both resistant and sensitive cells by performing <sup>13</sup>C-glucose tracer experiments. To this end, WT and BTZ/100 cells were grown in the presence of 8 mM [U-<sup>13</sup>C]-glucose and the incorporation of <sup>13</sup>C-carbon from glucose in downstream metabolites was followed over time using mass spectrometry. In addition, changes in extracellular metabolites levels were analysed. As a centrifugation step – which disturbs the cells – is inevitable to resuspend cells in [U-<sup>13</sup>C]-glucose medium, cells will only reach pseudo-steady states hours after being resuspended. Therefore, early time points (less than 4 hours) were excluded from the analysis. As expected, BTZ/100 cells displayed both an increased uptake of glucose from and increased secretion of lactate into the culture medium, indicative of a higher glycolytic activity (Fig. 2a, b). In addition, BTZ/100 cells displayed higher intracellular levels of <sup>13</sup>C-glucose, as well as higher levels of

$^{13}\text{C}$ -pyruvate and  $^{13}\text{C}$ -lactate, supporting higher glycolytic activity. No differences in the amount of  $^{13}\text{C}$ -citrate were observed between cell lines, suggesting no change in glucose flux to the TCA cycle (Fig. 2c). In contrast, sedoheptulose-7-phosphate (S7P), an intermediate of the PPP, was one of the most upregulated metabolites in BTZ/100 cells compared to WT cells. Substantially increased levels of *de novo* synthesized  $^{13}\text{C}$ -labeled S7P were present in BTZ/100 cells, indicating a higher PPP activity in resistant cells (Fig. 2c). Moreover, higher amounts of M+4 and M+6 isotopomers of S7P were present in BTZ/100 cells, which are indicative of increased PPP cycling and further support the higher PPP activity in these cells. After 8 hours, the S7P levels dropped in both cell lines, suggesting that the cells temporarily raised their PPP activity in response to some type of stress, most likely the centrifugation of the cells. We therefore hypothesize that bortezomib resistant cells have a higher basal PPP activity as well as a higher capability to increase PPP activity in response to stress [33].

To investigate whether these findings are general features of BTZ-resistant cells, we repeated the MS analysis on BTZ-sensitive AMO-1 multiple myeloma cells and its BTZ- and CFZ-resistant counterpart, again including RPMI-8226 cells. We also included BTZ-resistant ARH-77 cells, which have a different origin (plasmocytoid lymphoma) in these analyses (Supplemental Fig. S2a-c) [13, 29]. Whereas BTZ-resistant AMO-1 and RPMI-8226 cells all showed higher glucose uptake, lactate secretion and PPP activity compared to sensitive cells, AMO-1 CFZ/90 cells did not show these metabolic changes. Notably, overexpression of the drug efflux transporter ABCB1/P-glycoprotein, for which carfilzomib is a *bona fide* substrate, is an important underlying mechanism of carfilzomib resistance in CFZ/90 AMO-1 [29, 34]. It is thus likely that these cells do not require metabolic adaptations to oppose proteasome inhibitor induced apoptosis. ARH-77 BTZ-resistant cells on the other hand showed an opposite effect on glucose uptake, lactate secretion and PPP metabolism. Together, these findings show that BTZ-resistant MM cells have higher PPP activity compared to sensitive cells and suggest that this effect is specific for bortezomib as well as for multiple myeloma.

### **Enhanced pentose phosphate pathway activity increases anti-oxidant capacity of bortezomib resistant cells**

The PPP provides both ribose for purine nucleotide synthesis, and NADPH, which cells use for maintaining intracellular redox balance [33]. Since oxidative stress plays a role in the mechanism of action of BTZ, and BTZ/100 cells showed only moderately increased levels of the purines AMP and GMP (Fig. 2c), we hypothesized that BTZ-resistant cells increase their PPP activity predominantly to increase their anti-oxidant

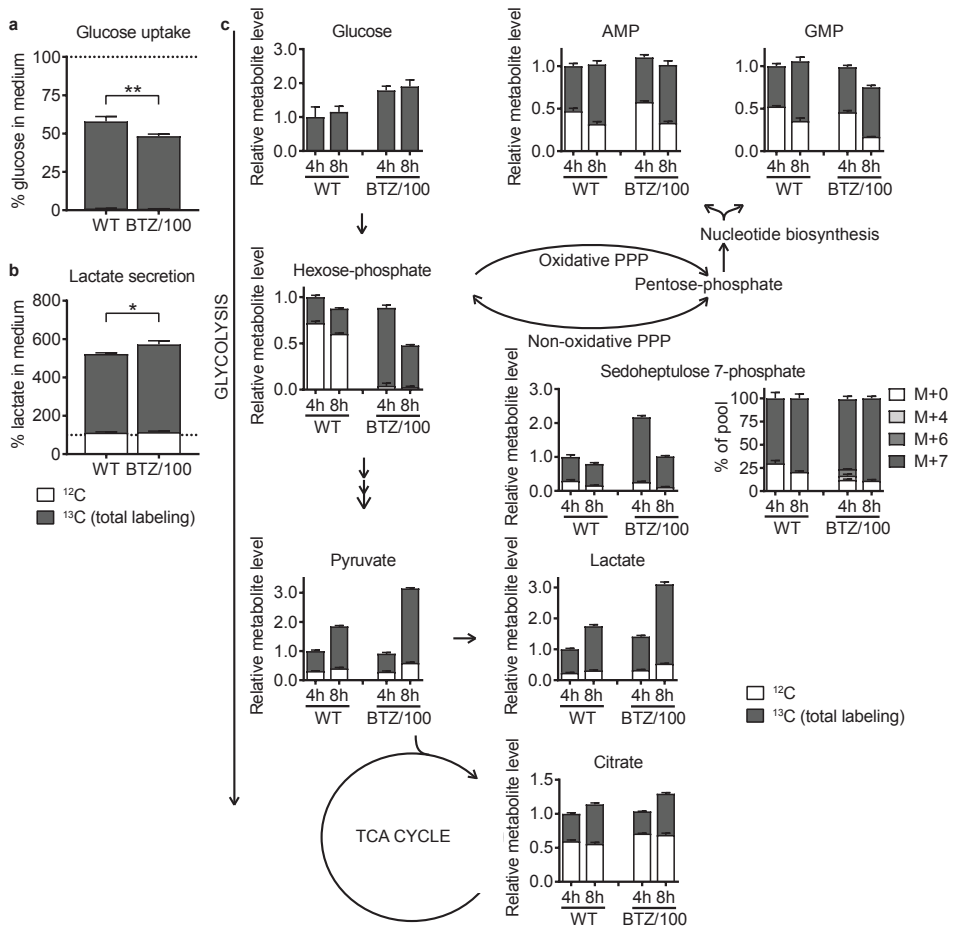


**Figure 2. Bortezomib resistant cells have an enhanced phosphate pathway activity.**

Intra- and extracellular metabolite analysis of RPMI-8226 wild type (WT) and bortezomib resistant (BTZ/100) cells. Cells were suspended in DMEM containing 8 mM [ $U\text{-}^{13}\text{C}$ ] D-glucose. **a,b** Media samples were collected after 8 hours, followed by LC-MS analysis of extracellular glucose (**a**) and lactate (**b**). Results represent % peak area  $\pm$  SD compared to cell-free media (n=3). Two-way ANOVA tests were performed (\*\* =  $p < 0.05$ , \*\* =  $p < 0.01$ ). **c** Intracellular metabolites were extracted after 4 and 8 hours and analyzed by LC-MS. Data are means  $\pm$  SD (n=3) of unlabelled (white) and  $^{13}\text{C}$ -labelled metabolites (grey). AMP = adenosine monophosphate, GMP = guanosine monophosphate, PPP = pentose phosphate pathway, TCA = tricarboxylic acid.

defenses and counteract the effect of the drug. Indeed, BTZ-resistant RPMI-8226 cells showed significantly higher concentrations of total glutathione (GSH), an important cellular antioxidant (Fig. 3a). Significantly higher levels of intracellular GSH were also found in BTZ-resistant AMO-1 cells as compared to BTZ-sensitive AMO-1 cells (Supplemental Fig. S2d). RPMI-8226 BTZ/100 cells were also less sensitive to hydrogen peroxide ( $\text{H}_2\text{O}_2$ ) ( $\text{IC}_{50}$  256 $\mu\text{M}$  vs. 67 $\mu\text{M}$ ) compared to WT cells (Fig. 3b).

When BTZ/100 cells were exposed to  $H_2O_2$  after a 24-hour pre-incubation with the PPP inhibitor trans-androsterone (TA), the  $IC_{50}$  of  $H_2O_2$  shifted from  $579\mu M$  to  $358\mu M$  (Fig. 3c), confirming that the resistance to oxidizing agents in these cells is at least partly mediated through their increased PPP activity. Furthermore, in line with our metabolomics data we found that the GSH/GSSG ratio was increased in BTZ/100 cells compared to WT cells (Fig. 3d), indicative of an increased anti-oxidant capacity. Finally, the ability of cells to reduce dehydroascorbate (DHA, oxidized vitamin C) to ascorbic acid (AA) can also be used as a tool to analyze cellular redox status [35]. DHA is rapidly taken up by the glucose transporters GLUT1 and GLUT3 and subsequently reduced either spontaneously or by GSH- and NADPH-dependent enzymes. As a consequence, DHA reduction is coupled to the ability of cells to regenerate NADPH and GSH [35]. We therefore developed an MS assay to measure the intracellular reduction of DHA to AA (Fig. 3e). Exposure to DHA resulted in similar intracellular

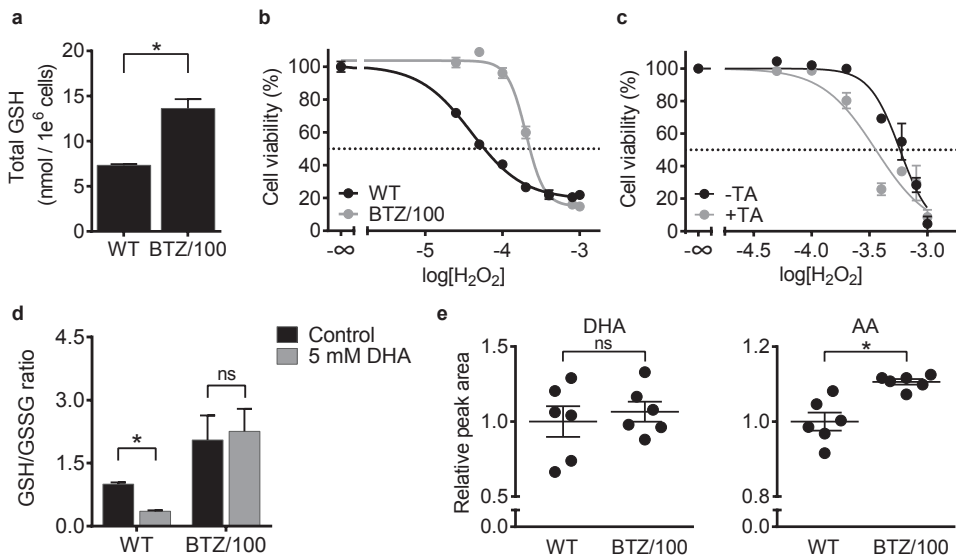


**Figure 3. Enhanced pentose phosphate pathway activity increases anti-oxidant capacity of bortezomib resistant cells.**

**a** Total GSH levels of RPMI-8226 wild type (WT) and bortezomib resistant (BTZ/100) cells. Data are means  $\pm$  SD ( $n=3$ ) **b** Cell viability of RPMI-8226 WT and BTZ/100 cells after a 16-hour treatment with increasing concentrations of  $H_2O_2$ . Results represent mean cell viability  $\pm$  SD compared to non-treated controls ( $n=3$ ). **c** Cell viability of RPMI-8226 BTZ/100 cells after treatment for 24 hours with  $50\mu M$  trans-androsterone (TA), followed by 24 hours with increasing concentrations of  $H_2O_2$ . Results represent mean cell viability  $\pm$  SD compared to non-treated control ( $n=3$ ). **d** GSH/GSSG ratio of RPMI-8226 WT and BTZ/100 cells after 5 minutes treatment with 5 mM DHA. Data are means  $\pm$  SD ( $n=3$ ). **e** Analysis of intracellular levels of DHA (left panel) and AA (right panel) in RPMI-8226 WT and BTZ/100 cells. Cells were treated with 5 mM DHA or vehicle for 5 minutes and subjected to LC-MS analyses. Data are means  $\pm$  SD ( $n=3$ ). Two-way ANOVA tests were performed (ns = not significant, \* =  $p < 0.05$ ). AA = ascorbic acid, DHA = dehydroascorbic acid, GSH = glutathione, TA = trans-androsterone.

levels of DHA in both WT and BTZ/100 cells. In contrast, significantly higher levels of AA were found in BTZ-resistant cells, indicating an increased conversion of DHA to AA. Because reduction of DHA will help maintain a DHA gradient over the cell membrane that favours transport [36], total DHA plus AA levels are also higher in the BTZ-resistant cells. Moreover, whereas DHA exposure decreased GSH/GSSG ratio in WT cells compared to control conditions, this ratio remained stable in BTZ/100 cells (Fig. 3d). These data indicate that the WT cells lack the capacity to regenerate GSH and NADPH, which render them more sensitive to oxidative stress compared to the resistant cells.

### **Bortezomib-resistant cells have a higher activity of the serine synthesis pathway**

The serine synthesis pathway (SSP), in which serine is synthesized from 3-phosphoglycerate, is another pathway that branches off from glycolysis and that is involved in both NADPH regeneration and GSH production. We therefore questioned whether BTZ-resistant cells also showed increased activity of the SSP. To investigate the basal activity of the SSP in BTZ sensitive and resistant cells, we performed tracer experiments in DMEM containing 8 mM  $^{13}\text{C}$ -glucose and normal levels of (unlabeled)  $^{12}\text{C}$ -serine. As the activity of the SSP is controlled primarily by the demand for serine and is only activated when serine is depleted from the extracellular environment [37–42], we expected only low levels of *de novo* serine synthesis under these conditions. Indeed, both RPMI-8226 WT and BTZ/100 cells contained predominantly  $^{12}\text{C}$  serine, obtained from the culture medium, and only small amounts of  $^{13}\text{C}$ -serine (M+1, M+2 and M+3) (Fig. 4a). However, the levels of serine M+3, which is synthesized *de novo* from glucose through the SSP [43], were higher in resistant cells compared to wild-type cells, indicative of a higher basal activity of the SSP in these cells. Moreover, BTZ/100 cells displayed a higher uptake of serine from the cell culture medium compared to the WT cells (Fig. 4b). Serine was almost depleted in the culture media in BTZ/100 cells after 24 hours, resulting in substantially lower serine levels 24 hours after fresh medium was added to cells (Fig. 4a, b). Although these data should be interpreted with care, as some nutrients are depleted at 24 hours, these data do indicate that BTZ/100 cells have an increased demand for serine compared to WT cells, which is met by increasing both serine synthesis and serine uptake.

Next, we investigated how BTZ-sensitive and -resistant cells behaved under conditions of serine starvation, when upregulation of the SSP would be a requirement to survive. To this end, cells were grown in the presence or absence of serine and glycine (SG), first for 24 hours in the presence of [U- $^{12}\text{C}$ ]-glucose, and subsequently for 4 hours using [U- $^{13}\text{C}$ ]-glucose, as described elsewhere [38]. To reduce extra stress on the cells and ensure ample glucose supply throughout the experiment, we

supplemented the cell culture medium with 25 mM glucose instead of 8 mM. These higher glucose levels did however not affect serine synthesis, at least under serine-fed conditions (compare Fig. 4a, 4-hour time point, to Fig. 4c and Supplemental Fig. S3a). In both WT and BTZ/100 cells, serine starvation resulted in a decrease in both total serine levels and  $^{13}\text{C}$ -serine levels (Fig. 4c, Supplemental Fig. S3a), probably reflecting the rapid conversion of serine to further downstream metabolites [37]. Although total glycine and GSH levels also decreased in both cell lines during serine starvation (Supplemental Fig. S3a), higher levels of  $^{13}\text{C}$ -glycine and  $^{13}\text{C}$ -GSH were found in BTZ/100 cells (Fig. 4c), indicating that SSP can be activated to a higher extent in resistant cells compared to WT cells when needed. Additionally, BTZ-resistant cells are able to maintain higher levels of GSH during serine starvation, supporting our findings that they have higher anti-oxidant capacity.

Given that cells with high SSP activity are able to proliferate in the absence of extracellular serine [43], we next hypothesized that especially WT cells, that have low SSP activity, would be sensitive to serine starvation both in the absence and presence of BTZ. Indeed, serine starvation lowered the viability of WT cells, while BTZ/100 cells remained viable after 48 hours of serine starvation (Fig. 4d), likely because they compensate for the lack of serine through serine synthesis. At the same time, serine starvation significantly increased the amount of cell death in WT cells, but not in BTZ/100 cells (Supplemental Fig. S3b). Importantly, a 24-hour serine starvation prior to BTZ treatment increased the cytotoxic effect of BTZ on WT cells (Fig. 4e). These data not only confirm that the presence of serine is important in the defense mechanism of cells against BTZ, but also suggest that serine starvation could be combined with BTZ to increase the efficacy of treatment in BTZ-sensitive patients.

### **Bortezomib resistance correlates to the expression of PHGDH**

Having established the importance of both PPP and SSP in the response of cells to BTZ, we next asked whether these differences were also found on the protein level. Hence, we performed proteomics on WT, BTZ/7 and BTZ/100 cells and quantified >3500 proteins, 395 of which were classified as metabolic enzymes (Fig. 5a, Supplemental Fig. S4a, Table S1, Table S2). The highest upregulated metabolic enzyme in both BTZ/7 and BTZ/100 cells was 3-phosphoglycerate dehydrogenase (PHGDH; fold change (FC) = 11.27 and 7.86, respectively), the first and rate-limiting enzyme in the SSP, underscoring the importance of the SSP in the response to BTZ. In agreement with our findings, overexpression of PHGDH has previously been associated with an increased glucose flux through the SSP and the ability to proliferate in the absence of extracellular serine [43, 44]. Of the other



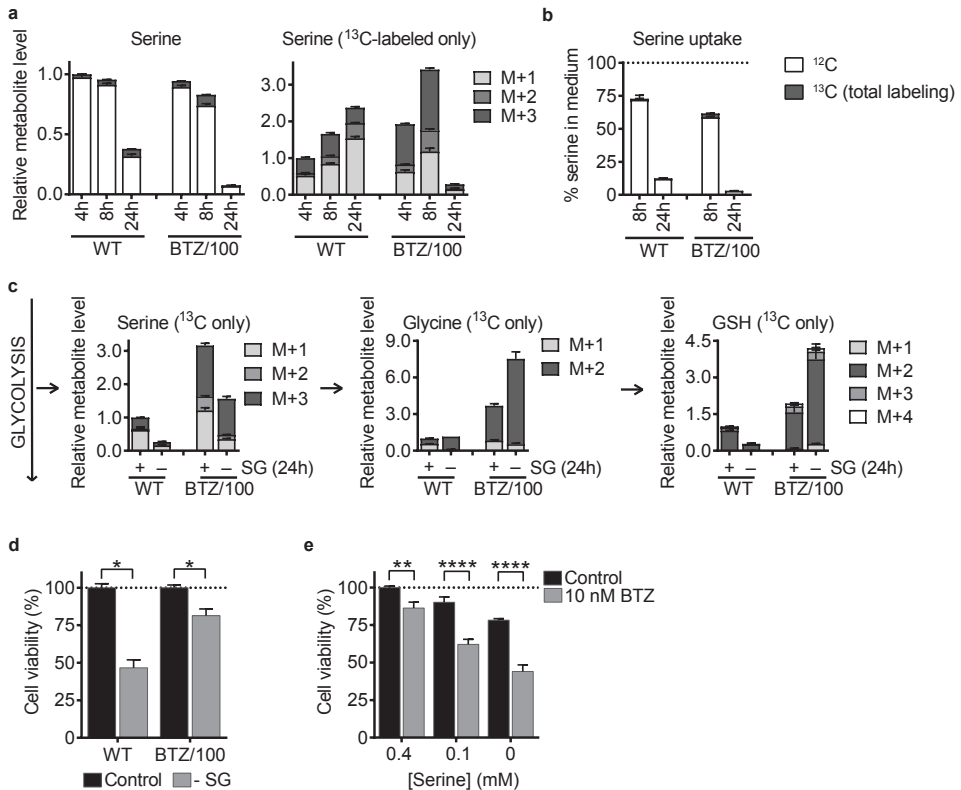


**Figure 4. Bortezomib resistant cells have a higher activity of the serine synthesis pathway.**

**a,b** Intra- and extracellular analysis of serine levels of RPMI-8226 wild type (WT) and bortezomib resistant (BTZ/100) cells. Cells were suspended in DMEM containing 8 mM [ $U\text{-}^{13}\text{C}$ ] D-glucose. Intracellular metabolites were extracted after 4, 8 and 24 hours and analyzed by LC-MS (**a**). Data are means  $\pm$  SD ( $n=3$ ) of unlabelled (white) and  $^{13}\text{C}$ -labelled serine (left panel). Labeled serine was plotted as M+1, M+2 and M+3 isotopomers (right panel). Media samples were collected after 8 and 24 hours, followed by LC-MS analysis of extracellular serine (**b**). Results represent % peak area  $\pm$  SD compared to non-treated media ( $n=3$ ). **c** Intracellular metabolite analysis of RPMI-8226 WT and BTZ/100 cells in the presence or absence of extracellular serine and glycine (-SG). Cells were grown complete medium in the presence or absence of 0.4 mM serine. After 24 hours, media were replaced with matched media containing 20 mM [ $U\text{-}^{13}\text{C}$ ] D-glucose and intracellular metabolites were extracted after 4 hours, followed by LC-MS analysis. Data are means  $\pm$  SD ( $n=3$ ) of labelled metabolites. **d** Cell viability of RPMI-8226 WT and BTZ/100 cells after 48 hours of serine starvation (-SG). Results represent mean cell viability  $\pm$  SD compared to non-treated control ( $n=3$ ). **e** Cell viability of RPMI-8226 WT cells after 48 hours in 0.4 mM, 0.1 mM or no serine, including 24 hours of 10 nM bortezomib. Results represent mean cell viability  $\pm$  SD compared to non-treated control ( $n=3$ ). One-way ANOVA tests were performed (ns = not significant, \* =  $p<0.05$ , \*\* =  $p<0.01$ , \*\*\*\* =  $p<0.0001$ ). BTZ = bortezomib, GSH = glutathione.

SSP enzymes, phosphoserine aminotransferase 1 (PSAT1) was downregulated in BTZ/100 cells, while the proteomics data showed no change in the expression of phosphoserine phosphatase (PSPH) in BTZ/100 cells compared to WT cells (Fig. 5b). However, since PHGDH is the rate-limiting enzyme in the SSP, the much higher PHGDH levels should allow for higher rates of serine synthesis. An 8-hour treatment

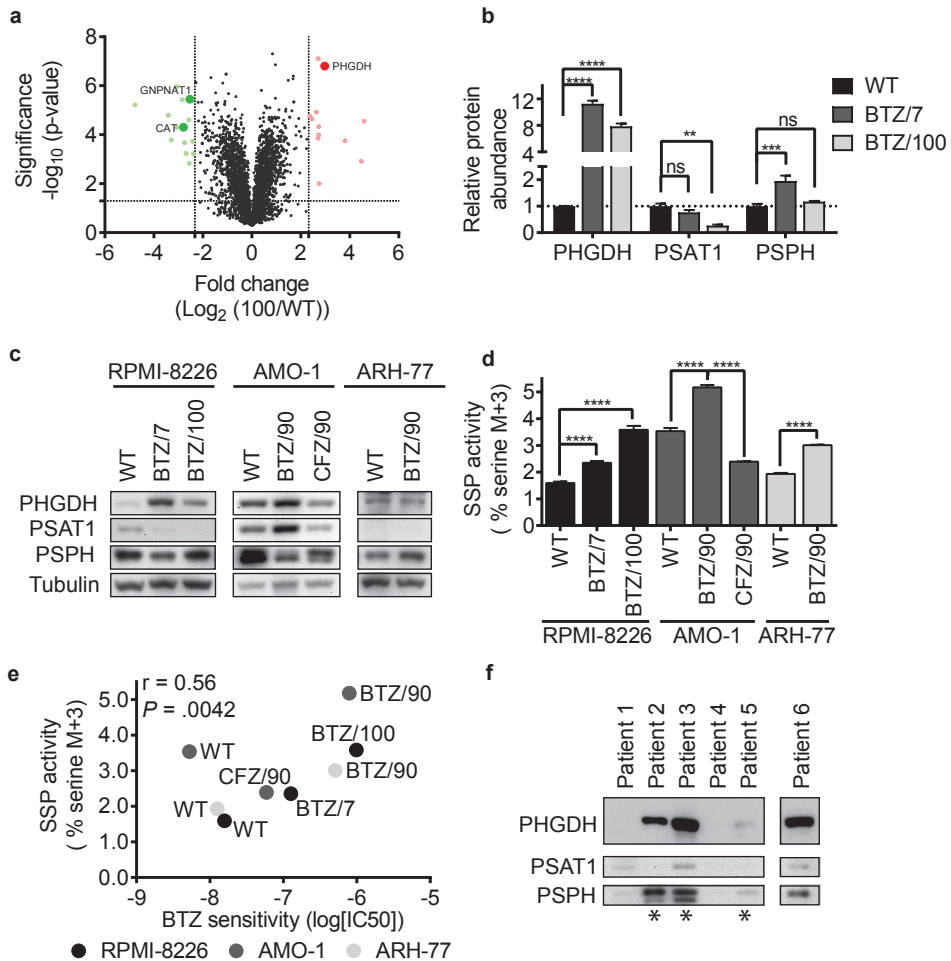


**Figure 5. Bortezomib resistance correlates to the expression of PHGDH.**

**a** Graphical representation of quantitative proteomics data. Proteins are ranked in volcano plot according to their statistically  $p$ -value (y-axis) and relative abundance ratio between RPMI-8226 wild type (WT) and bortezomib resistant (BTZ/100 cells) (x-axis). Coloured spots represent significantly upregulated (red) or downregulated (green) proteins in BTZ/100 cells with at least a 5-fold change. Significantly regulated metabolic enzymes are marked. **b** Quantitative proteomics data of enzymes involved in the serine synthesis pathway. Data represents means  $\pm$  SD ( $n=3$ ). **c** Immunoblot of 3-phosphoglycerate dehydrogenase (PHGDH), phosphoserine aminotransferase 1 (PSAT1), phosphoserine phosphatase (PSPH) and Tubulin expression in RPMI-8226, AMO-1 and ARH-77 bortezomib-sensitive and -resistant cells. **d** Fractions of serine M+3 in RPMI-8226, AMO-1 and ARH-77 bortezomib-sensitive and -resistant cells. Data represent % serine M+3 of total serine  $\pm$  SD ( $n=3$ ). One-way ANOVA tests were performed (\*\*\*\* =  $p < 0.0001$ ). **e** Correlation between serine M+3 fractions and bortezomib sensitivity in RPMI-8226, AMO-1 and ARH-77 bortezomib-sensitive and -resistant cells.  $\text{IC}_{50}$ s were determined in cell viability assay after 48 hours of increasing concentrations of bortezomib. Pearson correlation  $r = 0.56$  ( $p = .0042$ ). **f** Immunoblot of PHGDH, PSAT1 and PSPH in isolated CD1318+ plasma cells from diagnosed multiple myeloma patients ( $n=6$ ). Patients with progressive disease/refractory to BTZ-containing therapy are indicated with \*. PHGDH is blotted on a separate membrane. BTZ = bortezomib, CFZ = carfilzomib, PHGDH = 3-phosphoglycerate dehydrogenase, PSAT1 = phosphoserine aminotransferase 1, PSPH = phosphoserine phosphatase, SSP = serine synthesis pathway.

with BTZ had no effect on SSP enzyme levels cells in either cell line (Supplemental Fig. S4b), suggesting that the higher levels of PHGDH in BTZ/100 cells are not resulting from decreased proteasomal degradation of PHGDH but rather from an increase in PHGDH protein synthesis. Amongst the moderately upregulated metabolic enzymes (FC 1.5–5) in BTZ/100 cells were 6-phosphogluconolactonase (PGLS; FC=1.61) and transketolase (TKT1; FC=1.53), enzymes involved in NADPH production through PPP. In addition, glutamate-cysteine ligase (GCLC; FC=1.51) and cystathione  $\gamma$ -lyase (CTH; FC=2.27), both important enzymes in GSH synthesis, were upregulated. These results are in line with the increased anti-oxidant capacity of resistant cells and further validate the metabolomics results described above.

To validate that higher expression of PHGDH as well as higher SSP activity are general features of BTZ resistant cells, we performed a western blot for all SSP enzymes expression on our panel of BTZ- and CFZ-resistant cells (Fig. 5c). In all resistant cell lines, one or more SSP enzymes were upregulated. Both BTZ-resistant RPMI-8226 and AMO-1 cells showed higher expression of PHGDH compared to their sensitive counterparts, AMO-1 BTZ/90 cells also showed increased expression of PSAT1, while ARH-77 BTZ/90 cells showed higher expression of PSPH (Fig. 5c). In addition, we profiled the activity of the SSP in these 8 cell lines by measuring the abundance of  $^{13}\text{C}_3$ -serine (M+3) after incubation with [ $^{13}\text{C}$ ]-glucose (Fig. 5d). All BTZ-resistant cells showed a higher serine M+3 fraction compared to their WT counterparts, in line with higher expression of SSP enzymes in BTZ-resistant cells. Moreover, we observed a significant correlation between the serine M+3 fraction and the 48-hour  $\text{IC}_{50}$  towards BTZ in these cell lines (Fig. 5e). In the RPMI-8226 and AMO-1 BTZ-resistant cells, the increase in SSP activity was accompanied by an increased uptake of extracellular serine (Supplemental Fig. S4c). However, no difference in serine uptake was seen in ARH-77 cells, and no significant correlation was found between serine uptake and the 48-hour  $\text{IC}_{50}$  towards BTZ (Supplemental Fig. S4d). Together, these data suggest that the ability to perform serine synthesis rather than serine uptake is an important metabolic determinant for BTZ resistance. As expected, CFZ/90 AMO-1 cells did not show an increase in PHGDH expression or serine synthesis (Fig. 5c,d).

To verify the correlation between SSP and BTZ sensitivity, PHGDH expression was examined in CD138+ plasma cells from a small set (n=6) of multiple myeloma patients isolated either at diagnosis, during therapy or after relapse from various therapeutic interventions (Fig. 5f, Supplemental Fig. S3e,f, Table S3). For one MM patient (#1) at diagnosis, and for one patient (#4) with metastatic disease prior to therapy, PHGDH expression was negligible. Interestingly, 3 patients with progressive disease or refractory to BTZ therapy (indicated with \*) showed markedly increased

PHGDH expression, which was accompanied by higher PSPH expression but not PSAT1 expression. Notably, patient #6, that never received BTZ, but relapsed on melphalan, prednisone, lenalidomide therapy also displayed high PHGDH and PSPH expression. These results suggest that (BTZ)-therapy resistance in MM is associated with increased PHGDH expression in CD138+ cells.

## DISCUSSION

Metabolic alterations may play an essential role in the development of cellular resistance against anticancer drugs [24–27]. In the present study, we therefore aimed to identify metabolic mechanisms underlying BTZ resistance in MM. Here, we demonstrate for the first time that BTZ resistance in MM cells is sustained by metabolic rewiring, particularly of serine metabolism. Using tracer-based metabolomics, we show that the SSP has significantly increased activity in BTZ-resistant MM and plasmacytoid lymphoma cell lines. Importantly, we also observed a strong correlation between SSP activity and the ability of cells to withstand increasing BTZ concentrations in all BTZ-resistant cell lines tested.

The SSP is involved in the production of precursors for nucleotide synthesis, as well as glutathione synthesis and NADPH regeneration and has been shown to be an important pathway to sustain cancer growth and proliferation [41, 42]. PHGDH, the first and rate-limiting enzyme of the SSP, is often overexpressed in cancer and has been linked to tumorigenesis as well as poor diagnosis in different cancers [44–47], identifying PHGDH as an interesting pharmaceutical target [46, 48, 49]. Using proteomics, we show that PHGDH is the highest upregulated metabolic enzyme in BTZ-resistant RPMI-8226 MM cells, and western blots confirm that also in other BTZ-resistant cell lines one or more SSP enzymes are upregulated. The status of known regulators of the SSP in bortezomib resistance remains to be investigated.

We also demonstrate that PHGDH and PSPH are overexpressed in a small panel of CD138+ cells from BTZ-refractory MM patients compared to BTZ-responsive patients. This raises the possibility that high PHGDH expression, possibly in combination with PSPH expression, could be predictive of BTZ resistance. In line with these observations, we find that serine starvation enhances the efficacy of BTZ in sensitive RPMI-8226 cells, which have not yet upregulated PHGDH. This finding suggests that by removing serine from the diet, which is tolerated by mice and has been shown to reduce growth of some tumors [38, 50], the efficacy of current BTZ treatment might be enhanced in patients. Because patient sample size was limited in the current pilot study, confident conclusions about the role of PHGDH as a predictive

biomarker for bortezomib response cannot be drawn at this point. However, these results underscore our findings in cell lines and warrant further research with a larger, controlled patient cohort to validate the use of PHGDH as a diagnostic tool to determine BTZ sensitivity in MM and other hematologic diseases. Notably, one patient, that never received BTZ but was relapsing on melphalan, prednisone and lenalidomide, also displayed high PHGDH expression, raising the possibility that the observed changes in metabolism are also associated with other ROS-inducing agents. BTZ-resistant RPMI-8226 cells indeed show cross-resistance to CFZ, as has also been reported for AMO-1 cells [29], suggesting that the observed metabolic changes confer cross-resistance to other proteasome inhibitors to a certain extent, as expected. However, our data also show that BTZ-resistant RPMI-8226 cells do not display cross-resistance to either methotrexate or melphalan, both of which increase intracellular ROS levels, suggesting that the observed metabolic changes are specific for proteasome inhibitor resistance.

In addition to changes in the SSP, we find that the influx of glucose into the PPP is increased in BTZ-resistant multiple myeloma cell lines. Proteomics experiments confirm that several proteins involved in both the PPP and in GSH metabolism are upregulated in BTZ resistant cells, in line with previous reports [29]. These metabolic alterations ultimately result in an increased anti-oxidant capacity of BTZ-resistant cells, as evidenced by a lower susceptibility to hydrogen-peroxide induced oxidative stress, a higher GSH/GSSG ratio, and an increased ability to convert DHA to AA. Likely, this increased anti-oxidant capacity functions to protect resistant cells from BTZ-induced oxidative stress [6, 51]. Remarkably, increased PPP metabolism was not observed in ARH-77 plasmacytoid lymphoma cells. A recent report shows that BTZ resistance in leukemia was mediated through exocytosis of polyubiquitinated proteins [20], which may eliminate the need for extensive metabolic rewiring to induce resistance. The same holds true for CFZ-resistant cells, in which overexpression of ABCB1/P-glycoprotein has been described as an important mechanism of resistance [29]. It thus seems likely that the ability of cells to employ other mechanisms of resistance regulates the extent of metabolic resistance. Altered serine metabolism, however, occurred in all cell lines tested. Our data therefore strongly support for the hypothesis that altered serine metabolism is one of the core mechanisms of resistance, together with changes in proteasome abundance and composition. The clear correlation that we observe between PHGDH expression, SSP activity and BTZ sensitivity encourage further studies to determine whether increased SSP activity is causally related to BTZ and PHGDH can be targeted to overcome BTZ resistance.

## CONCLUSIONS

Here, we have identified specific metabolic mechanisms underlying bortezomib resistance. In particular, our results imply that BTZ resistance is associated with high activity of the serine synthesis pathway and overexpression of PHGDH. Interfering with serine metabolism, either by removal of serine from the diet or by PHGDH inhibition, are potential ways to increase BTZ efficiency in both sensitive and resistant patients. In addition, we propose PHGDH expression as a novel biomarker of bortezomib response.

## METHODS

### Reagents

The proteasome activity probe Me<sub>4</sub>BodipyFL-Ahx<sub>3</sub>L<sub>3</sub>VS was a gift from Huib Ovaa (Leiden University Medical Center, The Netherlands). Bortezomib (BTZ) and carfilzomib (CFZ) were purchased from Selleck Chemicals. All solvents were obtained from Biosolve. All other chemicals were obtained from Sigma-Aldrich, unless stated otherwise.

### Cell culture

Human multiple myeloma RPMI-8226 wild type (WT) were purchased from ATCC. BTZ resistant cells were obtained as described previously [11]. AMO-1 and ARH-77 WT, BTZ- and CFZ-resistant cells were kindly provided by C. Driessen (Kantonsspital St. Gallen, Switzerland). Cells were maintained in suspension culture in RPMI-1640 (Lonza) medium supplemented with 2mM L-glutamine (Lonza), 10% fetal bovine serum (FBS) (Gibco) and 100µg/ml penicillin/streptomycin (Lonza) and were kept at 37°C in humidified 5% CO<sub>2</sub> atmosphere. BTZ and CFZ resistant cells were continuously cultured in the presence of BTZ or CFZ as previous described [11, 13]. Cells were cultured without drugs 4-6 days prior to experiments. Media were supplemented with 10% FBS and 100µg/ml penicillin/streptomycin unless stated otherwise.

### Proteasome activity profiling

Proteasome activity was measured using Me<sub>4</sub>BodipyFL-Ahx<sub>3</sub>L<sub>3</sub>VS as described previously [31]. Cells were suspended in triplicate at a density of 1 x 10<sup>6</sup> cells in RPMI-1640 medium and incubated with the indicated concentrations of BTZ at 37°C for 1 hour, followed by a 1-hour incubation with 500nM Me<sub>4</sub>BodipyFL-Ahx<sub>3</sub>L<sub>3</sub>VS.

Cells were collected by centrifugation, washed with PBS and lysed for 30min in NP40 lysis buffer (50mM Tris, pH 7.4, 150mM NaCl, 1% NP40) at 4°C, followed by centrifugation at 14.000g to remove membrane fractions, nuclei and cell debris. Protein concentrations were determined using the Bradford assay (Bio-rad) and equal amounts of protein were denatured by boiling in XT Sample buffer (Bio-rad) with 9% b-mercaptoethanol. Proteins were separated on a 4-12% SDS-PAGE gel (Bio-rad) and fluorescence was measured with a Typhoon scanner (GE Healthcare) ( $\lambda_{\text{ex}}/\lambda_{\text{em}} = 488/526\text{nm}$ ). Protein loading was confirmed with a coomassie blue stain.

### **Cell viability and cell growth assays**

Cells were suspended in triplicate at a density of  $2-5 \times 10^4$  cells in RPMI-1640 medium in 96-well plates and incubated with drugs at the indicated concentrations for 24-48 hours. Cell growth was monitored continuously with the IncuCyte live-cell imager system. Images were automatically acquired every 2 hours for 1-2 days. Pictures were analysed using the IncuCyte Zoom software. Cell growth was defined as the amount of doubling times per 24/48 hours and calculated based on increase of confluency. Cell death was assessed after 24-48 hours by incubating each well with 30 $\mu\text{M}$  propidium iodide and measuring fluorescence after 15 minutes using the IncuCyte live-cell imager system. Cell death was calculated based on the area of the fluorescent signal, normalized to confluency of the wells. Cell viability was measured in parallel after 24-48 hours by incubation of cells with 50 $\mu\text{M}$  resazurin for an additional 2 hours, after which absorption was measured at 570nm and 600nm using a Multiskan GO microplate reader (Thermo Scientific). Results were calculated by subtraction of background absorbance at 600nm from absorbance at 570nm.

### **Liquid chromatography – Mass Spectrometry (LC-MS) based Metabolomics**

For all experiments, cells were diluted in fresh medium 16-24 hours prior to the start of the experiment.  $^{13}\text{C}$ -tracer experiments were performed as described [38, 52], with minor changes. At the start of all experiments, cells were counted and centrifuged for 5 minutes at 1400rpm to remove the old medium. Cells were then resuspended in DMEM containing 8mM [ $^{13}\text{C}$ ]D-glucose (Cambridge Isotopes) at a density of  $1 \times 10^6$  cells/ml, unless indicated otherwise. After 4 or 8 hours, samples were washed with PBS and harvested by centrifugation for 5 min at 1000g at 4°C. At these timepoints, cells had recovered from centrifugation and reached pseudo-steady state, without nutrients being depleted from the culture media. For all analysed metabolites, (near) isotopic steady state was reached at these time points. In addition, samples were harvested after 24 hours to analyse serine levels in the cells. Because at this point some nutrients were depleted, no other

metabolites were analysed in these samples. Metabolites were extracted by adding 100 – 200µl ice-cold MS lysis buffer (methanol/acetonitrile/uLCMS H<sub>2</sub>O (2:2:1)) to the cell pellets. To measure extracellular metabolites, medium samples were obtained prior to harvesting cells at 8 or 24 hours. Metabolites were extracted by diluting 10µL medium in 1mL MS lysis buffer. To measure differences in extracellular metabolites in different BTZ-resistant cell lines, cells were resuspended at a density of  $1 \times 10^6$  cells/ml in Minimal Essential Medium (MEM), supplemented with 1mM L-glutamine, 0.2mM L-serine and 0.2mM L-glycine. Medium samples were obtained after 8 hours and metabolites were extracted as described above. For serine starvation experiments, medium was formulated to match the composition of DMEM [38]. Medium consisted of MEM, supplemented with additional 1x MEM vitamins, 1x MEM amino acids, 10% dialyzed FBS and glucose up to 25mM, in the presence or absence of 0.4mM L-serine. Cells were resuspended at a density of  $0.7 \times 10^6$  in triplicate wells and were pre-incubated for 24 hours in the presence or absence of serine. After 24 hours, cells were centrifuged at 1400rpm for 5 minutes and media was replaced with matched media containing [U-<sup>13</sup>C]D-glucose. After 4 hours, cells were harvested as described above.

Metabolites were analysed by LC-MS. LC-MS analysis was performed on an Exactive mass spectrometer (Thermo Scientific) coupled to a Dionex Ultimate 3000 autosampler and pump (Thermo Scientific). The MS operated in polarity-switching mode with spray voltages of 4.5kV and -3.5kV. Metabolites were separated on a Sequant ZIC-pHILIC column (2.1 x 150mm, 5µm, Merck) with guard column (2.1 x 20mm, 5µm, Merck) using a linear gradient of acetonitrile and a buffer containing 20mM (NH<sub>4</sub>)<sub>2</sub>CO<sub>3</sub>, 0.1% NH<sub>4</sub>OH in ULC/MS grade water. Flow rate was set at 150 µL/min. Metabolites were identified based on exact mass within 5 ppm and further validated by concordance with retention times of standards. Peak areas of identified metabolites were in their respective linear range of detection. Metabolites were quantified using LCquan software (Thermo Scientific). Because cells were resuspended at equal cell densities, no substantial cell growth occurred between 0-8 hours and growth rates between resistant and sensitive cell lines were comparable up to 24 hours, samples were assumed to contain equal cell numbers. Peak intensities were additionally normalized based on median peak intensity to correct for technical variations during mass spectrometry analysis. Isotopomer distributions were corrected for natural abundance and data are plotted as relative peak area compared to WT cells under control conditions.



### DHA uptake assay

Cells were suspended at a density of  $0.5 \times 10^6$  cells in 200 $\mu$ L in MEM supplemented with 1mM L-glutamine and 0.2mM L-serine. Cells were incubated with 5mM dehydroascorbic acid (DHA) for 5 minutes at 37°C. DHA uptake was terminated by addition of 1.5mL cold PBS. Cells were centrifuged at 1000g for 5 minutes at 4°C and lysed in 75 $\mu$ L MS lysis buffer. Samples were centrifuged at 16.000g for 15 minutes at 4°C to remove precipitated proteins and cell debris and the supernatants were collected for LC-MS analysis.

### GSH/GSSG ratio

Cells were suspended at a density of  $5 \times 10^6$  cells in triplicate wells of 12-well plates and incubated in the indicated conditions. Cells were washed with cold PBS and lysed in 10mM HCl by two freeze/thaw cycles. Proteins were precipitated by addition of 1% 5-sulfosalicylic acid and pelleted by centrifugation at 4°C for 10 minutes at 8000g. The ratio of reduced to oxidized glutathione (GSH/GSSG) in the supernatant was measured using the quantification kit for oxidized and reduced glutathione (Sigma) according to the manufacturer's instructions.

### Proteomics

Cells were seeded in RPMI medium at a density of  $1 \times 10^6$  cells/ml and incubated for 2 hours. Three replicates of  $5 \times 10^6$  cells were washed with PBS and centrifuged for 5 minutes at 4°C. Cell pellets were lysed at room temperature by gentle vortexing in 8M urea, 50mM ammonium bicarbonate, 2% Triton X-100 and 0.1% SDS, supplemented with phosphatase inhibitor (PhosSTOP, Roche) and protease inhibitor (cOmplete mini EDTA-free, Roche). Total lysates were reduced in 4mM dithiothreitol (DTT), alkylated in 8mM iodoacetamide, and digested sequentially at 37°C with 1:75 LysC (Wako) and 1:50 Trypsin (Sigma-Aldrich) for 4 and 12 hours, respectively. Digested peptides were acidified with 0.1% formic acid (FA) and purified by strong cation exchange STAGE tips, using loading buffer 80% ACN, 0.1% FA and elution buffer 0.5M ammonium acetate, 20% ACN, 0.1% FA. Eluted peptides were dried by vacuum concentrator and 2 $\mu$ g equivalent of peptides was analyzed in 3hr reverse phase separation on the UHPLC 1290 system (Agilent) coupled to an Orbitrap Q Exactive Plus mass spectrometer (Thermo Scientific). Peptides were first trapped on a 2 cm x 100  $\mu$ m Repronil C18 pre-column (3  $\mu$ m) and then separated on a 50 cm x 75  $\mu$ m Poroshell EC-C18 analytical column (2.7  $\mu$ m). Trapping was performed for 10 min in 0.1M acetic acid (Solvent A) and elution with 80% ACN in 0.1M acetic acid (Solvent B) in gradients as follows: 10-36% solvent B in 155 min, 36-100% in 3min and finally 100% for 1min. Flow was passively split to 300 nl/min. MS data were

obtained in data-dependent acquisition mode. Full scans were acquired in the m/z range of 375-1600 at the resolution of 35,000 (m/z 400) with AGC target 3E6. Top 15 most intense precursor ions were selected for HCD fragmentation performed at NCE 25% after accumulation to target value of 5E4. MS/MS acquisition was performed at a resolution of 17,500.

Raw files were processed using MaxQuant version 1.5.3.30 and searched against the human Swissprot database (version Jan 2016) using Andromeda. Cysteine carbamidomethylation was set to fixed modification, while variable modifications of methionine oxidation and protein N-terminal acetylation, as well as up to 2 missed cleavages were allowed. False discovery rate (FDR) was restricted to 1% in both protein and peptide identification. Label-free quantification (LFQ) was performed with “match between runs” enabled.

### **Immunoblotting**

For drug treatment, cells were resuspended in RPMI medium at a density of  $1 \times 10^6$  cells/ml and incubated for 8 hours with the indicated concentrations of BTZ. Cells were lysed in a buffer containing 8M urea and 50mM ammonium bicarbonate, supplemented with phosphatase- and protease inhibitor. Protein content was determined using the Bradford assay (Bio-rad) and equal amounts of protein were denatured by boiling in XT Sample buffer (Bio-rad) with 15mM DTT. Proteins were separated on a 12% % SDS-PAGE gel (Bio-rad) and electroblotted onto PVDF membranes. The antibodies used were 3-phosphoglycerate dehydrogenase (PHGDH, Sigma), phosphoserine-aminotransferase antibody (PSAT1, Abcam), phosphoserine phosphatase antibody (PSPH, Abcam) and Tubulin antibody (Santa Cruz). For patient samples, protein loading was confirmed with a coomassie blue stain of the membrane.

### **Multiple Myeloma patient samples**

CD138-positive cells, isolated from bone marrow of 6 MM patients at diagnosis and during (BTZ) therapy, were available from the Hematology biobank. Patient characteristics are presented in additional file 1: Table S1. Research was approved by the Medical Ethics Committee of the VU University Medical Center and all patients gave written informed consent.

### **Acknowledgements**

CRB was supported by VENI grant (project 722.013.009) from the Netherlands Organization for Scientific Research (NWO). The authors would like to thank Pieter Langerhorst, Klaas Vermaas and Haley Baptist for technical assistance, Huib Ova

for providing Me<sub>4</sub>BodipyFLAhx<sub>3</sub>L<sub>3</sub>VS, Christoph Driessen for BTZ- and CFZ-resistant cell lines, and Albert Heck for constructive discussions.

### **Authors' Contributions**

CRB and EAZ developed this study, designed the experiments and wrote the manuscript. EAZ and WW performed the experiments. EAZ, CRB, WW, GJ, SZ and JC performed data analysis and interpretation. All authors reviewed the results and approved the final version of the manuscript.

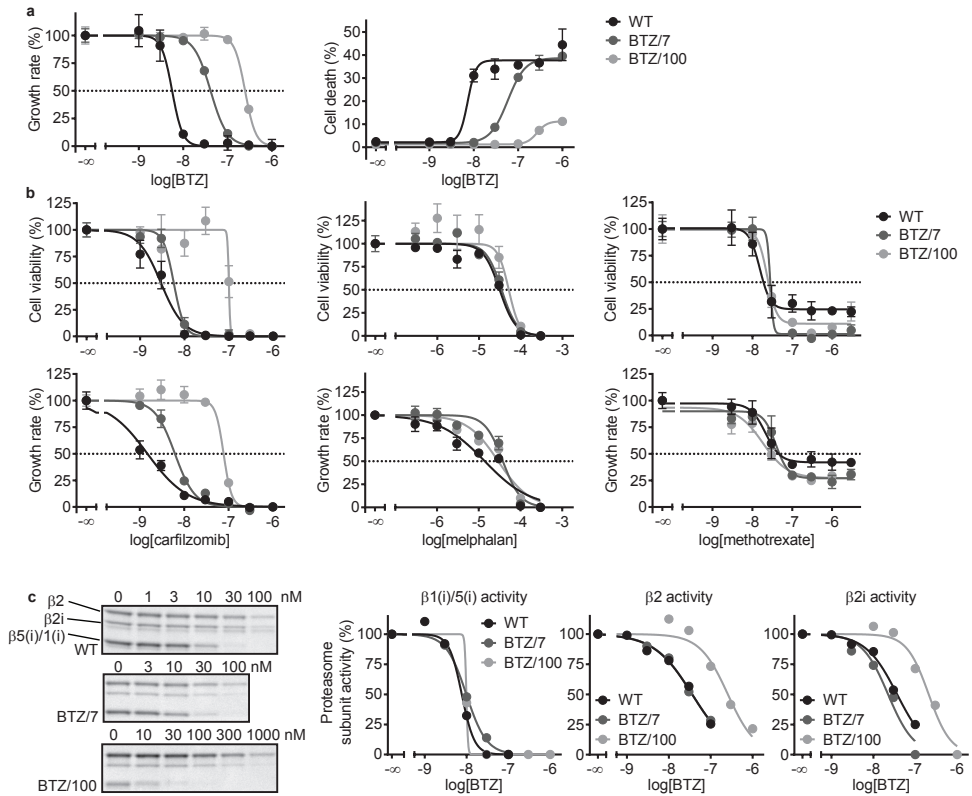
## REFERENCES

1. Moreau P, Richardson PG, Cavo M, Orlowski RZ, San Miguel JF, Palumbo A, et al. Proteasome inhibitors in multiple myeloma: 10 years later. *Blood*. 2012;120:947–59.
2. Anderson KC. The 39th David A. Karnofsky Lecture: bench-to bedside translation of targeted therapies in multiple myeloma. *J Clin Oncol*. 2012;30:445–52.
3. Raynes R, Pomatto LCD, Davies KJA. Degradation of oxidized proteins by the proteasome: Distinguishing between the 20S, 26S, and immunoproteasome proteolytic pathways. *Mol Aspects Med*. 2016;50:41–55.
4. Berkers CR, Ovaa H. Drug discovery and assay development in the ubiquitin-proteasome system. *Biochem Soc Trans*. 2010;38 Pt 1:14–20.
5. Obeng EA, Carlson LM, Gutman DM, Harrington WJ, Lee KP, Boise LH. Proteasome inhibitors induce a terminal unfolded protein response in multiple myeloma cells. *Blood*. 2006;107:4907–16.
6. Lipchick BC, Fink EE, Nikiforov MA. Oxidative stress and proteasome inhibitors in multiple myeloma. *Pharmacol Res*. 2016;105:210–5.
7. Niewerth D, Jansen G, Assaraf YG, Zweegman S, Kaspers GJL, Cloos J. Molecular basis of resistance to proteasome inhibitors in hematological malignancies. *Drug Resist Updat*. 2015;18:18–35.
8. McConkey DJ, Zhu K. Mechanisms of proteasome inhibitor action and resistance in cancer. *Drug Resist Updat*. 2008;11:164–79.
9. Orlowski RZ, Kuhn DJ. Proteasome inhibitors in cancer therapy: Lessons from the first decade. *Clin Cancer Res*. 2008;14:1649–57.
10. Oerlemans R, Franke NE, Assaraf YG, Cloos J, van Zantwijk I, Berkers CR, et al. Molecular basis of bortezomib resistance: proteasome subunit beta5 (PSMB5) gene mutation and overexpression of PSMB5 protein. *Blood*. 2008;112:2489–99.
11. Franke NE, Niewerth D, Assaraf YG, van Meerloo J, Vojtekova K, van Zantwijk CH, et al. Impaired bortezomib binding to mutant  $\beta 5$  subunit of the proteasome is the underlying basis for bortezomib resistance in leukemia cells. *Leukemia*. 2012;26:757–68.
12. de Wilt LHAM, Jansen G, Assaraf YG, van Meerloo J, Cloos J, Schimmer AD, et al. Proteasome-based mechanisms of intrinsic and acquired bortezomib resistance in non-small cell lung cancer. *Biochem Pharmacol*. 2012;83:207–17.
13. Rückrich T, Kraus M, Gogel J, Beck A, Ovaa H, Verdoes M, et al. Characterization of the ubiquitin-proteasome system in bortezomib-adapted cells. *Leukemia*. 2009;23:1098–105.
14. Balsas P, Galán-Malo P, Marzo I, Naval J. Bortezomib resistance in a myeloma cell line is associated to PSM $\beta 5$  overexpression and polyploidy. *Leuk Res*. 2012;36:212–8.
15. Niewerth D, Kaspers GJL, Jansen G, van Meerloo J, Zweegman S, Jenkins G, et al. Proteasome subunit expression analysis and chemosensitivity in relapsed paediatric acute leukaemia patients receiving bortezomib-containing chemotherapy. *J Hematol Oncol*. 2016;9:82.
16. Lichter DI, Danaee H, Pickard MD, Tayber O, Sintchak M, Shi H, et al. Sequence analysis of  $\beta$ -subunit genes of the 20S proteasome in patients with relapsed multiple myeloma treated with bortezomib or dexamethasone. *Blood*. 2012;120:4513–6.
17. Ling SCW, Lau EKK, Al-Shabeeb A, Nikolic A, Catalano A, Iland H, et al. Response of myeloma to the proteasome inhibitor bortezomib is correlated with the unfolded protein response regulator XBP-1. *Haematologica*. 2012;97:64–72.
18. Leung-Hagesteijn C, Erdmann N, Cheung G, Keats JJ, Stewart a. K, Reece DE, et al. Xbp1s-negative tumor B cells and pre-plasmablasts mediate therapeutic proteasome inhibitor resistance in multiple myeloma. *Cancer Cell*. 2013;24:289–304.
19. Driessen C, Kraus M, Joerger M, Rosing H, Bader J, Hitz F, et al. Treatment with the HIV protease inhibitor nelfinavir triggers the unfolded protein response and may overcome proteasome inhibitor resistance of multiple myeloma in combination with bortezomib: a phase I trial (SAKK 65/08). *Haematologica*. 2016;101:346–55.
20. Franke NE, Kaspers GL, Assaraf YG, van Meerloo J, Niewerth D, Kessler FL, et al. Exocytosis of polyubiquitinated proteins in bortezomib-resistant leukemia cells: a role for MARCKS in acquired resistance to proteasome inhibitors. *Oncotarget*. 2016;7:74779–96.
21. Ward PS, Thompson CB. Metabolic reprogramming: a cancer hallmark even

- warburg did not anticipate. *Cancer Cell*. 2012;21:297–308.
22. Vander Heiden MG, Cantley LC, Thompson CB. Understanding the Warburg effect: the metabolic requirements of cell proliferation. *Science*. 2009;324:1029–33.
  23. Galluzzi L, Kepp O, Vander Heiden MG, Kroemer G. Metabolic targets for cancer therapy. *Nat Rev Drug Discov*. 2013;12:829–46.
  24. Liu H, Liu Y, Zhang J-T. A new mechanism of drug resistance in breast cancer cells: fatty acid synthase overexpression-mediated palmitate overproduction. *Mol Cancer Ther*. 2008;7:263–70.
  25. Zhao Y, Liu H, Liu Z, Ding Y, Ledoux SP, Wilson GL, et al. Overcoming trastuzumab resistance in breast cancer by targeting dysregulated glucose metabolism. *Cancer Res*. 2011;71:4585–97.
  26. Stäubert C, Bhuiyan H, Lindahl A, Broom OJ, Zhu Y, Islam S, et al. Rewired metabolism in drug-resistant leukemia cells: a metabolic switch hallmarked by reduced dependence on exogenous glutamine. *J Biol Chem*. 2015;290:8348–59.
  27. Baenke F, Chaneton B, Smith M, Van Den Broek N, Hogan K, Tang H, et al. Resistance to BRAF inhibitors induces glutamine dependency in melanoma cells. *Mol Oncol*. 2016;10:73–84.
  28. Maiso P, Huynh D, Moschetta M, Sacco A, Aljawai Y, Mishima Y, et al. Metabolic signature identifies novel targets for drug resistance in multiple myeloma. *Cancer Res*. 2015;75:2071–82.
  29. Soriano GP, Besse L, Li N, Kraus M, Besse A, Meeuwenoord N, et al. Proteasome inhibitor-adapted myeloma cells are largely independent from proteasome activity and show complex proteomic changes, in particular in redox and energy metabolism. *Leukemia*. 2016;30:2198–207.
  30. Niewerth D, van Meerloo J, Jansen G, Assaraf YG, Hendrickx TC, Kirk CJ, et al. Anti-leukemic activity and mechanisms underlying resistance to the novel immunoproteasome inhibitor PR-924. *Biochem Pharmacol*. 2014;89:43–51.
  31. Berkers CR, van Leeuwen FWB, Groothuis T a, Peperzak V, van Tilburg EW, Borst J, et al. Profiling proteasome activity in tissue with fluorescent probes. *Mol Pharm*. 2007;4:739–48.
  32. Kraus M, Rückrich T, Reich M, Gogel J, Beck A, Kammer W, et al. Activity patterns of proteasome subunits reflect bortezomib sensitivity of hematologic malignancies and are variable in primary human leukemia cells. *Leukemia*. 2007;21:84–92.
  33. Kuehne A, Emmert H, Soehle J, Winnefeld M, Fischer F, Wenck H, et al. Acute Activation of Oxidative Pentose Phosphate Pathway as First-Line Response to Oxidative Stress in Human Skin Cells. *Mol Cell*. 2015;59:359–71.
  34. Verbrugge SE, Assaraf YG, Dijkmans B a C, Scheffer GL, Al M, den Uyl D, et al. Inactivating PSMB5 mutations and P-glycoprotein (multidrug resistance-associated protein/ATP-binding cassette B1) mediate resistance to proteasome inhibitors: ex vivo efficacy of (immuno)proteasome inhibitors in mononuclear blood cells from patients with rheumatoid arthritis. *J Pharmacol Exp Ther*. 2012;341:174–82.
  35. Bohndiek SE, Kettunen MI, Hu D, Kennedy BWC, Boren J, Gallagher FA, et al. Hyperpolarized [1-13C]-ascorbic and dehydroascorbic acid: vitamin C as a probe for imaging redox status in vivo. *J Am Chem Soc*. 2011;133:11795–801.
  36. Corti A, Casini AF, Pompella A. Cellular pathways for transport and efflux of ascorbate and dehydroascorbate. *Arch Biochem Biophys*. 2010;500:107–15.
  37. Labuschagne CF, van den Broek NJF, Mackay GM, Vousden KH, Maddocks ODK. Serine, but not glycine, supports one-carbon metabolism and proliferation of cancer cells. *Cell Rep*. 2014;7:1248–58.
  38. Maddocks ODK, Berkers CR, Mason SM, Zheng L, Blyth K, Gottlieb E, et al. Serine starvation induces stress and p53-dependent metabolic remodelling in cancer cells. *Nature*. 2013;493:542–6.
  39. Maddocks ODK, Labuschagne CF, Adams PD, Vousden KH. Serine Metabolism Supports the Methionine Cycle and DNA/RNA Methylation through De Novo ATP Synthesis in Cancer Cells. *Mol Cell*. 2016;61:210–21.
  40. Tedeschi PM, Markert EK, Gounder M, Lin H, Dvorzhinski D, Dolfi SC, et al. Contribution of serine, folate and glycine metabolism to the ATP, NADPH and purine requirements of cancer cells. *Cell Death Dis*. 2013;4:e877.
  41. Locasale JW. Serine, glycine and one-carbon units: cancer metabolism in full circle. *Nat Rev Cancer*. 2013;13:572–83.

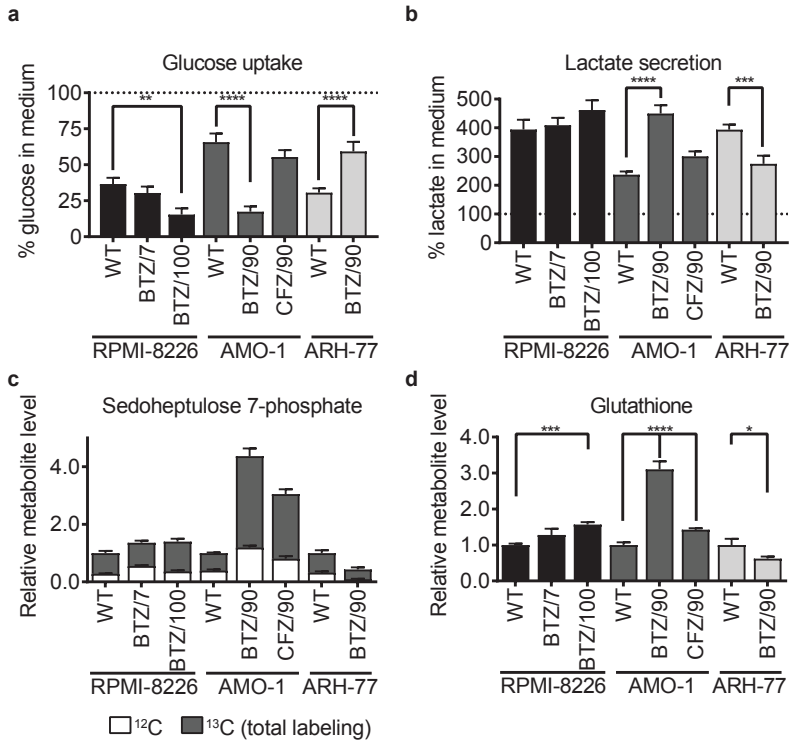
42. Amelio I, Cutruzzolá F, Antonov A, Agostini M, Melino G. Serine and glycine metabolism in cancer. *Trends Biochem Sci.* 2014;39:191–8.
43. Mullarky E, Lucki NC, Beheshti Zavareh R, Anglin JL, Gomes AP, Nicolay BN, et al. Identification of a small molecule inhibitor of 3-phosphoglycerate dehydrogenase to target serine biosynthesis in cancers. *Proc Natl Acad Sci U S A.* 2016;113:1778–83. doi:10.1073/pnas.1521548113.
44. DeNicola GM, Chen P-H, Mullarky E, Sudderth JA, Hu Z, Wu D, et al. NRF2 regulates serine biosynthesis in non-small cell lung cancer. *Nat Genet.* 2015;47:1475–81.
45. Pollari S, Kähkönen S-M, Edgren H, Wolf M, Kohonen P, Sara H, et al. Enhanced serine production by bone metastatic breast cancer cells stimulates osteoclastogenesis. *Breast Cancer Res Treat.* 2011;125:421–30.
46. Mullarky E, Mattaini KR, Vander Heiden MG, Cantley LC, Locasale JW. PHGDH amplification and altered glucose metabolism in human melanoma. *Pigment Cell Melanoma Res.* 2011;24:1112–5.
47. Locasale JW, Grassian AR, Melman T, Lyssiotis CA, Mattaini KR, Bass AJ, et al. Phosphoglycerate dehydrogenase diverts glycolytic flux and contributes to oncogenesis. *Nat Genet.* 2011;43:869–74.
48. Possemato R, Marks KM, Shaul YD, Pacold ME, Kim D, Birsoy K, et al. Functional genomics reveal that the serine synthesis pathway is essential in breast cancer. *Nature.* 2011;476:346–50.
49. Pacold ME, Brimacombe KR, Chan SH, Rohde JM, Lewis CA, Swier LJYM, et al. A PHGDH inhibitor reveals coordination of serine synthesis and one-carbon unit fate. *Nat Chem Biol.* 2016;12:452–8.
50. Maddocks ODK, Athineos D, Cheung EC, Lee P, Zhang T, van den Broek NJF, et al. Modulating the therapeutic response of tumours to dietary serine and glycine starvation. *Nature.* 2017;544:372–6.
51. Du Z-X, Zhang H-Y, Meng X, Guan Y, Wang H-Q. Role of oxidative stress and intracellular glutathione in the sensitivity to apoptosis induced by proteasome inhibitor in thyroid cancer cells. *BMC Cancer.* 2009;9:56.
52. Buescher JM, Antoniewicz MR, Boros LG, Burgess SC, Brunengraber H, Clish CB, et al. A roadmap for interpreting (13)C metabolite labeling patterns from cells. *Curr Opin Biotechnol.* 2015;34:189–201.

## SUPPLEMENTAL MATERIAL



**Supplemental figure S1. Response of RPMI-8226 WT, BTZ/7 and BTZ/100 cells to bortezomib and other chemotherapeutic agents.**

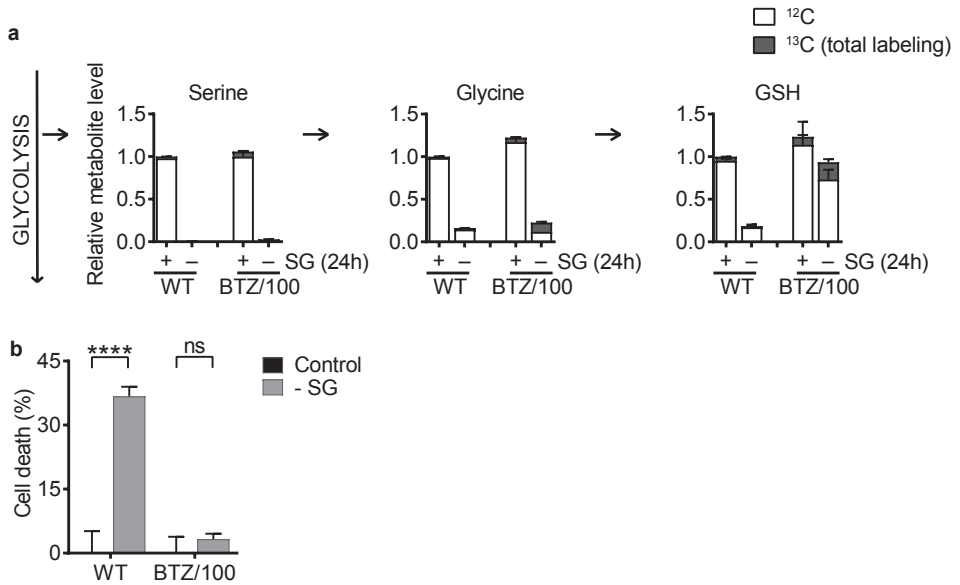
**a** Growth rate and cell death of RPMI-8226 wild type (WT) and bortezomib-resistant (BTZ/100) cells after a 48-hour treatment with increasing concentrations of bortezomib (BTZ). Results represent % growth rate (left panel) or % cell death (right panel)  $\pm$  SD compared to non-treated controls (n=3). **b** Cell viability and growth rate of RPMI-8226 wild type (WT) and bortezomib-resistant (BTZ/100) cells after a 48-hour treatment with increasing concentrations of carfilzomib, melphalan and methotrexate. Results represent % cell viability (upper panel) or % growth rate (lower panel)  $\pm$  SD compared to non-treated controls (n=3). **c** In gel fluorescence measurements showing representative proteasome activity profiles of RPMI-8226 WT, BTZ/7 and BTZ/100 cells after 2 hour of bortezomib treatment in increasing concentrations, including 1 hour treatment with proteasome activity probe Me<sub>2</sub>BodipyFLAhx<sub>3</sub>L<sub>3</sub>VS (left panel). Quantification of gel images, with results plotted as fractions of subunit activity compared to non-treated controls (right panel). BTZ = bortezomib



**Supplemental figure S2. Intra- and extracellular metabolite analysis of BTZ- and CFZ-resistant cell lines.**

**a,b** Extracellular metabolite analysis of RPMI-8226, AMO-1 and ARH-77 wild type (WT) and bortezomib- and carfilzomib-resistant cells. Cells were suspended in MEM with 1mM L-glutamine, 0.2mM L-serine and 0.2mM L-glycine. Media samples were collected after 8 hours, followed by LC-MS analysis of extracellular glucose (**a**) and lactate (**b**). Results represent % peak area  $\pm$  SD compared to cell-free media (n=3). **c,d** Intracellular metabolite analysis of RPMI-8226, AMO-1 and ARH-77 wild type (WT) and bortezomib- and carfilzomib-resistant cells. Cells were suspended in DMEM containing 8mM [<sup>13</sup>C] D-glucose. Intracellular metabolites were extracted after 8 hours and analyzed by LC-MS. Data are means  $\pm$  SD (n=3) of unlabelled (white) and <sup>13</sup>C-labelled metabolites (grey) for sedoheptulose 7-phosphate (**c**) and total glutathione (**d**). One-way ANOVA tests were performed (\* = p<0.05, \*\* = p<0.01, \*\*\* = p<0.001, \*\*\*\* = p<0.0001)

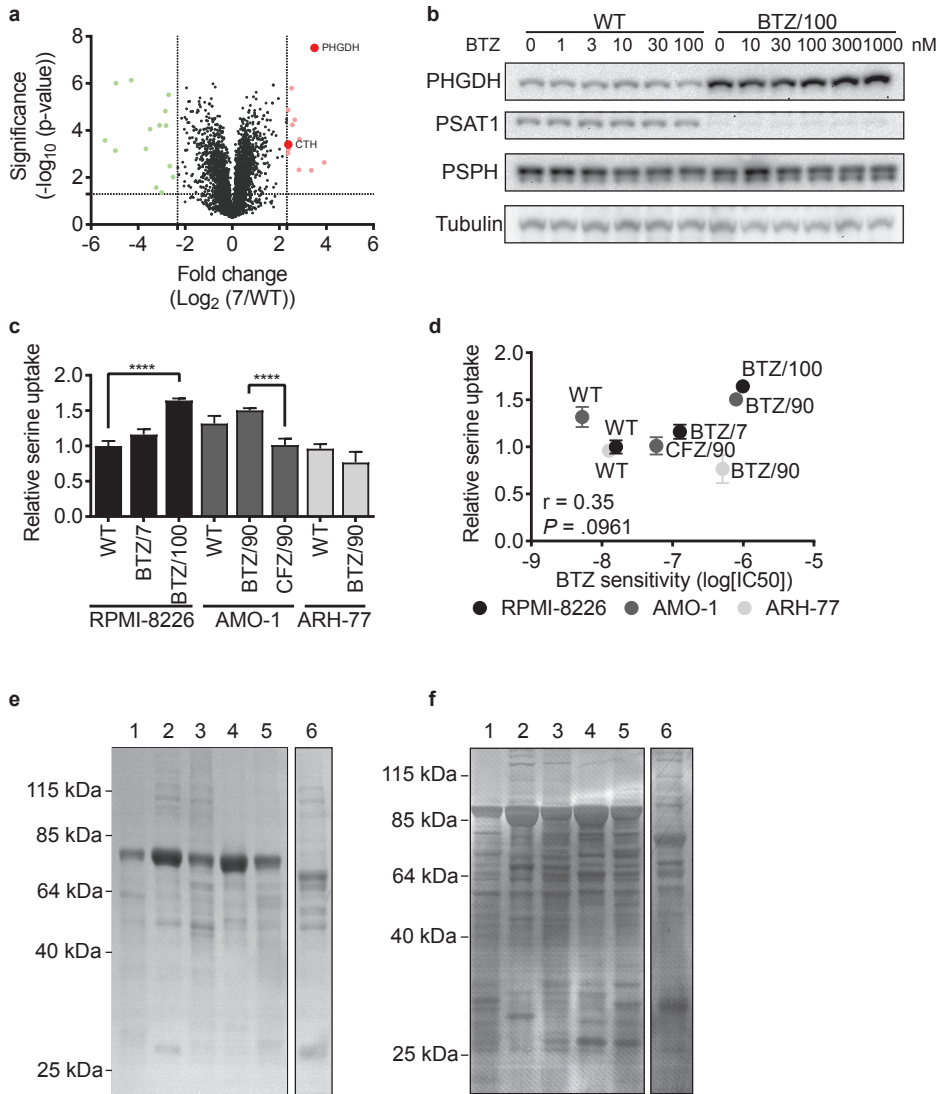




**Supplemental figure S3. Response to serine starvation of RPMI-8226 WT and BTZ/100 cells.**

**a** Intracellular metabolite analysis of RPMI-8226 WT and BTZ/100 cells in the presence or absence of extracellular serine (-SG). Cells were grown complete medium in the presence or absence of 0.4mM serine. After 24 hours, medium were replaced with matched media containing 20 mM [U- $^{13}\text{C}$ ]D-glucose. Cells were harvested after 4 hours and subjected to LC-MS analysis. Data are means  $\pm$  SD (n=3) of unlabelled (white) and labelled metabolites (grey).

**b** Cell death assay of RPMI-8226 WT and BTZ/100 cells in the presence or absence of extracellular serine (-SG). Data are means  $\pm$  SD of % death cells after 24 hours. Two-way ANOVA tests were performed (\*\*\*\* =  $p < 0.0001$ ). BTZ = bortezomib. GSH = glutathione.



#### Supplemental figure S4. Bortezomib resistance correlates to the expression of PHGDH.

**a** Graphical representation of quantitative proteomics data. Proteins are ranked in volcano plot according to their statistically p-value (y-axis) and relative abundance ratio between RPMI-8226 WT and BTZ/7 cells (x-axis). Coloured spots represent significantly upregulated (red) or downregulated (green) proteins in BTZ/7 cells with at least a 5-fold change. Significantly regulated metabolic enzymes are marked. **b** Immunoblot of 3-phosphoglycerate dehydrogenase (PHGDH), phosphoserine aminotransferase 1 (PSAT1), phosphoserine phosphatase (PSPH) and Tubulin expression in RPMI-8226 WT and BTZ/100 cells after 8 hour incubation with increasing concentrations of bortezomib. **c** Extracellular metabolite analysis of RPMI-8226, AMO-1 and ARH-77 wild type (WT) and bortezomib- and carfilzomib-resistant cells. Cells were suspended in MEM with 1mM L-glutamine, 0.2mM L-serine and 0.2mM L-glycine. Media samples were collected after 8 hours, followed by LC-MS analysis of extracellular serine. Results represent % peak area  $\pm$  SD compared to cell-free media (n=3). One-way ANOVA tests were performed (\*\*\*\* =  $p < 0.0001$ ). **d** Correlation between serine uptake and IC<sub>50</sub> of bortezomib in RPMI-8226, AMO-1 and ARH-77 bortezomib-sensitive and -resistant sublines. Pearson correlation:  $r = 0.35$  ( $p = .0961$ ). **e, f** Coomassie stained membrane for loading control of PHGDH (**e**) and PSAT1 and PSPH (**f**) with isolated CD138+ plasma cells from diagnosed multiple myeloma patients (n=6). BTZ = bortezomib, CFZ = carfilzomib, PHGDH = 3-phosphoglycerate dehydrogenase, PSAT1 = phosphoserine aminotransferase 1, PSPH = phosphoserine phosphatase.

**Supplemental Table S1.** Characteristics of multiple myeloma patients

Patient	Gender	Age (yr)	BTZ treatment	Remarks
1	Male	68	no	Sample at diagnosis
2	Male	46	yes	Initial response to BTZ/dexamethasone therapy, autologous stem cell transplantation, relapse after 2 years, second BTZ/dexamethasone therapy and tandem auto/allo-transplantation. Relapse with development of plasma cell leukemia when sample was taken.
3	Female	66	yes	Relapse after autologous STC, start BTZ/dexamethasone therapy, development of plasma cell leukemia after 4 months therapy when sample was taken (BTZ-refractory)
4	Female	68	no	MM with breast cancer metastasis; starting therapy with melphalan when sample was taken
5	Female	65	yes	Progressive disease during BTZ/dexamethasone therapy when sample was taken (BTZ-refractory)
6	Male	70	no	Sample taken at first relapse after melphalan/dexamethasone/ lenalidomide therapy.

**Supplemental Table S2.** Upregulated metabolic enzymes in RPMI-8226 BTZ/100 and BTZ/7 cells compared to WT

Protein ID	Gene name	Protein name	BTZ/100 : WT		BTZ/7 : WT	
			FC	p-value	FC	p-value
O43175	PHGDH	D-3-phosphoglycerate dehydrogenase	7.86	1.57E-07*	11.27	3.08E-08*
Q5T6L4	ASS	Argininosuccinate synthase	3.29	4.57E-06*	1.61	6.78E-04*
O60701	UGDH	UDP-glucose 6-dehydrogenase	2.92	1.92E-05*	2.54	2.34E-05*
X5D767	ADA	Adenosine deaminase	2.66	1.37E-04*	2.80	3.60E-05*
Q16222	UAP1	UDP-N-acetylhexosamine pyrophosphorylase	2.56	4.35E-05*	3.36	1.17E-06*
F5H5V4	PSMD9	26S proteasome non-ATPase regulatory subunit 9	2.41	8.44E-05*	1.16	1.31E-02*
P16152	CBR1	Carbonyl reductase [NADPH] 1	2.30	1.12E-04*	1.40	7.60E-02*
Q6LET3	HPRT1	Hypoxanthine-guanine phosphoribosyltransferase	2.28	7.40E-05*	1.58	9.22E-03*
P32929	CTH	Cystathionine gamma-lyase	2.27	1.41E-03*	5.22	3.94E-04*
D6RFF8	GNPDA1	Glucosamine-6-phosphate isomerase	2.15	2.87E-03*	1.40	4.93E-03*
B3KN05	ACSL3	Long-chain-fatty-acid-CoA ligase 3	2.13	7.59E-04*	2.70	3.16E-04*
Q8NFW8	CMAS	N-acylneuraminase cytidylyltransferase	2.06	5.09E-04*	1.64	7.62E-04*
E9PNU1	NME7	Nucleoside diphosphate kinase 7	1.97	2.51E-03*	1.33	4.31E-02*
A0A024R275	RFK	Riboflavin kinase	1.95	1.75E-03*	1.10	1.21E-01
HOYMB3	GMPR2	GMP reductase	1.92	1.91E-05*	2.03	1.25E-04*
A0A024R912	UCK2	Uridine kinase	1.88	1.72E-03*	1.60	1.65E-03*
Q86TP1	PRUNE	Protein prune homolog	1.87	1.53E-04*	2.18	5.81E-03*
A8K8N7	PFAS	Phosphoribosylformylglycinamide synthase	1.85	5.26E-04*	1.90	2.05E-04*
Q5M7Z5	GRHPR	Glyoxylate reductase/hydroxypyruvate reductase	1.82	2.07E-03*	1.25	1.56E-01
P23526	AHCY	Adenosylhomocysteinase	1.81	8.66E-05*	2.83	1.74E-05*
B2ZZ90	ACACA	Acetyl-CoA carboxylase 1	1.76	2.49E-05*	1.48	2.67E-03*
Q53HM1	UCKL1	Uridine kinase	1.74	5.86E-03*	1.25	5.64E-02
Q9NZL9	MAT2B	Methionine adenosyltransferase 2 subunit beta	1.74	6.97E-05*	1.27	5.14E-02
B4DM26	LCLAT1	Lysocardiolipin acyltransferase 1	1.74	3.53E-03*	1.48	1.00E-02*
P28070	PSMB4	Proteasome subunit beta type-4	1.73	2.47E-03*	0.78	2.41E-01
B7Z1Y2	ALDOC	Fructose-bisphosphate aldolase	1.72	1.86E-04*	3.28	6.84E-06*
P28074	PSMB5	Proteasome subunit beta type-5	1.71	3.93E-04*	1.28	3.02E-02*
Q504W7	OCRL	Inositol polyphosphate 5-phosphatase OCRL-1	1.70	3.08E-03*	1.33	2.59E-02*
B2R9X3	GMD5	GDP-mannose 4,6 dehydratase	1.68	3.27E-04*	2.15	5.15E-05*
P08243	ASNS	Asparagine synthetase	1.67	1.14E-04*	1.52	6.16E-03*
X5D8S6	ADSL	Adenylosuccinate lyase	1.66	1.09E-03*	1.01	4.86E-01
P52788	SMS	Spermine synthase	1.66	2.50E-04*	1.25	1.92E-02*
A0A024QZW7	NUP153	Nuclear pore complex protein Nup153	1.63	2.42E-05*	1.63	1.66E-05*
P15531	NME1	Nucleoside diphosphate kinase A	1.62	1.16E-02*	1.57	3.01E-02*
A8K6Y2	PPP2R5D	Phosphatase 2A, regulatory subunit B56 delta isoform	1.62	1.35E-03*	1.90	1.37E-04*
O95336	PGLS	6-phosphogluconolactonase	1.61	7.07E-03*	1.26	6.40E-02*
Q96HT3	POLR1C	DNA-directed RNA polymerases I and III subunit RPAC1	1.60	1.21E-03*	1.37	2.01E-02*
C9JFR7	CYCS	Cytochrome c	1.59	5.91E-02	2.66	6.90E-03
A0A024R652	MTHFD1	Methylenetetrahydrofolate dehydrogenase	1.58	2.07E-04*	1.49	1.23E-04*
P25787	PSMA2	Proteasome subunit alpha type	1.58	3.26E-03*	1.15	7.93E-02
Q53HS0	QARS	Glutaminyl-tRNA synthetase variant	1.56	1.42E-04*	1.02	3.90E-01
V9HWD9	TKT1	Transketolase	1.53	8.06E-06*	0.74	1.95E-03*
P25325	MPST	3-mercaptopyruvate sulfurtransferase	1.53	4.98E-02*	1.26	2.01E-01
P12268	IMPDH2	Inosine-5-monophosphate dehydrogenase 2	1.52	5.95E-04*	0.82	5.20E-04*
E9PF10	NUP155	Nuclear pore complex protein Nup155	1.51	1.47E-04*	1.56	1.49E-04*
Q14TF0	GCLC	Glutamate-cysteine ligase	1.51	7.48E-04*	1.21	6.59E-02*

Metabolic enzymes that are upregulated in RPMI-8226 BTZ/100 cells compared to WT cells with fold change (FC) &gt; 1.5

\* = p&lt;0.05 based on Student's T-Test

**Supplemental Table S3.** Downregulated metabolic enzymes in RPMI-8226 BTZ/100 and BTZ/7 cells compared to WT

Protein ID	Gene name	Protein name	BTZ/100 : WT		BTZ/7 : WT	
			FC	p-value	FC	p-value
P04040	CAT	Catalase	0.14	4.98E-05 *	0.65	2.90E-02 *
G3V4W4	A0A024R5K6	Glucosamine 6-phosphate N-acetyltransferase	0.17	3.56E-06 *	0.29	2.11E-04 *
A0A024R5K6	NDUFC2	NADH dehydrogenase [ubiquinone] 1 subunit C2	0.23	5.67E-02 *	0.54	3.62E-01
J3KS22	DCXR	L-xylulose reductase	0.25	2.32E-04 *	0.25	6.93E-04 *
Q6FGU2	DTYMK	Thymidylate kinase	0.25	1.01E-04 *	0.43	8.87E-05 *
A0A087WX1	HIBCH	3-hydroxyisobutyryl-CoA hydrolase	0.27	3.06E-05 *	0.40	3.50E-04 *
A0A024R222	PSAT1	Phosphoserine aminotransferase	0.27	6.72E-05 *	0.77	1.75E-02 *
Q9P2X2	SLC1A4	Amino acid transporter	0.27	1.40E-04 *	0.38	4.17E-03 *
B4DEA8	ACADVL	Very long-chain specific acyl-CoA dehydrogenase	0.28	6.96E-04 *	0.21	7.66E-03 *
P36871	PGM1	Phosphoglucomutase-1	0.33	8.47E-05 *	0.35	9.04E-05 *
A0A024QZ78	AGMAT	Agmatinase	0.33	2.67E-02 *	0.36	1.62E-02 *
A0A024RBX9	PDHA1	Pyruvate dehydrogenase E1 component subunit alpha	0.34	5.71E-04 *	0.50	2.72E-03 *
Q53GL5	IDH2	Isocitrate dehydrogenase [NADP]	0.34	1.27E-03 *	0.33	3.21E-04 *
Q71UA6	SLC1A5	Amino acid transporter	0.34	1.63E-01	1.11	2.64E-01
E9PN17	ATP5L	ATP synthase subunit g	0.37	5.76E-03 *	0.71	6.93E-02
A0A024QYX0	EBP	3-beta-hydroxysteroid-Delta(8),Delta(7)-isomerase	0.37	3.30E-04 *	0.48	9.19E-04 *
Q5T0S4	PPT1	Palmitoyl-protein thioesterase 1	0.37	1.93E-04 *	0.63	9.87E-03 *
Q53X12	ATP6V0A1	V-type proton ATPase subunit a	0.40	5.84E-02	0.67	9.44E-03 *
Q8TCJ2	STT3B	Dolichyl-diphosphooligosaccharide-protein glycosyltransferase subunit STT3B	0.40	1.50E-03 *	0.67	4.23E-02 *
B4DJ81	NDUFS1	NADH-ubiquinone oxidoreductase 75 kDa subunit	0.40	8.00E-03 *	0.67	1.03E-02 *
B3KM58	DKFZp686O15119	Putative uncharacterized protein DKFZp686O15119	0.41	9.83E-04 *	0.38	3.97E-04 *
P11177	PDHB	Pyruvate dehydrogenase E1 component subunit beta	0.42	1.50E-03 *	0.38	5.60E-04 *
B2R7W0	MTHFD2	methylenetetrahydrofolate dehydrogenase	0.42	2.35E-03 *	0.62	3.33E-03 *
Q15067	ACOX1	Peroxisomal acyl-coenzyme A oxidase 1	0.42	5.34E-04 *	0.43	6.81E-03 *
A0A024R6G6	NDUFB1	NADH dehydrogenase [ubiquinone] 1 beta subcomplex	0.42	9.24E-02	0.70	7.18E-02
B4E072	ACAA1	3-ketoacyl-CoA thiolase	0.43	1.46E-04 *	0.60	5.84E-03 *
A0A087WTV6	PYCR2	Pyrraline-5-carboxylate reductase 2	0.43	1.62E-03 *	0.53	2.09E-03 *
A0A024QZ30	SDHA	Succinate dehydrogenase [ubiquinone] flavoprotein subunit	0.43	2.46E-05 *	0.70	2.96E-03 *
P22695	UQCRC2	Cytochrome b-c1 complex subunit 2	0.43	2.76E-03 *	0.60	2.66E-02 *
A0A0C4DGS1	DDOST	Dolichyl-diphosphooligosaccharide-protein glycosyltransferase 48 kDa subunit	0.44	1.81E-04 *	0.77	5.46E-02
P32321	DCTD	Deoxycytidylate deaminase	0.44	2.50E-02 *	0.65	5.71E-03 *
B4DZ08	ACO2	Aconitate hydratase	0.44	4.81E-05 *	0.56	9.45E-04 *
Q13057	COASY	Bifunctional coenzyme A synthase	0.45	2.84E-03 *	0.41	4.68E-04 *
Q5QNZ2	ATP5F1	ATP synthase F(0) complex subunit B1	0.45	1.34E-04 *	0.59	1.11E-03 *
Q2TB59	NNT	NAD(P) transhydrogenase	0.45	7.85E-04 *	0.43	8.22E-03 *
P31930	UQCRC1	Cytochrome b-c1 complex subunit 1	0.46	7.51E-04 *	0.64	1.17E-02 *
P21912	SDHB	Succinate dehydrogenase [ubiquinone] iron-sulfur subunit	0.46	2.57E-03 *	0.73	1.40E-01
Q0QEN7	ATP5B	ATP synthase subunit beta	0.47	6.82E-04 *	0.51	2.83E-03 *
B3KUZ8	GOT2	Aspartate aminotransferase	0.47	7.87E-04 *	0.52	2.83E-03 *
P24752	ACAT1	Acetyl-CoA acetyltransferase	0.47	3.26E-04 *	0.68	6.34E-03 *
A0A024R7A8	AKR1B1	Aldose reductase	0.47	1.69E-04 *	0.75	1.09E-04 *
A8K168	ME1	Malic enzyme	0.48	6.98E-02	0.97	4.81E-01
A0A024R3W5	SLC39A10	Zinc transporter ZIP10	0.48	6.04E-02	0.58	5.93E-02
B4DRH6	HADHA	Long-chain enoyl-CoA hydratase	0.48	3.32E-07 *	0.64	4.16E-04 *
P53602	MVD	Diphosphomevalonate decarboxylase	0.49	4.35E-03 *	0.61	1.42E-02 *
B4DY96	HADHB	3-ketoacyl-CoA thiolase	0.49	4.49E-04 *	0.50	3.64E-03 *
Q53GR7	SLC25A13	Calcium-binding mitochondrial carrier protein Aralar2	0.49	3.91E-02 *	0.77	2.94E-01
B4E0N9	GLUD1	Glutamate dehydrogenase	0.49	5.53E-04 *	0.49	2.03E-03 *
Q53FM7	NDUFS3	NADH dehydrogenase [ubiquinone] iron-sulfur protein 3	0.50	3.71E-03 *	0.91	2.50E-01
D3DVH3	INPP4A	Type I inositol 3,4-bisphosphate 4-phosphatase	0.50	2.01E-03 *	0.68	1.03E-02 *
A0A087WVM4	MTHFD1L	Monofunctional C1-tetrahydrofolate synthase	0.50	2.19E-03 *	0.87	2.11E-01

Supplemental Table S3. Continued

Protein ID	Gene name	Protein name	BTZ/100 : WT		BTZ/7 : WT	
			FC	p-value	FC	p-value
H7C3G9	NAGK	N-acetyl-D-glucosamine kinase	0.50	3.20E-05 *	0.46	4.39E-04 *
Q6IB54	ATP5J	ATP synthase-coupling factor 6	0.51	3.06E-04 *	0.61	4.60E-03 *
P13073	COX4I1	Cytochrome c oxidase subunit 4 isoform 1	0.51	1.66E-03 *	0.64	6.51E-03 *
A4D1K0	ATP6V1F	V-type proton ATPase subunit F	0.52	1.06E-02 *	0.64	1.46E-03 *
Q5QP19	NFS1	Cysteine desulfurase	0.52	6.18E-04 *	0.66	2.54E-03 *
C9JJU1	SLC38A5	Sodium-coupled neutral amino acid transporter 5	0.52	5.86E-02	0.47	1.53E-01
Q96HA1	POM121	Nuclear envelope pore membrane protein POM 121	0.52	2.77E-04 *	0.68	1.35E-03 *
B2RE46	RPN2	Dolichyl-diphosphooligosaccharide-protein glycosyltransferase subunit 2	0.52	7.94E-04 *	0.86	4.72E-02 *
B2R659	HSD17B4	Peroxisomal multifunctional enzyme type 2	0.53	1.04E-03 *	0.74	7.46E-03 *
E9PC15	AGK	Acylglycerol kinase	0.53	8.21E-05 *	0.66	5.82E-03 *
P47985	UQCRFS1	Cytochrome b-c1 complex subunit 11	0.54	1.78E-02 *	0.55	6.43E-02
B7Z9J8	IDH3A	Isocitrate dehydrogenase [NAD] subunit	0.54	1.12E-01	1.65	2.12E-01
O75947	ATP5H	ATP synthase subunit d	0.54	1.49E-03 *	0.67	6.89E-02
B4DFL1	DLD	Dihydrolipoyl dehydrogenase	0.55	1.94E-02 *	0.54	2.65E-03 *
Q0QF37	MDH2	Malate dehydrogenase	0.56	6.85E-04 *	0.59	4.21E-03 *
K7EPM1	ENO3	Enolase	0.56	9.11E-03 *	0.60	4.53E-03 *
E9PDF2	OGDH	2-oxoglutarate dehydrogenase	0.56	1.29E-04 *	0.62	3.95E-03 *
E7D7X9	PYCR1	Pyrraline-5-carboxylate reductase	0.57	2.23E-04 *	0.55	9.36E-06 *
Q6FHM4	COX5B	Cytochrome c oxidase subunit 5B	0.57	1.05E-02 *	0.65	2.35E-02 *
Q9GZS1	POLR1E	DNA-directed RNA polymerase I subunit RPA49	0.58	9.82E-03 *	1.00	5.00E-01
F5GZS6	SLC3A2	4F2 cell-surface antigen heavy chain	0.59	1.61E-03 *	0.75	5.05E-03 *
Q8N4P3	HDDC3	Guanosine-3,5-bis(diphosphate) 3-pyrophosphohydrolase MESH1	0.59	5.10E-03 *	0.97	3.51E-01
O00116	AGPS	Alkylidihydroxyacetonephosphate synthase	0.59	1.94E-03 *	0.83	8.40E-02
B3KNL8	ALG2	Alpha-1,3/1,6-mannosyltransferase ALG2	0.59	4.21E-03 *	0.59	7.66E-03 *
B2R761	SCP2	Non-specific lipid-transfer protein	0.59	9.38E-03 *	0.67	1.83E-02 *
E9PF18	HADH	Hydroxyacyl-coenzyme A dehydrogenase	0.59	1.76E-03 *	0.55	9.66E-04 *
Q99714	HSD17B10	3-hydroxyacyl-CoA dehydrogenase type-2	0.59	1.43E-03 *	0.64	5.16E-03 *
B4DL14	ATP5C1	ATP synthase subunit gamma	0.59	3.99E-03 *	0.64	2.87E-02 *
Q9NRN7	AASDHPPT	L-aminoadipate-semialdehyde dehydrogenase-phosphopantetheinyl transferase	0.60	4.63E-04 *	1.03	4.39E-01
A0A075X871	COX3	Cytochrome c oxidase subunit 3	0.60	2.40E-02 *	0.91	2.60E-01
Q9NR45	NANS	Sialic acid synthase	0.60	1.16E-03 *	0.60	5.31E-03 *
A0A087WUV8	BSG	Basigin	0.61	9.33E-04 *	0.74	1.85E-02 *
A0A087WZN1	IDH3B	Isocitrate dehydrogenase [NAD] subunit	0.61	1.76E-04 *	0.98	3.98E-01
E9PPM8	DERA	Deoxyribose-phosphate aldolase	0.61	6.77E-04 *	0.69	3.45E-03 *
Q53H22	PPAT	Amidophosphoribosyltransferase	0.62	1.89E-04 *	0.58	3.24E-05 *
Q5JU21	FPGS	Folylpolyglutamate synthase	0.62	6.92E-03 *	0.28	2.27E-02 *
P06132	UROD	Uroporphyrinogen decarboxylase	0.63	3.97E-04 *	0.70	1.53E-03 *
E9PGM4	GBE1	1,4-alpha-glucan-branching enzyme	0.63	4.41E-05 *	0.94	3.51E-02 *
Q6ZRI6	C1orf57	Uncharacterized protein C15orf39	0.64	2.87E-02 *	0.90	2.68E-01
A0A024RB32	PTGES3	Prostaglandin E synthase 3	0.64	2.58E-03 *	0.58	9.06E-03 *
P17858	PFKL	ATP-dependent 6-phosphofructokinase	0.65	8.97E-05 *	0.51	7.45E-06 *
Q3T7C7	TRIT1	tRNA dimethylallyltransferase	0.65	1.11E-02 *	0.96	3.27E-01
A0A087X211	PSMC6	26S protease regulatory subunit 10B	0.66	9.08E-04 *	0.95	2.18E-01
Q6FHU0	PSMB8	Proteasome subunit beta type	0.66	2.15E-02 *	0.65	3.82E-03 *
ALDH18A1	ALDH18A1	Glutamate 5-kinase	0.66	7.33E-04 *	0.74	1.61E-02 *
Q01970	PLCB3	1-phosphatidylinositol 4,5-bisphosphate phosphodiesterase beta-3	0.66	3.43E-02 *	1.18	6.41E-02

Metabolic enzymes that are downregulated in RPMI-8226 BTZ/100 cells compared to WT cells with fold change (FC) > 1.5

\* = p<0.05 based on Student's T-Test







---

## Part I

# Chapter

## Mitochondrial respiration as a target in bortezomib-resistant multiple myeloma cells

Esther A. Zaal<sup>1</sup>, Pieter Langerhorst<sup>1</sup>, Haley Baptist<sup>1</sup>, Harm-Jan de Grooth<sup>2</sup>, Maaïke Meerlo<sup>3</sup>, Boudewijn M. Burgering<sup>3</sup>, Wei Wu<sup>1</sup>, Celia R. Berkers<sup>1</sup>

<sup>1</sup> Biomolecular Mass Spectrometry and Proteomics, Bijvoet Center for Biomolecular Research, Utrecht University, Utrecht, The Netherlands

<sup>2</sup> Department of Intensive Care, VU University Medical Centre, Amsterdam, The Netherlands

<sup>3</sup> Molecular Cancer Research, Center Molecular Medicine, University Medical Center Utrecht, Utrecht, The Netherlands

## ABSTRACT

Metabolic alterations are an important aspect of cancer and also play a role in anticancer drug resistance. As drug-resistant cells can become reliant on their altered metabolism, a better understanding of this metabolic rewiring aids in finding novel strategies to improve current therapies.

The proteasome inhibitor bortezomib is widely used in the treatment of multiple myeloma, but its clinical success is hampered by the occurrence of resistance. Previously, we have shown that bortezomib-resistant cells rewire their glucose metabolism to divert glycolytic metabolites to biosynthetic pathways. Here, we aimed to further characterize this metabolic rewiring of bortezomib-resistant cells by using a combination of mass spectrometry-based metabolomics and proteomics.

Our data indicate that bortezomib-resistant cells have increased activity of the mitochondrial tricyclic acid (TCA) cycle and electron transport chain (ETC). We also demonstrate that BTZ-resistant cells use more glutamine to maintain TCA cycle activity, but are less dependent on extracellular glutamine for survival as compared to sensitive cells. Our data suggests that BTZ-resistant cells have activated multiple pathways to replenish the TCA cycle, underlining the importance of this pathway in BTZ-resistant cells. Using gene expression profiles, we further show that high expression of genes related to mitochondrial respiration results in lower response to BTZ in patients. Moreover, BTZ-resistant cells are more dependent on oxidative phosphorylation for ATP production and are more vulnerable to inhibition of the electron transport chain.

Overall, our data provides novel mechanistic insights in the increased mitochondrial energy production in bortezomib resistance and indicates that inhibition of oxidative phosphorylation with biguanides or simvastatin can be a novel strategy to overcome bortezemib resistance.

## INTRODUCTION

Changes in metabolism are increasingly regarded as one of the emerging hallmarks of cancer cells [1]. In addition to rapid adenosine triphosphate (ATP) production and maintenance of redox state of malignant cells, metabolic rewiring plays an important role in fulfilling the higher demand for building blocks needed for proliferation [2, 3]. For example, cancer cells have a rewired glucose metabolism and convert pyruvate preferentially into lactate instead of diverting it to the tricarboxylic acid (TCA) cycle for ATP production, a process better known as the Warburg effect [4]. In addition, cancer cells are also more dependent on nutrients such as glutamine and other amino acids as well as fatty acids [5, 6], making them more vulnerable for interference with these metabolic pathways [7, 8]. Metabolic alterations have also been shown to be involved in resistance towards chemotherapeutic agents (see chapter 1), illustrating the potential of metabolic drugs to treat chemo-resistant cancers.

The proteasome inhibitor bortezomib (BTZ) is widely used in the treatment of multiple myeloma. However, not all patients respond to BTZ and many responding patients develop resistance during the course of therapy [9, 10]. Although several mechanisms involved in BTZ-resistance are described, specific targets to overcome BTZ-resistance are still missing [11–17].

Various studies indicate that metabolic alterations play a role in the response of cells to BTZ [18–21]. Higher glycolytic activity lowers BTZ sensitivity under hypoxic conditions [18]. In a previous study, we have shown that in addition to increased glycolysis, BTZ-resistant cells use glucose to fuel the pentose phosphate pathway (PPP) and serine synthesis pathway (SSP). This metabolic rewiring of glucose metabolism is accompanied with upregulation of 3-phosphoglycerate dehydrogenase (PHGDH) in various BTZ-resistant cell lines [21]. This metabolic rewiring results in an increased antioxidant capacity, likely to protect cells from BTZ-induced oxidative stress [22, 23].

Here, we hypothesize that if BTZ-resistant cells use glucose mainly for redox metabolism, other sources must be used to generate the energy needed for proliferation. Previous studies suggest that BTZ-resistant cells have increased energy metabolism and ATP production [19, 20]. In addition, in particular carfilzomib-resistant cells seem dependent on glutamine metabolism to sustain oxidative phosphorylation (OXPHOS), at least *in vitro* [20]. However, whether and how energy metabolism can be exploited to counteract bortezomib resistance is unclear.

We further characterised the role of energy metabolism in BTZ-resistant cells by combining a targeted proteomics approach, in which we enrich for metabolic enzymes, with metabolomics and  $^{13}\text{C}$  tracer studies. Our data indicate that BTZ-

resistant cells have increased activity of the TCA cycle and electron transport chain (ETC), and that this signature also results in lower response to BTZ in multiple myeloma patients. Surprisingly, BTZ-resistant cells are less dependent on extracellular glutamine for survival as compared to sensitive cells. Instead, these cells are more vulnerable to inhibition of the ETC by phenformin and simvastatin, suggesting that inhibition of OXPHOS can be a novel strategy to overcome BTZ resistance.

## RESULTS

### **Bortezomib-resistant cells have higher activity of mitochondrial energy metabolism**

To study the metabolic alterations contributing to BTZ resistance, we compared human BTZ-sensitive wild-type (WT) to BTZ-resistant (BTZ/100) RPMI-8226 multiple myeloma cells [12] and performed liquid chromatography-mass spectrometry (LC-MS)-based proteomics and metabolomics in parallel, as detailed in Figure 1. In order to get a more comprehensive view on the metabolic alterations in BTZ-resistant cells we took a targeted proteomic approach, focussing on proteins that are involved in cellular metabolism. Since many metabolic reactions take place in membranes and mitochondria of cells, we fractionated cytosolic proteins from membrane proteins, in order to improve coverage of metabolic enzymes. A total of 7210 proteins was identified, with >5380 proteins quantified in at least 2 out of 4 biological replicates. Amongst these, 1807 proteins identified were reportedly involved in cellular metabolism, based on KEGG pathways, many of which were significantly up- or downregulated in BTZ-resistant cells (Fig. 2a). Amongst the highly upregulated metabolic proteins ( $\geq 5$ -fold) is 3-phosphoglycerate dehydrogenase (PHGDH; fold change (FC) = 6.4), which we previously associated with BTZ-resistance [21]. Also pyruvate dehydrogenase kinase 1 (PDK1) was highly upregulated in BTZ-resistant cells (FC = 8.5). By inhibiting pyruvate dehydrogenase, PDK1 regulates glucose flux into the SSP and PPP, both of which are upregulated in BTZ-resistant cells [21]. PDK1 upregulation thus confirms our previous findings. Although PDK1 inhibition with dichloroacetate (DCA) has been shown to increase sensitivity towards BTZ in (BTZ-sensitive) multiple myeloma cells [24, 25], PDK1 inhibition is not more effective in BTZ-resistant cells as compared to sensitive cells (Supplemental Fig. S1). As expected, many metabolites, involved in different metabolic pathways, were also up- or downregulated in BTZ-resistant cells (Supplemental Table. S1).

Next, differentially expressed metabolic enzymes ( $\geq 2$ -fold,  $p < 0.05$ ) were subjected to a Gene Ontology (GO) enrichment analysis. The most enriched

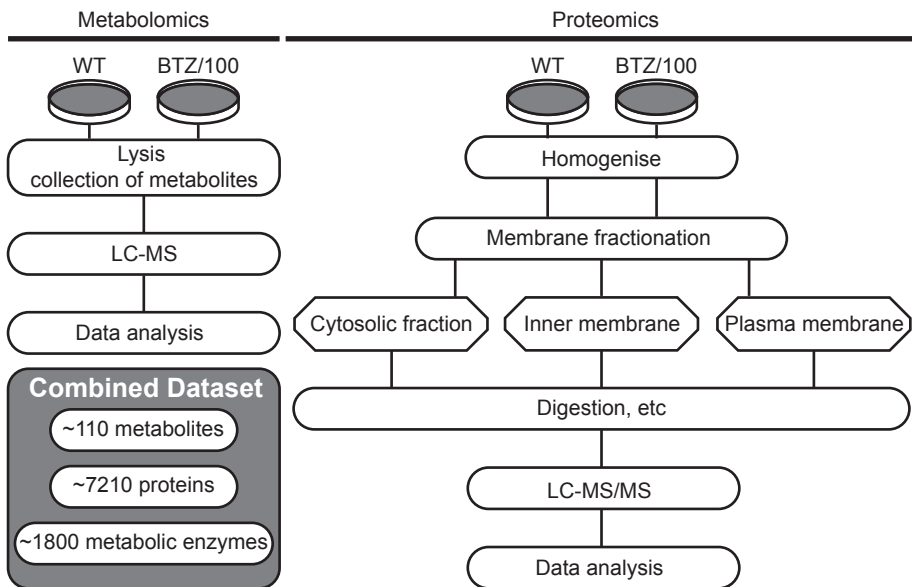


**Figure 1. Metabolomics and proteomics workflow.**

Metabolomic and proteomic characterization of RPMI-8226 wild type (WT) and bortezomib-resistant (BTZ/100) cells. Cells were suspended in RPMI medium and harvested after 2 hours and either subjected to mass spectrometry (MS) based metabolomics or –proteomics. For proteomic analysis, homogenized cell samples were fractionated in a cytosolic-, inner membrane-, and plasma membrane fraction. The inset on the bottom left corner depicts the cumulative identifications of our combined dataset.

GO term in BTZ-resistant cells was isocitrate dehydrogenase (NAD<sup>+</sup>) activity. Upregulated metabolic proteins were also associated with nicotinamide adenine dinucleotide (NAD<sup>+</sup>), oxidoreductase activity and electron carrier activity in several go terms (Fig. 2b). Both isocitrate dehydrogenase (IDH) and NAD<sup>+</sup>, together with its reduced form NADH, play important roles in cellular energy production. IDH is part of the tricarboxylic acid (TCA) cycle, which produces the NADH and FADH<sub>2</sub> that are oxidized by protein complexes (I-V) of the ETC to ultimately ATP (Fig. 3a,b) [26, 27]. Based on our previous findings [21], we hypothesized that alterations in energy metabolism are essential to sustain diversion of glucose into anti-oxidant pathways rather than to the TCA cycle.

We next mapped changes in TCA cycle metabolism on both the proteome and metabolome level. Almost all metabolic enzymes involved in the TCA cycle as well as almost all identified TCA intermediates were upregulated in BTZ-resistant cells as compared to WT cells (Fig. 3a), suggesting that the TCA cycle is more active in BTZ-resistant cells. Also most of the proteins involved in complexes I-IV as well as enzymes involved ubiquinone (Q) synthesis (COQ3,5,6,7) were upregulated in

BTZ-resistant cells (FC = 3–5) (Fig. 3b, Supplemental Table S2). The higher levels of both TCA cycle and ETC proteins suggest that BTZ-resistant cells have more capability for mitochondrial ATP production. Indeed, BTZ-resistant cells had a higher basal oxygen consumption rate (OCR) (Fig. 3c,d), as well as higher ATP-coupled respiration (the difference in OCR in the presence or absence of the ATP-synthase inhibitor oligomycin) (Fig. 3e). These findings are in line with studies on other BTZ-resistant cell lines [19, 20]. Together, these results suggest that BTZ-resistant cells have higher activity of the TCA cycle, which is coupled to higher ETC rate, resulting in increased mitochondrial ATP production.

### BTZ-resistant cells need more glutamine to sustain high TCA cycle activity

We next questioned which nutrients were preferentially used by BTZ-resistant cells to sustain the high TCA cycle rates. Many cells use glucose as one of the main sources of carbon for the TCA cycle, but as BTZ-resistant cells use glucose predominantly to fuel anti-oxidant pathways [21], these cells are likely depending on other carbon sources.

Glutamine is the main carbon source for TCA cycle in many cancerous cells, including multiple myeloma [28–30]. Glutamine is converted to glutamate by glutaminase (GLS), which is subsequently converted by transaminases (GPT2 or GOT2) or glutamate dehydrogenases (GLUD1), to form  $\alpha$ -ketoglutarate (Fig. 4a). GPT2, GOT2 and GLUD1 were all significantly upregulated in BTZ/100 cells ( $\geq 2$ -fold,  $p < 0.05$ ), suggesting that BTZ-resistant cells have higher capacity to convert

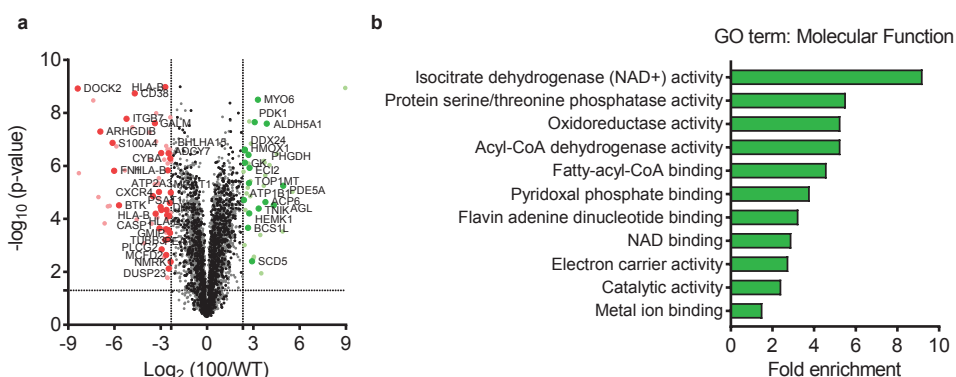


**Figure 2. Analysis of metabolic enzymes associated with bortezomib resistance.**

**a** Graphical representation of quantitative proteomics data. Proteins are ranked in volcano plot according to their statistically p-value (y-axis) and relative abundance ratio between RPMI-8226 wild type (WT) and bortezomib resistant (BTZ/100) cells (x-axis). Coloured spots represent significantly upregulated (red) or downregulated (green) proteins in BTZ/100 cells with at least a 5-fold change. Significantly regulated metabolic enzymes are marked. **b** Gene Ontology (GO) enrichment analysis of upregulated metabolic enzymes in BTZ/100 cells ( $\geq 2$ -fold,  $p < 0.05$ ).

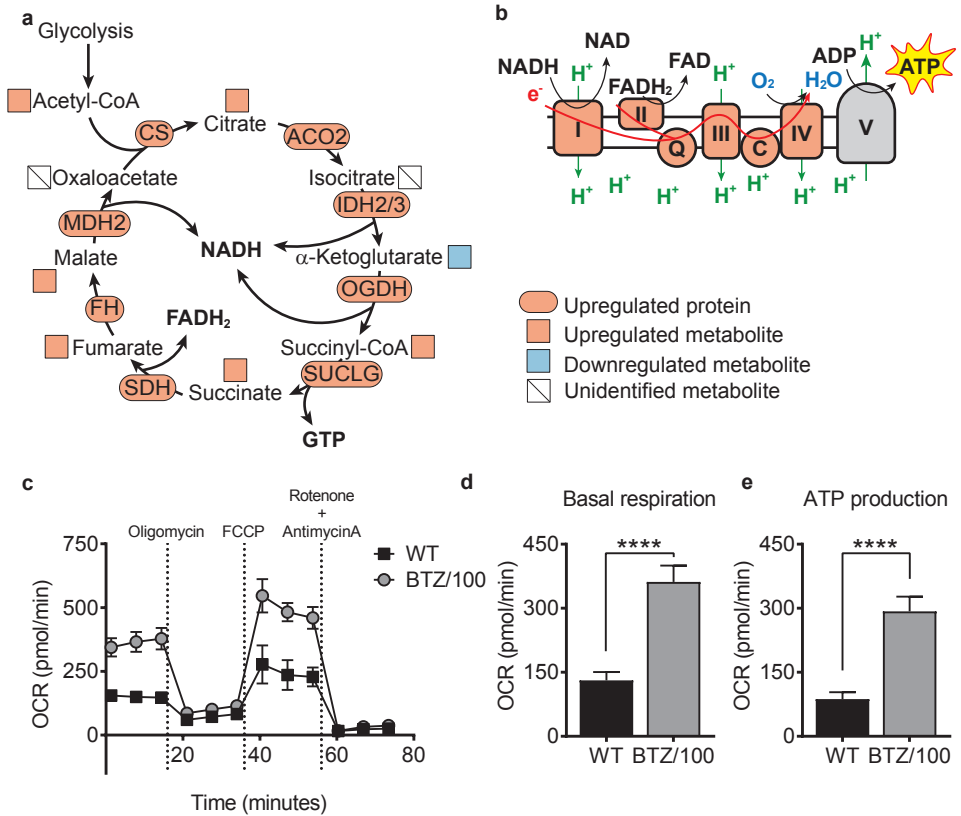


**Figure 3. Bortezomib-resistant cells have higher activity of mitochondrial energy metabolism.**

**a** Schematic overview of identified metabolites (square) and proteins (oval) involved in the TCA cycle that were significantly up- (orange) or downregulated (blue) in RPMI-8226 bortezomib-resistant (BTZ/100) cells compared to wild type (WT) cells. **b** Schematic overview of proteins involved in the electron transport chain that were significantly upregulated (orange) in RPMI-8226 bortezomib-resistant (BTZ/100) cells compared to wild type (WT) cells. **cde** WT and BTZ/100 cells were plated in XF base medium exposed to the Seahorse XF Cell Mito Stress Test, consisting of automated treatment with oligomycin, FCCP, and the combination of antimycin A and rotenone at the indicated times. The oxygen consumption rate (OCR) was measured over time using the XFe24 Analyzer (**c**). Basal OCR (**d**) and ATP production (**e**) are shown. Data are mean OCR  $\pm$  SD (n=5). One-way ANOVA tests were performed (\*\*\*\* =  $p < 0.0001$ ).

glutamate to  $\alpha$ -ketoglutarate. Analysis of cell culture medium by LC-MS revealed that BTZ-resistant cells have a higher uptake of extracellular glutamine (Fig. 4b). Together with the higher levels of TCA cycle intermediates and enzymes, these results suggest that BTZ-resistant use glutamine as the main carbon source for the production of TCA cycle intermediates.

To further test this hypothesis, we performed tracer experiments using <sup>13</sup>C-glutamine. To this end, WT and BTZ/100 cells were grown in the presence of [U-<sup>13</sup>C]-glutamine for 8h, after which the incorporation of <sup>13</sup>C-carbon from glutamine in

downstream metabolites was analysed using mass spectrometry. BTZ-resistant cells showed lower intracellular levels of total glutamine, glutamate and  $\alpha$ -ketoglutarate (Fig. 4c), which could be indicative of a fast conversion of these molecules to downstream metabolites [31]. Increased levels of TCA intermediates succinate and citrate were present in BTZ-resistant cells (Fig. 4c), suggesting that BTZ-resistant cells use glutamine to sustain a higher TCA cycle activity.

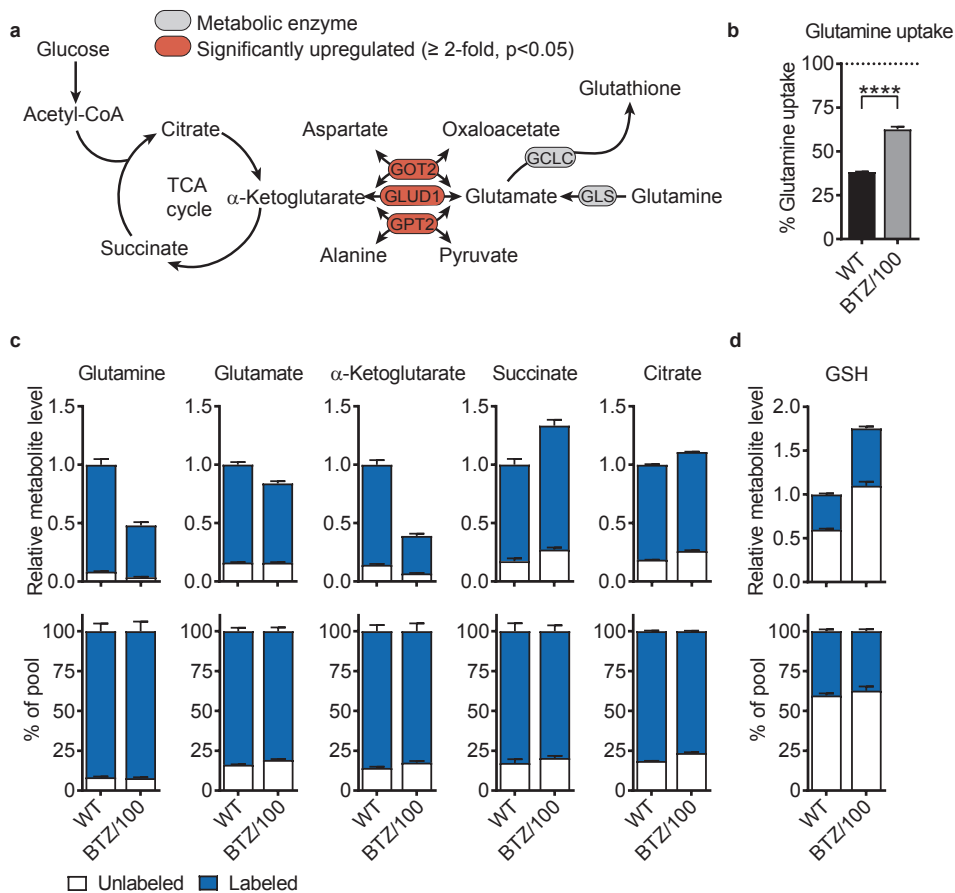


**Figure 4. BTZ-resistant cells need more glutamine to sustain high TCA cycle activity.**

**a** Schematic overview of identified metabolic enzymes involved in glutaminolysis. Metabolic enzymes that were significantly upregulated in BTZ/100 cells are depicted in orange. **b** Extracellular metabolite analysis of RPMI-8226 wild type (WT) and bortezomib resistant (BTZ/100) cells. Cells were suspended in RPMI medium containing 1mM L-glutamine. Media samples were collected after 8 hours, followed by LC-MS analysis of extracellular glutamine. Results represent uptake of glutamine as compared to cell-free media ( $n=3$ ). One-way ANOVA tests were performed (\*\*\*\* =  $p < 0.0001$ ). **cd** Intracellular analysis of TCA cycle intermediates (**c**) and GSH (**d**) of WT and BTZ/100 cells. Cells were suspended in DMEM containing 2 mM [ $U$ - $^{13}C$ ]D-Glutamine. Intracellular metabolites were extracted after 8 hours and analyzed by LC-MS. Data are means  $\pm$  SD ( $n=3$ ) of unlabelled (white) and  $^{13}C$ -labelled (blue) metabolites as compared to WT (upper panel) or as % of metabolite level (lower panel). GCLC = glutamate-cysteine ligase, GLS = glutaminase, GLUD 1 = glutamate dehydrogenase 1, GOT2 = aspartate aminotransferase, GPT2 = alanine aminotransferase 2, GSH = glutathione.



All TCA cycle metabolites were predominantly  $^{13}\text{C}$ -labelled in both WT and BTZ/100 cells (Fig 4c), confirming the importance of glutamine as a carbon source for TCA cycle in multiple myeloma cells [29, 30]. While there was no significant difference in the percentage of  $^{13}\text{C}$ -labeled intermediates, higher absolute levels of  $^{13}\text{C}$ -labeled intermediates were present in BTZ-resistant cells, especially in succinate (Fig. 4c). Together, these results indicate that glutamine is the main carbon source in both WT and BTZ/100 cells and because BTZ/100 cells have higher activity of the TCA cycle, it is likely that they need more extracellular glutamine to maintain high TCA cycle activity.

Besides the conversion to  $\alpha$ -ketoglutarate, glutamate can also be incorporated into glutathione (GSH) (Fig. 4a). Previously, we showed that BTZ-resistant have higher levels of GSH and have a higher anti-oxidant capacity [21]. Indeed, elevated levels of both  $^{12}\text{C}$  and  $^{13}\text{C}$ -GSH were found in BTZ-resistant cells (Fig. 4d), suggesting that the higher levels of GSH are, at least in part, a result of more GSH synthesis.

### **Bortezomib-resistant cells are less dependent on extracellular glutamine for survival**

Having found that BTZ-resistant cells have a higher uptake of glutamine, we tested whether BTZ-resistant cells were more dependent on extracellular glutamine for survival and cell proliferation. Withdrawal of glutamine from the cell culture medium resulted in a loss in cell growth for both BTZ-sensitive and -resistant cells (Fig. 5a). Interestingly, with 25% of glutamine left in the culture medium, WT cells showed 25% of growth inhibition, while BTZ-resistant cells showed no change in growth rate. While complete glutamine starvation stopped proliferation of both cell lines (Fig. 5a), the addition of extracellular glutamine after 24 hours of glutamine starvation restored cell proliferation of BTZ/100 cells but not of WT cells (Supplemental Fig. S2a), suggesting glutamine starvation induces a reversible growth inhibition in BTZ-resistant cells. In line with these data, cell death assays showed that WT cells underwent complete cell death within 24 hours of glutamine starvation, while less than 50% of BTZ-resistant cells died under the same conditions (Fig. 5b). OCR measurements in the presence or absence of glutamine showed that ATP production dropped severely in BTZ/100 cells under glutamine-starved conditions, confirming that glutamine is a major source for mitochondrial energy production (Fig. 5c,d). However, while WT cells have no measurable basal respiration in the absence of glutamine, the OCR of BTZ/100 cells without glutamine is comparable to the OCR of WT cells under control conditions. In addition, BTZ-resistant cells were not more sensitive to inhibition of transaminases or GLUD1. (Supplemental Fig. S2b). Together, these results show that, although BTZ-resistant cells take up more extracellular glutamine, they are less dependent

on extracellular glutamine for survival and maintain sufficient mitochondrial activity to survive.

Since glutamine is the main carbon source for the TCA cycle under normal growth conditions, we questioned how BTZ-resistant cells fuel the TCA cycle in the absence of glutamine. We performed a metabolic flux experiment using  $^{13}\text{C}$ -glucose under glutamine starved conditions. To this end, WT and BTZ/100 cells were grown for 4 hours in culture media supplemented with  $[\text{U-}^{13}\text{C}]$ -glucose in the presence or absence of glutamine (Fig. 5e). Under normal conditions, a smaller fraction of acetyl-CoA and citrate become  $^{13}\text{C}$  labelled in BTZ-resistant cells compared to

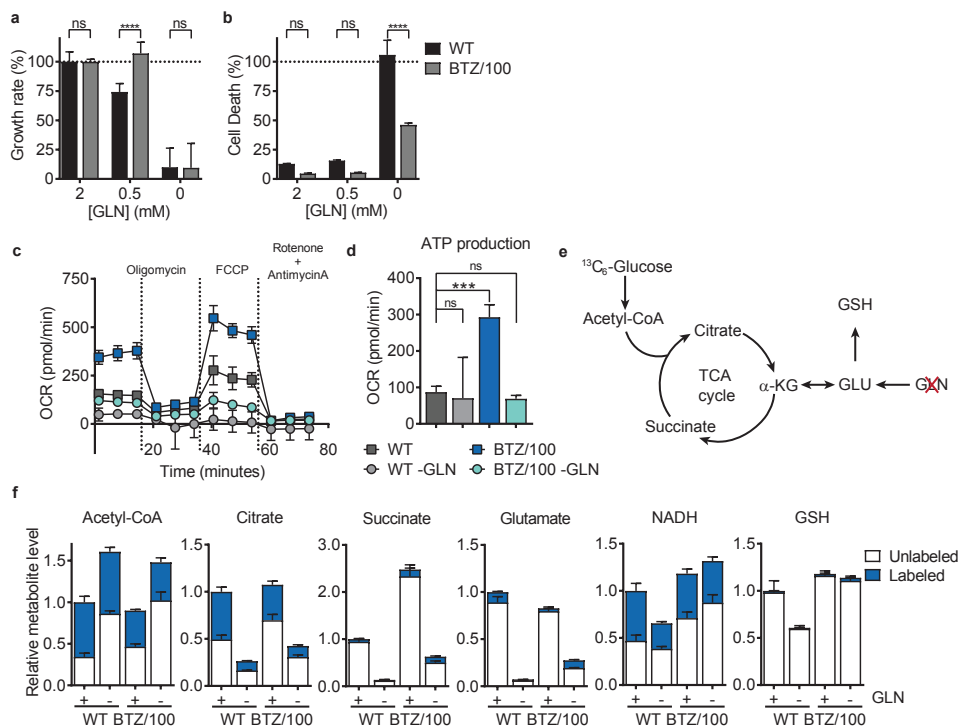


**Figure 5. Bortezomib-resistant cells are less dependent on extracellular glutamine for survival.**

**a,b** Growth rate (**a**) and cell death (**b**) of RPMI-8226 wild type (WT) and bortezomib-resistant (BTZ/100) cells after a 24-hour treatment with decreasing concentrations of glutamine (GLN) present in the culture medium. Results represent % growth rate (left panel) or % cell death (right panel)  $\pm$  SD compared to non-treated controls (n=3). **cd** Seahorse XF Cell Mito Stress Test (**c**) of WT and BTZ/100 cells and ATP production (**d**) in the presence and absence (-GLN) of extracellular glutamine, consisting of automated treatment with oligomycin, FCCP, and the combination of antimycin A and rotenone at the indicated times. Data are mean OCR  $\pm$  SD (n=5). **ef** Intracellular metabolite analysis of RPMI-8226 WT and BTZ/100 cells in the presence or absence of extracellular glutamine (**e**) Cells were grown complete medium containing 25 mM  $[\text{U-}^{13}\text{C}]$  D-glucose in the presence (+) or absence (-) of 2 mM glutamine and intracellular metabolites were extracted after 4 hours, followed by LC-MS analysis. Data are means  $\pm$  SD (n=3) of unlabelled (white) and  $^{13}\text{C}$ -labelled (blue) metabolites (**f**). Two-way ANOVA tests were performed (ns = not significant, \*\*\* =  $p < 0.001$  \*\*\*\* =  $p < 0.0001$ ). GLN = glutamine, GLU = glutamate, GSH = glutathione, ATP = adenosine triphosphate,  $\alpha$ -KG =  $\alpha$ -Ketoglutarate.

WT cells (Fig. 5f), in line with previous observations that BTZ-resistant cells divert glycolytic metabolites to biosynthetic pathways [21]. As expected, levels of TCA intermediates dropped when glutamine was depleted from the culture medium in both WT and BTZ-resistant cells. However, BTZ/100 cells maintained higher levels of TCA intermediates under glutamine-starved conditions as compared to sensitive cells. In addition, BTZ/100 cells were able to maintain their levels of NADH and GSH in the absence of glutamine, while these levels decreased in WT cells (Fig. 5f). Surprisingly, a large part of the citrate and succinate in BTZ/100 cells remained unlabelled from glucose in the absence of glutamine (Fig. 5f), suggesting that these cells can deploy sources other than glutamine and glucose to maintain the levels of TCA cycle metabolites and ETC activity.

Carbons from both fatty acids [32] and the branched chain amino acids (BCAA) leucine, isoleucine and valine [33] can also enter the TCA cycle (Fig. S3a). Almost all proteins involved in both  $\beta$ -oxidation of fatty acids and breakdown of BCAA were significantly upregulated in BTZ-resistant cells (Fig. S3b). In line with this, BTZ/100 cells displayed a higher uptake of BCAA from the culture media (Fig. S3c) as well as elevated intracellular levels of  $\alpha$ -ketoisocaproate, the first breakdown product of leucine (Fig. S3d). Together, these results suggest that both these pathways aid in sustaining mitochondrial ATP production in the absence of glutamine.

### **BTZ-resistant cells are more vulnerable to ETC inhibition**

Together, our data show that BTZ-resistant cells have more TCA cycle activity and that metabolic enzymes involved in multiple pathways surrounding the TCA cycle and ETC are upregulated in these cells. We therefore hypothesized that BTZ-resistant cells were dependent on mitochondrial respiration and more vulnerable to inhibition of the ETC compared to WT cells. To test this hypothesis, we performed cell growth assays in the presence of both phenformin, an inhibitor of complex 1 of the ETC [34], and simvastatin, a HMG-CoA reductase inhibitor that lowers ubiquinone (Q) levels [35, 36], an important coenzyme in the ETC (Fig. 6a). Phenformin was cytostatic and not cytotoxic to both cell types, but cell growth was inhibited in BTZ-resistant cells at lower concentrations than WT-cells (Fig. 6b). BTZ-resistant cells were also more sensitive to growth inhibition by simvastatin, as compared to WT cells (Fig. 6c). Interestingly, simvastatin was cytotoxic to BTZ-resistant cells, while almost no cell death was present in WT cells, even at higher concentrations (Fig. 6c). Overall, these data shows that BTZ-resistant cells are more susceptible to ETC inhibition as compared to WT cells. More importantly, these results suggest that ETC inhibitors such as phenformin and simvastatin are potent drugs to target bortezomib resistance and improve therapy.

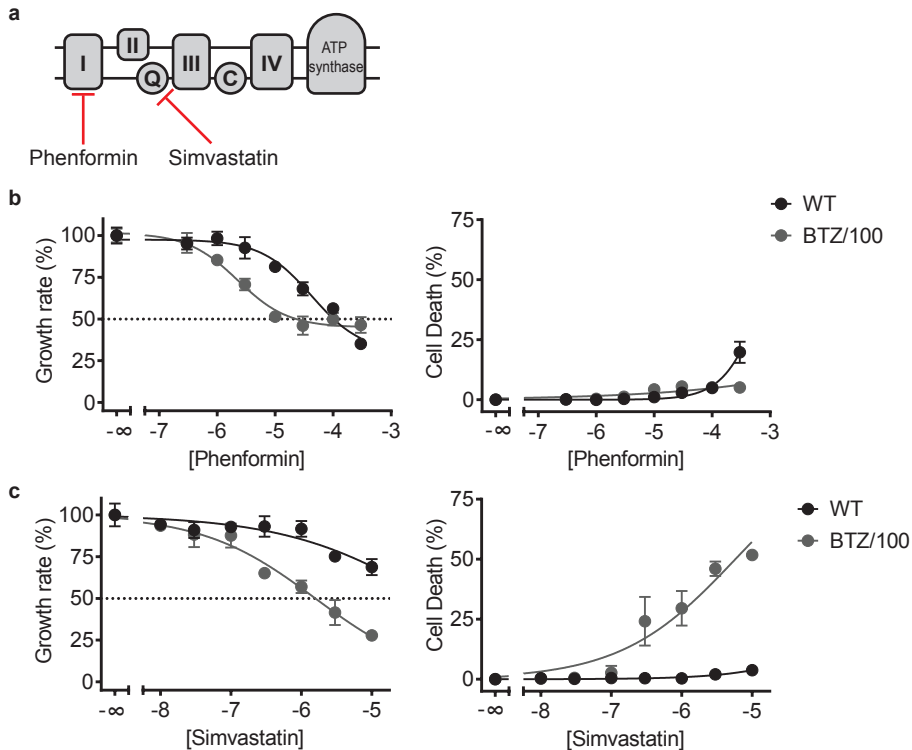


**Figure 6. BTZ-resistant cells are more vulnerable to ETC inhibition.**

**a** Schematic representation of the electron transport chain and used inhibitors. **bc** Growth rate (left panel) and cell death (right panel) of RPMI-8226 wild type (WT) and bortezomib-resistant (BTZ/100) cells after a 48-hour treatment with increasing concentrations of phenformin (**b**) or Simvastatin (**c**). Results represent % growth rate (left panel) or % cell death (right panel)  $\pm$  SD compared to non-treated controls ( $n=3$ ).

### OXPHOS gene expression in multiple myeloma patients is correlated to BTZ response

To verify if the increased activity of OXPHOS is linked to BTZ response and outcome in patients, we investigated the expression of OXPHOS-related genes in genome-wide data of 264 multiple myeloma samples from the APEX trial [37]. In this study, purified multiple myeloma samples were collected prior to treatment with BTZ (188 patients) or dexamethasone (DEX) (76 patients). For each patient, an OXPHOS expression index was defined based on the mean expression of genes involved in ETC (GO:0022904, 193 genes). This OXPHOS expression index was significantly higher in BTZ non-responders (NR) than in BTZ responding (R) patients ( $p<0.01$ ) (Fig 7a). In addition, response (ordinal progressive disease (PD) – no change (NC) – minimal response (MR) – partial response (PR) – complete response (CR)) was

proportionally associated with OXPPOS expression index (proportional odds logistic regression ( $p < 0.001$ )) (Fig 7b). The opposite effect was present in patients that were treated with DEX, indicating that high OXPPOS expression is specific for BTZ-resistance (data not shown). At the same time, the mean expression of all other genes was decreased rather than increased in BTZ non-responders (mean difference in expression index  $-0.067$ , 95%CI  $-0.122$  to  $-0.011$ ,  $p = 0.018$ ). These results indicate that patients with higher expression of ETC-related genes are more likely to be resistant to BTZ therapy, substantiating our findings in BTZ-resistant cells.

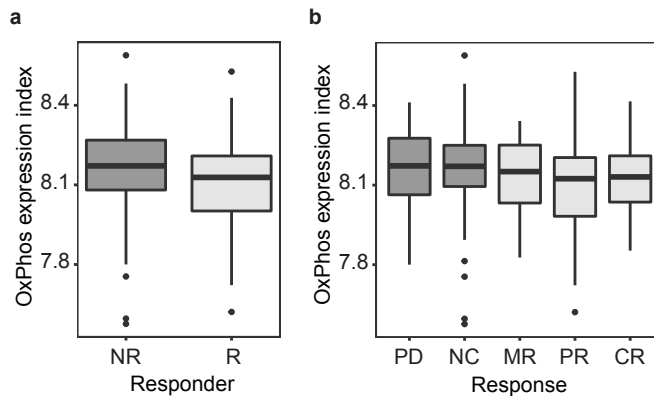


**Figure 7. Oxidative phosphorylation gene expression in multiple myeloma patients is correlated to BTZ response.**

OXPPOS expression index was defined based on the mean expression of genes involved in ETC (GO:0022904, 193 genes) in genome-wide data of 264 multiple myeloma samples. **a** OXPPOS expression index of BTZ non-responders (NR) than and BTZ responding (R) patients ( $p < 0.01$ ). **b** OXPPOS expression index of patients categorized based on response to BTZ (proportional odds logistic regression ( $p < 0.001$ )). PD = progressive disease, NC = no change, MR = minimal response PR = partial response CR = complete response

## DISCUSSION

The occurrence of resistance in BTZ treatment remains a leading problem of multiple myeloma therapy. Considering that metabolism plays an essential role in resistance against anticancer drugs, we aimed to search for metabolic pathways involved in BTZ resistance. By combining a targeted, metabolism-oriented proteomics approach with metabolomics and  $^{13}\text{C}$  tracer studies, we show that metabolic pathways enabling higher mitochondrial oxygen consumption are specifically upregulated in BTZ-resistant cells. As a result, BTZ-resistant cells were more vulnerable to inhibition of the ETC. This suggests that combination treatments of BTZ and ETC-inhibitors might be a novel strategy to treat BTZ-resistant patients. Finally, we demonstrate that

patients that do not respond to BTZ treatment have a higher expression of genes related to OXPHOS, suggesting that our findings are translatable to patients.

Previously, BTZ resistance has been linked to higher glycolytic activity [18, 21]. The higher conversion of glucose into lactate, known as the Warburg effect, has been postulated to promote cell proliferation by diverting glycolytic intermediates to pathways for biosynthesis [2]. Indeed, we previously showed that in BTZ-resistant cells glucose is used for anti-oxidant pathways that branch off from glycolysis, such as the serine synthesis pathway and pentose phosphate pathway [21]. In the targeted proteomics screen described in the current study, we also identify PDK1 as one of the highest upregulated metabolic enzyme in BTZ-resistant cells. PDK prevents pyruvate flux into the TCA cycle by phosphorylating and inhibiting pyruvate dehydrogenase, thereby promoting the use of glucose for other biosynthetic pathways. We showed that BTZ-resistant cells are not more sensitive towards the PDK1 inhibitor DCA. DCA has been shown to enhance the effect of BTZ in (BTZ-sensitive) multiple myeloma cells due to increased oxidative stress [24, 25]. Because BTZ-resistant cells have an increased antioxidant mechanism, it is expected that PDK1 inhibition does not affect BTZ-resistant cells.

The Warburg effect has been linked to impaired mitochondrial function in cancer cells [4]. However, most cancer cells that display the Warburg effect have intact mitochondrial respiration, which remains the major source for ATP production in many cancer cells, despite their higher glycolytic activity [38]. We here show that also BTZ-resistant cells have higher activity of the TCA cycle and that glutamine is the major source for TCA cycle in both BTZ-sensitive and –resistant cells, as in many cancers [28, 38]. Overall, this results in a higher consumption rate of glutamine in BTZ-resistant cells in particular. As a result of high glutamine consumption, many cancer cells are highly dependent on glutamine for survival and proliferation [28, 39]. In addition, withdrawal of glutamine from the culture media results in growth arrest and cell death of multiple myeloma cells [29, 30]. In contrast, our results show that BTZ-resistant cells are dependent on glutamine for proliferation, but do not undergo apoptosis after glutamine starvation, whilst WT cells do. Moreover, our data show that BTZ-resistant cells remain higher levels of TCA cycle intermediates and mitochondrial oxygen consumption under conditions of glutamine starvation. Surprisingly, glucose is not the major carbon source for TCA cycle intermediates under glutamine-starved conditions and most likely fatty acid oxidation and the breakdown of branched chain amino acids also contribute to the TCA flux.

A recent study showed that proteasome inhibitor-resistant cells are more sensitive to glutaminase inhibition compared to wild-type cells [20], especially in combination with carfilzomib. Notably, overexpression of the drug efflux transporter

ABCB1/P-glycoprotein, an ATP-dependent efflux pump, is an important underlying mechanism of carfilzomib resistance [19, 40]. It is therefore conceivable that carfilzomib-resistant cells are especially sensitive to the lower ATP levels that result from glutamine starvation or glutaminase inhibition. However, our data show that BTZ-resistant cells are not sensitive to glutaminase inhibition and can compensate glutamine loss by the activation of several other pathways that fuel the TCA cycle. The sensitivity to glutamine starvation or glutaminase inhibition therefore seems to be specifically associated with carfilzomib resistance, rather than a general feature of proteasome inhibitor resistant cells.

The higher activity of the TCA cycle in BTZ-resistant cells is coupled to higher mitochondrial respiration. Proteasome inhibition induces mitochondrial damage, which results in oxidative stress and eventually leads to apoptosis [41]. It is therefore likely that BTZ-resistant cells upregulate their mitochondrial activity and anti-oxidant capacity to counteract these effects. Previously, mitochondrial activity was also linked to bortezomib sensitivity in multiple myeloma cell lines [19, 20, 42]. In the current study, we show that higher gene expression of OXPHOS related genes are also found in BTZ-resistant patients, in line with others [37, 43]. Together, this shows that higher activity of mitochondrial respiration is likely to contribute to BTZ-resistance in patients.

Finally, our combined proteomics and metabolomics approach shows that this higher OXPHOS is sustained by specific metabolic alterations in BTZ-resistant cells, which can be targeted by the biguanides phenformin and simvastatin. Both phenformin and the anti-diabetic compound metformin inhibit complex 1 of the ETC and have been shown to have anticancer effects [7]. Metformin inhibits proliferation of multiple myeloma cells [44], but the current literature shows contrasting results on the enhancement of metformin on the effect of BTZ [44, 45]. More importantly, retrospective studies show that the use of biguanides is associated with better prognosis in multiple myeloma patients [46–48]. Our data suggest that this effect could be the result of increased sensitivity to proteasome inhibitor therapy in combination with complex 1 inhibition.

Simvastatin is an approved drug for the treatment of hypercholesterolaemia and is currently under investigation for cancer therapy [7, 49]. Simvastatin inhibits HMG-CoA reductase, the rate limiting step in cholesterol synthesis, which is also involved in the biosynthesis of ubiquinone [50]. Hence, statins lower the levels of ubiquinone in statin treated patients [35, 36]. Ubiquinone is an essential component of mitochondrial electron transport and simvastatin treatment lowers mitochondrial respiration and increase oxidative stress, which can be reversed by addition of ubiquinone [51, 52]. Our proteomics experiment revealed an upregulation of many

enzymes involved in ubiquinone synthesis, suggesting that simvastatin is more effective in inducing cell death in resistant compared to WT cells via its ability to lower ubiquinone levels.

In conclusion, our findings demonstrate that BTZ-resistant cells have rewired their metabolism to increase mitochondrial energy production. By performing tracer-based metabolomics and proteomics, we have identified an increased activity of the TCA cycle and surrounding pathways that are linked to BTZ resistance. Moreover, we here show that this increased TCA cycle activity is linked to higher energy production via the ETC and BTZ-resistant cells are more sensitive towards the ETC inhibitors. In addition, expression of ETC related genes is increased in BTZ non-responding patients, supporting our findings. We propose that a combination of ETC inhibition and BTZ could be a novel therapy to overcome BTZ resistance.

## METHODS

### Reagents

The proteasome activity probe Me<sub>4</sub>BodipyFL-Ahx<sub>3</sub>L<sub>3</sub>VS was a gift from Huib Ovaa (Leiden University Medical Center, The Netherlands). RPMI-8226 WT and Bortezomib-resistant cells were a kind gift from Gerrit Jansen (VU University Medical Center, Amsterdam). Bortezomib (BTZ) and carfilzomib (CFZ) were purchased from Selleck Chemicals. All solvents were obtained from Biosolve. All other chemicals were obtained from Sigma-Aldrich, unless stated otherwise.

### Cell culture

Human multiple myeloma RPMI-8226 wild type (WT) were purchased from ATCC. BTZ resistant cells were obtained as described previously [12]. Cells were maintained in suspension culture in RPMI-1640 (Lonza) medium supplemented with 2mM L-glutamine (Lonza), 10% fetal bovine serum (FBS) (Gibco) and 100µg/ml penicillin/streptomycin (Lonza) and were kept at 37°C in humidified 5% CO<sub>2</sub> atmosphere. BTZ-resistant cells were continuously cultured in the presence of 100 nM BTZ as previous described [12, 14]. Cells were cultured without drugs 4-6 days prior to experiments. Media were supplemented with 10% FBS and 100µg/ml penicillin/streptomycin unless stated otherwise.

### LC-MS based Metabolomics

For all experiments, cells were diluted in fresh medium 16-24 hours prior to the start of the experiment. At the start of all experiments, cells were counted and centrifuged



for 5 minutes at 1400 rpm to remove the old medium. For metabolic screens, cells were resuspended in fresh RPMI medium at a density of  $1 \times 10^6$  cells/ml. After 2 hours, samples were washed with PBS and harvested by centrifugation for 5 min at 1000g at 4°C. Metabolites were extracted by adding 100 – 200µl ice-cold MS lysis buffer (methanol/acetonitrile/uLCMS H<sub>2</sub>O (2:2:1)) to the cell pellets. Samples were shaken for 10 minutes at 4°C, centrifuged at 14,000g for 15 minutes at 4°C and supernatants were collected for LC-MS analysis.

<sup>13</sup>C-tracer experiments were performed as described [53, 54], with minor changes. For glutamine flux studies, cells were resuspended in DMEM containing 2 mM [U-<sup>13</sup>C] D-Glutamine (Cambridge Isotopes and harvested after 4 hours as described above. For glutamine starvation experiments, medium consisted of DMEM, supplemented with 25 mM [U-<sup>13</sup>C]D-Glucose and 10% dialyzed FBS in the presence or absence of 2 mM L-glutamine. Cells were resuspended at a density of  $0.7 \times 10^6$  in triplicate wells and were After 4 hours, cells were harvested as described above. To measure extracellular metabolites, medium samples were obtained prior to harvesting cells at 8 or 24 hours. Metabolites were extracted by diluting 10µL medium in 1mL MS lysis buffer.

Metabolites were analysed by LC-MS. LC-MS analysis was performed on an Exactive mass spectrometer (Thermo Scientific) coupled to a Dionex Ultimate 3000 autosampler and pump (Thermo Scientific). The MS operated in polarity-switching mode with spray voltages of 4.5kV and -3.5kV. Metabolites were separated on a Sequant ZIC-pHILIC column (2.1 x 150mm, 5µm, Merck) with guard column (2.1 x 20mm, 5µm, Merck) using a linear gradient of acetonitrile and a buffer containing 20mM (NH<sub>4</sub>)<sub>2</sub>CO<sub>3</sub>, 0.1% NH<sub>4</sub>OH in ULC/MS grade water. Flow rate was set at 150 µL/min. Metabolites were identified based on exact mass within 5 ppm and further validated by concordance with retention times of standards. Metabolites were quantified using LCquan software (Thermo Scientific). Peak intensities were normalized based on median peak intensity. Isotopomer distributions were corrected for natural abundance and data are plotted as relative peak area compared to WT cells under control conditions. Peak areas of identified metabolites were in their respective linear range of detection.

### **Proteomics with membrane fractionation**

RPMI-8226 WT and BTZ-resistant cells were seeded in RPMI medium at a density of  $1 \times 10^6$  cells/ml and incubated for 2 hours. Per treatment category, four biological replicates of  $3 \times 10^7$  cells were washed with PBS and harvested for fractionation using a plasma membrane isolation kit (Abcam, ab65400). Cell pellets were gently lysed on ice using a dounce homogenizer in the presence of protease inhibitor (cComplete

mini EDTA-free, Roche) and phosphatase inhibitor (PhosSTOP, Roche). Differential centrifugation according to manufacturer's instructions yielded the cytosolic fraction (CF), inner membrane (IM) and finally plasma membrane (PM). Thirty micrograms of protein each from the cytosolic, inner membrane and plasma membrane fraction were reduced in 4mM Dithiothreitol (DTT), alkylated in 8mM iodoacetamide (IAA), and digested sequentially at 37°C with 1:75 Lys C (Wako) and 1:50 Trypsin (Sigma-Aldrich) for 4 and 12 hours respectively. Digested peptides were acidified to 0.1% formic acid (FA) and purified by strong cation exchange (SCX) STAGE tips. Eluted peptides were dried by vacuum and 2µg equivalent of peptides was analysed in each 3hr reverse phase separation on the UHPLC 1290 system (Agilent) coupled to an Orbitrap Q Exactive Plus mass spectrometer (Thermo Scientific).

### **RP-nanoLC-MS/MS**

Proteomics data were acquired using an UHPLC 1290 system (Agilent) coupled to an Orbitrap Q Exactive Plus mass spectrometer (Thermo Scientific). Peptides were first trapped on a 2 cm x 100 µm Reprosil C18 pre-column (3 µm) and then separated on a 50 cm x 75 µm Poroshell EC-C18 analytical column (2.7 µm). Trapping was performed for 5 min in 0.1 M acetic acid (Solvent A) and elution with 80% ACN in 0.1M acetic acid (Solvent B) in gradients as follows: 10-36% solvent B in 155 min, 36-100% in 3min and finally 100% for 1min. Flow was passively split to 300 nL/min. MS data were obtained in data-dependent acquisition mode. Full scans were acquired in the  $m/z$  range of 375-1600 at the resolution of 35,000 ( $m/z$  400) with AGC target 3E6. Top 15 most intense precursor ions were selected for HCD fragmentation performed at NCE 25% after accumulation to target value of 5E4. MS/MS acquisition was performed at a resolution of 17,500.

### **Database search**

Raw files were processed using MaxQuant version 1.5.3.30 and searched against the human Swissprot database (version Jan 2016, 147933 entries) using Andromeda. Cysteine carbamidomethylation was set to fixed modification, while variable modifications of methionine oxidation and protein N-terminal acetylation, as well as up to 2 missed cleavages were allowed. False discovery rate (FDR) was restricted to 1% in both protein and peptide identification. Label-free quantification (LFQ) was performed with "match between runs" enabled.

### **Extracellular flux analysis**

Extracellular flux analysis was performed using a Seahorse Bioscience XFe24 Analyzer. RPMI-8226 WT and BTZ-resistant cells were resuspended at a density of 1

$\times 10^6$  cells / ml in Seahorse XF Base medium (Seahorse Bioscience), supplemented with 25mM glucose and 1M NaOH, in the presence or absence of 2mM L-glutamine.  $1 \times 10^6$  cells (100  $\mu$ L) were added to 5 wells of XF24 cell culture microplates (Seahorse Bioscience). After 30 minutes, microplates were centrifuged at 400 rpm to ensure cells were adhered to the bottom of the plates. 425  $\mu$ L of corresponding media was added and cells were incubated for 60 min at 37 °C. The oxygen consumption rate (OCR) in pmol  $O_2$ /min was measured in triplicate at basal conditions, and after the injection of 1  $\mu$ M oligomycin, 0.1 $\mu$ M FCCP and 2  $\mu$ M of Rotenone and Antimycin A after 18, 36 and 54 min, respectively. After injections, measurements of 3 min were performed in triplicate, preceded by 1 min of mixture time and 2 min waiting time.

### **Cell viability and cell growth assays**

Cells were suspended in triplicate at a density of  $2-5 \times 10^5$  cells/ml in RPMI-1640 medium in 96-well plates and incubated with drugs at the indicated concentrations for 24-48 hours. Cell growth was monitored continuously with the IncuCyte live-cell imager system (Essen Instruments). Images were acquired every 2 hours for 1-2 days, and analysed using the IncuCyte Zoom software (Essen Instruments). Cell growth was defined as population doublings per 48 hours and calculated based on increased confluence.

Cell death was assessed after 24-48 hours by incubating each well with 30  $\mu$ M propidium iodide and measuring fluorescence after 15 minutes using the IncuCyte instrument. Cell death was calculated based on the area of the fluorescent signal, normalized to confluency of the wells.

### **Gene expression analysis**

Gene expression profiles were analysed from a dataset downloaded from Gene Expression Omnibus with accession number GSE9782 [37]. In this study, purified multiple myeloma samples were collected prior to treatment with BTZ (188 patients) or dexamethasone (DEX) (76 patients). Patients were classified based on their response to therapy: complete response (CR), partial response (PR), minimal response (MR), no change (NC), or progressive disease (PD) [37]. For each patient, an OXPHOS expression index was defined based on the mean expression of genes involved in ETC (GO:0022904, 193 genes).

### **Acknowledgements**

CRB was supported by VENI grant (project 722.013.009) from the Netherlands Organization for Scientific Research (NWO). The authors would like to thank Gerrit

Jansen for providing BTZ-resistant cell lines and Anna Hoekstra for assistance in proteomic data analysis.

**Author contributions**

CRB and EAZ developed this study, designed the experiments and wrote the manuscript. EAZ, PL, HB and WW performed the experiments. EAZ, WW and CRB performed data analysis and interpretation. MM and BMB contributed to extracellular flux analyses. HJdG performed gene expression analysis.

## REFERENCES

1. Hanahan D, Weinberg RA. Hallmarks of cancer: The next generation. *Cell*. 2011;144:646–74.
2. Vander Heiden MG, Cantley LC, Thompson CB. Understanding the Warburg effect: the metabolic requirements of cell proliferation. *Science*. 2009;324:1029–33.
3. Cairns RA, Harris IS, Mak TW. Regulation of cancer cell metabolism. *Nat Rev Cancer*. 2011;11:85–95.
4. Warburg O. On the Origin of Cancer Cells. *Science* (80- ). 1956;123:309–14.
5. DeBerardinis RJ, Chandel NS. Fundamentals of cancer metabolism. *Sci Adv*. 2016;2:e1600200.
6. Vander Heiden MG, DeBerardinis RJ. Understanding the Intersections between Metabolism and Cancer Biology. *Cell*. 2017;168:657–69.
7. Galluzzi L, Kepp O, Vander Heiden MG, Kroemer G. Metabolic targets for cancer therapy. *Nat Rev Drug Discov*. 2013;12:829–46.
8. Vander Heiden MG. Targeting cancer metabolism: A therapeutic window opens. *Nat Rev Drug Discov*. 2011;10:671–84.
9. Anderson KC. The 39th David A. Karnofsky Lecture: bench-to bedside translation of targeted therapies in multiple myeloma. *J Clin Oncol*. 2012;30:445–52.
10. Orlowski RZ, Kuhn DJ. Proteasome inhibitors in cancer therapy: Lessons from the first decade. *Clin Cancer Res*. 2008;14:1649–57.
11. Oerlemans R, Franke NE, Assaraf YG, Cloos J, van Zantwijk I, Berkers CR, et al. Molecular basis of bortezomib resistance: proteasome subunit beta5 (PSMB5) gene mutation and overexpression of PSMB5 protein. *Blood*. 2008;112:2489–99.
12. Franke NE, Niewerth D, Assaraf YG, van Meerloo J, Vojtekova K, van Zantwijk CH, et al. Impaired bortezomib binding to mutant  $\beta 5$  subunit of the proteasome is the underlying basis for bortezomib resistance in leukemia cells. *Leukemia*. 2012;26:757–68.
13. de Wilt LHAM, Jansen G, Assaraf YG, van Meerloo J, Cloos J, Schimmer AD, et al. Proteasome-based mechanisms of intrinsic and acquired bortezomib resistance in non-small cell lung cancer. *Biochem Pharmacol*. 2012;83:207–17.
14. Rückrich T, Kraus M, Gogel J, Beck A, Ovaa H, Verdoes M, et al. Characterization of the ubiquitin-proteasome system in bortezomib-adapted cells. *Leukemia*. 2009;23:1098–105.
15. Balsas P, Galán-Malo P, Marzo I, Naval J. Bortezomib resistance in a myeloma cell line is associated to PSM $\beta 5$  overexpression and polyploidy. *Leuk Res*. 2012;36:212–8.
16. Niewerth D, Kaspers GJL, Jansen G, van Meerloo J, Zweegman S, Jenkins G, et al. Proteasome subunit expression analysis and chemosensitivity in relapsed paediatric acute leukaemia patients receiving bortezomib-containing chemotherapy. *J Hematol Oncol*. 2016;9:82.
17. Driessen C, Kraus M, Joerger M, Rosing H, Bader J, Hitz F, et al. Treatment with the HIV protease inhibitor nelfinavir triggers the unfolded protein response and may overcome proteasome inhibitor resistance of multiple myeloma in combination with bortezomib: a phase I trial (SAKK 65/08). *Haematologica*. 2016;101:346–55.
18. Maiso P, Huynh D, Moschetta M, Sacco A, Aljawai Y, Mishima Y, et al. Metabolic signature identifies novel targets for drug resistance in multiple myeloma. *Cancer Res*. 2015;75:2071–82.
19. Soriano GP, Besse L, Li N, Kraus M, Besse A, Meeuwenoord N, et al. Proteasome inhibitor-adapted myeloma cells are largely independent from proteasome activity and show complex proteomic changes, in particular in redox and energy metabolism. *Leukemia*. 2016;30:2198–207.
20. Thompson RM, Dytfeld D, Reyes L, Robinson RM, Smith B, Manevich Y, et al. Glutaminase inhibitor CB-839 synergizes with carfilzomib in resistant multiple myeloma cells. 2017;8:35863–76.
21. Zaal EA, Wu W, Jansen G, Zweegman S, Cloos J, Berkers CR. Bortezomib resistance in multiple myeloma is associated with increased serine synthesis. *Cancer Metab*. 2017;5:7.
22. Lipchick BC, Fink EE, Nikiforov MA. Oxidative stress and proteasome inhibitors in multiple myeloma. *Pharmacol Res*. 2016;105:210–5.
23. Du Z-X, Zhang H-Y, Meng X, Guan Y, Wang H-Q. Role of oxidative stress and intracellular glutathione in the sensitivity to apoptosis

- induced by proteasome inhibitor in thyroid cancer cells. *BMC Cancer*. 2009;9:56.
24. Sanchez WY, McGee SL, Connor T, Mottram B, Wilkinson A, Whitehead JP, et al. Dichloroacetate inhibits aerobic glycolysis in multiple myeloma cells and increases sensitivity to bortezomib. *Br J Cancer*. 2013;108:1624–33.
  25. Fujiwara S, Kawano Y, Yuki H, Okuno Y, Nosaka K, Mitsuya H, et al. PDK1 inhibition is a novel therapeutic target in multiple myeloma. *Br J Cancer*. 2013;108:170–8.
  26. Nicholls DG, Budd SL. Mitochondria and neuronal survival. *Physiol Rev*. 2000;80:315–60.
  27. Pavlova NN, Thompson CB. The Emerging Hallmarks of Cancer Metabolism. *Cell Metab*. 2016;23:27–47.
  28. DeBerardinis RJ, Mancuso A, Daikhin E, Nissim I, Yudkoff M, Wehrli S, et al. Beyond aerobic glycolysis: transformed cells can engage in glutamine metabolism that exceeds the requirement for protein and nucleotide synthesis. *Proc Natl Acad Sci U S A*. 2007;104:19345–50.
  29. Bolzoni M, Chiu M, Accardi F, Vescovini R, Airolidi I, Storti P, et al. Dependence on glutamine uptake and glutamine addiction characterize myeloma cells: a new attractive target. *Blood*. 2016;128:667–79.
  30. Bajpai R, Matulis SM, Wei C, Nooka AK, Von Hollen HE, Lonial S, et al. Targeting glutamine metabolism in multiple myeloma enhances BIM binding to BCL-2 eliciting synthetic lethality to venetoclax. *Oncogene*. 2016;35:3955–64.
  31. Labuschagne CF, van den Broek NJF, Mackay GM, Vousden KH, Maddocks ODK. Serine, but not glycine, supports one-carbon metabolism and proliferation of cancer cells. *Cell Rep*. 2014;7:1248–58.
  32. Carracedo A, Cantley LC, Pandolfi PP. Cancer metabolism: fatty acid oxidation in the limelight. *Nat Rev Cancer*. 2013;13:227–32.
  33. Mayers JR, Torrence ME, Danai L V, Papagiannakopoulos T, Davidson SM, Bauer MR, et al. Tissue of origin dictates branched-chain amino acid metabolism in mutant Kras-driven cancers. *Science*. 2016;353:1161–5.
  34. Bridges HR, Jones AJY, Pollak MN, Hirst J. Effects of metformin and other biguanides on oxidative phosphorylation in mitochondria. *Biochem J*. 2014;462:475–87.
  35. Mabuchi H, Higashikata T, Kawashiri M, Katsuda S, Mizuno M, Nohara A, et al. Reduction of serum ubiquinol-10 and ubiquinone-10 levels by atorvastatin in hypercholesterolemic patients. *J Atheroscler Thromb*. 2005;12:111–9.
  36. Passi S, Stancato A, Aleo E, Dmitrieva A, Littarru GP. Statins lower plasma and lymphocyte ubiquinol/ubiquinone without affecting other antioxidants and PUFA. *Biofactors*. 2003;18:113–24.
  37. Mulligan G, Mitsiades C, Bryant B, Zhan F, Chng WJ, Roels S, et al. Gene expression profiling and correlation with outcome in clinical trials of the proteasome inhibitor bortezomib. *Blood*. 2007;109:3177–88.
  38. Fan J, Kamphorst JJ, Mathew R, Chung MK, White E, Shlomi T, et al. Glutamine-driven oxidative phosphorylation is a major ATP source in transformed mammalian cells in both normoxia and hypoxia. *Mol Syst Biol*. 2013;9:712.
  39. Wise DR, Thompson CB. Glutamine addiction: a new therapeutic target in cancer. *Trends Biochem Sci*. 2010;35:427–33. doi:10.1016/j.tibs.2010.05.003.
  40. Verbrugge SE, Assaraf YG, Dijkmans B A C, Scheffer GL, Al M, den Uyl D, et al. Inactivating PSMB5 mutations and P-glycoprotein (multidrug resistance-associated protein/ATP-binding cassette B1) mediate resistance to proteasome inhibitors: ex vivo efficacy of (immuno)proteasome inhibitors in mononuclear blood cells from patients with rheumatoid arthritis. *J Pharmacol Exp Ther*. 2012;341:174–82.
  41. Maharjan S, Oku M, Tsuda M, Hoseki J, Sakai Y. Mitochondrial impairment triggers cytosolic oxidative stress and cell death following proteasome inhibition. *Sci Rep*. 2014;4:5896.
  42. Song IS, Kim HK, Lee SR, Jeong SH, Kim N, Ko KS, et al. Mitochondrial modulation decreases the bortezomib-resistance in multiple myeloma cells. *Int J cancer*. 2013;133:1357–67.
  43. Zhan X, Yu W, Franqui-machin R, Bates ML, Nadiminti K, Cao H, et al. Alteration of mitochondrial biogenesis promotes disease progression in multiple myeloma. *Oncotarget*. 2017;8:11213–24.
  44. Zi FM, He JS, Li Y, Wu C, Yang L, Yang Y, et al. Metformin displays anti-myeloma activity and synergistic effect with dexamethasone in

- in vitro and in vivo xenograft models. *Cancer Lett.* 2015;356:443–53.
45. Jagannathan S, Abdel-Malek MAY, Malek E, Vad N, Latif T, Anderson KC, et al. Pharmacologic screens reveal metformin that suppresses GRP78-dependent autophagy to enhance the anti-myeloma effect of bortezomib. *Leukemia.* 2015;29:2184–91.
  46. Wu W, Merriman K, Nabaah A, Seval N, Seval D, Lin H, et al. The association of diabetes and anti-diabetic medications with clinical outcomes in multiple myeloma. *Br J Cancer.* 2014;111:628–36.
  47. Chang S-H, Luo S, O'Brian KK, Thomas TS, Colditz GA, Carlsson NP, et al. Association between metformin use and progression of monoclonal gammopathy of undetermined significance to multiple myeloma in US veterans with diabetes mellitus: a population-based retrospective cohort study. *Lancet Haematol.* 2015;2:e30-6.
  48. Boursi B, Mamtani R, Yang Y-X, Weiss BM. Impact of metformin on the progression of MGUS to multiple myeloma. *Leuk Lymphoma.* 2017;58:1265–7.
  49. Martinez-Outschoorn UE, Peiris-Pagés M, Pestell RG, Sotgia F, Lisanti MP. Cancer metabolism: a therapeutic perspective. *Nat Rev Clin Oncol.* 2017;14:11–31.
  50. Mullen PJ, Yu R, Longo J, Archer MC, Penn LZ. The interplay between cell signalling and the mevalonate pathway in cancer. *Nat Rev Cancer.* 2016;16:718–31.
  51. Vaughan RA, Garcia-Smith R, Bisoffi M, Conn CA, Trujillo KA. Ubiquinol rescues simvastatin-suppression of mitochondrial content, function and metabolism: implications for statin-induced rhabdomyolysis. *Eur J Pharmacol.* 2013;711:1–9.
  52. Kettawan A, Takahashi T, Kongkachuichai R, Charoenkiatkul S, Kishi T, Okamoto T. Protective effects of coenzyme q(10) on decreased oxidative stress resistance induced by simvastatin. *J Clin Biochem Nutr.* 2007;40:194–202.
  53. Maddocks ODK, Berkers CR, Mason SM, Zheng L, Blyth K, Gottlieb E, et al. Serine starvation induces stress and p53-dependent metabolic remodelling in cancer cells. *Nature.* 2013;493:542–6.
  54. Buescher JM, Antoniewicz MR, Boros LG, Burgess SC, Brunengraber H, Clish CB, et al. A roadmap for interpreting (13)C metabolite labeling patterns from cells. *Curr Opin Biotechnol.* 2015;34:189–201.

## SUPPLEMENTAL

Supplemental Table S1. Intracellular metabolite levels of bortezomib-sensitive and –resistant cells

Metabolite	WT (peak area)	BTZ/100 (peak area)	FC (BTZ/100:WT)
PHE	40483886	70383949	1.74
LEU	99351203	171669537	1.73
ILE	116798970	173437399	1.48
MET	28441323	47911014	1.68
TRP	5179828	11562706	2.23
VAL	50051115	71195125	1.42
PRO	1269420514	1872845564	1.48
TYR	19833998	33170402	1.67
THR	50214151	60816653	1.21
ALA	41707335	56940642	1.37
GLN	323834368	302057164	0.93
ASN	15680953	19594539	1.25
b-ALA	53166314	34283584	0.64
GLU	190644339	159763437	0.84
GLY	3048247	5037437	1.65
SER	9014892	10064065	1.12
ASP	24675090	14497570	0.59
HIS	3661789	6629239	1.81
LYS	987508	1243628	1.26
ARG	47041878	55269962	1.17
4-Methyl-2-Oxopentanoate	1129599	2100190	1.86
4-Hydroxyphenylpyruvate	18384	18360	1.00
Kynurenine	118714	227003	1.91
Trimethyllysine	998936	1062859	1.06
Dimethyllysine	347166	452659	1.30
ADMA	1492278	1770845	1.19
NMMA	37775	39692	1.05
Monomethyllysine	2277906	3433537	1.51
Pyruvate	1144568	479663	0.42
Lactate	48582141	66144955	1.36
Glucose	2097398	1277711	0.61
Dihydroxyacetone3P	234845	138967	0.59
HexP	1381259	255914	0.19
Glyceraldehyde3P	838805	1438254	1.71
2P-glycerate	1316879	736127	0.56
G6P	209011	81107	0.39
PEP	163843	142209	0.87
Fructose16bisP	240866	204708	0.85
Erythrose4P	15828	4404	0.28
Ribulose5P	104033	102496	0.99
Sedoheptulose7P	126155	204297	1.62
6P-gluconate	20312	12621	0.62
AcetylCoA	884503	1111638	1.26
GABA	35157365	35858355	1.02
Succinate	7349456	11044334	1.50
a-Ketoglutarate	33505207	13436038	0.40
Malate	85535143	127303657	1.49
SuccinylCoA	100585	127566	1.27
cis-Aconitate	2839238	3826322	1.35
Citrate	71738411	84370508	1.18
Creatinine	41207592	55703707	1.35
Creatine	532323387	604782449	1.14
n-Acetylglutamate	520865	377502	0.72
Citrulline	437993	336138	0.77



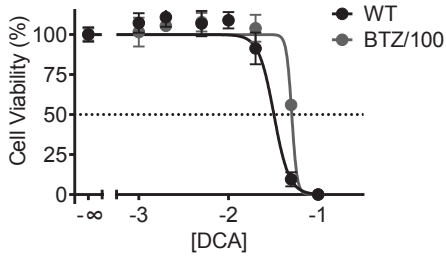
Supplemental Table S1. Continued

Metabolite	WT (peak area)	BTZ/100 (peak area)	FC (BTZ/100:WT)
Fumarate	6050046	9293370	1.54
Ornithine	1643711	2122029	1.29
N-Ac-Glucosamine	144497	161487	1.12
N-Ac-Glucosamine-6P	64180	56470	0.88
UDP-N-Ac-Glucosamine	37150969	44144593	1.19
Nicotinamide	24275863	12564413	0.52
Betaine	110589462	226906111	2.05
Cystine	200731	403284	2.01
S-Adenosyl-Methionine	432025	452619	1.05
Choline	26690938	17490873	0.66
Cystathionine	176857	235197	1.33
8-oxo-guanine	720674	616329	0.86
NADH	2431412	4518373	1.86
Glutathione	95077069	126351845	1.33
NAD+	14542206	22706009	1.56
NADP+	157618	187177	1.19
NADPH	1020547	1160754	1.14
GSSG	274234	624795	2.28
Adenosine	193092	640977	3.32
Adenine	295682	420854	1.42
cAMP	397102	51644	0.13
Inosine	16178	41779	2.58
AMP	1243779	1029065	0.83
IMP	63554	41203	0.65
GMP	130522	98611	0.76
Orotate	793525	1099297	1.39
Uracil	162784	226592	1.39
Dihydroorotate	119358	78820	0.66
Cytidine	53373	152940	2.87
UMP	336478	333554	0.99
CMP	64531	59823	0.93
N-Carbamoyl-aspartate	85801	90380	1.05
16.0Palmitoyl-L-carnitine	330144	406163	1.23
18.0Stearoyl-L-carnitine	212315	258563	1.22
18.1Oleoyl-L-carnitine	288380	427369	1.48
14.0Myristoyl-L-carnitine	228446	178589	0.78
6.0Hexanoyl-L-carnitine	768434	424522	0.55
4.0Butyryl-L-carnitine	78982188	196888508	2.49
3-HydroxybutanoicAcid(BHBA)	63629	163833	2.57
3.0Propionyl-L-carnitine	19316333	53089991	2.75
Glycerol	2468891	2589675	1.05
2.0Acetyl-L-Carnitine	72403538	245007714	3.38
FAD(adhH-1)	347226	421890	1.22
L-Carnitine	282143694	475940294	1.69
Glycerol-3P	1917625	21444249	11.18
HMG-CoA	6490	4787	0.74
Niacinamide	26696226	13736089	0.51
Pyridoxin	6922439	7419442	1.07
Pantothenate	19748364	19066585	0.97
Biotin	1409251	485362	0.34
Riboflavin	51822	49870	0.96
Inositol	4047506	3208269	0.79
Thiamine	3962380	10650657	2.69
Folic acid	16975	10887	0.64

**Supplemental Table S2.** Proteins involved in oxidative phosphorylation

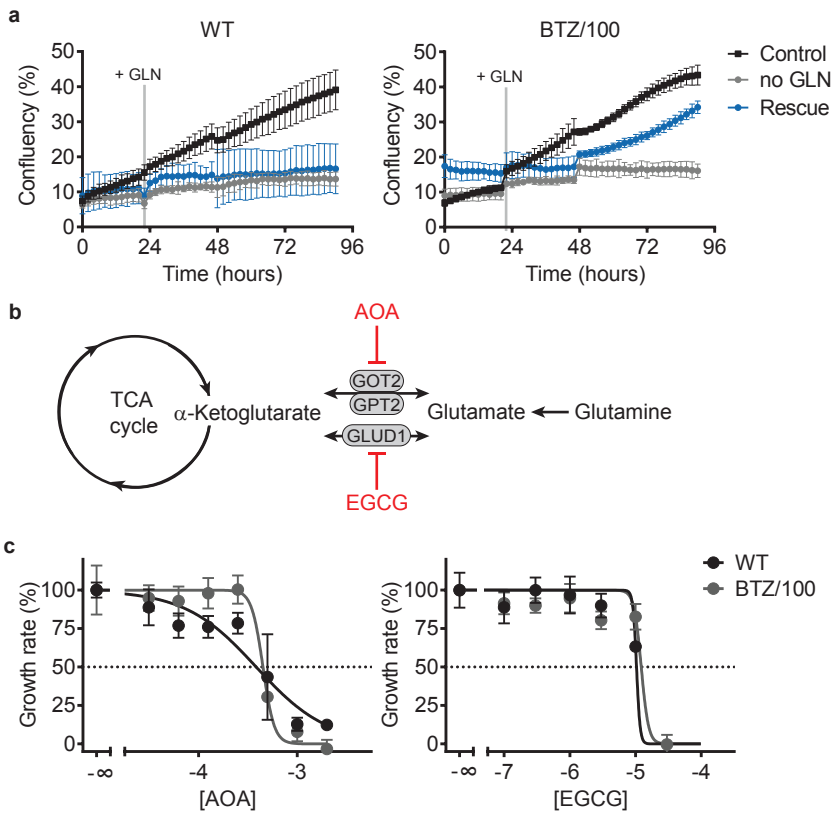
Complex I			Complex II		
Gene name	BTZ/100 : WT	FC	Gene name	BTZ/100 : WT	FC
NDUFA10	1.528867	*	SDHA	1.7083014	*
NDUFA11	1.703058	*	SDHD	0.9231727	
NDUFA12	1.282812	*	<b>Complex III</b>		
NDUFA13	1.781574	*	CYC1	1.640397	*
NDUFA2	1.652314	*	UQCR10	1.0984297	
NDUFA5	1.80498	*	UQCRB	1.6849432	*
NDUFA6	1.383658	*	UQCRC1	1.6692847	*
NDUFA7	1.51635	*	UQCRC2	1.6448289	*
NDUFA8	1.344293	*	UQCRFS1	2.3798366	*
NDUFA9	1.603948	*	UQCRH	2.1174861	*
NDUFAB1	2.207697	*	UQCRQ	1.409609	*
NDUFAF1	1.472125	*	<b>Complex IV</b>		
NDUFB1	2.439909	*	COX15	1.8899231	*
NDUFB10	1.582346	*	COX4I1	1.6397092	*
NDUFB11	1.32969	*	COX5A	1.5931918	*
NDUFB2	1.001866		COX5B	1.8057116	*
NDUFB3	1.463926	*	COX6B1	2.1825996	*
NDUFB4	1.415444	*	COX6C	1.6313344	*
NDUFB5	1.416075	*	COX7A2L	2.0403972	*
NDUFB6	1.52835		COX7C	2.3325249	*
NDUFB7	1.787651	*	NDUFA4	2.6567316	*
NDUFB8	1.936062	*	<b>ATP-synthase</b>		
NDUFB9	1.766737	*	ATP5C1	1.3356898	*
NDUFC1	1.14072		ATP5D	1.4557827	*
NDUFC2	1.353474	*	ATP5E	0.577633	
NDUFS1	1.417631	*	ATP5O	1.1317929	
NDUFS2	1.961235	*	ATP6AP1	0.7176091	*
NDUFS3	1.482105	*	ATP6V0C	0.3518177	*
NDUFS4	1.683434	*	<b>Q-synthesis</b>		
NDUFS5	1.536556	*	COQ3	2.7543034	*
NDUFS6	1.50231	*	COQ5	4.1320279	*
NDUFS7	1.63212	*	COQ6	4.6771348	*
NDUFS8	1.908845	*	COQ7	4.3295362	*
NDUFV1	1.659234	*			
NDUFV2	1.23852	*			
NDUFV3	2.166648				

Metabolic enzymes that are upregulated in RPMI-8226 BTZ/100 cells compared to WT cells  
 \* = p<0.05 based on Student's T-Test



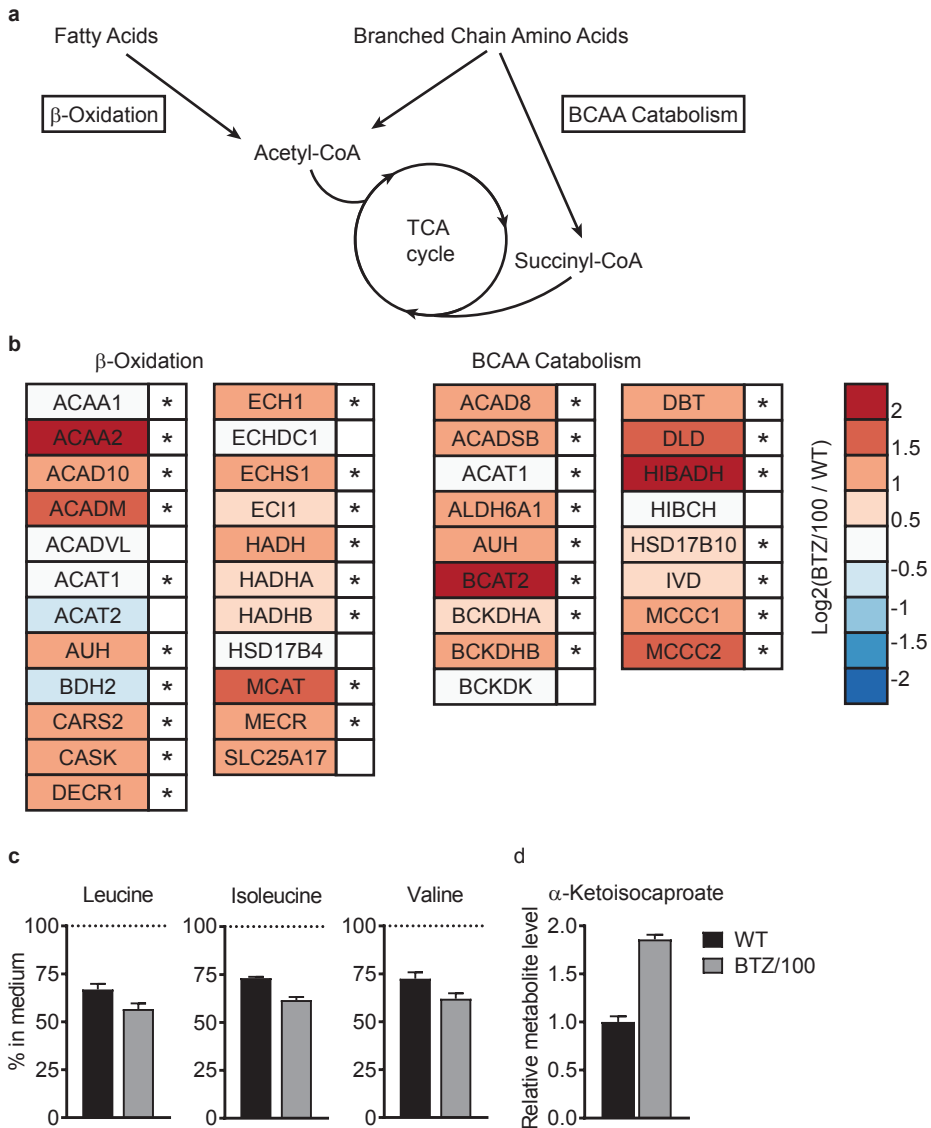
**Supplemental figure S1. Inhibition of PDK1 in bortezomib-sensitive and -resistant cells.**

Cell viability of RPMI-8226 wild type (WT) and bortezomib-resistant (BTZ/100) cells after a 48-hour treatment with increasing concentrations of DCA. Results represent % cell viability  $\pm$  SD compared to non-treated controls (n=3).



**Supplemental figure S2. Bortezomib-resistant cells are less dependent on extracellular glutamine for survival.**

**a** Confluency of RPMI-8226 wild type (WT) (left panel) and bortezomib-resistant (BTZ/100) (right panel) cells followed over time in the presence (black) or absence (grey) of glutamine (GLN). Glutamine was added after 24 hours in cells that were starved for glutamine (blue). Results represent % of confluence (n=3). **b** Schematic representation of the TCA cycle and glutaminolysis inhibitors (upper panel). **c** Growth rate of WT and BTZ/100 cells after a 48-hour treatment with increasing concentrations of aminooxyacetic acid (AOA) (left panel) and Epigallocatechin gallate (EGCG) (right panel). Results represent % growth rate  $\pm$  SD compared to non-treated controls (n=3). AOA = aminooxyacetic acid, EGCG = Epigallocatechin gallate, GLUD 1 = glutamate dehydrogenase 1, GOT2 = aspartate aminotransferase, GPT2 = alanine aminotransferase 2.



**Supplemental figure S3. Bortezomib-resistant cells have higher levels of proteins involved in  $\beta$ -oxidation and BCAA catabolism.**

**a** Schematic overview of pathways. **b** Heatmap of identified proteins involved in  $\beta$ -oxidation (GO:0006635) and BCAA catabolism (GO:0009083). The colour indicates the amount of up- (red) or down (blue) regulation of the proteins in BTZ/100 cells as compared to sensitive cells. Proteins that were significantly regulated are marked with \*. **c** Extracellular analysis of leucine, isoleucine and valine in RPMI-8226 wild type (WT) and bortezomib resistant (BTZ/100) cells. Cells were suspended in RPMI medium containing 1mM L-glutamine. Media samples were collected after 8 hours, followed by LC-MS analysis. Results represent metabolite levels as compared to cell-free media (n=3). **d** Intracellular analysis of  $\alpha$ -ketoisocaproate.





---

## Part II

# Metabolomics in multi-omics approaches to study responses to anticancer therapy

*Although I am not first author of the publications in this part, I believe that my contribution to both projects warrants their inclusion in this thesis. In both chapters, I performed metabolomic analysis, contributed to the metabolomics-related figures and was involved in writing and editing the manuscript.*





---

## Part II

# Chapter 4

## Lapatinib resistance in breast cancer cells is accompanied by phosphorylation-mediated reprogramming of glycolysis

Benjamin Ruprecht<sup>1,2</sup>, Esther Zaal<sup>3</sup>, Jana Zecha<sup>1,4,5</sup>, Wei Wu<sup>3</sup>, Celia Berkers<sup>3</sup>, Bernhard Kuster<sup>1,2,4,5,6</sup> and Simone Lemeer<sup>1,2,3</sup>

<sup>1</sup> Chair of Proteomics and Bioanalytics, Technical University of Munich, Freising, Germany

<sup>2</sup> Center for Integrated Protein Science Munich (CIPSM), Freising, Germany

<sup>3</sup> Biomolecular Mass Spectrometry and Proteomics, Bijvoet Center for Biomolecular Research Utrecht University, Utrecht, The Netherlands

<sup>4</sup> German Cancer Consortium (DKTK), Heidelberg, Germany

<sup>5</sup> German Cancer Research Center (DKFZ), Heidelberg, Germany

<sup>6</sup> Bavarian Biomolecular Mass Spectrometry Center, Technical University of Munich, Freising, Germany

## ABSTRACT

Despite initially high response rates to the small molecule kinase inhibitor lapatinib in *ERBB2* overexpressing breast cancer, the acquisition of drug resistance frequently occurs. Here, we used an established BT-474 cell line model of lapatinib resistance and employed explorative mass spectrometry to profile the proteome, kinome and phosphoproteome changes in an effort to systematically investigate initial inhibitor response and concomitant kinome reprogramming and signaling rewiring in resistance. The resulting dataset, which collectively contains quantitative data for > 7,800 proteins, > 300 protein kinases and > 15,000 phosphopeptides enabled deep insight into signaling recovery and molecular reprogramming upon resistance. Our data-driven approach confirms previously described mechanism of resistance (e.g. *AXL* overexpression and *PIK3* reactivation), reveals novel, pharmacologically actionable targets (e.g. *CDK1* and the spliceosome) and furthermore suggests a great heterogeneity in molecular resistance drivers inducing distinct phenotypical changes. Furthermore, we identified an extensive and exclusively phosphorylation-mediated reprogramming of glycolytic activity which is further supported by widespread changes of corresponding metabolites and an increased sensitivity towards glycolysis inhibition. Collectively, this multi omic analysis offers a new perspective on the molecular mechanisms of resistance which points to new therapeutically relevant markers and treatment options for lapatinib sensitive and resistant *ERBB2* overexpressing breast cancer.

## INTRODUCTION

The receptor tyrosine kinase *ERBB2* is overexpressed in 20 % - 30 % of all breast tumors and leads to an increase in the proliferative and invasive potential which is associated with poor prognosis for patient survival [1, 2]. Mechanistically, high levels of *ERBB2* cause homodimerization, autophosphorylation and activation of downstream signaling pathways even in the absence of an activating ligand [3]. Pharmacological efforts directed against *ERBB2* activity resulted in the FDA approval of e.g. trastuzumab [4–6], a monoclonal antibody which prevents *ERBB2* dimerization, and lapatinib [7, 8], a small molecule *EGFR/ERBB2* inhibitor which blocks the kinases' active site. However, despite initially high response rates, breast tumors frequently acquire resistance against targeted therapy. Owing to the early FDA approval of *ERBB2* targeted therapies and their clinical prevalence in breast cancer, a wealth of different resistance mechanisms has been described to date.

For example, Liu *et al.* found the overexpression of the receptor tyrosine kinase *AXL* to be driving lapatinib resistance in the *ERBB2* overexpressing breast cancer cell line BT-474 [9]. They showed that *AXL* engaged *PIK3* which in turn restored proliferation by recovery of the *AKT/MTOR* signaling branch. Other examples include signaling switches to other receptor tyrosine kinases (RTKs; *EGFR* [10], *ERBB3* [11], *EPHA2* [12], *IGF1R* [12, 13], *MET* [15] or *MERTK* [16], the activation of downstream kinases *PRKACA* [17], *SRC* [18, 19, 20] or *PIK3CA* [21] and non-kinase mediated mechanisms (*CCNE* [22], *PTEN* [23], *CDKN1B* [24], *ESR1* [25]).

Metabolic alterations provide another mechanism by which cancer cells can evade the selective pressure of inhibitor treatment. Overexpression of *LDHA* [26], as well as increased expression of the glucose deprivation response network [27] are described mechanisms in lapatinib resistant breast cancer. In addition, two independent studies recently found that small molecule inhibitor resistance can be mediated by the Estrogen Related Receptor Alpha (*ESRRA*) which is capable of altering metabolism through transcriptional regulation induced by oncogenic signaling changes [28, 29]. Deblois *et al.* showed that *MTOR*-dependent *ESRRA* re-expression contributes to lapatinib resistance via increased glutamine metabolism and Park *et al.* provided evidence for intrinsic resistance of breast cancer cells to *PIK3/MTOR* inhibition, which is caused by alteration of mitochondrial function and lactate metabolism. Both studies reveal a tight orchestration of kinase signaling, protein expression changes and metabolic adaptation which clearly highlights the importance of a systems level understanding of resistance and furthermore suggests the existence of several parallel and targetable alterations which are co-dependent.

Mass spectrometry-based technologies nowadays allow for the explorative and large-scale assessment of (phospho)proteins and metabolites, thus rendering the study of such complex associations feasible. Here, we used an established, lapatinib resistant BT-474 cell line model [9] and applied a combination of proteomics, chemoproteomics, phosphoproteomics and metabolomics in an effort to globally assess the molecular consequences of lapatinib treatment and resistance. Collectively, our analysis offers a systems-wide view on the molecular mechanisms of resistance and shows that the acquisition is accompanied by many pharmacologically exploitable alterations. Specifically, the data suggests that posttranslational regulation of glycolysis leads to increased glycolytic addiction in lapatinib resistance. In combination with results from other studies, this observation implies that increased glucose addiction in resistance can occur via multiple different routes. Hence, this phenotype might represent a common and targetable convergence point and, as such, a universal “Achilles’ heel” of resistance to *ERBB2* targeted therapies in breast cancer.

## RESULTS

### **Mass spectrometry-based multi proteomic profiling of lapatinib action and resistance**

With the aim to globally study lapatinib action and lapatinib resistance, we performed a mass spectrometry-based (phospho)proteomic analysis on a previously established cell line model system, consisting of both a lapatinib sensitive and a lapatinib resistant cell line [9]. Triple dimethyl-labeling of proteome digests in combination with Fe-IMAC column-based phosphopeptide enrichment allowed us to compare the (phospho)proteome of parental cells to cells exposed to 1  $\mu$ M lapatinib and to lapatinib resistant cells (Fig. 1a; four independent biological replicates). To gain further insight into protein kinase expression changes, we additionally performed kinase affinity enrichment using Kinobeads  $\gamma$  (KBy) in triplicate [30] (Fig. 1a). The collective dataset (Supplemental Tables S1–3) comprised quantitative information for > 7,800 proteins (Supplemental Fig. 1a), > 300 protein kinases and > 15,000 unique phosphopeptides (> 9,800 unique phosphorylation sites; Supplemental Fig. 1b). The correlation between biological replicates was excellent (average Pearson R of > 0.98 for phosphopeptides and > 0.99 for proteins from replicates of the same condition, Supplemental Fig. 1c) and Principal Component Analysis (PCA) of the twelve experimental states (three dimethyl channels in four replicates) revealed that the proteome and phosphoproteome samples cluster according to biology rather than batch (Fig. 1b).

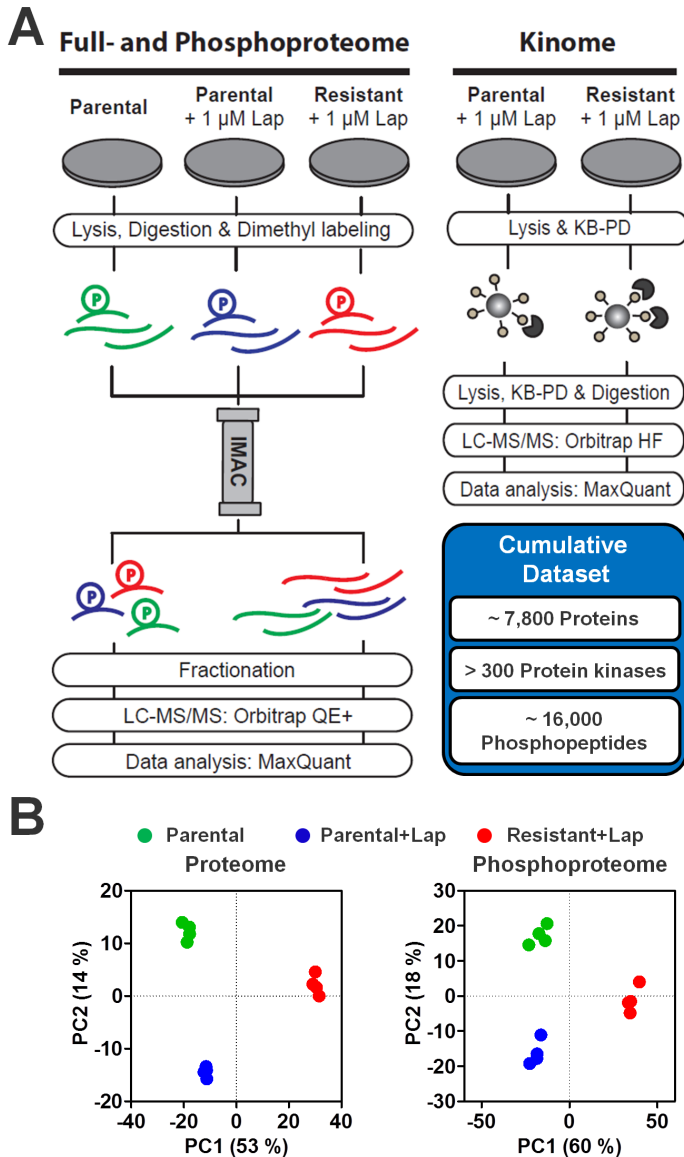


**Figure 1. Multi-proteomic characterization of lapatinib treatment in parental BT-474 cells (Parental) and their resistant counterpart BT-474-J4 (Resistant).**

**a** For the mass spectrometry-based (phospho) proteomic workflow used in this study, digested peptides from three different experimental conditions were dimethyl-labeled, combined and enriched for phosphopeptides using Fe-IMAC chromatography. To increase proteome and phosphoproteome coverage, the column flow through was separated using hydrophilic strong anion exchange (hSAX) chromatography and the phosphopeptide containing eluate was fractionated using high-pH reversed-phase micro-columns. The whole procedure was repeated in four independent biological replicates. In order to increase kinome coverage, Kinobead pull downs were conducted in three replicates. The inset on the bottom right corner depicts the cumulative identifications of our combined dataset **b** PCA analysis of the three dimethyl-encoded experimental states which were conducted in four biological replicates shows that samples cluster tightly according to biology.

### Phosphoproteomic analysis of lapatinib mode of action in parental cells

We first analyzed phosphorylation changes induced by treatment of the parental cell line with 1  $\mu$ M lapatinib for 30 min. To assess statistical significance, a FDR controlled t-test (FDR < 0.01, SO of 0.5) was performed on localized sites (localization probability > 0.75) which were observed in a minimum of three biological replicates. Despite the inhibitor's exquisite selectivity, a total of 332 sites (5 % of the 6421 sites) changed significantly upon short term lapatinib treatment (178 sites down and 154 sites up; Fig. 2a). As expected, less than one percent of the measured proteins changed significantly within the same period of time (Supplemental Fig. 2a). Figure 2b shows that the 178 downregulated sites contain several known, *ERBB2* pathway and protein activity regulating kinase phosphorylation sites such as *ERBB2* pY-1233 ( $\log_2$  FC of -1.3; *p*-value of 3.6E-4) or *MAPK3* pY-204 ( $\log_2$  FC -3.2; *p*-value of 1.2E-08). Enrichment analysis of combined kinase substrates and linear motifs amongst regulated sites [31] showed strong inhibition of *AKT-MTOR-RPS6KB1* and *EGFR-MAPK1/3-RPS6KA3* signaling upon lapatinib treatment (Fishers Exact test, FDR < 0.01; Supplementary Fig. 2b). The analysis additionally uncovered regulation of receptor tyrosine kinase adaptor proteins such as *IRS1/2*, *SHC1* or *GAB2* and the inactivation of central transcription factors such as *JUN* and *MYC* (Fig. 2c). Global protein interaction analysis of changing phosphoproteins using the STRING database in combination with KEGG annotation of the extracted network confirmed the perturbation of *MTOR* signaling (FDR = 7.5E-07), *ERBB* signaling (FDR = 7.6E-05; Fig. 2c and Supplemental Table S1) and *MEK-ERK* signaling directly downstream of *ERBB2*. Moreover, it revealed a previously unknown impact of the inhibitor on the spliceosome (FDR = 7.5E-07; inset in Fig. 2c).

### Resistance acquisition is accompanied by extensive reprogramming of cellular signaling

Having analyzed the impact of short term lapatinib treatment, we next looked at signaling changes occurring upon acquisition of resistance. In line with what has been reported before [9], resistant BT-474 cells are insensitive to lapatinib treatment ( $IC_{50}$  of 4.4  $\mu$ M for the resistant cells and 56 nM for the parental cells; Supplemental Fig. S3a), responsive to *AXL* inhibition ( $IC_{50}$  of 82 nM for the multi kinase inhibitor BMS-777607 which also targets *AXL*; Supplemental Fig. S3b) and have a proliferation rate comparable to the parental cells (Supplemental Fig. S3c). Since *AXL* expression was found to be directly dependent on the selective pressure of lapatinib, the growth medium of the resistant cell line was supplemented with 1  $\mu$ M lapatinib throughout the study (Supplemental Fig. S3d).

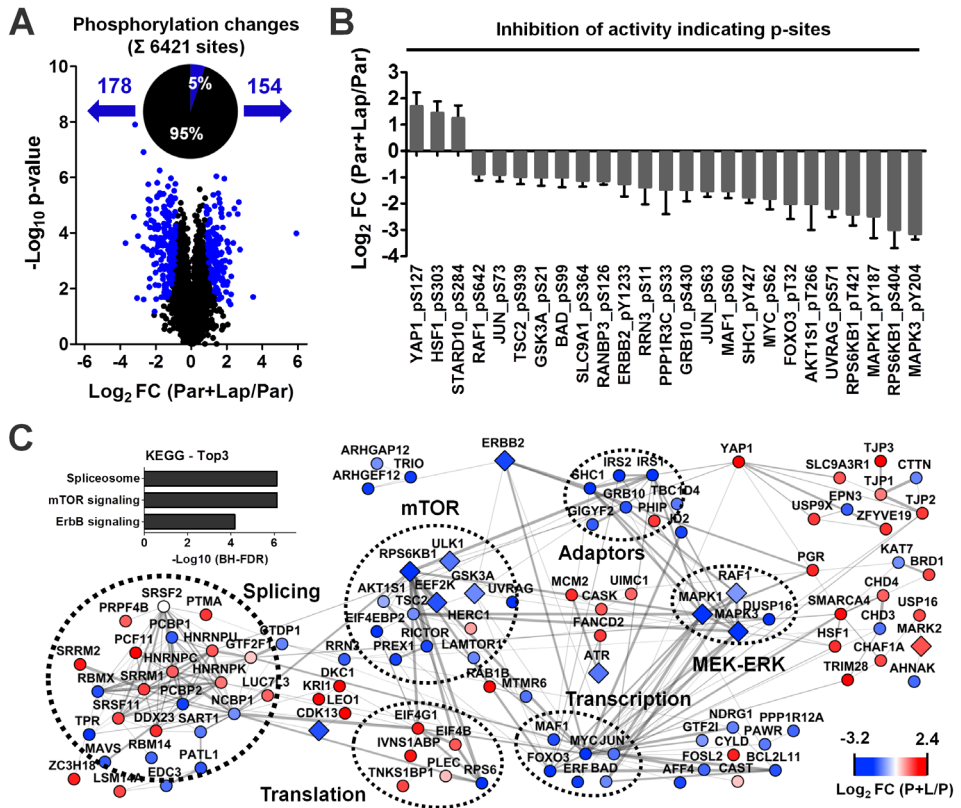


**Figure 2. (Phospho)proteomic analysis of lapatinib mode of action in parental cells.**

**a** A volcano plot shows that 332 localized phosphorylation sites (found in a minimum of three biological replicates) change significantly ( $\text{FDR} < 0.01$ ,  $S_0$  of 0.5; blue dots) upon 30 min treatment with  $1 \mu\text{M}$  lapatinib. **b** Bar plots display the average  $\text{log}_2$  FC of sites which are known to have a functional impact on protein activity. Among those are several sites expected to be responsive to lapatinib treatment (e.g. *ERBB2* pY-1233 or *SHC* pY-427). **c** Protein-protein interaction map of phosphoproteins whose sites are significantly changing upon short term lapatinib treatment. The node color represents the  $\text{log}_2$  FC upon lapatinib treatment, whereas the thickness of the edge represents the STRING combined interaction score ( $> 0.7$ ). Kinases are indicated by diamond shaped nodes. Known and annotated associations are highlighted by dotted circles. The top three KEGG terms overrepresented among regulated phosphoproteins are shown in the inset: this confirms the known (inactivation of *MAPK*, *MTOR* signaling) and uncovers a new (spliceosome) mode of lapatinib action.

Global proteome and phosphoproteome analysis of resistant versus parental cells showed that 767 out of 6,318 proteins (247 up and 521 down; Supplemental Fig. S3e) and 2,247 out of 6421 phosphorylation sites (1,111 up and 1,136 down; Fig. 3a) changed significantly. The latter corresponds to over one third of all covered sites, which is surprisingly large in comparison to the moderate changes elicited by short term treatment with lapatinib (5 % of all sites; Fig. 2A). To study signaling recovery in resistance we divided the 332 sites which were initially inhibited by lapatinib in the parental cells into the categories “remain responsive” (182 sites), “medium recovery”

(99 sites) and “strong recovery” (51 sites) according to statistical criteria and the magnitude of the  $\log_2$  FC between lapatinib treated parental and resistant cells (Supplemental Methods). Figure 3b shows protein activity indicating sites assigned to those categories. Whereas the activity of the kinases *ERBB2* or *MAPK1* and the transcription factors *FOXO3* and *BAD* remained strongly inhibited, the activity of the kinases *RAF1*, *MAPK3*, *GSK3A* and the transcription factor *JUN* recovered in lapatinib resistant compared to sensitive cells. Globally, 2D annotation enrichment (FDR < 0.01) [31] confirmed the re-activation of the *PIK3/AKT/MTOR* signaling axis (e.g. kinases *AKT*, *RPS6KB1* and *RPS6KA1* based on combined kinase substrates and *ERBB*- and *MTOR*-signaling based on differential KEGG terms; Supplemental Fig. S3f and Supplemental Table S1).

As kinases are frequently involved in the resistant phenotype and contain a high proportion of pharmacologically actionable targets, kinome perturbations were of special interest. Complementing the phosphoproteomic data which suggested *de novo* activation of several kinases (e.g. *CDK1* and *SRC*; Supplemental Fig. 3g), kinobead pull-downs in combination with kinome expression changes derived from the full proteome dataset confirmed the known overexpression of *AXL* and highlighted many other kinases with known or emerging roles in breast cancer biology (e.g. *ERN1* [32], *FGRF2* [33], *ATR* [34] and *EEF2K* [35], with a  $\log_2$  FC of 3.1, 2.9, 2.0 and 1.9; Fig. 3c and Supplemental Table S5). Notably, expression of the primary lapatinib targets *EGFR* and *ERBB2* remained constant (Fig. 3c). This extensive kinome reprogramming highlights a pool of potentially relevant kinases in resistance, of which several are druggable targets.

### Pharmacological exploitation of reprogrammed cellular signaling

Our multilayered (phospho)proteomic dataset allowed us to paint a detailed molecular picture of lapatinib resistance. The pathway map depicted in Figure 4a, summarizes both protein expression and protein phosphorylation changes in lapatinib treated compared to resistant cells. Proteins highly overexpressed in resistance are highlighted and phosphorylation events were classified as remaining inhibited, moderately recovering, strongly recovering or *de novo* activated depending on the fold change detected between lapatinib treated and resistant cells (Supplemental Methods).

We next followed up on some selected observations in order to demonstrate the utility of such a resistance map. First, the model revealed a moderate recovery of a *RAF1/BRAF-MAPK3-JUN* which implied that this signaling axis is controlled independently of *ERBB2-MAPK1* which remained responsive to lapatinib. This was surprising given that *RAF1/BRAF* phosphorylated *MEK* usually activates both



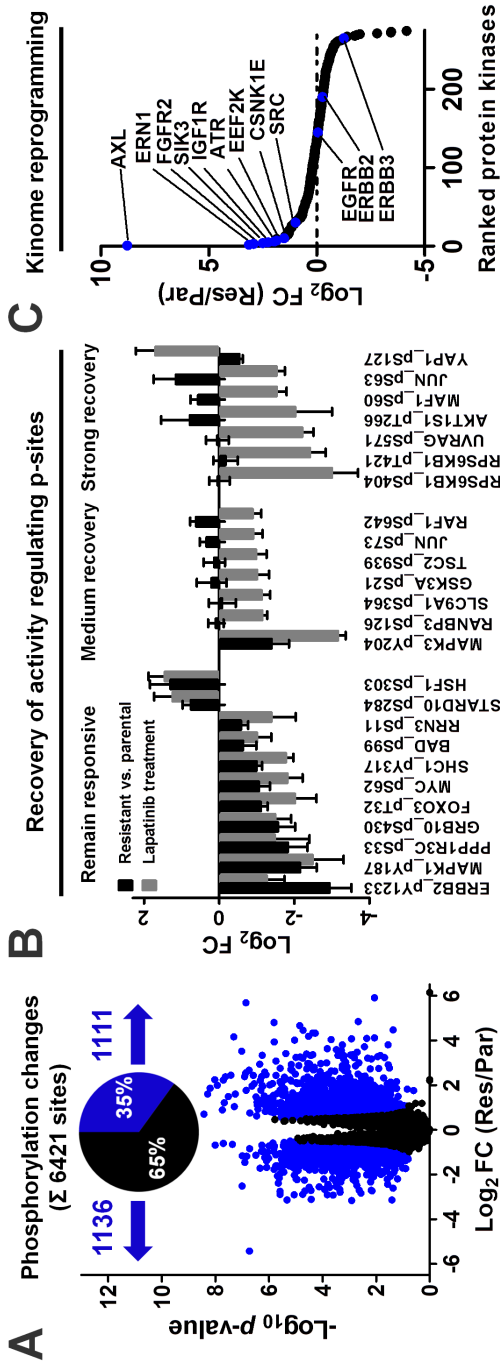


**Figure 3. Signaling reprogramming in lapatinib resistance.**  
**a** A volcano plot depicts significantly changing localized phosphorylation sites (found in a minimum of three biological replicates; FDR < 0.01, S0 of 0.5) in the resistant (Res) compared to the parental (Par) cell line. The magnitude of phosphoproteome alterations (35 % of all sites) suggest that resistance is accompanied by a fundamental impact on tumor cell signaling. **b** To study signaling rewiring, phosphorylation sites responsive to short term lapatinib treatment were classified as “remain responsive” or “recovering” in resistance (depending on the magnitude of change, recovery was classified as “medium” or “strong”). The bar chart shows log<sub>2</sub> FC of activity associated sites from those categories in resistance and compares it to their initial log<sub>2</sub> FC in response to short term lapatinib treatment. **c** Averaged quantitative kinase data from the full proteome and the affinity purification dataset were ranked according to their log<sub>2</sub> FC between the parental (Par) and the resistant (Res) cell line.

*MAPK1* and *MAPK3*. Further support for both signaling axis being uncoupled came from differential responsiveness of the resistant cells towards *MEK* and *RAF1/BRAF* inhibition (Fig. 4b). This uncoupling might for example be caused by a differentially activated phosphatase. In contrast, the *AKT-MTOR* pathway fully recovered and resistant cells were this exquisitely sensitive towards *AKT* inhibition (sensitivity increases roughly twofold compared to parental cells; Supplemental Fig. S4a). Collectively, this suggests that our approach is capable of dissecting differentially recovering signaling nodes which can support the rational targeting of functionally relevant pathways.

Second, we asked if the *de novo* activated kinases can be pharmacologically exploited. *CDK1* was selected as a promising target owing to the strongest observed activation of any protein kinase present in our dataset (activity associated site pT-161 increases with a  $\log_2$ FC of 2.7, Supplemental Fig. S3g). Indeed, a much higher proportion of the resistant cell population was susceptible to the *CDK1* inhibitors BMS-387032 (Fig. 4c) and SCH-727965 (Supplemental Fig. S4b) which implies increased dependence on *CDK1* signaling despite similar proliferation rates (Supplemental Fig. S3c).

Third and motivated by the fact that resistance against *ERBB2* inhibition in breast cancer is one of the best studied model systems of resistance against targeted therapy, we asked if common molecular drivers of resistance acquisition exist. Strikingly, our dataset contained quantitative information for virtually all of the molecules and phosphorylation events described in 20 previous studies investigating trastuzumab or lapatinib resistance in *ERBB2* overexpressing breast cancer (Supplemental Fig. S4c). Whereas large-scale (phospho)proteomic measurement readily confirmed Western Blot based read-outs from the same resistant cell line [28] (e.g. *AXL* overexpression or loss of *BAD* pS-99 and *FOXO* pT-32) the majority of alterations found in other studies were not evident in our datasets (Supplemental Fig. S4c). However, we were able to confirm the previously described activation of *SRC* [18–20] and the overexpression of *IGF1R* [13] (Supplemental Fig. S3f,g for *SRC* and Fig. 3c for *IGF1R*). Dose-dependent addition of an *IGF1R* inhibitor linsitinib (Supplemental Fig. S4d) or the *SRC* inhibitors dasatinib and saracatinib (Supplemental Fig. S4e) showed that neither of those kinases is required for proliferation in our resistance model. Owing to clear morphological changes of the resistant cell line (Supplemental Fig. S4f) and the well-established role of the *de novo* activated *SRC* in invasion [36], we additionally examined the invasive behavior in resistance and found it to be three fold higher compared to the parental cell line (Fig. 4d). Interestingly, the removal of lapatinib increased the invasiveness to roughly six fold (Supplemental Fig. S4f), which calls discontinued inhibitor exposure of patients upon the development of

resistance into question. The invasive phenotype was reduced nearly back to the level of parental cells by addition of low doses of *SRC* inhibitors, indicating that *SRC* family kinases may be driving the invasiveness in resistance cells (Fig. 4d). Collectively, the obtained results suggest that resistance acquisition is molecularly very heterogeneous, that previously identified drivers of resistance can have diverse functional roles (e.g. *SRC*) and that activation or increased expression of proteins is not necessarily a direct indicator for functional relevance (e.g. *IGF1R* and proliferation).

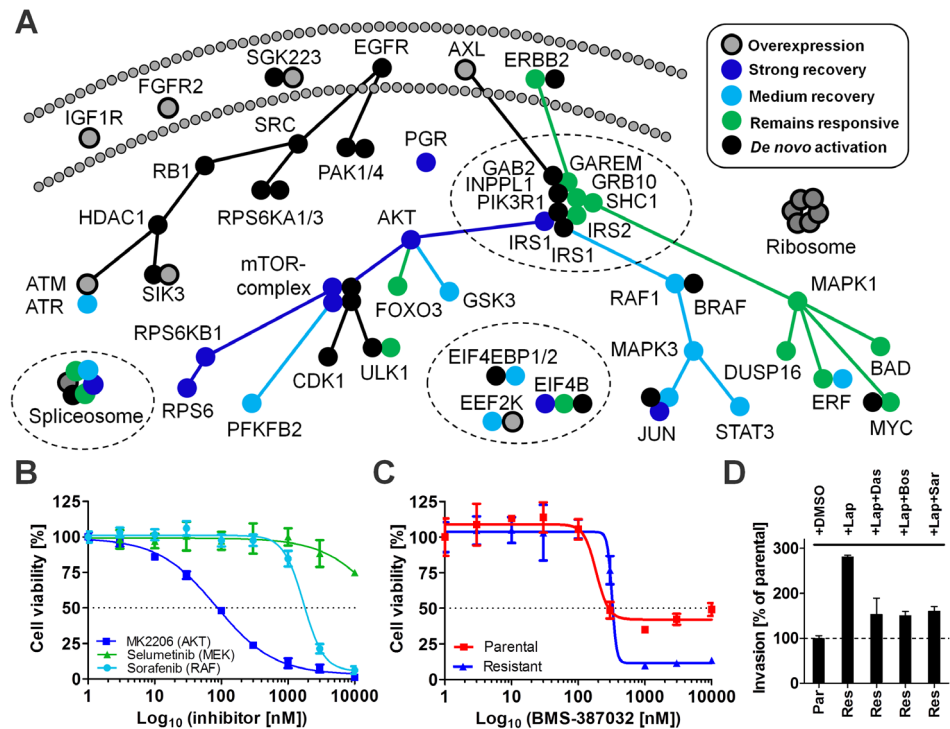


**Figure 4. Identification of pharmacologically actionable targets and phenotypes based on a breast cancer model of lapatinib resistance.**

**a** A manually compiled pathway model of signaling reprogramming in resistance identifies phosphorylated nodes which remain responsive to lapatinib also in resistance (green), nodes that are reactivated and might thus re-establish proliferation (blue shades) and nodes which are *de novo* regulated in resistance (black). Grey dots represent overexpression in resistance. Different nodes/colors for the same (phospho)protein indicate that multiple such events occur simultaneously. The dotted circles highlight a strong involvement of adaptor proteins, the spliceosome and general translational control. **b** The extent of signaling recovery in the resistant cell line compared to the lapatinib treated parental cell line might provide a means to prioritize pathways based on functional importance. Whereas resistant (Res) cells are not responsive to MEK inhibition, they are responsive to RAF and highly responsive to AKT inhibition. **c** In line with strong CDK1 activation in resistance, a dose-response curve for resistant and parental cells treated with the CDK1 inhibitor BMS-387032 shows that a higher proportion of the resistant cell population is dependent on CDK signaling. **d** A triplicate matrigel invasion assay shows that resistant cells cultured in the presence of 1  $\mu$ M lapatinib are more invasive than their parental counterpart (cultured in 0.5 % DMSO). This invasiveness can be reduced almost back to parental (Par) levels by addition of SRC inhibitors dasatinib (Das; 250 nM), bosutinib (Bos; 300 nM) or saracatinib (Sar; 250 nM).

### Lapatinib resistance leads to phosphorylation-mediated changes in glycolysis

Two other described molecular mechanisms of resistance are based on glycolytic addiction caused by metabolic reprogramming [27, 37] (Supplemental Fig. S4c). One of these mechanisms involves *HSF1* dependent overexpression of *LDHA*, a metabolic protein that enhances glycolytic flux [37]. Whereas *LDHA* was not significantly regulated in our model, we found a massive (60-fold) increase of *LDAH* Y-10 phosphorylation, a site which is known to cause enzymatic activation [38] ( $p$ -value of  $8.7E-03$ ; Supplemental Fig. S3g). Also *ENO1* pY-44, *PKM* pY-175, *PGAM1* pY-92, phosphotyrosine sites on three other important glycolytic enzymes were highly upregulated in resistance ( $\log_2$  FC of 4.9, 2.8 and 3.7). In addition, several phosphoserine sites such as *ALDOA* pS-39, *ALDOA* pS-46, *PFKP* pS-386 and *GAPDH* pS-83 ( $\log_2$  FC of 1.4, 1.3, 1.3 and 2.5) showed a strong gain in phosphorylation without a significant increase in protein abundance (except for *ALDOA*). Apart from core glycolytic enzymes, enzymes involved in glycogen catabolism were also found to be phosphorylated to a significantly higher degree in lapatinib resistant cells compared to the parental cell line (*PYGB* pT-59, *PGM1* pS-117 and *PGM2* pS-165;  $\log_2$  FC of 5.0, 2.3 and 2.1 respectively). Moreover, we observed a 1.4  $\log_2$  fold recovery of *PFKFB2* pS-466 phosphorylation in resistance ( $p$ -value of  $5.9E-06$ ). This site was initially inhibited by lapatinib treatment and its recovery likely indicates its functional importance in resistance. Phosphorylation of pS-466 has been shown to stimulate *PFKFB2* kinase activity, which catalyzes the production of fructose-2,6-bisphosphate, an allosteric activator of glycolysis [39]. Finally we observed posttranslational inactivation of *PDHA1*, caused by strong phosphorylation of the enzymatic activity inhibiting sites pS-293 and pS-300 (40) ( $\log_2$  FC of 1.9 and 4.8). This enzyme catalyzes the conversion of pyruvate into acetyl-CoA, which is the starting point of the citric acid cycle. Taken together these results suggested a strong, phosphorylation mediated, regulation of glucose metabolism.

In order to investigate if these changes affected the levels of glycolytic metabolites, we quantitatively and time-dependently determined the levels of 86 metabolites in the resistant and parental cells 2 h, 8 h and 24 h after medium change (in triplicates) (Fig. 5a, Supplemental Table S4). To summarize the obtained results and facilitate integrated analysis, we assembled the key observations from all acquired “-omics” datasets in a quantitative glycolysis map (Fig. 6a). Metabolic analysis confirmed higher intracellular levels of glucose ( $\log_2$  FC of 1.9 after 8 h) in resistant cells together with higher levels of glycolytic intermediates, which was especially apparent for glucose-6-phosphate ( $\log_2$  FC of 1.6 after 8 h), glyceraldehyde-3-phosphate ( $\log_2$  FC of 1.4 after 2 h) and phosphoenolpyruvate ( $\log_2$  FC of 1.7 after 8 h; Fig. 5, Supplemental Table S4). Moreover, time-dependent measurement of extracellular metabolites after

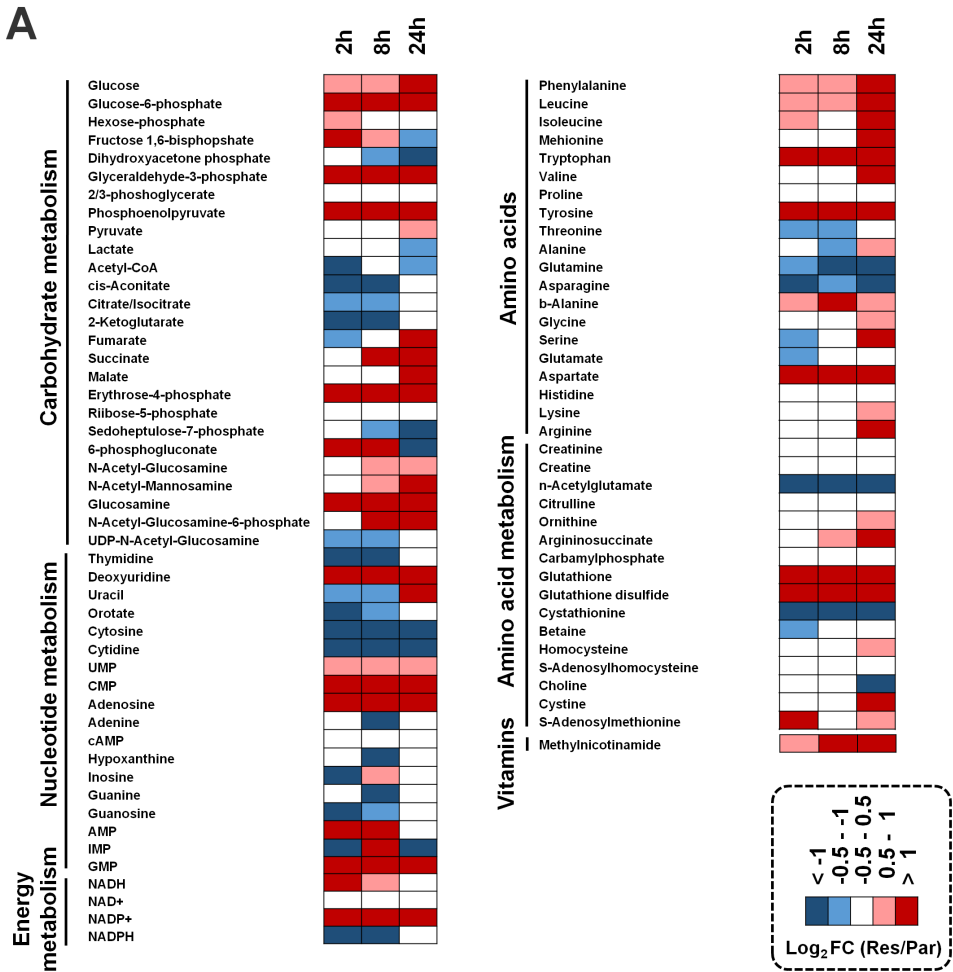


**Figure 5. Metabolic changes in lapatinib resistant cell line model.**

The levels of 86 different metabolites have been quantitatively determined at different time points after medium change (2 h, 8 h, 24 h). The overview summarizes the color-coded  $\log_2$ FC between resistant (Res) and parental (Par) cells.

8 h and 24 h revealed that the resistant cells import higher amounts of glucose, export more lactate and massively secrete pyruvate compared to their parental counterpart (Fig. 6b). Collectively, the acquired intracellular and extracellular metabolomic data clearly provide compelling evidence for a higher glycolytic activity which supports conclusions drawn from phosphorylation changes.

Finally, we investigated if the increased glycolytic activity in resistant cells can be therapeutically exploited. Hence, we treated resistant and parental cells with the competitive Hexokinase inhibitor 2-deoxy glucose. Figure 6c shows that the resistant

cells were indeed more sensitive to glycolysis inhibition by 2-deoxy-glucose (2-DO-Glc), in line with our metabolomic and phosphoproteomic results. Importantly, glycolysis inhibitors such as 2-DO-Glc or the antidiabetic drug metformin are actively evaluated in clinical breast cancer trials which renders their application a viable therapeutic option.

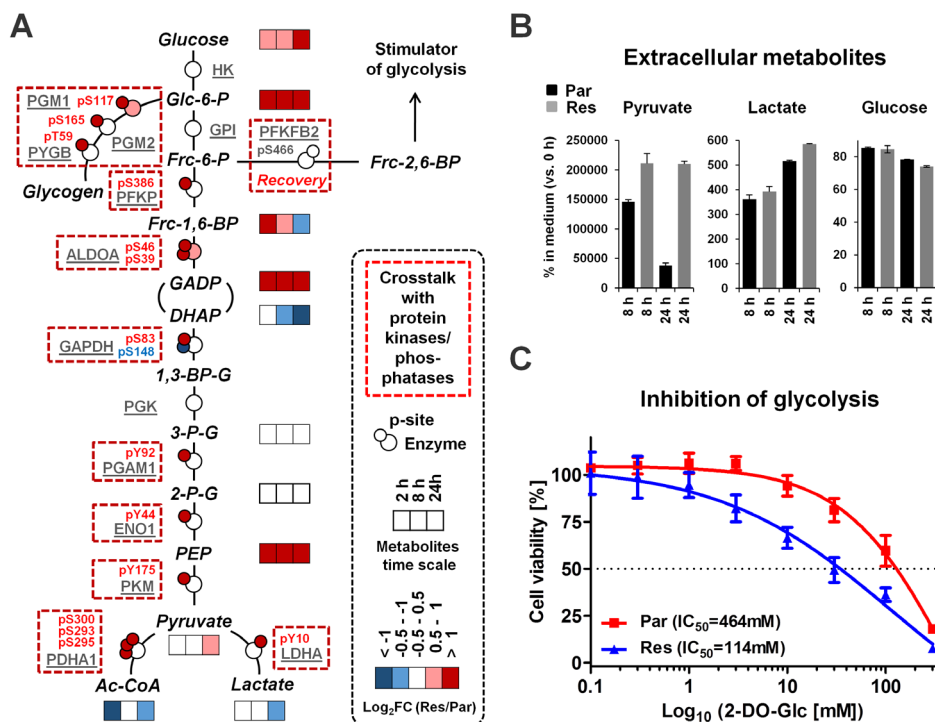


**Figure 6. Phosphorylation mediated rewiring of glycolysis as a targetable alteration in lapatinib resistant breast cancer cells.**

**a** A metabolic pathway model summarizes expression (significant with a FDR < 0.01), phosphorylation (significant with a FDR < 0.01) and time-dependent (after 2 h, 8 h and 24 h) metabolite changes of resistant (Res) and parental (Par) cells. Big dots represent metabolic enzymes and small dots represent phosphorylation sites. The color code indicating magnitude of FC is consistent for all data types. The absence of protein expression changes suggests that glycolytic rewiring is driven by phosphorylation on a post-translational level. Phosphorylation affects many known glycolytic enzymes which provides widespread evidence for crosstalk with oncogenic protein kinases and/or phosphatases (indicated by red boxes). **b** Metabolite levels present in media of resistant (Res) and parental (Par) cells were determined after 8 h and 24 h. **c** Compared to the parental cell line, the resistant cells show a decrease viability upon treatment with increasing doses of 2-deoxy-glucose (2-DO-Glc) for 96 h.

## DISCUSSION

In this study we used a multilayered proteomic approach to investigate how the small molecule kinase inhibitor lapatinib acts on responsive, *ERBB2* overexpressing breast cancer cells and compared this to the rewired signaling of lapatinib resistant cells. This setup allowed us to functionally prioritize phosphorylation site and pathway changes in resistance in light of their initial responsiveness to lapatinib, with the rationale that re-activation of initially inhibited pathways must be crucial for the resistant phenotype. Collectively, the data confirmed previous observations made using classical biochemical approaches (e.g. *PIK3-AKT-MTOR* recovery or *AXL* overexpression [9]), but also provided many new additional molecular insights of which we are only able to discuss a few. First, splicing was shown to be heavily affected by short term lapatinib treatment of parental cells. Splicing is already well known to be implicated in virtually all steps of tumor biology and is frequently involved in oncogenic transformation [41]. Hence, the spliceosome is increasingly recognized as druggable tumor target [42]. Moreover, spliceostatsins (or analogues thereof) are known to inhibit parental BT-474 cells with low nanomolar affinity [43, 44]. Impairment of splicing mechanisms might thus represent a previously unrecognized mechanism of lapatinib action in breast cancer. Second, the data allowed us to propose a detailed model of signaling adaptor rewiring in resistance. Re-established phosphorylation might imply a higher relevance of *IRS1*, *GAB2* and *INPPL1* for resistance acquisition as compared to several other adaptor proteins which remain de-phosphorylated (e.g. *SHC1* or *IRS2*). Whereas *GAB2* pY-452 is known to confer resistance against *BCR/ABL* targeted therapy, we found *GAB2* pY-476 to be important in *AXL* mediated resistance (the site is not responsive to short term lapatinib treatment, highly upregulated in resistance and known to induce interaction with *PIK3R1*, the regulatory subunit of *PIK3* [45]). *GAB2* is an amplifier of oncogenic signaling, serves as a signaling integrator and also confers imatinib resistance in chronic myeloid leukemia which might make it an ideal target for the effective treatment of a diverse set of cancers addicted to deregulated RTKs [46, 47]. The same applies to *IRS1* and *INPPL1*, which are known to confer the mitogenic signals of several oncoproteins and have potential therapeutic value [48, 49].

Third, the integrative data analysis suggests that the cell tries to surmount initial inhibitor action by excessive re-activation of initially targeted nodes and pathways (e.g. the spliceosome; Supplemental Fig. S5b), the hormone-receptor *PGR* or the translation associated kinase *EEF2K*). Hence, our analysis also singles out phosphorylation sites which might be useful as early markers of resistance onset. The immediate upregulation of the *PGR* transcription inducing site pS-102 indicates

a direct and posttranslational link between lapatinib action and *PGR* activation, which further emphasizes the emerging paradigm of *ERBB2-PGR* crosstalk [50]. The fact, that this activity is lost in resistance (probably at least in part due the loss of *PGR* expression itself) makes it intriguing to speculate that *PGR* activity needs to be low to ensure proper survival of *ERBB2* overexpressing breast cancer cells.

Fourth, lapatinib treatment of sensitive BT-474 cells is known to affect glycolysis [27] and our analysis unveiled that phosphorylation of S466 on *PFKFB2*, a regulator indirectly affecting a rate limiting step in glycolysis, is inhibited in response to lapatinib treatment but is recovering to initial phosphorylation levels (i.e. to the same extent as non-treated parental cells) in resistance, providing a molecular connection between lapatinib mode of action and therapeutically relevant metabolic reprogramming in resistance. This specific example shows that the analysis of the initial drug mode of action is crucial for the interpretation of phosphorylation changes in resistance, as this observation would have gone unnoticed if parental cells would be compared to resistant cells directly.

Our study demonstrates that resistance in our cell line is characterized by extensive post-translational changes on glycolytic enzymes. Importantly, the fact that this reprogramming was not apparent from protein expression changes underscores the importance to study post-translational events in general and phosphorylation in particular. Moreover, metabolic alterations are an established hallmark of cancer and phosphorylation is emerging as a major switch connecting oncogenic protein kinase signaling to modified metabolic activity [51]. Indeed, we found many examples where phosphorylation on metabolic enzymes co-occurs with the expected shift of metabolite levels. For example, phosphorylation of *PDHA1* at S-293/S-300 which is known to inhibit its enzymatic activity [39] is co-detected with a decrease in intracellular Acetyl-CoA abundance and a concomitant secretion of pyruvate. The latter might additionally be promoted by a strong increase in Y-175 phosphorylation of *PKM* which is responsible for pyruvate production. *PKM* is particularly interesting, since it is one of the rate limiting enzymes in glycolysis and well known to be controlled by kinase signaling [52]. Another example is pY-44 of *ENO1* which co-occurs with strong and sustained elevation of its enzymatic product 2-phosphoglycerat. Our analysis further uncovered a massive increase in intracellular glucose-6-phosphate levels and phosphorylation of several key enzymes responsible for glycogenolysis (which ultimately results in glucose-6-phosphate production). This might be another way for the resistant cells to fuel glycolysis which can be targeted.

Some of the detected phosphorylation sites have previously been connected to specific oncogenic kinases. As mentioned above, *LDHA* Y-10 is known to be phosphorylated by several tyrosine kinases (e.g. *FGFR* or *ABL* [38]). Activated



*SRC* is capable of phosphorylating *ENO1* and *PGAM1* and *PDHA1* S-293 and S-300 are known to be phosphorylated by *PDK* isoenzymes [53, 54]. Other sites on glycolytic enzymes (e.g. *PFKP* pS-386, *GAPDH* pS-83) are not yet associated with a specific kinase/phosphatase and provide starting points for further analysis of kinase mediated metabolic control. Overall, the extent of glycolytic rewiring, the occurrence of various phosphoserine/-threonine as well as phosphotyrosine sites and the diversity of functionally involved kinases suggest that post-translational mediated glycolytic addiction is a collective phenomenon rather than being caused by one single kinase.

Metabolic alterations are increasingly implicated in resistance against kinase inhibitors in general [55] and lapatinib in particular [27–29]. Importantly though, all previously described mechanisms are dependent on expression changes. To the best of our knowledge, this is the first study to show that such a metabolic shift involved in lapatinib resistance can occur exclusively by change of enzymatic activity which is likely caused by post-translational regulation. Interestingly, recent reports suggest that metabolites are themselves capable of affecting kinase pathways. For example, lactate which is found to accumulate in our resistant cell line has been shown to engage *AXL* and activate the *PIK3* pathway [56]. This reciprocal crosstalk might open up exciting new therapeutic opportunities and shows how important it is to understand resistance on a systems-wide level.

Furthermore, our proteomic datasets revealed that mechanisms of resistance acquisition are very heterogeneous and that previously identified resistance drivers can result in different phenotypic changes, depending on the resistant cell line used. This heterogeneity might pose a great challenge in terms of unifying treatment options. Thus, it might be a more efficient strategy to search for common alterations and molecular integrators of different, heterogeneous resistance mechanisms. As an example, several resistance mechanisms observed in *ERBB2* overexpressing breast cancer, whether it is *AXL*, *EPHA2* or *MET*, lead to the reactivation of *PIK3*, which might consequently be a more attractive node to target [9, 12, 15]. Glycolysis is another example: both, our cell line and the resistant cell line from Komurov *et al.*, are sensitive to inhibition of the glycolysis rate limiting enzyme hexokinase via 2-deoxy glucose treatment independent of the way glycolytic addiction has been acquired [27]. Moreover, recent reports also establish a link between hormone receptor overexpression, altered metabolism, *MTOR* signaling and lapatinib resistance [28, 29]. Although all three aberrations represent individually targetable entities, they seem to depend on each other. Indeed, also in our cell line model estrogen receptor upregulation is responsible for *AXL* overexpression as shown by Liu and colleagues [9]. This interplay between different molecular aberrations implies that there are

diverse ways of targeting the resistant phenotype. Selecting the mechanism most commonly occurring might thus emerge as a key step in resistance management.

Finally, our dataset contains many additional observations (e.g. multiple deregulated intracellular/extracellular metabolites (Supplemental Fig. S5c), signaling events and kinase targets). For example, we observed a massive secretion of the acidic metabolite glutamate which is known to promote growth and invasion [57]. Given the prevalence of brain metastasis in breast cancer and the observed invasive phenotype connected to lapatinib resistance, knowledge about potential metabolic mechanisms causing or amplifying invasion might ultimately result in better cure of disease. In addition, not only glycolysis is deregulated but we rather find a strong global impact of resistance acquisition on diverse metabolic pathways such as the citric acid cycle, redox signaling, amino acid metabolism and several more (Fig. 5). These and many other observations resulting from the acquired datasets clearly merit closer inspection which places this work as a rich resource for further studies.

## METHODS

### Cell culture and reagents

Parental BT-474 cells and its lapatinib resistant clone BT-474-J4 were grown in DMEM/Ham's F-12 medium (Biochrom) supplemented with 15 % (v/v) Fetal Bovine Serum (Biochrom) and 1 % (v/v) Antibiotic/Antimycotic solution (Sigma). Resistant BT-474-J4 cells were cultured in the continuous presence of 1  $\mu$ M lapatinib. Biological replicates were prepared at different days using a different cell line passage. Lapatinib, sorafenib, dasatinib and bosutinib were purchased from LC Laboratories, 2-deoxy-D-glucose was purchased from Sigma Aldrich and saracatinib, selumetinib, linsitinib, BMS-387032, SCH-727965 and MK-2206 were purchased from Selleckchem.

### Viability and invasion assay

For viability/drug treatment assays, cells were seeded in 96-well plates at a concentration of  $4 \times 10^4$  cells/well with complete culture medium. Cell viability was measured using the AlamarBlue® Cell Viability Assay (ThermoFisher Scientific) according to manufacturer's instructions. Sigmoidal dose response curves were fitted using a nonlinear regression model in GraphPad Prism v.5.01. The invasive potential of parental and resistant BT-474 cell lines was assessed in a transwell assay using BD matrigel (VWR).

### Cell lysis

Prior to harvest, cells were washed two times with PBS. For (phospho)proteome preparation, cells were lysed in 8 M Urea, 40 mM Tris/HCl (pH 7.6), 1 x EDTA-free protease inhibitor mixture (complete mini, Roche) and 1 x phosphatase inhibitor cocktail 1, 2 and 3 (Sigma). The lysate was centrifuged at 20,000 g for 45 min at 4 °C. For Kinobead experiments, cells were lysed in 1 x CP buffer (50 mM Tris-HCl, pH 7.5, 5 % glycerol, 1.5 mM MgCl<sub>2</sub>, 150 mM NaCl) supplemented with 0.8 % NP-40, 1 mM DTT, 25 mM NaF and freshly added protease and phosphatase inhibitors (5 x phosphatase inhibitor cocktail 1 and 2, Sigma–Aldrich; 1 x phosphatase inhibitor cocktail 3, Sigma–Aldrich; 1 mM Na<sub>3</sub>VO<sub>4</sub>). CP buffer protein extracts were clarified by ultracentrifugation at 150,000 g for 1 h at 4 °C. Protein concentration for phosphoproteome and kinome samples was determined by the Bradford method (Coomassie (Bradford) Protein Assay Kit, Thermo Scientific) and the cleared lysates were stored at -80 °C until further use.

### Digestion and dimethyl labeling for phospho- and full proteome preparation

The urea containing lysate was reduced with 10 mM DTT at 56 °C for 30 min and alkylated with 55 mM CAA for 30 min at room temperature in the dark. The protein mixture was diluted with 40 mM Tris/HCl to a final urea concentration of 1.6 M. Digestion was performed by adding sequencing grade trypsin (Promega) in an enzyme-to-substrate ratio of 1 : 100 and incubation for 4 h at 37 °C. Subsequently, another 1 : 100 trypsin was added for overnight digestion at 37 °C. The next day, samples were acidified with TFA to a pH of 2 and desalted using SepPak columns (C18 cartridges Sep-Pak Vac 1 cc (50 mg), Waters Corp., solvent A: 0.07 % TFA, solvent B: 0.07 % TFA, 50 % ACN). Dimethyl labeling was performed on column as described previously [58].

### Fe-IMAC column enrichment and (phospho)peptide fractionation

Phosphopeptide enrichment was essentially performed as previously described [59]. Detailed description of high pH reversed-phase micro-column fractionation can be found in the Supplementary Materials and Methods section. hSAX fractionation of 300 µg Fe-IMAC column flow through into 24 fractions was performed as previously described [59].

### Sample preparation for metabolomics experiments

BT-474 and BT-474-J4 cells were seeded in triplicates on 6-well plates at a density of 4x10<sup>5</sup> cells per well. Extra wells were seeded for cell counting. After 24 h, media was replaced and after 2 h, 8 h and 24 h, cells were washed with ice cold PBS and

metabolites were extracted in 0.25 mL lysis buffer containing MeOH/ACN/ddH<sub>2</sub>O (2:2:1). Samples were centrifuged at 16,000 g for 15 min at 4 °C and supernatants were collected for LC-MS analysis. In addition, the media were sampled 8 h and 24 h after exchange. For this, 10 µL of medium was added to 1 mL of lysis buffer containing MeOH/ACN/ddH<sub>2</sub>O (2:2:1) and prepared as described above.

### **Kinase affinity pull downs**

Kinobead pull downs were conducted in a 96 well plate format as described previously [30].

### **LC-MS/MS measurements**

For full- and phosphoproteome fractions, nanoflow LC-MS/MS was performed by coupling an Agilent 1290 (Agilent technologies, Middelburg, Netherlands) to an Orbitrap Q Exactive Plus mass spectrometer (Thermo Scientific, Bremen, Germany). For Kinobead eluates, nanoflow LC-MS/MS was performed by coupling an UltiMate 3000 nano LC system (Thermo Scientific) to a Q Exactive HF mass spectrometer (Thermo Scientific). For metabolomics experiments, LC-MS analysis was performed on a Q Exactive mass spectrometer (Thermo Scientific) coupled to a Dionex Ultimate 3000 autosampler and pump (Thermo, Scientific). Detailed LC and MS parameters can be found in the Supplementary Materials and Methods section.

### **Data analysis**

Processing of raw mass spectrometric data was performed using MaxQuant v1.4.0.5 [60]. To facilitate further data analysis, the results were either imported into the MaxQuant associated software suite Perseus (v.1.5.0.15) [31] or into Excel (Microsoft). Data normalization was performed according to a procedure that will be published elsewhere. A two-sided student's t-test was used to assess statistical significance. Phosphopeptide and protein *p*-values were corrected for multiple testing using a permutation based 1 % FDR cut-off (250 randomizations; S0 of 0.5). Metabolites were quantified using LCQUAN™ software (Thermo Scientific).

Additional information on materials and methods used in this study is provided in the Supplemental Information.

### **Authors Contributions**

Conception and design, BR, BK and SL; Development of methodology, BR, BK and SL; Administrative, technical, or material support (i.e., reporting or organizing data, constructing databases): BR., EZ., JZ, WW..and SL.; Analysis and interpretation of data (e.g., statistical analysis, biostatistics, computational analysis): BR, EZ, JZ, WW

and SL; Writing – Original Draft, BR and SL; Writing – Review & Editing, BR, JZ, EZ, BK and SL; Funding Acquisition, CB, BK and SL; Supervision, CB, BK and SL.

### **Acknowledgements**

This work was in part funded by the Center for Integrated Protein Science Munich (CIPSM). SL acknowledges support from the Netherlands Organization for Scientific Research (NWO) through a VIDI grant (project 723.013.008). CB acknowledge support from the Netherlands Organization for Scientific Research (NWO) through a VENI grant (project 722.013.009)The authors would like to express their sincere gratitude to Andrea Hubauer for excellent technical assistance and the Department of Translational Research, GlaxoSmithKline in Pennsylvania, USA for kindly providing the lapatinib resistant and parental cell line.

## REFERENCES

1. Slamon DJ, Clark GM, Wong SG, Levin WJ, Ullrich A, McGuire WL. Human breast cancer: correlation of relapse and survival with amplification of the HER-2/neu oncogene. *Science*. 1987;235:177–82.
2. Slamon DJ, Godolphin W, Jones LA, Holt JA, Wong SG, Keith DE, et al. Studies of the HER-2/neu proto-oncogene in human breast and ovarian cancer. *Science*. 1989;244:707–12.
3. Fiore PD, Pierce JH, Kraus MH, Segatto O, King CR, Aaronson SA. erbB-2 is a potent oncogene when overexpressed in NIH/3T3 cells. *Science*. 1987;237:178–82.
4. Cobleigh MA, Vogel CL, Tripathy D, Robert NJ, Scholl S, Fehrenbacher L, et al. Multinational Study of the Efficacy and Safety of Humanized Anti-HER2 Monoclonal Antibody in Women Who Have HER2-Overexpressing Metastatic Breast Cancer That Has Progressed After Chemotherapy for Metastatic Disease. *J Clin Oncol*. 1999;17:2639–2639.
5. Hudziak RM, Lewis GD, Winget M, Fendly BM, Shepard HM, Ullrich A. p185HER2 monoclonal antibody has antiproliferative effects in vitro and sensitizes human breast tumor cells to tumor necrosis factor. *Mol Cell Biol*. 1989;9:1165–72.
6. Slamon DJ, Leyland-Jones B, Shak S, Fuchs H, Paton V, Bajamonde A, et al. Use of Chemotherapy plus a Monoclonal Antibody against HER2 for Metastatic Breast Cancer That Overexpresses HER2. *N Engl J Med*. 2001;344:783–92.
7. Xia W, Mullin RJ, Keith BR, Liu L-H, Ma H, Rusnak DW, et al. Anti-tumor activity of GW572016: a dual tyrosine kinase inhibitor blocks EGF activation of EGFR/erbB2 and downstream Erk1/2 and AKT pathways. *Oncogene*. 2002;21:6255–63.
8. Geyer CE, Forster J, Lindquist D, Chan S, Romieu CG, Pienkowski T, et al. Lapatinib plus Capecitabine for HER2-Positive Advanced Breast Cancer. *N Engl J Med*. 2006;355:2733–43.
9. Liu L, Greger J, Shi H, Liu Y, Greshock J, Annan R, et al. Novel mechanism of lapatinib resistance in HER2-positive breast tumor cells: activation of AXL. *Cancer Res*. 2009;69:6871–8.
10. Ritter CA, Perez-Torres M, Rinehart C, Guix M, Dugger T, Engelman JA, et al. Human Breast Cancer Cells Selected for Resistance to Trastuzumab In vivo Overexpress Epidermal Growth Factor Receptor and ErbB Ligands and Remain Dependent on the ErbB Receptor Network. *Clin Cancer Res*. 2007;13:4909–19.
11. Garrett JT, Olivares MG, Rinehart C, Granja-Ingram ND, Sánchez V, Chakrabarty A, et al. Transcriptional and posttranslational up-regulation of HER3 (ErbB3) compensates for inhibition of the HER2 tyrosine kinase. *Proc Natl Acad Sci*. 2011;108:5021–6.
12. Zhuang G, Brantley-Sieders DM, Vaught D, Yu J, Xie L, Wells S, et al. Elevation of receptor tyrosine kinase EphA2 mediates resistance to trastuzumab therapy. *Cancer Res*. 2010;70:299–308.
13. Lu Y, Zi X, Zhao Y, Mascarenhas D, Pollak M. Insulin-Like Growth Factor-I Receptor Signaling and Resistance to Trastuzumab (Herceptin). *J Natl Cancer Inst*. 2001;93:1852–7.
14. Nahta R, Yuan LXH, Zhang B, Kobayashi R, Esteva FJ. Insulin-like growth factor-I receptor/human epidermal growth factor receptor 2 heterodimerization contributes to trastuzumab resistance of breast cancer cells. *Cancer Res*. 2005;65:11118–28.
15. Shattuck DL, Miller JK, Carraway KL, Sweeney C. Met Receptor Contributes to Trastuzumab Resistance of Her2-Overexpressing Breast Cancer Cells. *Cancer Res*. 2008;68:1471–7.
16. Wang Q, Quan H, Zhao J, Xie C, Wang L, Lou L. RON confers lapatinib resistance in HER2-positive breast cancer cells. *Cancer Lett*. 2013;340:43–50.
17. Moody SE, Schinzel AC, Singh S, Izzo F, Strickland MR, Luo L, et al. PRKACA mediates resistance to HER2-targeted therapy in breast cancer cells and restores anti-apoptotic signaling. *Oncogene*. 2015;34:2061–71.
18. Zhang S, Huang W-C, Li P, Guo H, Poh S-B, Brady SW, et al. Combating trastuzumab resistance by targeting SRC, a common node downstream of multiple resistance pathways. *Nat Med*. 2011;17:461–9.
19. De Luca A, D'Alessio A, Gallo M, Maiello MR, Bode AM, Normanno N. Src and CXCR4 are involved in the invasiveness of breast cancer cells with acquired resistance to lapatinib. *Cell Cycle Georget Tex*. 2013;13.
20. Rexer BN, Ham A-JL, Rinehart C, Hill S, Granja-Ingram N de M, González-Angulo AM,

- et al. Phosphoproteomic mass spectrometry profiling links Src family kinases to escape from HER2 tyrosine kinase inhibition. *Oncogene*. 2011;30:4163–74.
21. Campbell IG, Russell SE, Choong DYH, Montgomery KG, Ciavarella ML, Hooi CSF, et al. Mutation of the PIK3CA Gene in Ovarian and Breast Cancer. *Cancer Res*. 2004;64:7678–81.
  22. Scaltriti M, Eichhorn PJ, Cortés J, Prudkin L, Aura C, Jiménez J, et al. Cyclin E amplification/overexpression is a mechanism of trastuzumab resistance in HER2+ breast cancer patients. *Proc Natl Acad Sci*. 2011;108:3761–6.
  23. Nagata Y, Lan K-H, Zhou X, Tan M, Esteva FJ, Sahin AA, et al. PTEN activation contributes to tumor inhibition by trastuzumab, and loss of PTEN predicts trastuzumab resistance in patients. *Cancer Cell*. 2004;6:117–27.
  24. Nahta R, Takahashi T, Ueno NT, Hung M-C, Esteva FJ. P27kip1 Down-Regulation Is Associated with Trastuzumab Resistance in Breast Cancer Cells. *Cancer Res*. 2004;64:3981–6.
  25. Xia W, Bacus S, Hegde P, Husain I, Strum J, Liu L, et al. A model of acquired autoresistance to a potent ErbB2 tyrosine kinase inhibitor and a therapeutic strategy to prevent its onset in breast cancer. *Proc Natl Acad Sci*. 2006;103:7795–800.
  26. Zhao Y, Liu H, Liu Z, Ding Y, LeDoux SP, Wilson GL, et al. Overcoming Trastuzumab Resistance in Breast Cancer by Targeting Dysregulated Glucose Metabolism. *Cancer Res*. 2011;71:4585–97.
  27. Komurov K, Tseng J-T, Muller M, Seviour EG, Moss TJ, Yang L, et al. The glucose-deprivation network counteracts lapatinib-induced toxicity in resistant ErbB2-positive breast cancer cells. *Mol Syst Biol*. 2012;8:596.
  28. Deblois G, Smith HW, Tam IS, Gravel S-P, Caron M, Savage P, et al. ERRA mediates metabolic adaptations driving lapatinib resistance in breast cancer. *Nat Commun*. 2016;7:12156.
  29. Park S, Chang C-Y, Safi R, Liu X, Baldi R, Jasper JS, et al. ERRA-Regulated Lactate Metabolism Contributes to Resistance to Targeted Therapies in Breast Cancer. *Cell Rep*. 2016;15:323–35.
  30. Médard G, Pachi F, Ruprecht B, Klaeger S, Heinzlmeier S, Helm D, et al. Optimized Chemical Proteomics Assay for Kinase Inhibitor Profiling. *J Proteome Res*. 2015;14:1574–86.
  31. Tyanova S, Temu T, Sinitcyn P, Carlson A, Hein MY, Geiger T, et al. The Perseus computational platform for comprehensive analysis of (prote)omics data. *Nat Methods*. 2016;13:731–40.
  32. Rajapaksa G, Nikolos F, Bado I, Clarke R, Gustafsson J-Å, Thomas C. ERβ decreases breast cancer cell survival by regulating the IRE1/XBP-1 pathway. *Oncogene*. 2015;34:4130–41.
  33. Wei W, Liu W, Serra S, Asa SL, Ezzat S. The breast cancer susceptibility FGFR2 provides an alternate mode of HER2 activation. *Oncogene*. 2015;
  34. Abdel-Fatah TMA, Middleton FK, Arora A, Agarwal D, Chen T, Moseley PM, et al. Untangling the ATR-CHEK1 network for prognostication, prediction and therapeutic target validation in breast cancer. *Mol Oncol*. 2015;9:569–85.
  35. Yao Z, Li J, Liu Z, Zheng L, Fan N, Zhang Y, et al. Integrative bioinformatics and proteomics-based discovery of an eEF2K inhibitor (cefatrizine) with ER stress modulation in breast cancer cells. *Mol Biosyst*. 2016;
  36. Guarino M. Src signaling in cancer invasion. *J Cell Physiol*. 2010;223:14–26.
  37. Zhao YH, Zhou M, Liu H, Ding Y, Khong HT, Yu D, et al. Upregulation of lactate dehydrogenase A by ErbB2 through heat shock factor 1 promotes breast cancer cell glycolysis and growth. *Oncogene*. 2009;28:3689–701.
  38. Fan J, Hitosugi T, Chung T-W, Xie J, Ge Q, Gu T-L, et al. Tyrosine phosphorylation of lactate dehydrogenase A is important for NADH/NAD(+) redox homeostasis in cancer cells. *Mol Cell Biol*. 2011;31:4938–50.
  39. Marsin AS, Bertrand L, Rider MH, Deprez J, Beauloye C, Vincent MF, et al. Phosphorylation and activation of heart PFK-2 by AMPK has a role in the stimulation of glycolysis during ischaemia. *Curr Biol CB*. 2000;10:1247–55.
  40. Korotchkina LG, Patel MS. Probing the mechanism of inactivation of human pyruvate dehydrogenase by phosphorylation of three sites. *J Biol Chem*. 2001;276:5731–8.
  41. Oltean S, Bates DO. Hallmarks of alternative splicing in cancer. *Oncogene*. 2014;33:5311–8.
  42. van Alphen RJ, Wiemer E a. C, Burger H, Eskens F a. LM. The spliceosome as target

- for anticancer treatment. *Br J Cancer*. 2008;100:228–32.
43. Eustáquio AS, Janso JE, Ratnayake AS, O'Donnell CJ, Koehn FE. Spliceostatin hemiketal biosynthesis in *Burkholderia* spp. is catalyzed by an iron/ $\alpha$ -ketoglutarate-dependent dioxygenase. *Proc Natl Acad Sci U S A*. 2014;111:E3376–85.
  44. He H, Ratnayake AS, Janso JE, He M, Yang HY, Loganzo F, et al. Cytotoxic Spliceostatins from *Burkholderia* sp. and Their Semisynthetic Analogues. *J Nat Prod*. 2014;77:1864–70.
  45. Crouin C, Arnaud M, Gesbert F, Camonis J, Bertoglio J. A yeast two-hybrid study of human p97/Gab2 interactions with its SH2 domain-containing binding partners. *FEBS Lett*. 2001;495:148–53.
  46. Adams SJ, Aydin IT, Celebi JT. GAB2—a Scaffolding Protein in Cancer. *Am Assoc Cancer Res*. 2012;10:1265–70.
  47. Wöhrle FU, Halbach S, Aumann K, Schwemmers S, Braun S, Auberger P, et al. Gab2 signaling in chronic myeloid leukemia cells confers resistance to multiple Bcr-Abl inhibitors. *Leukemia*. 2013;27:118–29.
  48. Reuveni H, Flashner-Abramson E, Steiner L, Makedonski K, Song R, Shir A, et al. Therapeutic destruction of insulin receptor substrates for cancer treatment. *Cancer Res*. 2013;73:4383–94.
  49. Suwa A, Kurama T, Shimokawa T. SHIP2 and its involvement in various diseases. *Expert Opin Ther Targets*. 2010;14:727–37.
  50. Daniel AR, Hagan CR, Lange CA. Progesterone receptor action: defining a role in breast cancer. *Expert Rev Endocrinol Metab*. 2011;6:359–69.
  51. Humphrey SJ, James DE, Mann M. Protein Phosphorylation: A Major Switch Mechanism for Metabolic Regulation. *Trends Endocrinol Metab*. 2015;26:676–87.
  52. Lim S-O, Li C-W, Xia W, Lee H-H, Chang S-S, Shen J, et al. EGFR Signaling Enhances Aerobic Glycolysis in Triple-Negative Breast Cancer Cells to Promote Tumor Growth and Immune Escape. *Cancer Res*. 2016;76:1284–96.
  53. Cooper JA, Reiss NA, Schwartz RJ, Hunter T. Three glycolytic enzymes are phosphorylated at tyrosine in cells transformed by Rous sarcoma virus. *Nature*. 1983;302:218–23.
  54. Korotchkina LG, Patel MS. Site specificity of four pyruvate dehydrogenase kinase isoenzymes toward the three phosphorylation sites of human pyruvate dehydrogenase. *J Biol Chem*. 2001;276:37223–9.
  55. Bhattacharya B, Mohd Omar MF, Soong R. The Warburg effect and drug resistance. *Br J Pharmacol*. 2016;173:970–9.
  56. Ruan G-X, Kazlauskas A. Lactate engages receptor tyrosine kinases Axl, Tie2, and vascular endothelial growth factor receptor 2 to activate phosphoinositide 3-kinase/Akt and promote angiogenesis. *J Biol Chem*. 2013;288:21161–72.
  57. Li L, Hanahan D. Hijacking the neuronal NMDAR signaling circuit to promote tumor growth and invasion. *Cell*. 2013;153:86–100.
  58. Boersema PJ, Raijmakers R, Lemeer S, Mohammed S, Heck AJR. Multiplex peptide stable isotope dimethyl labeling for quantitative proteomics. *Nat Protoc*. 2009;4:484–94.
  59. Ruprecht B, Koch H, Medard G, Mundt M, Kuster B, Lemeer S. Comprehensive and Reproducible Phosphopeptide Enrichment Using Iron Immobilized Metal Ion Affinity Chromatography (Fe-IMAC) Columns. *Mol Cell Proteomics*. 2015;14:205–15.
  60. Cox J, Mann M. MaxQuant enables high peptide identification rates, individualized p.p.b.-range mass accuracies and proteome-wide protein quantification. *Nat Biotechnol*. 2008;26:1367–72.



**SUPPLEMENTAL INFORMATION**

Supplemental information for this chapter is available at Cancer Research Online (<https://doi.org/10.1158/0008-5472.CAN-16-2976>).



---

## Part II

# Chapter 5

## Multi-omic profiling of survival and metabolic signaling networks in cells subjected to photodynamic therapy

Ruud Weijer<sup>1</sup>, Séverine Clavier<sup>2†</sup>, Esther A. Zaal<sup>2†</sup>, Maud M. E. Pijls<sup>1†</sup>, Robert T. van Kooten<sup>1†</sup>, Klaas Vermaas<sup>2</sup>, René Leen<sup>3</sup>, Aldo Jongejan<sup>4</sup>, Perry D. Moerland<sup>4</sup>, Antoine H.C. van Kampen<sup>4</sup>, André B.P. van Kuilenburg<sup>3</sup>, Celia R. Berkers<sup>2§</sup>, Simone Lemeer<sup>2§</sup>, Michal Heger<sup>1§#</sup>

<sup>1</sup> Department of Experimental Surgery, Academic Medical Center, University of Amsterdam, Amsterdam, the Netherlands

<sup>2</sup> Biomolecular Mass Spectrometry and Proteomics, Bijvoet Center for Biomolecular Research, Utrecht University, Utrecht, The Netherlands

<sup>3</sup> Department of Clinical Chemistry, Laboratory Genetic Metabolic Diseases, Academic Medical Center, University of Amsterdam, Amsterdam, the Netherlands

<sup>4</sup> Bioinformatics Laboratory, Academic Medical Center, University of Amsterdam, Amsterdam, the Netherlands

<sup>†</sup> *These authors equally contributed to this work*

<sup>§</sup> *Shared senior authorship*

## ABSTRACT

Photodynamic therapy (PDT) is an established palliative treatment for perihilar cholangiocarcinoma that is clinically promising. However, tumors tend to regrow after PDT, which may result from the PDT-induced activation of survival pathways in sublethally afflicted tumor cells. In this study, tumor-comprising cells (*i.e.*, vascular endothelial cells, macrophages, perihilar cholangiocarcinoma cells, EGFR-overexpressing epidermoid cancer cells) were treated with the photosensitizer zinc phthalocyanine that was encapsulated in cationic liposomes (ZPCLs). The post-PDT survival pathways and metabolism were studied following sublethal ( $LC_{50}$ ) and supralethal ( $LC_{90}$ ) PDT.

Sublethal PDT induced survival signaling in perihilar cholangiocarcinoma (SK-ChA-1) cells via mainly HIF-1-, NF- $\kappa$ B-, AP-1-, and heat shock factor (HSF)-mediated pathways. In contrast, supralethal PDT damage was associated with a dampened survival response. PDT-subjected SK-ChA-1 cells downregulated proteins associated with EGFR signaling, particularly at  $LC_{90}$ . PDT also affected various components of glycolysis and the tricarboxylic acid cycle as well as metabolites involved in redox signaling.

In conclusion, sublethal PDT activates multiple pathways in tumor-associated cell types that transcriptionally regulate cell survival, proliferation, energy metabolism, detoxification, inflammation/angiogenesis, and metastasis. Accordingly, sublethally afflicted tumor cells are a major therapeutic culprit. Our multi-omics analysis unveiled multiple druggable targets for pharmacological co-intervention.

## INTRODUCTION

Photodynamic therapy (PDT) is a non-to-minimally invasive treatment modality for solid cancers that entails the photosensitization of a tumor using light-sensitive compounds called photosensitizers. After the photosensitizer molecules have sufficiently accumulated in the target tissue, the tumor is illuminated with light to activate the photosensitizer molecules [1]. Activated photosensitizers interact with molecular oxygen through energy or electron transfer, leading to the photochemical production of singlet oxygen and superoxide anion, respectively. These reactive oxygen species (ROS) subsequently attack biomolecules in the vicinity of their production site and induce a state of hyperoxidative stress in the illuminated tumor cells in case of an optimal PDT regimen. The oxidative damage in turn results in tumor cell death, microvascular shutdown and corollary tumor hypoxia and hyponutrition, and induction of an anti-tumor immune response (reviewed in [2]), altogether culminating in tumor destruction and removal.

Some types of cancers respond well to PDT and are associated with excellent cure rates, including esophageal carcinoma [3] and basal cell carcinoma [4]. In contrast, the cure rates for nasopharyngeal carcinomas [5] and superficial recurrent urothelial carcinomas [6,7] are suboptimal with respect to PDT and warrant improvement. Moreover, non-resectable perihilar cholangiocarcinomas respond better to PDT than to any other last-line treatment such as chemotherapy [8], but all available treatments (including PDT) are currently palliative and not curative. The recalcitrant nature of these tumor types to PDT is believed to stem from the use of photosensitizers with suboptimal spectral properties and poor pharmacokinetics as well as the activation of cell survival pathways by tumor cells following PDT [9,2].

In order to resolve these issues with a single therapeutic modality, we have developed a 4<sup>th</sup>-generation photosensitizer-based PDT platform that aims to target pharmacologically relevant locations in the tumor, namely the tumor cells [10], the tumor endothelium [11-13], and the tumor interstitium [14]. The platform employs a 2<sup>nd</sup>-generation photosensitizer (zinc phthalocyanine, ZnPC) encapsulated in targeted liposomes (making it a 3<sup>rd</sup>-generation photosensitizer, which was employed in this study) with co-encapsulated molecular inhibitors of survival pathways (making it a 4<sup>th</sup>-generation photosensitizer) [14,10,13,9,12,2,11]. Previously, we demonstrated that PDT of human skin and bile duct cancer cells with liposomal ZnPC and acriflavine, an inhibitor of hypoxia-inducible factor 1 $\alpha$  (HIF-1 $\alpha$ ) [15], increases therapeutic efficacy by downmodulation of HIF-1 $\alpha$ -driven survival signaling following PDT [13,11]. In light of this combined therapy and the broader scope of applicability of the PDT platform technology, it is imperative to map post-PDT survival pathways [9] for every

liposomal formulation so as to identify druggable targets beyond those already tested [9]. So far we have mapped PDT-activated survival pathways with respect to the interstitially targeted ZnPC-liposomes [16], but not yet for the endothelium- and tumor cell-targeting liposomes.

Of the three different liposomal formulations that were developed, the most promising is the tumor endothelium-targeting ZnPC formulation. These liposomes, which are cationic and PEGylated, are taken up by cultured endothelial cells [14], macrophages (manuscript in preparation), and tumor cells [14,13,11], enabling multi-targeted delivery of the photosensitizer to key locations. Moreover, the liposomes are relatively non-toxic in the absence of light (this study), but become highly toxic to cultured cells upon illumination in the low nanomolar photosensitizer concentration range [13,11]. Finally, ZnPC distributes to multiple intracellular loci after uptake of the liposomes [17,18], from which different cell death pathways but also cell survival pathways are activated [2]. In preliminary experiments it was discovered that epidermal growth factor receptor (EGFR), a receptor overexpressed in a multitude of cancers [19] including perihilar cholangiocarcinoma [20,21], was afflicted by PDT with ZnPC-liposomes. EGFR constitutes an important druggable target in cancer therapy, as evidenced by the approval status of the monoclonal antibodies cetuximab and panitumumab as well as the kinase inhibitors gefitinib and erlotinib [22].

This study therefore examined the cell survival pathways induced by ZnPC-encapsulating PEGylated cationic liposomes (ZPCLs) in tumor parenchymal and non-parenchymal cell types using a multi-omics approach: transcriptomics, (phospho)proteomics, and metabolomics. The cells that were employed are human umbilical vein endothelial cells (HUVECs) as a model for vascular endothelium; RAW 264.7 murine macrophages as a model for tumor-resident macrophages; human biliary adenocarcinoma (SK-ChA-1) cells as model for PDT-recalcitrant perihilar cholangiocarcinomas; and EGFR-overexpressing human epidermoid carcinoma (A431) cells to further elaborate on the preliminary experimental results. The studies were performed at supralethal light dose (90% lethal concentration,  $LC_{90}$ ), reflective of cells fully affected by PDT, and at sublethal light dose ( $LC_{50}$ ), representative of cells in the distant and peripheral portions of the illuminated tumor, where the fluence rates are insufficient due to light absorption and scattering [23]. Therapeutically, the low-fluence sites are the most important tumor regions because survival signaling is expected to predominate, which may negatively impact therapeutic outcome and facilitate tumor recurrence as has been observed in PDT-treated patients [24].

The most important results of the study were that (1) ZPCLs were not toxic *in vitro*, which is key for clinical translation, (2) sublethal PDT was associated with extensive

survival signaling, which is detrimental to therapeutic outcome, (3) PDT resulted in downregulation of proteins involved in EGFR signaling and cell adhesion, in particular after optimal PDT, and (4) sublethal and optimal PDT both downregulated metabolic pathways involved in energy production, including glycolysis and the tricarboxylic acid (TCA) cycle. The latter two findings are chiefly advantageous for therapeutic efficacy.

## RESULTS

### PDT induces photosensitizer concentration- and time-dependent cell death

To correlate the transcriptomic-, (phospho)proteomic-, and metabolomic responses to the extent of PDT-induced cell death, the viability of HUVEC, RAW 264.7, SK-ChA-1, and A431 cells was determined first as a function of time after PDT at previously calculated  $LC_{50}$  and  $LC_{90}$  concentrations (details can be found in Supplemental Table S1). The effect of PDT on cells was assessed with the *water*-soluble tetrazolium salt (WST-1) and sulforhodamine B (SRB) assays. WST-1 is a measure of mitochondrial metabolic activity [33] and therefore represents a parameter of early-onset cell demise. In contrast, SRB stains total protein and is therefore used as a parameter of late, fully executed cell death.

The ZPCLs exhibited no deleterious effect on metabolic activity (Fig. 1A-D) or cell viability (Fig. 1E-H) in any of the cell types in the absence of laser irradiation, indicating that the ZPCLs imparted no dark toxicity. The loss of metabolic activity (Fig. 1A-D) and extent of cell death (Fig. 1E-H) were more pronounced in the  $LC_{90}$  group versus the  $LC_{50}$  group and occurred in a time-dependent manner. The loss of metabolic activity is in line with the localization of ZnPC to mitochondrial membranes [2] and the post-PDT induction of mitochondrial permeability transition [12]. Typically, cells were most afflicted at the longest incubation time, underscoring that metabolic perturbations and execution of cell death pathways are progressive during at least 24 hours after PDT. Unexpectedly, the  $LC_{90}$  HUVECs showed significantly higher cell viability 24 hours after PDT compared to 2 hours post-PDT (Fig. 1E). HUVECs in the  $LC_{90}$  group were also more resilient to treatment 24 hours following PDT than HUVECs in the  $LC_{50}$  group (Fig. 1E).

### PDT at $LC_{90}$ has greater transcriptional effects than at $LC_{50}$ , but the effect size is cell type-dependent

To gain insight in the early transcriptomic response after PDT with ZPCLs, non-illuminated and PDT-treated cells were harvested 90 minutes after (control) treatment

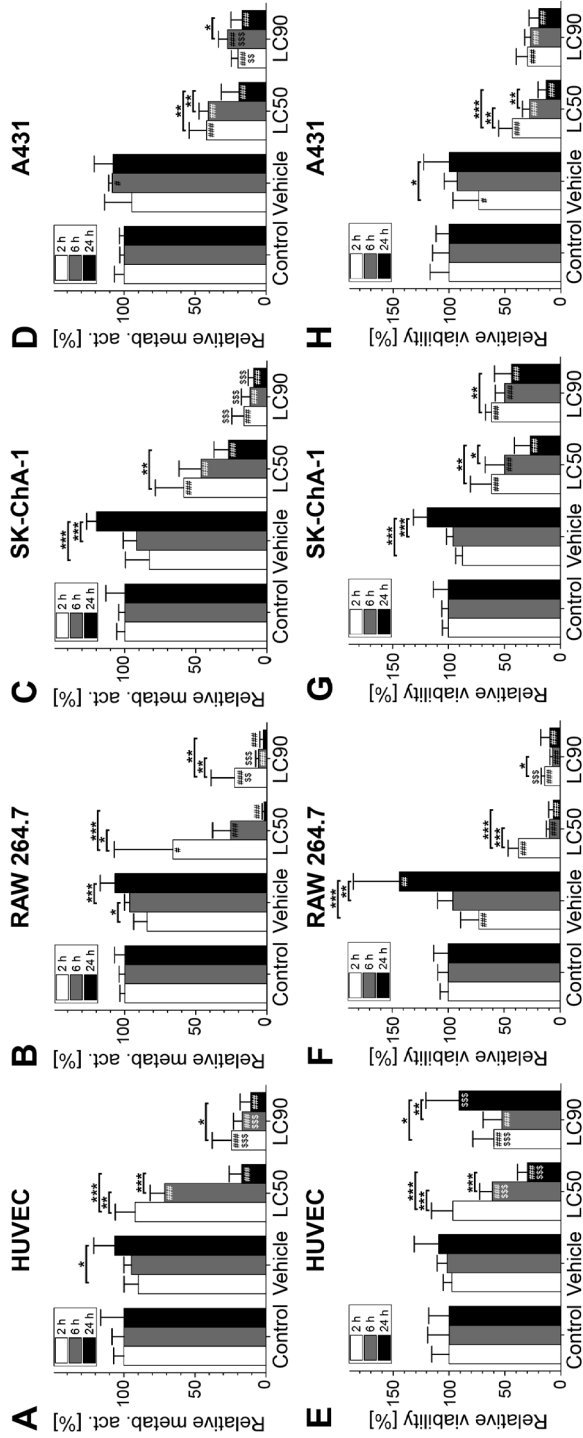


**Figure 1. Cell viability after ZPCL-PDT.** a-h HUVEC, RAW 264.7, SK-ChA-1, and A431 cells were incubated with ZPCLs (concentrations can be found in Table S1) and treated with PDT. Two hours (white bar), 6 hours (light grey bar), and 24 hours (dark grey bar) after PDT, cell viability was determined using the a-d WST-1 and (E-H) SRB assay ( $n = 8$  per group). Readers are referred to the experimental section for the significance of the statistical symbols. Abbreviation: metab. act., metabolic activity.



and the transcriptome was analyzed by whole genome microarray, summarized in Fig. 2, and correlated to cell viability. This toxicogenomics approach corroborated the absence of dark toxicity of ZPCLs (Fig. 2, vehicle vs control), given that of all screened genes, none were dysregulated compared to control. The same had been observed previously with the ZnPC-encapsulating interstitially-targeted liposomes [16], which differ from the ZPCLs in that they lack DC-cholesterol in the membrane and therefore bear a neutral surface charge rather than a cationic charge.

In case of the interstitially targeted liposomes, the milder PDT protocol (irradiation of cells at 50 mW) induced more profound transcriptional dysregulation than the severe PDT regimen (500 mW laser irradiation) [16]. In contrast, the extent of mRNA dysregulation following PDT with ZPCLs was most pronounced in the LC<sub>90</sub> groups compared to the LC<sub>50</sub> groups (Fig. 2). The overlap between genes dysregulated in both the LC<sub>90</sub> and LC<sub>50</sub> groups was also cell type-specific. The highest number of commonly afflicted genes was observed in RAW 264.7 cells (3363), followed by A431 (790), SK-ChA-1 (638), and HUVEC (134) cells.

### **PDT-mediated induction of survival signaling**

The basis of therapeutic recalcitrance towards PDT may partly originate from the induction of survival signaling after PDT [16]. PDT activates six major pathways that encompass a nuclear factor of kappa light polypeptide gene enhancer in B cells (NF-κB)-mediated inflammatory response, a proteotoxic stress response via the unfolded protein response (UPR) and heat shock transcription factor (HSF)-mediated response, an activator protein 1 (AP-1)-mediated immediate early gene response, a HIF-1-mediated hypoxia-induced stress response, and a nuclear factor (erythroid-derived 2)-like (NFE2L2)-mediated antioxidant response [9]. The pathways have been described in detail in [16,34]. The microarray expression data were superimposed on these pathways (Fig. S3 (with pathways and transcriptional targets) and Fig. 3 (transcriptional targets only)).

The downstream targets of the survival pathways were analyzed with a ROAST gene test to determine whether a pathway was differentially regulated in response to PDT. All cell types upregulated the NF-κB, AP-1, and HSF survival pathways at LC<sub>50</sub> and LC<sub>90</sub>, whereas only the LC<sub>50</sub> groups exhibited upregulation of HIF-1-mediated signaling (Table S4). Importantly, HIF-1-, UPR-, AP-1-, and NF-κB-associated genes were less extensively dysregulated in the LC<sub>90</sub> group of the tumor-derived cell lines (A431, SK-ChA-1) compared to the LC<sub>50</sub> group. In contrast, the LC<sub>90</sub> group of the non-tumor derived cells (RAW 264.7, HUVEC) displayed more HSF-mediated signaling than the LC<sub>50</sub> group. Altogether, these findings indicate that PDT induced

extensive survival signaling in all cell types tested, whereby survival signaling was more prominent in cells treated by sublethal PDT.

### ***NF-κB-mediated inflammatory response***

NF-κB mediates an inflammatory response following PDT [35,36]. As shown in Fig. 3, the transcription of various pro-inflammatory cytokines that are under the control of NF-κB, including interleukin 1A (*IL1A*), *IL1B*, *IL6*, and chemokine (C-X-C motif) ligand 8 (*CXCL8*), increased following PDT in the human cell types. Murine *Il1b* and *Cxcl2* were also considerably induced following PDT in RAW 264.7 cells. Sublethal PDT

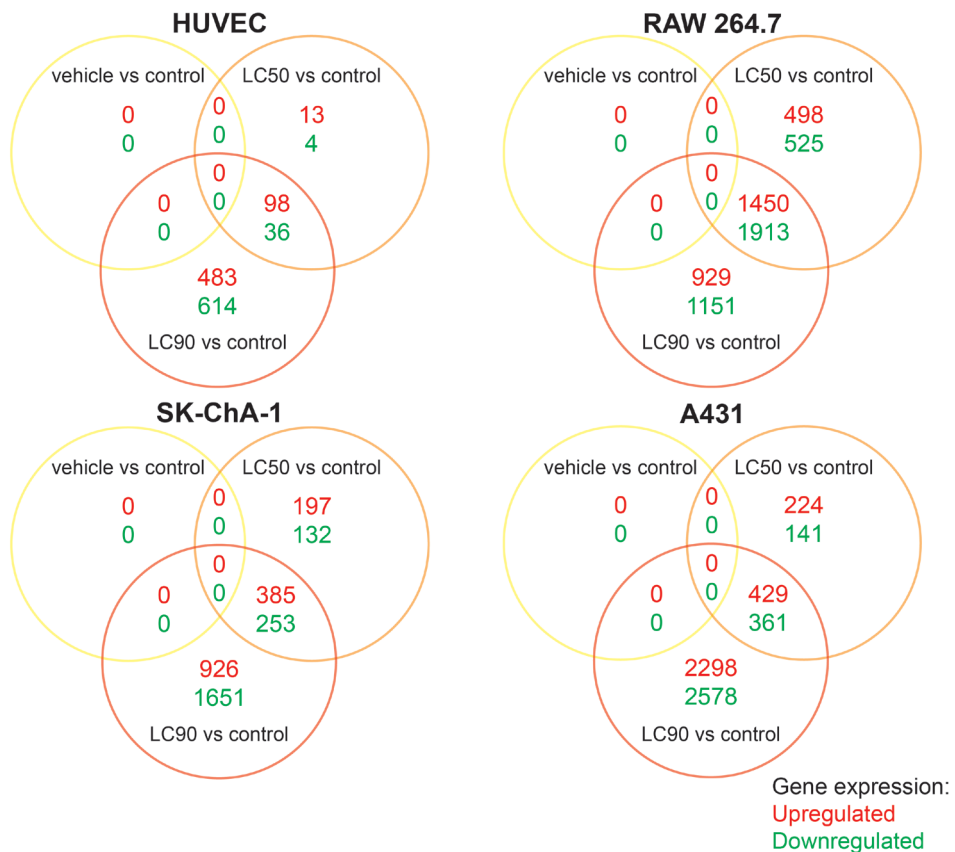


**Figure 2. Gross transcriptional response 90 minutes after ZPCL-PDT.**

The Venn diagrams show the number of upregulated (red) and downregulated (green) genes compared to the control group (FDR < 0.05), as well as the overlapping genes between the vehicle (dark toxicity), LC<sub>50</sub>, and LC<sub>90</sub> groups (*n* = 3 per group). The total number of upregulated and downregulated genes per PDT regimen (full circle) equals the sum of all values enveloped by the respective circle.

resulted in upregulation of vascular endothelial growth factor (*VEGF*) in SK-ChA-1 and A431 cells, which was downregulated in HUVEC cells. The pro-inflammatory factor prostaglandin-endoperoxide synthase 2 (*PTGS2*, *Ptgs2*) was also highly upregulated following PDT in HUVEC, RAW 264.7, and A431 cells.

### ***Proteotoxic stress response***

The proteotoxic stress response can be induced by ROS-mediated endoplasmic reticulum (ER) stress that leads to the accumulation of misfolded and unfolded proteins in the ER [37]. As a result, the UPR is initiated together with the activation of HSF1 [38]. ZPCL-PDT at both regimens induced upregulation of the UPR-associated genes DNA-damage-inducible transcript 3 (*DDIT3*, *Ddit3*), activating transcription factor 3 (*ATF3*, *Atf3*), protein phosphatase 1, and regulatory subunit 15A (*PPP1R15A*, *Ppp1r15a*) in all cell types (Fig. 3). PDT at LC<sub>50</sub> triggered upregulation of DnaJ (Hsp40) homolog, subfamily B, member 9 (*DNAJB9*) in all cell types, of which the protein product protects cells from apoptosis [39]. With respect to HSF signaling, all cell types exhibited elevated *DNAJB1* (*Dnajb1*) and heat shock 70kDa protein 1A (*HSPA1A*, *Hspa1a*) mRNA levels following PDT (Fig. 3). In contrast to RAW 264.7, SK-ChA-1, and A431 cells, HUVECs revealed a dose-dependent effect on the transcript levels of *HSPA1A*, *DNAJB1*, *JUN*, and *FOS*, where PDT at LC<sub>90</sub> caused the most pronounced upregulation of these genes.

### ***AP-1-mediated immediate early gene response***

In response to various extracellular and intracellular (e.g., ROS) stimuli, the immediate early response is activated via apoptosis signal-regulating kinase 1 (ASK-1) that enables AP-1-mediated transcription [40]. The AP-1 transcription factors FBJ murine osteosarcoma viral oncogene homolog (*FOS*, *Fos*) and jun B proto-oncogene (*JUNB*, *Junb*) were upregulated in RAW 264.7, SK-ChA-1, and A431 cells in both the LC<sub>50</sub> and LC<sub>90</sub> groups (Fig. 3). Furthermore, the survival factor heparin-binding EGF-like growth factor (*HGEGF*, *Hbegf*) was strongly upregulated in all cell types following both PDT regimens. *EGFR* was downregulated in HUVEC, SK-ChA-1, and A431 cells, particularly in the LC<sub>90</sub> group.

In addition, the effect of PDT on EGFR signaling in EGFR-overexpressing A431 cells versus SK-ChA-1 cells is shown in more detail in Fig. S4. This subanalysis revealed that PDT had an inhibitory effect on the various ErbB isoforms, which was observed in both cell lines, although *EGFR* (*ERBB1*) was mostly afflicted. Also, known downstream targets of EGFR [41] appeared to be more inhibited in A431 cells compared to SK-ChA-1 cells after supralethal PDT (Fig. S4).

### **HIF-1-mediated hypoxia-induced stress response**

HIF-1 is a transcription factor that is induced by ROS and hypoxia [42], which promotes the transcription of genes involved in cell survival and angiogenesis [43]. ZPCL-PDT caused upregulation of various HIF-1-associated genes, including *VEGFA* (not in HUVECs), *PTGS2*, endothelin 1 (*EDN1*), myeloid cell leukemia 1 (*MCL1*), and phorbol-12-myristate-13-acetate-induced protein 1 (*PMAIP1*) (Fig. 3). The effects were more pronounced after sublethal PDT. PDT also upregulated several HIF-1-associated genes in RAW 264.7 cells, including *Vegfa*, *Ptgs2*, *Edn1*, and *Pmaip1* but not *Mcl1*. However, RAW 264.7 cells did not exhibit any dose-dependent differences as observed in the human cell types.

### **NFE2L2-mediated antioxidant response**

The NFE2L2-mediated antioxidant response is activated by oxidative stress and serves to restore the cellular redox balance. As shown in Fig. 3, the NFE2L2 pathway was largely unaffected. In fact, PDT reduced the expression of genes involved in detoxification (e.g., *ATP binding cassette subfamily C member 4* (*ABCC4*, *Abcc4*), *ATP binding cassette subfamily G member 2* (*ABCG2*, *Abcg2*)), and antioxidant activity (e.g., *epoxide hydrolase 1* (*EPHX1*, *Ephx1*)). Heme oxygenase 1 (*HMOX1*, *Hmox1*) is linked to cell survival following PDT [44]. In addition to NFE2L2, HIF-1 (section 3.3.4) is also able to mediate transcription of *HMOX1* [45]. Its gene expression after PDT was higher in RAW 264.7, SK-ChA-1, and A431 cells but not in HUVEC cells. This effect was more pronounced in the LC<sub>50</sub> cells compared to the LC<sub>90</sub> cells as evidenced by the log<sub>2</sub> fold-changes in *HMOX1/Hmox1* gene expression: A431 (2.1 versus 1.3, respectively), SK-ChA-1 (2.1 versus 1.4, respectively), and RAW 264.7 cells (1.7 versus 1.5, respectively).

### **PDT upregulates transcription-related proteins and downregulates proteins linked to EGFR signaling**

To explore the cellular response in a cell line derived from a tumor that is refractory towards PDT [24], SK-ChA-1 cells were subjected to more in-depth analysis using an untargeted (phospho)proteomic-based approach 90 minutes after PDT. The EGFR-overexpressing A431 cell line was excluded from the (phospho)proteomic analysis to eliminate redundancy, given that SK-ChA-1 cells also express high basal levels of EGFR [46]. The differentially expressed phosphorylated and non-phosphorylated proteins (compared to non-treated cells) are presented in Table S5. A no-liposome, irradiation-only group was excluded because we have shown previously that red light irradiation has no effect on cells [14].

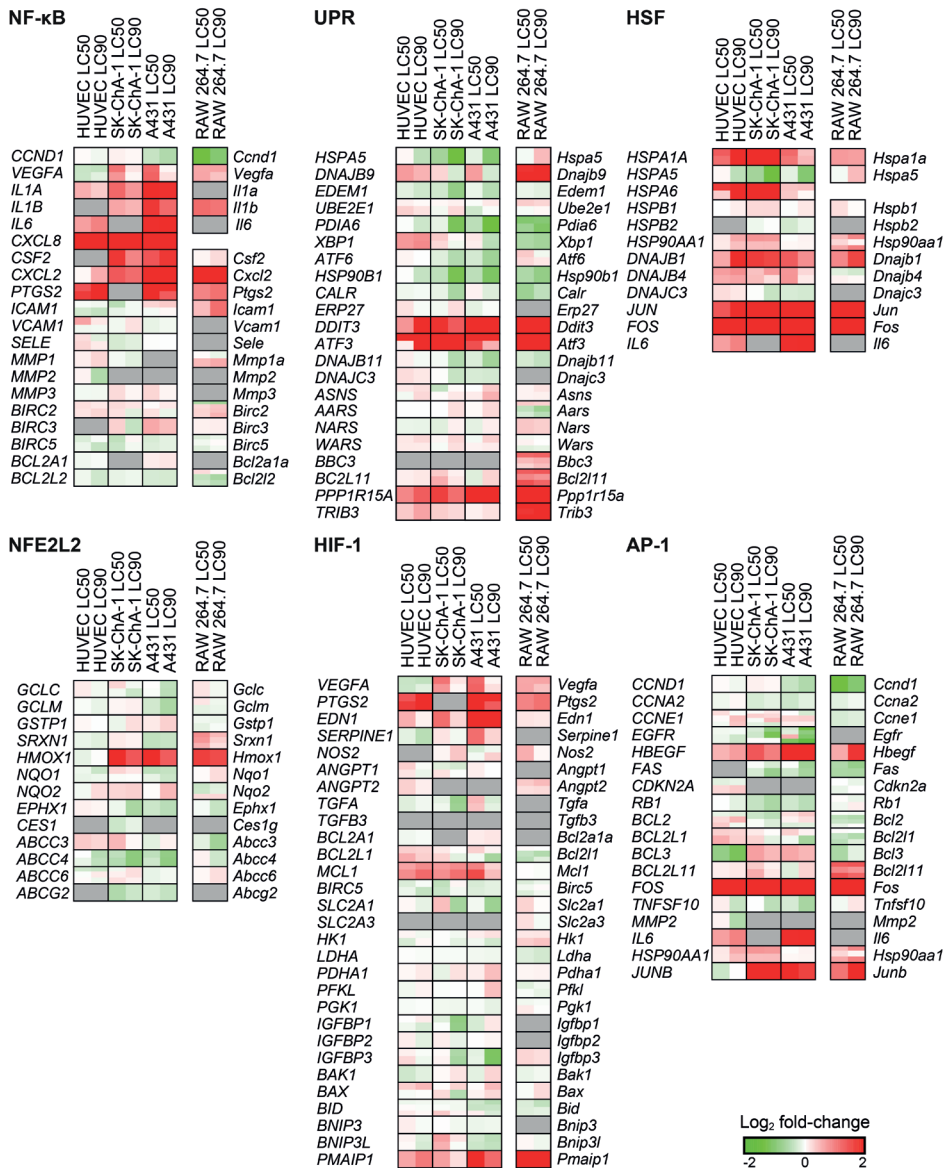


**Figure 3. Transcriptional response following ZPCL-PDT.**

Expression analysis of genes that are involved in NF-κB, UPR, HSF, NFE2L2, HIF-1, and AP-1 signaling as shown by the log<sub>2</sub> fold-change (lower right corner). All comparisons were made between the PDT-treated groups versus the control group ( $n = 3$  per group). A gene may correspond to multiple probes as indicated by horizontal splits. Each gene is divided in two halves corresponding to the LC<sub>50</sub> (left) and LC<sub>90</sub> (right) group. Grey boxes signify probes that exhibited poor quality or were not included in the gene expression analysis.

The proteome data revealed a dose-dependent response in the number of differentially expressed proteins (Fig. S5). To gain more insight in the affected molecular pathways, the data were analyzed with Reactome [47,48] (Fig. 4). Based on the proteomics data, PDT caused downregulation of various proteins involved in endocytosis in the LC<sub>50</sub> group, but more predominantly in the LC<sub>90</sub> group (AP-2 complex subunit alpha-1 (AP2A1), AP2M1, AP2B1, AP3B1). Furthermore, SK-ChA-1 cells that had been treated at LC<sub>90</sub> upregulated proteins involved in pre-RNA splicing (serine/arginine-rich splicing factor 4 (SRSF4), SRSF6) and epigenetic control of transcription (protein dpy-30 homolog (DPY30), WD repeat-containing protein 5 (WDR5)) (Fig. 4).

Phosphoproteomic data were analyzed with the Phosphopath plugin in Cytoscape [32] and only phosphosites which were differentially regulated in either LC<sub>50</sub> or LC<sub>90</sub> groups were analyzed. PDT of SK-ChA-1 cells induced the phosphorylation of heat shock protein beta-1 (HSPB1) (Fig. 5), which is involved in the defense against oxidative stress [49,50]. Furthermore, PDT decreases phosphorylation of proteins involved in EGFR signaling, such as mitogen-activated protein kinase 1 (MAPK1), son of sevenless homolog 1 (SOS1), and catenin delta-1 (CTNND1). This effect was more evident at LC<sub>90</sub> inasmuch as these cells downregulated the EGFR-associated proteins EGFR (confirmed by Western blotting, Fig. S2), proto-oncogene tyrosine-protein kinase Src (SRC), caveolin-1 (CAV1), and phosphorylated proteins SOS1, related RAS viral (r-ras) oncogene homolog 2 (RRAS2), MAPK1, and MAPK3. Altogether, it seems that PDT induced the expression of transcription-related proteins and downregulated proteins involved in EGFR signaling.

### **PDT affects metabolites that are involved in energy production and redox signaling**

Finally, PDT-treated SK-ChA-1 cells were investigated in terms of metabolomics at 90 minutes post-PDT. Incubation of cells with ZPCLs in the absence of light only marginally affected the metabolomic profile (Fig. 6A, Table S6), again confirming the *in vitro* safety of the ZPCLs.

PDT highly influenced almost all studied metabolites, whereby the effects observed in the LC<sub>50</sub> group were essentially exacerbated in the LC<sub>90</sub> group. PDT-subjected SK-ChA-1 cells upregulated multiple amino acid levels as well as metabolites involved in nucleotide metabolism. In contrast, metabolites involved in the TCA cycle and urea cycle were downregulated, reflecting perturbations in anaerobic energy production as evidenced by the lactate and succinate accumulation. Moreover, PDT also affected metabolites that modulate the redox balance (Fig. 6B). Glutathione and oxidized glutathione (GSSG) were downregulated, while nicotinamide adenine dinucleotide phosphate (NADP<sup>+</sup>) was upregulated. Possibly as a consequence of

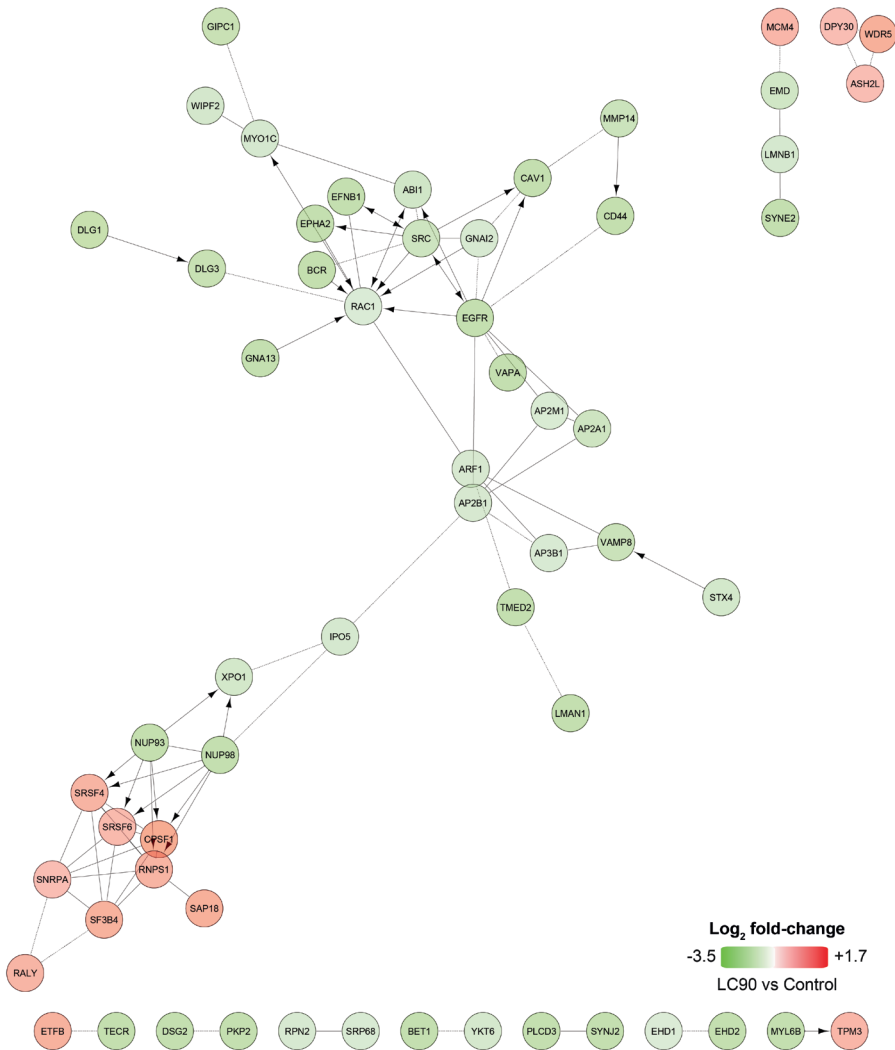


**Figure 4. Differentially expressed proteins observed after ZPCL-PDT of SK-ChA-1 cells in the LC90 group.** Up- (in red) and downregulated (in green) proteins between the PDT-treated groups and control group ( $n = 4$  per group) were analyzed using Reactome to assess functional interactions [48,47]. Arrows indicate activating/catalyzing reactions, whereas straight and dashed lines indicate functional and predicted functional interactions, respectively. Proteins without functional interactions are not displayed in the figure.

the pro-oxidative state, metabolites in the oxidative branch of the pentose phosphate pathway were upregulated (Table S6). Lastly, the nucleotide profile was also determined in PDT-treated cells, which showed slightly lower uridine triphosphate (UTP), cytidine triphosphate (CTP), and guanosine triphosphate (GTP) levels in the LC<sub>50</sub> group (Fig. S6). The lower ATP:ADP ratio in PDT-treated cells may be indicative of dying cells (Fig. S6).

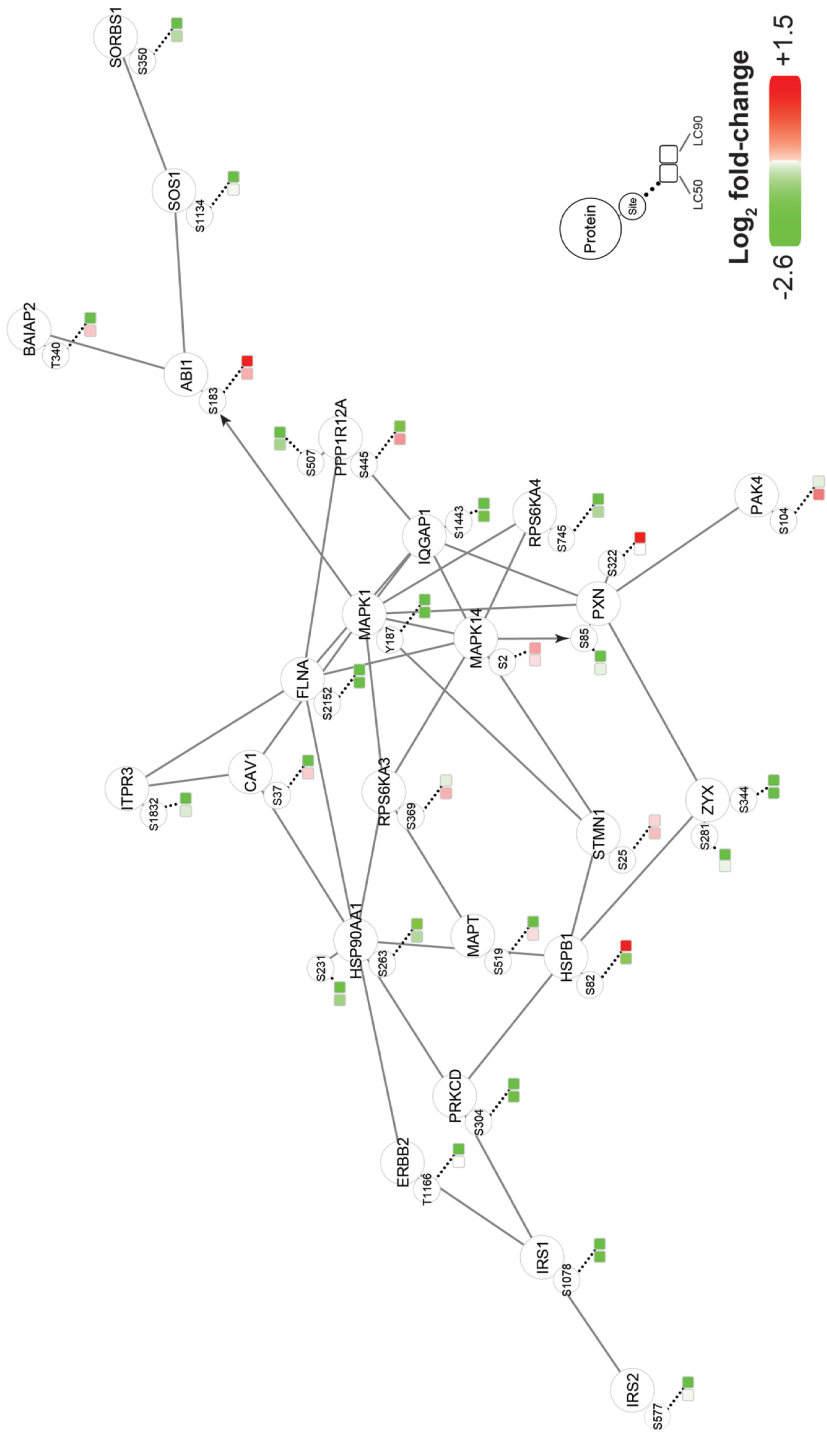


**Figure 5. Phosphoproteomic analysis of SK-ChA-1 cells after ZPCL-PDT.**

The data ( $n = 4$  per group) were analyzed with the PhosphoPath plugin in Cytoscape [32] and increased and decreased phosphorylation of proteins in the PDT-treated groups versus the control group are indicated in red and green, respectively. Straight lines and arrows indicate protein interactions (derived from the Biogrid database [78]) and kinase-substrate interactions (imported from PhosphoSitePlus [79]), respectively. WikiPathways was used for pathway analysis [80], where the dataset was queried against this database to identify pathways. For this figure, EGF, VEGF, insulin, FAK, and MAPK signaling pathways were selected.



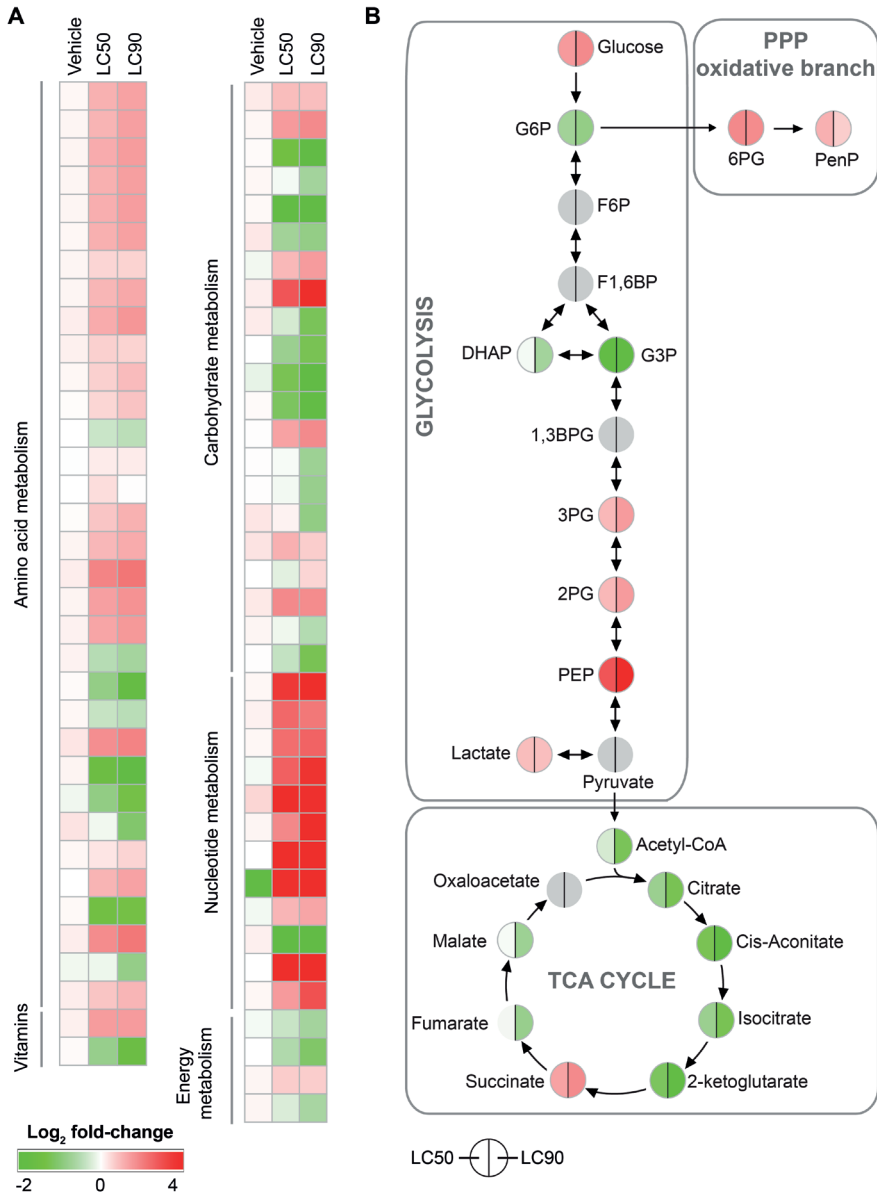


**Figure 6. Metabolomic analysis of SK-ChA-1 cells after ZPCL-PDT.**

**a** Metabolites were classified into pathways and metabolite expression is depicted as the  $\log_2$  fold-change (bottom left corner) between treated and control cells ( $n = 3$  per group). Numerical values can be found in Table S6.

**b**  $\log_2$  fold-change of metabolites in the category carbohydrate metabolism grouped per pathway. Changes in LC<sub>50</sub>-treated (left) and LC<sub>90</sub>-treated (right) SK-ChA-1 cells compared to control cells are depicted. Identical  $\log_2$  fold-change values are plotted for 3PG and 2PG and for citrate and isocitrate, as these metabolites could not be resolved. Metabolites indicated in grey could not be quantified. Abbreviations: TCA cycle, tricarboxylic acid cycle; PPP, pentose phosphate pathway; G6P, glucose-6-phosphate; F6P, fructose-6-phosphate; F1,6BP, fructose-1,6-bisphosphate; DHAP, dihydroxyacetone phosphate; G3P, glyceraldehyde-3-phosphate; 1,3 BPG, 1,3-bisphosphoglycerate; 3PG, 3-phosphoglycerate; 2PG, 2-phosphoglycerate; PEP, phosphoenolpyruvate; 6pG, 6-phosphogluconate; PenP, pentose-phosphate.

**Table 1.** Potential druggable targets that were identified in this study.

	Identified target	Druggable target	General function	Inhibitor	PDT efficacy	Ref.
Transcriptomics	↑ <i>HMOX1</i>	<i>HMOX1</i>	Cytoprotective, antioxidative properties	SnPPiX	↑	[75]
	↑ AP-1 pathway	AP-1	Proliferation, inflammation, apoptosis	ZnPPiX	↑	[44,76]
	↑ HIF-1 pathway	HIF-1	Survival, angiogenesis, glycolysis	Acridiflavine	n.d.	[9]
	↑ HSF pathway	HSF1	Proteostasis, survival	HIF-1 $\alpha$ siRNA	↑	[13,11]
	↑ NF- $\kappa$ B pathway	NF- $\kappa$ B	Inflammation, proliferation, anti-apoptosis	-	↑	[57]
	↑ HSPB1	HSPB1	Anti-apoptosis, cell invasion	NF- $\kappa$ B siRNA	n.d.	[9]
Proteomics	↑ Succinate	SUCNR1	Inflammation, HIF-1 stabilization	-	↑	[35]
Metabolomics				Dihydroartemisinin	↑	[58]
				BAY 11-7082	↑	[59]
				-	↑↓	[50,77]
				-	n.d.	[73]

For all the molecular targets, its general function is listed, as well as whether inhibition improves (indicated with ↑) or hampers (indicated with ↓) PDT efficacy. Abbreviations: SnPPiX, tin protoporphyrin; ZnPPiX, zinc protoporphyrin; siRNA, small interfering RNA; n.d., not determined; SUCNR1, succinate receptor 1.

## DISCUSSION

Clinical PDT may be enhanced by pharmacologically interfering in molecular pathways that mediate resistance to therapy [2]. During PDT, light intensity attenuates in the tumor tissue as a result of absorption and scattering, creating a gradient of cumulative light dose (fluence) across the tumor. Since PDT-mediated ROS production is proportional to the fluence [14], tumor cells that are more distal from the light source, or tumor cells that are insufficiently oxygenated, may experience less oxidative stress than fully exposed cells [23], allowing the sublethally afflicted cells to activate survival pathways. Inasmuch as tumor cell survival may ultimately enable recurrence and metastasis, it is critical that the tumor bulk is completely eradicated in a single PDT session.

One potential strategy to optimize PDT is by using pharmacological adjuvants that inhibit post-PDT survival signaling, which may be co-administered with the photosensitizer [13,12,11]. This study was conducted to determine which pathways are activated and hence eligible for pharmacological targeting. The response of tumor parenchymal and non-parenchymal cells subjected to sublethal ( $LC_{50}$ ) and supralethal PDT ( $LC_{90}$ ) was therefore investigated in the acute phase of PDT – a time point where the transcriptome and acute phase proteins were expected to be dysregulated. SK-ChA-1 and A431 cells were used because the former are derived from a tumor known to be refractory to PDT [51,52] and because both overexpress EGFR, which was shown to be profoundly affected by PDT. It is critical to underscore that the post-PDT environment temporally evolves in a dynamic manner at the level of the transcriptome, lipidome, proteome, and metabolome [53]. In support of this, the extent of PDT-induced cell death progressively increased at 2, 4, and 24 hours after PDT and transcriptomic and (phospho)proteomic analysis revealed that mRNA and protein expression was discordant at 90 minutes post-PDT (Fig. S7). Firstly, mRNA and protein expression profiles may be more in sync at later time points, *i.e.*, when the mRNA has been translated to functional proteins. Secondly, the transcriptome and proteome are also expected to change over time, potentially necessitating an acclimating pharmacological inhibition strategy after PDT. Because the transcriptomic-, (phospho)proteomic-, and metabolomic temporal changes are vital to therapeutic outcome, studies in our labs are underway to establish post-PDT molecular signatures across the 24-hour time span.

In the acute phase, transcriptomic analysis revealed that PDT-treated tumor cells (SK-ChA-1, A431) were afflicted at multiple physiological and biochemical junctions and activated extensive survival signaling via HIF-1, NF- $\kappa$ B, AP-1, and HSF. Survival signaling was most pronounced in the low-dose PDT group, which is detrimental to

the desired clinical outcome. Second, PDT-treated SK-ChA-1 cells downregulated proteins involved in EGFR signaling. Third, metabolomic analysis of PDT-treated SK-ChA-1 cells pointed to downregulation of metabolites involved in energy metabolism (glycolysis, TCA cycle), altered cellular redox state, and upregulation of metabolites involved in nucleotide metabolism and the pentose phosphate pathway. These latter two findings are expected to be beneficial for PDT outcome, as EGFR downregulation and perturbed energy metabolism negatively affect cell viability and proliferation and hence offset the survival signaling.

The ROAST gene set analysis supports our hypothesis that suboptimally treated tumor cells ( $LC_{50}$ ) engage in more extensive survival signaling in response to PDT. Especially the HIF-1- and NF- $\kappa$ B-mediated pathways may be attractive for therapeutic interventions. PDT of SK-ChA-1 and A431 cells upregulated genes downstream of HIF-1 and NF- $\kappa$ B (*IL1A*, *IL1B*, *IL6*, *CXCL8*, *VEGFA*, *HMOX1*) that mediate inflammation, survival, and angiogenesis [54,55]. These findings have been echoed in literature (Table 1). Whereas overexpression of HIF-1 was associated with therapeutic resistance in 5-aminolevulinic acid (5-ALA)-PDT-treated human esophageal carcinoma cells [56], combination therapy of siRNA-mediated knockdown of HIF-1 with Photosan-PDT significantly improved therapeutic efficacy in human head-and-neck cancer (SCC4, SAS) tumor-bearing mice [57]. Corroboratively, treatment of A431 and SK-ChA-1 cells with the HIF-1 inhibitor acriflavine significantly improved PDT efficacy [11,13]. Similarly, it was shown in various studies that combined treatment comprising NF- $\kappa$ B inhibitors and PDT augmented therapeutic efficacy [35,58,59].

In addition to the tumor-derived cell lines, murine macrophages (RAW 264.7) responded fervently to PDT, inasmuch as these cells significantly upregulated all survival pathways (except for NFE2L2 in the  $LC_{90}$  group). This hyperactive state may in part have been caused by the fact that macrophages become activated upon exposure to dying cells and cell debris [60], including post-PDT [35]. The same pattern was observed for HUVEC cells, but in contrast to the tumor cell lines, only few differences were observed between the  $LC_{50}$  and  $LC_{90}$  groups. Unexpectedly, after PDT the endothelial cells slightly downregulated *VEGF*, which is a growth factor for (tumor) endothelium that stimulates angiogenesis. Zhang *et al.* also observed downregulated VEGF protein levels after hypericin-PDT in HUVECs [61], which may indicate that PDT is able to induce growth inhibition of tumor endothelium.

SK-ChA-1 cells were also subjected to (phospho)proteomic and metabolomic analysis, of which the main results are summarized in Fig. 7. At the proteomic level, PDT mediated phosphorylation of HSPB1, which is a stress protein that acts as a chaperone to stimulate survival under stress conditions [50]. PDT at  $LC_{90}$

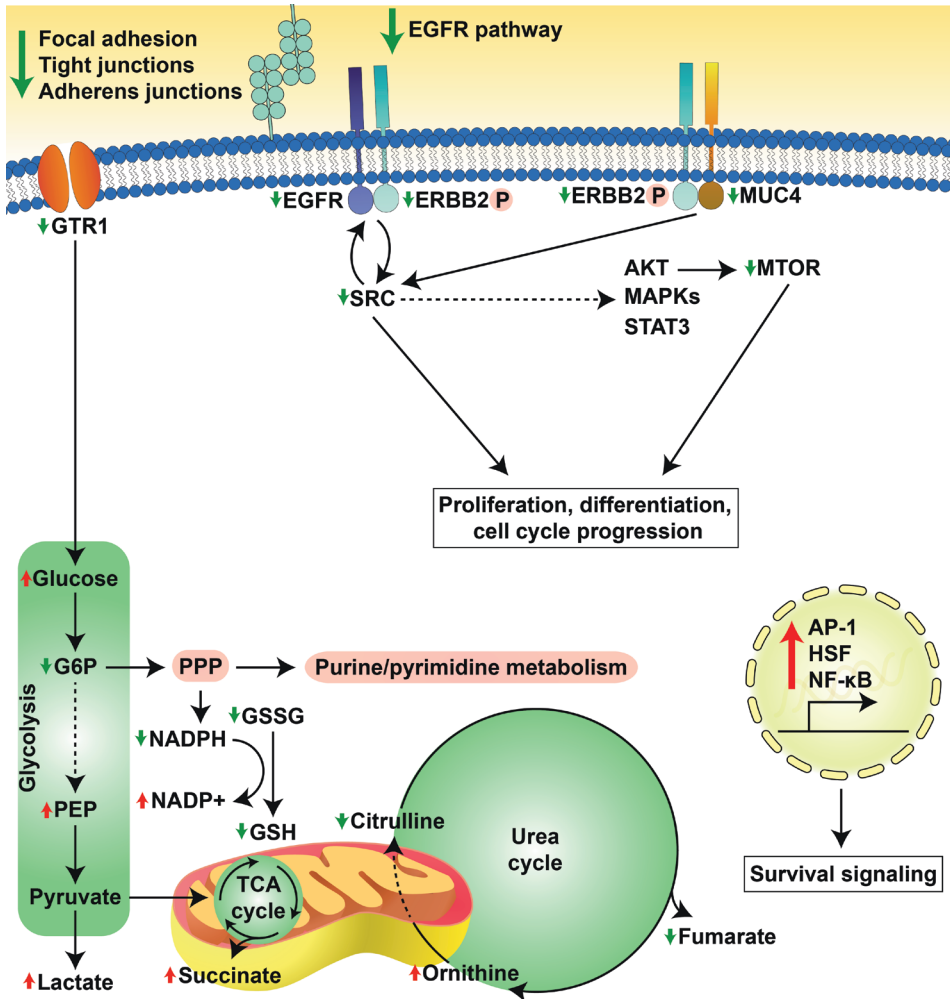


Figure 7. Overview of the cellular response of SK-ChA-1 cells to supralethal (LC90) PDT.

In response to PDT, SK-ChA-1 cells downregulate proteins involved in focal adhesion, tight and adherens junctions, and EGFR signaling. Metabolic processes that are dependent on mitochondria (TCA cycle, urea cycle) appear to be downmodulated, whereas the antioxidant response was activated. On the transcriptomic level, SK-ChA-1 cells demonstrated an upregulation of AP-1-, HSF-, and NF-κB-mediated signaling that may contribute to cell survival.

downregulated proteins involved in focal adhesion (CAV1, integrin alpha-2 (ITA2)), adherens junctions (CTNND1, EPCAM), and tight junctions (phosphorylated ZO1 and ZO3). As reported in [62-64], PDT may oxidatively damage proteins involved in cell-cell adhesion, cytoskeletal structure, and focal adhesion, which appears to be dependent on cell type, photosensitizer concentration, and light dose. However, it may also contribute to a higher metastatic potential after PDT, inasmuch as loss

of adhesion proteins is associated with invasion [62]. Further research is warranted to establish whether PDT enhances the metastatic potential of cancer cells, as activation of both survival and metastasis pathways by PDT may hamper clinical safety of the procedure.

Supralethal PDT also downregulated various proteins involved in EGFR signaling, which is an important therapeutic target as it is overexpressed in numerous cancer types [19]. Previous studies have shown that SK-ChA-1 and A431 cells in the absence of PDT are sensitive to EGFR inhibitors, as these compounds inhibited cell growth [46,65]. ZPCL-PDT of SK-ChA-1 cells with LC<sub>90</sub> revealed downregulation of EGFR on both the transcriptomic and proteomic level. Both SK-ChA-1 and A431 cells exhibited a reduction in *EGFR* mRNA levels after PDT and this effect was enhanced in the LC<sub>90</sub> group. Although the exact mechanism is still unknown, the general trend is that PDT is able to inhibit and/or degrade EGFR, thereby deterring tumor growth and inducing apoptosis [66]. However, exceptions do exist. For instance, Edmonds and co-workers showed that human ovarian carcinoma (OVCAR-5) and non-small cell lung cancer (H460) cell lines upregulated EGFR after PDT with verteporfin (log  $P = 3.74$ ) [67,68]. Inhibition of EGFR with erlotinib increased PDT efficacy and resulted in apoptotic cell death [67], linking pharmacological EGFR inhibition to cell demise. Also, a more recent study demonstrated that erlotinib treatment prior to PDT induced higher complete response rates in NSCLC (H460, A549)-xenografted mice [69]. Interestingly, treatment of various cancer cell lines with the photosensitizer Photofrin (porfimer sodium, log  $P = 8.5$  [2]) alone downregulated EGFR protein expression, which was enhanced upon PDT, indicating that Photofrin alone is able to downmodulate EGFR expression [70]. ZnPC is a highly lipophilic photosensitizer (log  $P = 8.5$  [2]) that intercalates into biomembranes [13]. Given that EGFR is a transmembrane protein, ZnPC is expected to reside in the direct vicinity of the transmembrane domain of EGFR, where it can subsequently cause oxidative modification of EGFR's transmembrane structures and impede its functional properties. The same applies to verteporfin and Photofrin. However, apparently the site of ROS generation is not ubiquitously linked to protein dysfunctionalization. Instead, EGFR expression after PDT is photosensitizer-dependent, whereby inhibition of EGFR by PDT may contribute to an anti-cancer effect when photosensitizers are employed that induce its downregulation, such as ZnPC, by an as yet undefined mechanism.

The metabolomics data of PDT-treated SK-ChA-1 cells showed similar trends between the LC<sub>50</sub> and LC<sub>90</sub> groups, although the effects were more pronounced in the LC<sub>90</sub> group. PDT-treated cells exhibited increased glucose levels, whereas a number of glycolytic-associated metabolites were reduced, suggesting that glucose is shuttled into pathways that branch off glycolysis, such as the pentose phosphate

pathway. Also, the TCA cycle appeared to be downregulated following PDT, as evidenced by a downregulation of acetyl-CoA, citrate,  $\alpha$ -ketoglutarate, and malate. As a result of ROS production during PDT, the redox status of a cell may be seriously affected. This is also observed in PDT-treated SK-ChA-1 cells, as regulators of the redox response differed (*e.g.*, reduction of glutathione and GSSG, increase of NADP<sup>+</sup>). The post-PDT pro-oxidative state may also explain the upregulation of the pentose phosphate pathway (Fig. 6B), as the pentose phosphate pathway contributes to the production of NADPH – a major player in the antioxidant response [71]. Another important factor that was increased in PDT-treated SK-ChA-1 cells is succinate. Mitochondria are a known target of ZnPC-based PDT [17,2], after which mitochondria-localized succinate may be released to the cytoplasm [72]. Succinate has been shown to mediate ATP generation in mitochondria, activation of HIF-1, and pro-inflammatory signaling (reviewed in [73]). Pharmacological strategies that limit succinate production could therefore serve as a strategy to augment PDT efficacy, although succinate build-up in mitochondria is also a precursor condition for latent oxidative stress [74] that in turn may promote tumor cell death.

To our knowledge, this is the first study that explored the PDT response in such detail. Therefore, it may provide novel information that could be valuable to design new therapeutic strategies, possibly based on therapeutic targets that were found in this study (Table 1). Consistent with earlier reports, the combined use of PDT and inhibitors of survival pathways may be an attractive approach to improve therapeutic efficacy in the aforementioned clinically recalcitrant cancer types.

## METHODS

### Chemicals

1,2-dipalmitoyl-*sn*-glycero-3-phosphocholine (DPPC) and  $3\beta$ -[N-(N',N'-dimethylaminoethane)-carbimoyl]cholesterol (DC-cholesterol) were purchased from Avanti Polar Lipids (Alabaster, AL).  $\beta$ -mercaptoethanol, cholesterol, chloroform, 1,2-distearoyl-*sn*-glycero-3-phosphoethanolamine-polyethylene glycol (DSPE-PEG, average PEG molecular mass of 2,000 amu), ZnPC (97% purity), acetonitrile, 4-(2-hydroxyethyl)-1-piperazineethanesulfonic acid (HEPES), potassium carbonate (K<sub>2</sub>CO<sub>3</sub>), pyridine, sodium chloride (NaCl), sodium deoxycholate, sodium fluoride, sodium orthovanadate, SRB, tris(hydroxymethyl)aminomethane (Tris), and Triton X-100 were obtained from Sigma-Aldrich (St. Louis, MO). Glycerol was purchased from Fisher Scientific (Hampton, NH), and sodium dodecyl sulfate (SDS) and bromophenol blue were obtained from Bio-Rad Laboratories (Hercules, CA).

Methanol, perchloric acid (HClO<sub>4</sub>), and sodium hydroxide (NaOH) were from Merck (Darmstadt, Germany).

All lipids were dissolved in chloroform and stored under a nitrogen atmosphere at -20 °C. ZnPC was dissolved in pyridine at a 178- $\mu$ M concentration and stored under nitrogen at room temperature (RT) in the dark.

### Cell culture

Human epidermoid carcinoma (A431) cells and murine macrophages (RAW 264.7) were cultured in Dulbecco's Modified Eagle's medium (DMEM, Lonza, Walkersville, MD) supplemented with 10% fetal bovine serum (FBS) (Bodinco, Alkmaar, the Netherlands), 100 U/mL penicillin, 100  $\mu$ g/mL streptomycin, and 2 mM L-glutamine (all from Lonza). Human umbilical vein endothelial cells (HUVECs) were isolated as described in [25] and maintained in EndoGro-LS complete culture medium (Merck Millipore, Billerica, MA). HUVECs were grown in Primaria cell culture flasks (Corning Life Sciences, Tewksbury, MA). Human perihilar cholangiocarcinoma (SK-ChA-1) cells were cultured in Roswell Park Memorial Institute (RPMI) 1640 culture medium (Lonza) supplemented with 10% FBS, 100 U/mL penicillin, 100  $\mu$ g/mL streptomycin, 2 mM L-glutamine, and 143  $\mu$ M  $\beta$ -mercaptoethanol. All cells were maintained at standard culture conditions (37 °C, 5% CO<sub>2</sub>, 95% air, humidified atmosphere).

### Preparation of ZPCLs

ZPCLs were composed of DPPC, DC-cholesterol, cholesterol, and DSPE-PEG (66:25:5:4, molar ratio) and prepared by the lipid film hydration technique as described previously [16,13]. Physiological buffer composed of 10 mM HEPES, 0.88% (w/v) NaCl, pH = 7.4, 0.293 osmol/kg [14] was used as hydration solution. ZnPC was incorporated in the liposomal formulation at a ZnPC:lipid molar ratio of 0.003. Liposomal formulations were purged with nitrogen gas and stored at 4 °C in the dark. Under these conditions the liposomal ZnPC remains stable for at least 56 days [13].

### PDT protocol

Cells were seeded in either 6-well (2 mL per well) or 24-well (0.5 mL per well) culture plates (Corning Life Sciences) as specified in the corresponding subsections and grown under standard culture conditions. HUVEC, RAW 264.7, SK-ChA-1, and A431 cells were seeded at a density of  $0.5 \times 10^5$  cells/mL,  $0.5 \times 10^6$  cells/mL,  $0.25 \times 10^6$  cells/mL, and  $0.5 \times 10^6$  cells/mL, respectively, and cultured until confluence in 24 hours (48 hours for SK-ChA-1 cells). HUVECs were cultured in Primaria culture plates (Corning Life Sciences) throughout the study. After reaching confluence, cells were washed



with PBS and incubated with ZPCLs in serum-free supplemented phenol red-free medium for 1 hour (drug-light interval) at 37 °C under standard culture conditions. Control cells received an equal volume of physiological buffer. The concentrations of ZPCLs that were used for the different cell types are specified in Table S1. Next, cells were washed with PBS and fresh supplemented phenol red-free medium was added. Cells were either returned to the incubator (control and dark toxicity) or irradiated with a 671-nm diode laser (CNI, Changchun, China) at a laser power of 500 mW with a fluence of 15 J/cm<sup>2</sup>. The spot size was set to the exact dimensions of the well (6-wells plate: 9.5 cm<sup>2</sup>, 24-wells plate: 1.9 cm<sup>2</sup>). During the application of PDT, cells were maintained at 37 °C using a hotplate (cat. no. 97042-616, VWR, Radnor, PA).

### **Cell metabolic activity and viability assays**

Cell metabolic activity was assessed using the WST-1 reagent (Roche Diagnostics, Basel, Switzerland). Cells were seeded in 24-wells plates and cultured until confluence. After a predetermined time interval after PDT, the culture medium was removed and 300 µL of WST-1-containing serum-free and phenol red-free medium (at a 1:25 volume ratio) was added to the wells. After 30 minutes of incubation under standard culture conditions, the absorbance was read at 450 nm using 600 nm as a reference wavelength (BioTek Synergy HT multi-well plate reader, Winooski, VT). Data were normalized to the average values of the control cells that was set at a viability of 100%.

After the measurement, the wells were washed with PBS, and the protein content was determined with the SRB total protein assay as described by Vichai *et al.* [26]. SRB absorbance was read at 564 nm using 690 nm as a reference wavelength (BioTek Synergy HT). Data were normalized to the average values of the control cells that was set at a viability of 100%.

### **Whole genome expression analysis**

Cells were seeded in 6-wells plates and cultured until confluence. Cells were treated using the PDT protocol as described in section 2.4 ( $n = 3$  per group). Total cellular RNA was extracted using 1 mL of TRIzol (Life Technologies, Carlsbad, CA) according to the manufacturer's protocol. RNA samples were purified using the NucleoSpin RNA kit (Machery-Nagel, Düren, Germany) and eluted in 30 µL RNase-free water. The quality control, RNA labeling, hybridization, and data extraction were performed at ServiceXS (Leiden, the Netherlands), and the procedure can be found in [16]. Samples for human cell lines were randomly assigned to three Human-HT12 v4 arrays. For the RAW 264.7 cell line, MouseWG-6 v2 arrays were used with control and vehicle samples on one chip and LC<sub>50</sub> and LC<sub>90</sub> samples on a second chip.

### Microarray data preprocessing and analysis

Microarray data preprocessing and analysis were performed as described previously [16]. In short, each cell line was analyzed separately with Bioconductor packages (version 2.13) using the statistical software package R (version 3.1.0). Normalization was performed starting from the Illumina sample and control probe profiles by a normexp-by-control background correction, quantile normalization, and  $\log_2$  transformation (limma package). Probes with a detection  $P$ -value of  $> 0.05$  (non-expressed) on all arrays for the cell line under study were filtered out. Differential expression between the experimental conditions was assessed with a moderated t-test using the linear model framework (limma package). Resulting  $P$ -values were corrected for multiple testing using the Benjamini-Hochberg false discovery rate. Corrected  $P$ -values  $\leq 0.05$  were considered statistically significant. Probes were reannotated using the Bioconductor IlluminaHumanv4.db and IlluminaMousev2.db packages. The microarray data have been deposited in NCBI Gene Expression Omnibus in a MIAME compliant format and are accessible under GEO series accession number GSE84758. Microarray data were confirmed using quantitative reverse transcription polymerase chain reaction (qRT-PCR) since the qRT-PCR data were in agreement with the microarray data (Fig. S1). This also strongly suggests that for the RAW 264.7 cells potential confounding of effects due to systematic differences between chips and biological effects of interest (comparison of  $LC_{50}/LC_{90}$  versus control/vehicle) is limited. In addition, a ROAST gene set test [27] was performed on the downstream targets of each survival pathway (Table S2) to statistically determine whether a survival pathway was either upregulated or downregulated using 10,000 rotations with Benjamini-Hochberg-based multiple testing correction of the mid  $P$ -values.

### qRT-PCR

RNA was extracted as described in section 2.6. cDNA synthesis and qRT-PCR reactions were performed as described previously [16]. Primer sequences can be found in Table S3. The quantitative analysis of the qRT-PCR data was performed according to Ruijter *et al.* [28] to calculate the starting concentration ( $N_0$ ) of each cDNA template. Gene expression levels were normalized to the expression level of the reference gene ribosomal protein S18 (*RPS18*).  $\log_2$  fold-changes of the target genes were calculated based on the mean values of the control group.

## **Proteomics**

### ***Harvesting***

SK-ChA-1 cells were seeded in 6-wells plates and cultured until confluence. Cells were treated using the PDT protocol as described in section 2.4 ( $n = 12$  per group). Ninety minutes post-PDT, cells were washed three times with 2 mL PBS and 150  $\mu\text{L}$  of lysis buffer (8 M urea, 0.5% sodium deoxycholate, 50 mM  $\text{NH}_4\text{HCO}_3$ , supplemented with cOmplete Mini protease inhibitor cocktail and phosSTOP (both from Roche)) was added to each well that was ensued by 30-minute incubation on ice. Lysates were scraped, collected, pooled (to yield  $n = 4$  per treatment group), and centrifuged for 15 minutes at  $20,000 \times g$ . The supernatant was stored at  $-80^\circ\text{C}$  for further analysis. Protein concentrations were determined with the bicinchoninic acid (BCA) assay (Thermo Fisher Scientific, Waltham, MA).

### ***Affinity purification and digestion***

For each sample, 400  $\mu\text{g}$  of proteins was reduced by incubating with 2  $\mu\text{L}$  of 1 M DTT at  $56^\circ\text{C}$  for 25 minutes, alkylated by adding 4  $\mu\text{L}$  of 200 mM IAA for 30 minutes at RT in the dark, and digested by Lys-C (enzyme:protein ratio of 1:75) for 4 hours at  $37^\circ\text{C}$ . Samples were then diluted 4 times with 50 mM  $\text{NH}_4\text{HCO}_3$  and digested overnight at  $37^\circ\text{C}$  with trypsin (enzyme:protein ratio of 3:100). Next, 100  $\mu\text{L}$  of acetic acid was added to each sample to precipitate sodium deoxycholate, after which samples were centrifuged for 15 minutes at  $20,000 \times g$ . The obtained digests were desalted using 1cc Sep-Pak C18 cartridges. Phosphoenrichment was performed with Ti-IMAC microcolumns with 250  $\mu\text{g}$  of digests following the protocol previously described in detail [29], while the rest of the digests was kept for proteome analysis.

### ***NanoLC-MS/MS analysis***

Phosphoproteome and proteome were analyzed by NanoLC-MS/MS using an Agilent 1100 HPLC system (Agilent Technologies, Santa Clara, CA) coupled to a Q Exactive Plus Orbitrap (Thermo Scientific) mass spectrometer. Peptides were trapped at 5  $\mu\text{L}$ /minute in 100% solvent A (0.1 M acetic acid in water) on an in-house packed 20 mm  $\times$  100  $\mu\text{m}$  ID trapping column (ReproSil-Pur C18-AQ, 3  $\mu\text{m}$ , Dr. Maisch, Ammerbuch, Germany) and then transferred to an in-house packed 50-cm  $\times$  50- $\mu\text{m}$  ID analytical column (Poroshell 120 EC-C18, 2.7  $\mu\text{m}$ , Agilent Technologies) maintained at  $40^\circ\text{C}$ . The gradient used for proteome analysis ranged from 10 to 40% solvent B (0.1 M acetic acid in 8:2 (v/v) acetonitrile/water) in 180 minutes at  $\sim 100$  nL/minute, whereas the gradient for phosphopeptides ranged from 4 to 40% in 120 minutes. The eluent was sprayed via distal coated emitter tips (New Objective, Woburn, MA) connected to the analytical column. The Q Exactive Plus was operated in data-dependent

mode, automatically switching between MS and MS/MS. Full-scan MS spectra (from  $m/z$  350 to 1500) were acquired in the Orbitrap with a resolution of 60,000 at  $m/z$  400 (after accumulation to a target value of 500,000). The 20 most intense ions at a threshold above  $m/z$  500 were successively selected and fragmented in HCD cells at normalized collision energy of 35% after accumulation to a target value of 10,000.

### ***Protein quantification and identification***

Data analysis was performed using MaxQuant (version 1.5.2.8) [30] and the integrated search engine Andromeda [31]. For peptide and protein identification, raw files were searched against the human Swissprot database (20,201 entries) with carbamidomethylated cysteine as fixed modification and phosphorylation of serine, threonine, and tyrosine, and oxidation of methionine as variable modifications. Trypsin/P was set as the proteolytic enzyme for which up to two missed cleavage sites were allowed. Precursor tolerance was set to 4.5 ppm and fragment ion tolerance to 0.05 Da. Peptide identifications required a minimal length of 7 amino acids and all datasets were adjusted to 1% PSM FDR. For label-free quantification (LFQ), match between runs was selected with a maximum shift time window of 3 minutes and the intensities of razor and unique peptides were summed up. Resulting protein intensities were then normalized to obtain LFQ intensities. To facilitate further data analysis, the results were imported into Perseus (version 1.5.2.4). Replicates were grouped per condition, and proteins or phosphopeptides identified in less than 3 out of 4 replicates were discarded. A two-tailed t-test was used to assess statistical significance. Phosphopeptide and protein  $P$ -values were corrected by permutation-based FDR correction (FDR 5%). Phosphopeptides were filtered for a localization probability  $> 0.75$  (class 1 sites). Regulated proteins were analyzed using Reactome within the Cytoscape environment and regulated phosphorylation sites were analyzed by Phosphopath [32] within Cytoscape. The mass spectrometry proteomics data have been deposited to the ProteomeXchange Consortium via the PRIDE partner repository with the dataset identifier PXD004320.

### **Western Blotting**

Western Blotting was performed to validate the (phospho)proteomic data (Fig. S2). As such, SK-ChA-1 cells were seeded in 6-wells plates, cultured until confluence, and treated by PDT as described in section 2.4 ( $n = 3$  per group). Ninety minutes after PDT, cells were washed twice with ice-cold PBS, placed on ice, and lysed in ice-cold RIPA buffer (50 mM Tris, 150 mM NaCl, 1% Triton X-100, 0.5% sodium deoxycholate, 1% SDS) supplemented with cOmplete Mini protease inhibitor cocktail, 10 mM sodium fluoride, and 1 mM sodium orthovanadate. The samples

were centrifuged for 15 minutes at  $14,000 \times g$  ( $4\text{ }^{\circ}\text{C}$ ) and the supernatant was stored for further analysis. Protein lysates were mixed with  $4 \times$  SDS sample buffer (200 mM Tris (pH = 6.8), 8% SDS, 40% glycerol, 0.02% bromophenol blue) and boiled for 5 minutes at  $95\text{ }^{\circ}\text{C}$ . Next, samples (20-30  $\mu\text{g}$ ) were loaded on a TGX 10% precast gel (Bio-Rad Laboratories) and electrophoresis was performed at 150 V. The gels were blotted onto Amersham Hybond P 0.45 PVDF membranes (GE Healthcare, Little Chalfont, UK) for 2 hours at 250 mA at  $4\text{ }^{\circ}\text{C}$ . The membranes were blocked for 1 hour with 5% BSA (Sigma-Aldrich) in 0.1% Tween 20 Tris-buffered saline (TBST, 20 mM Tris, 150 mM NaCl, pH = 7.6), after which the membranes were incubated overnight with the primary antibody at  $4\text{ }^{\circ}\text{C}$  on a rocker. The primary antibodies used were (dilution factor, catalogue number, company): EGFR (1:1000, #4267, Cell Signaling (Danvers, MA)), phospho-ERK (1:1000, #4370, Cell Signaling), phospho-p38 MAPK (1:500, #9216, Cell Signaling), p38 MAPK (1:1000, #9228, Cell Signaling), COX IV (1:1000, #4844, Cell Signaling), and ERK (1:1000, sc-2711270, Santa Cruz Biotechnology (Dallas, TX)). All primary antibodies were diluted in 5% BSA in TBST. Next, the membranes were washed three times in TBST and incubated with a HRP-conjugated secondary antibody (1:2,000, Dako Cytomation (Glostrup, Denmark)) for 1 hour at RT. Subsequently, membranes were washed three times with TBST. The enhanced chemiluminescence (ECL) kit (Thermo Scientific) was used as substrate and protein bands were visualized on an ImageQuant LAS 4000 luminometer (GE Healthcare).

### Metabolomics

SK-ChA-1 cells were seeded in 6-wells plates and cultured until confluence. Cells were treated using the PDT protocol as described in section 2.4 ( $n = 3$  per group). After 90 minutes, the cells were washed with 1 mL cold PBS and the cells were lysed in 1 mL lysis buffer (40% acetonitrile, 40% methanol, 20% water). The cells were scraped and transferred to 2-mL centrifuge tubes that were shaken for 10 minutes at  $4\text{ }^{\circ}\text{C}$ . Next, the samples were centrifuged for 15 minutes at  $20,000 \times g$  ( $4\text{ }^{\circ}\text{C}$ ), after which the supernatant was aspirated and stored at  $-80\text{ }^{\circ}\text{C}$ . LC-MS analysis was performed on an Exactive mass spectrometer (Thermo Scientific) coupled to a Dionex Ultimate 3000 autosampler and pump (Thermo Scientific). The MS operated in polarity-switching mode with spray voltages of 4.5kV and -3.5kV. Metabolites were separated using a Sequant ZIC-pHILIC column ( $2.1 \times 150\text{ mm}$ ,  $5\text{ }\mu\text{m}$ , guard column  $2.1 \times 20\text{ mm}$ ,  $5\text{ }\mu\text{m}$  (Merck)) using a linear gradient of acetonitrile and eluent A (20 mM  $(\text{NH}_4)_2\text{CO}_3$ , 0.1%  $\text{NH}_4\text{OH}$  in ULC/MS grade water (Biosolve, Valkenswaard, the Netherlands)). The flow rate was set at 150  $\mu\text{L}/\text{min}$ . Metabolites were identified and quantified using LCquan software (Thermo Scientific) on the basis of exact

mass within 5 ppm and further validated in accordance with the retention times of standards. Peak intensities were normalized based on total ion count (TIC).

### **Nucleotide profiles**

SK-ChA-1 cells were seeded in 6-wells plates and cultured until confluence. Cells were treated using the PDT protocol as described in section 2.4 ( $n = 3$  per group). After 90 minutes, the cells were washed twice with PBS, placed on ice, and nucleotides were extracted using 200  $\mu\text{L}$  ice-cold 0.4 M  $\text{HClO}_4$ . After 10-minute incubation on ice, the samples were centrifuged for 5 minutes at  $10,000 \times g$  ( $4^\circ\text{C}$ ) and the nucleotide-containing supernatant was neutralized using 7.5  $\mu\text{L}$  5 M  $\text{K}_2\text{CO}_3$ . The wells were washed twice with 150  $\mu\text{L}$  0.2 M NaOH to remove residual proteins, which was added to the protein-containing dry pellet as obtained in the previous centrifugation step. In addition, 300  $\mu\text{L}$  0.8 M  $\text{HClO}_4$  was added to the protein fraction. After mixing thoroughly, the samples were centrifuged for 5 minutes at  $10,000 \times g$  ( $4^\circ\text{C}$ ) and the protein-containing pellet was dissolved in 200  $\mu\text{L}$  0.2 M NaOH. Protein content was determined using the bicinchoninic acid assay protein kit (Thermo Scientific).

Nucleotide extracts were analyzed by high-performance liquid chromatography (HPLC) using a Partisphere 5- $\mu\text{m}$  SAX cartridge column (cat. no. 4621-0505, Hichrom, Reading, United Kingdom). Nucleotides were eluted with a gradient from 100% buffer A (100-fold dilution of buffer B) to 70% buffer B (0.75 M  $\text{NaH}_2\text{PO}_4$ , pH = 4.55) in 50 minutes at a flow rate of 1 mL/min.

### **Statistical analysis**

Statistical analysis was performed in GraphPad Prism 6 (GraphPad Software, La Jolla, CA). Normality was tested with the D'Agostino Pearson omnibus test. Differences between normally distributed variables were analyzed with a one-way ANOVA with Bonferroni post-hoc test. Intergroup differences were indicated with (\*) and differences between the treated groups and the control group at the same time point were indicated with (#). Differences between a condition and the previous condition at the same time point are, when relevant, indicated with (\$) (Fig. 1). A single, double, and triple sign indicate a  $P$ -value of  $\leq 0.05$ ,  $\leq 0.01$ , and  $\leq 0.001$ , respectively. Data are presented as mean  $\pm$  SD throughout the manuscript.

### **Acknowledgements**

MH has received grants from Stichting Technologische Wetenschap (STW 12064), the Phospholipid Research Center in Heidelberg, the Dutch Anticancer Foundation in Amsterdam (Stichting Nationaal Fonds Tegen Kanker), and the Nijbakker Morra

Foundation. SL and SC were supported by the Netherlands Organization for Scientific Research (NWO) through a VIDI grant (project 723.013.008). CRB was supported by NWO through a VENI grant (project 722.013.009). The A431 cell line was a kind a gift from Gerben Koning (Erasmus Medical Center, the Netherlands). The SK-ChA-1 cell line was a kind gift from Alexander Knuth and Claudia Matter (University Hospital Zurich, Switzerland). The RAW 264.7 cell line was a kind gift from Joan Kwakkel (Academic Medical Center, the Netherlands).

**Author contributions**

RW, CRB, SL, and MH designed the experiments. RW, SC, EAZ, MMEP, and RL conducted the experiments. Microarray data were processed and statistically analyzed by AJ and PDM. Microarray data interpretation was performed by RW, RTvK, AJ, PDM, and MH. Proteome data were analyzed by SC and SL and metabolome data were analyzed by EAZ, KV, and CRB. RW and MH wrote the manuscript. AHCvK and ABPvK critically reviewed the manuscript. All authors have read and approved the final version of the manuscript.

## REFERENCES

1. Plaetzer K, Krammer B, Berlanda J, Berr F, Kiesslich T (2009) Photophysics and photochemistry of photodynamic therapy: fundamental aspects. *Lasers Med Sci* 24 (2):259-268.
2. Weijer R, Broekgaarden M, Kos M, van Vught R, Rauws EAJ, Breukink E, van Gulik TM, Storm G, Heger M (2015) Enhancing photodynamic therapy of refractory solid cancers: Combining second-generation photosensitizers with multi-targeted liposomal delivery. *J Photochem Photobiol C Photochem Rev* 23 (0):103-131.
3. Sibille A, Lambert R, Souquet JC, Sabben G, Descos F (1995) Long-term survival after photodynamic therapy for esophageal cancer. *Gastroenterology* 108 (2):337-344
4. Zeitouni NC, Shieh S, Oseroff AR (2001) Laser and photodynamic therapy in the management of cutaneous malignancies. *Clin Dermatol* 19 (3):328-338
5. Sun ZQ (1992) Photodynamic therapy of nasopharyngeal carcinoma by argon or dye laser - An analysis of 137 cases. *Zhonghua Zhong Liu Za Zhi* 14 (4):290-292
6. Benson RC, Jr. (1986) Laser photodynamic therapy for bladder cancer. *Mayo Clin Proc* 61 (11):859-864
7. Nseyo UO, Dougherty TJ, Boyle DG, Potter WR, Wolf R, Huben R, Pontes JE (1985) Whole bladder photodynamic therapy for transitional cell carcinoma of bladder. *Urology* 26 (3):274-280
8. Quyn AJ, Ziyaie D, Polignano FM, Tait IS (2009) Photodynamic therapy is associated with an improvement in survival in patients with irresectable hilar cholangiocarcinoma. *HPB (Oxford)* 11 (7):570-577.
9. Broekgaarden M, Weijer R, van Gulik TM, Hamblin MR, Heger M (2015) Tumor cell survival pathways activated by photodynamic therapy: a molecular framework for inhibition strategies. *Cancer Metastasis Rev*:1-48
10. Broekgaarden M, van Vught R, Oliveira S, Roovers RC, van Bergen en Henegouwen PM, Pieters RJ, van Gulik TM, Breukink E, Heger M (2016) Site-specific conjugation of single domain antibodies to liposomes enhances photosensitizer uptake and photodynamic therapy efficacy. *Nanoscale* 8 (12):6490-6494
11. Weijer R, Broekgaarden M, Krekorian M, Alles LK, van Wijk AC, Mackaaij C, Verheij J, van der Wal AC, van Gulik TM, Storm G, Heger M (2016) Inhibition of hypoxia inducible factor 1 and topoisomerase with acriflavine sensitizes perihilar cholangiocarcinomas to photodynamic therapy. *Oncotarget* 7 (3):3341-3356.
12. Broekgaarden M, Weijer R, van Wijk AC, Cox RC, Egmond MR, Hoebe R, van Gulik TM, Heger M (2016, in press) Photodynamic therapy with liposomal zinc phthalocyanine and tirapazamine increases tumor cell death via DNA damage. *J Biomed Nanotechnol*
13. Broekgaarden M, Weijer R, Krekorian M, van den IJssel B, Kos M, Alles LK, van Wijk AC, Bikadi Z, Hazai E, van Gulik TM, Heger M (2016) Inhibition of hypoxia-inducible factor 1 with acriflavine sensitizes hypoxic tumor cells to photodynamic therapy with zinc phthalocyanine-encapsulating cationic liposomes. *Nano Res*
14. Broekgaarden M, de Kroon AI, Gulik TM, Heger M (2014) Development and in vitro proof-of-concept of interstitially targeted zinc-phthalocyanine liposomes for photodynamic therapy. *Curr Med Chem* 21 (3):377-391
15. Lee K, Zhang H, Qian DZ, Rey S, Liu JO, Semenza GL (2009) Acriflavine inhibits HIF-1 dimerization, tumor growth, and vascularization. *Proc Natl Acad Sci U S A* 106 (42):17910-17915.
16. Weijer R, Broekgaarden M, van Golen RF, Bulle E, Nieuwenhuis E, Jongejan A, Moerland PD, van Kampen AH, van Gulik TM, Heger M (2015) Low-power photodynamic therapy induces survival signaling in perihilar cholangiocarcinoma cells. *BMC Cancer* 15 (1):1014.
17. Alexandratou E, Yova D, Loukas S (2005) A confocal microscopy study of the very early cellular response to oxidative stress induced by zinc phthalocyanine sensitization. *Free Radic Biol Med* 39 (9):1119-1127.
18. Fabris C, Valduga G, Miotto G, Borsetto L, Jori G, Garbisa S, Reddi E (2001) Photosensitization with zinc (II) phthalocyanine as a switch in the decision between apoptosis and necrosis. *Cancer Res* 61 (20):7495-7500



19. Herbst RS, Shin DM (2002) Monoclonal antibodies to target epidermal growth factor receptor-positive tumors: a new paradigm for cancer therapy. *Cancer* 94 (5):1593-1611
20. Harder J, Waiz O, Otto F, Geissler M, Olschewski M, Weinhold B, Blum HE, Schmitt-Graeff A, Opitz OG (2009) EGFR and HER2 expression in advanced biliary tract cancer. *World J Gastroenterol* 15 (36):4511-4517
21. Yang X, Wang W, Wang C, Wang L, Yang M, Qi M, Su H, Sun X, Liu Z, Zhang J, Qin X, Han B (2014) Characterization of EGFR family gene aberrations in cholangiocarcinoma. *Oncol Rep* 32 (2):700-708.
22. Joseph SO, Wu J, Muggia FM (2012) Targeted therapy: its status and promise in selected solid tumors. Part II: Impact on selected tumor subsets, and areas of evolving integration. *Oncology (Williston Park)* 26 (11):1021-1030, 1035
23. Postiglione I, Chiaviello A, Palumbo G (2011) Enhancing photodynamic therapy efficacy by combination therapy: dated, current and oncoming strategies. *Cancers (Basel)* 3 (2):2597-2629
24. Shim CS, Cheon YK, Cha SW, Bhandari S, Moon JH, Cho YD, Kim YS, Lee LS, Lee MS, Kim BS (2005) Prospective study of the effectiveness of percutaneous transhepatic photodynamic therapy for advanced bile duct cancer and the role of intraductal ultrasonography in response assessment. *Endoscopy* 37 (5):425-433.
25. Post IC, de Boon WM, Heger M, van Wijk AC, Kroon J, van Buul JD, van Gulik TM (2013) Endothelial cell preservation at hypothermic to normothermic conditions using clinical and experimental organ preservation solutions. *Exp Cell Res* 319 (17):2501-2513.
26. Vichai V, Kirtikara K (2006) Sulforhodamine B colorimetric assay for cytotoxicity screening. *Nat Protoc* 1 (3):1112-1116.
27. Wu D, Lim E, Vaillant F, Asselin-Labat ML, Visvader JE, Smyth GK (2010) ROAST: rotation gene set tests for complex microarray experiments. *Bioinformatics* 26 (17):2176-2182.
28. Ruijter JM, Ramakers C, Hoogaars WM, Karlen Y, Bakker O, van den Hoff MJ, Moorman AF (2009) Amplification efficiency: linking baseline and bias in the analysis of quantitative PCR data. *Nucleic Acids Res* 37 (6):e45.
29. Zhou H, Ye M, Dong J, Corradini E, Cristobal A, Heck AJ, Zou H, Mohammed S (2013) Robust phosphoproteome enrichment using monodisperse microsphere-based immobilized titanium (IV) ion affinity chromatography. *Nat Protoc* 8 (3):461-480.
30. Cox J, Mann M (2008) MaxQuant enables high peptide identification rates, individualized p.p.b.-range mass accuracies and proteome-wide protein quantification. *Nat Biotechnol* 26 (12):1367-1372.
31. Cox J, Neuhauser N, Michalski A, Scheltema RA, Olsen JV, Mann M (2011) Andromeda: a peptide search engine integrated into the MaxQuant environment. *J Proteome Res* 10 (4):1794-1805.
32. Raaijmakers LM, Giansanti P, Possik PA, Mueller J, Peeper DS, Heck AJ, Altelaar AF (2015) PhosphoPath: Visualization of phosphosite-centric dynamics in temporal molecular networks. *J Proteome Res* 14 (10):4332-4341.
33. Berridge MV, Herst PM, Tan AS (2005) Tetrazolium dyes as tools in cell biology: new insights into their cellular reduction. *Biotechnol Annu Rev* 11:127-152.
34. Kutmon M, Riutta A, Nunes N, Hanspers K, Willighagen EL, Bohler A, Melius J, Waagmeester A, Sinha SR, Miller R, Coort SL, Cirillo E, Smeets B, Evelo CT, Pico AR (2016) WikiPathways: capturing the full diversity of pathway knowledge. *Nucleic Acids Res* 44 (D1):D488-494.
35. Broekgaarden M, Kos M, Jurg FA, van Beek AA, van Gulik TM, Heger M (2015) Inhibition of NF-kappaB in tumor cells exacerbates immune cell activation following photodynamic therapy. *Int J Mol Sci* 16 (8):19960-19977.
36. Karin M, Cao Y, Greten FR, Li ZW (2002) NF-kappaB in cancer: from innocent bystander to major culprit. *Nat Rev Cancer* 2 (4):301-310.
37. Iurlaro R, Munoz-Pinedo C (2015) Cell death induced by endoplasmic reticulum stress. *The FEBS journal*.
38. Fujimoto M, Nakai A (2010) The heat shock factor family and adaptation to proteotoxic stress. *The FEBS journal* 277 (20):4112-4125
39. Lee HJ, Kim JM, Kim KH, Heo JI, Kwak SJ, Han JA (2015) Genotoxic stress/p53-induced DNAJB9 inhibits the pro-apoptotic function of p53. *Cell Death Differ* 22 (1):86-95.

40. Nishitoh H, Saitoh M, Mochida Y, Takeda K, Nakano H, Rothe M, Miyazono K, Ichijo H (1998) ASK1 is essential for JNK/SAPK activation by TRAF2. *Mol Cell* 2 (3):389-395.
41. Brand TM, Iida M, Li C, Wheeler DL (2011) The nuclear epidermal growth factor receptor signaling network and its role in cancer. *Discov Med* 12 (66):419-432
42. Movafagh S, Crook S, Vo K (2015) Regulation of hypoxia-inducible factor-1 $\alpha$  by reactive oxygen species: new developments in an old debate. *J Cell Biochem* 116 (5):696-703.
43. Carmeliet P, Dor Y, Herbert JM, Fukumura D, Brusselmans K, Dewerchin M, Neeman M, Bono F, Abramovitch R, Maxwell P, Koch CJ, Ratcliffe P, Moons L, Jain RK, Collen D, Keshert E (1998) Role of HIF-1 $\alpha$  in hypoxia-mediated apoptosis, cell proliferation and tumour angiogenesis. *Nature* 394 (6692):485-490.
44. Grimm S, Mvondo D, Grune T, Breusing N (2011) The outcome of 5-ALA-mediated photodynamic treatment in melanoma cells is influenced by vitamin C and heme oxygenase-1. *Biofactors* 37 (1):17-24.
45. Ockaili R, Natarajan R, Salloum F, Fisher BJ, Jones D, Kukreja RC (2005) HIF-1 activation attenuates postischemic myocardial injury: role for heme oxygenase-1 in modulating microvascular chemokine generation. *Am J Physiol Heart Circ Physiol* 289 (2):H542-H548
46. Wiedmann M, Feisthammel J, Bluthner T, Tannapfel A, Kamenz T, Kluge A, Mossner J, Caca K (2006) Novel targeted approaches to treating biliary tract cancer: the dual epidermal growth factor receptor and ErbB-2 tyrosine kinase inhibitor NVP-AEE788 is more efficient than the epidermal growth factor receptor inhibitors gefitinib and erlotinib. *Anticancer Drugs* 17 (7):783-795.
47. Fabregat A, Sidiropoulos K, Garapati P, Gillespie M, Hausmann K, Haw R, Jassal B, Jupe S, Korninger F, McKay S, Matthews L, May B, Milacic M, Rothfels K, Shamovsky V, Webber M, Weiser J, Williams M, Wu G, Stein L, Hermjakob H, D'Eustachio P (2016) The Reactome pathway knowledgebase. *Nucleic Acids Res* 44 (D1):D481-487.
48. Croft D, Mundo AF, Haw R, Milacic M, Weiser J, Wu G, Caudy M, Garapati P, Gillespie M, Kamdar MR, Jassal B, Jupe S, Matthews L, May B, Palatnik S, Rothfels K, Shamovsky V, Song H, Williams M, Birney E, Hermjakob H, Stein L, D'Eustachio P (2014) The Reactome pathway knowledgebase. *Nucleic Acids Res* 42 (Database issue):D472-477.
49. Zhang J, Zhang Y, Liu S, Zhang Q, Wang Y, Tong L, Chen X, Ji Y, Shang Q, Xu B, Chu M, Wei L (2013) Metadherin confers chemoresistance of cervical cancer cells by inducing autophagy and activating ERK/NF-kappaB pathway. *Tumour Biol* 34 (4):2433-2440.
50. Wang HP, Hanlon JG, Rainbow AJ, Espiritu M, Singh G (2002) Up-regulation of Hsp27 plays a role in the resistance of human colon carcinoma HT29 cells to photooxidative stress. *Photochem Photobiol* 76 (1):98-104
51. Wagner A, Wiedmann M, Tannapfel A, Mayr C, Kiesslich T, Wolkersdorfer GW, Berr F, Hauss J, Witzigmann H (2015) Neoadjuvant down-sizing of hilar cholangiocarcinoma with photodynamic therapy - Long-term outcome of a phase II pilot study. *Int J Mol Sci* 16 (11):26619-26628.
52. Zoepf T, Jakobs R, Arnold JC, Apel D, Riemann JF (2005) Palliation of nonresectable bile duct cancer: improved survival after photodynamic therapy. *Am J Gastroenterol* 100 (11):2426-2430.
53. Buescher JM, Driggers EM (2016) Integration of omics: more than the sum of its parts. *Cancer & metabolism* 4:4.
54. Masoud GN, Li W (2015) HIF-1 $\alpha$  pathway: role, regulation and intervention for cancer therapy. *Acta Pharm Sin B* 5 (5):378-389.
55. DiDonato JA, Mercurio F, Karin M (2012) NF-kappaB and the link between inflammation and cancer. *Immunol Rev* 246 (1):379-400.
56. Ji Z, Yang G, Shahzidi S, Tkacz-Stachowska K, Suo Z, Nesland JM, Peng Q (2006) Induction of hypoxia-inducible factor-1 $\alpha$  overexpression by cobalt chloride enhances cellular resistance to photodynamic therapy. *Cancer Lett* 244 (2):182-189.
57. Chen WH, Lecaros RL, Tseng YC, Huang L, Hsu YC (2015) Nanoparticle delivery of HIF1 $\alpha$  siRNA combined with photodynamic therapy as a potential treatment strategy for head-and-neck cancer. *Cancer Lett* 359 (1):65-74.
58. Li YJ, Zhou JH, Du XX, Jia de X, Wu CL, Huang P, Han Y, Sui H, Wei XL, Liu L, Yuan HH, Zhang TT, Zhang WJ, Xie R, Lang XH, Liu T, Jiang CL, Wang LY, Bai YX (2014) Dihydroartemisinin accentuates the anti-tumor effects of photodynamic therapy via inactivation of NF-kappaB in Eca109 and

- Ec9706 esophageal cancer cells. *Cell Physiol Biochem* 33 (5):1527-1536.
59. Coupieenne I, Bontems S, Dewaele M, Rubio N, Habraken Y, Fulda S, Agostinis P, Piette J (2011) NF-kappaB inhibition improves the sensitivity of human glioblastoma cells to 5-aminolevulinic acid-based photodynamic therapy. *Biochem Pharmacol* 81 (5):606-616.
  60. Porta C, Riboldi E, Ippolito A, Sica A (2015) Molecular and epigenetic basis of macrophage polarized activation. *Semin Immunol* 27 (4):237-248.
  61. Zhang Q, Li ZH, Li YY, Shi SJ, Zhou SW, Fu YY, Zhang Q, Yang X, Fu RQ, Lu LC (2015) Hypericin-photodynamic therapy induces human umbilical vein endothelial cell apoptosis. *Sci Rep* 5:18398.
  62. Di Venosa G, Perotti C, Battle A, Casas A (2015) The role of cytoskeleton and adhesion proteins in the resistance to photodynamic therapy. Possible therapeutic interventions. *Photochem Photobiol Sci* 14 (8):1451-1464.
  63. Acedo P, Stockert JC, Canete M, Villanueva A (2014) Two combined photosensitizers: a goal for more effective photodynamic therapy of cancer. *Cell Death Dis* 5:e1122.
  64. Galaz S, Espada J, Stockert JC, Pacheco M, Sanz-Rodriguez F, Arranz R, Rello S, Canete M, Villanueva A, Esteller M, Juarranz A (2005) Loss of E-cadherin mediated cell-cell adhesion as an early trigger of apoptosis induced by photodynamic treatment. *J Cell Physiol* 205 (1):86-96.
  65. Gendreau SB, Ventura R, Keast P, Laird AD, Yakes FM, Zhang W, Bentzien F, Cancilla B, Lutman J, Chu F, Jackman L, Shi Y, Yu P, Wang J, Aftab DT, Jaeger CT, Meyer SM, De Costa A, Engell K, Chen J, Martini JF, Joly AH (2007) Inhibition of the T790M gatekeeper mutant of the epidermal growth factor receptor by EXEL-7647. *Clin Cancer Res* 13 (12):3713-3723.
  66. Martinez-Carpio PA, Trelles MA (2010) The role of epidermal growth factor receptor in photodynamic therapy: a review of the literature and proposal for future investigation. *Lasers Med Sci* 25 (6):767-771.
  67. Edmonds C, Hagan S, Gallagher-Colombo SM, Busch TM, Cengel KA (2012) Photodynamic therapy activated signaling from epidermal growth factor receptor and STAT3: Targeting survival pathways to increase PDT efficacy in ovarian and lung cancer. *Cancer Biol Ther* 13 (14):1463-1470.
  68. Kawczyk-Krupka A, Bugaj AM, Potempa M, Wasilewska K, Latos W, Sieron A (2015) Vascular-targeted photodynamic therapy in the treatment of neovascular age-related macular degeneration: Clinical perspectives. *Photodiagnosis Photodyn Ther* 12 (2):161-175.
  69. Gallagher-Colombo SM, Miller J, Cengel KA, Putt ME, Vinogradov SA, Busch TM (2015) Erlotinib pretreatment improves photodynamic therapy of non-small cell lung carcinoma xenografts via multiple mechanisms. *Cancer Res* 75 (15):3118-3126.
  70. Yang PW, Hung MC, Hsieh CY, Tung EC, Wang YH, Tsai JC, Lee JM (2013) The effects of Photofrin-mediated photodynamic therapy on the modulation of EGFR in esophageal squamous cell carcinoma cells. *Lasers Med Sci* 28 (2):605-614.
  71. Tomanek L (2015) Proteomic responses to environmentally induced oxidative stress. *J Exp Biol* 218 (Pt 12):1867-1879.
  72. Ariza AC, Deen PM, Robben JH (2012) The succinate receptor as a novel therapeutic target for oxidative and metabolic stress-related conditions. *Front Endocrinol* 3:22.
  73. Mills E, O'Neill LA (2014) Succinate: a metabolic signal in inflammation. *Trends Cell Biol* 24 (5):313-320.
  74. Chouchani ET, Pell VR, Gaude E, Aksentijevic D, Sundier SY, Robb EL, Logan A, Nadtochiy SM, Ord EN, Smith AC, Eyassu F, Shirley R, Hu CH, Dare AJ, James AM, Rogatti S, Hartley RC, Eaton S, Costa AS, Brookes PS, Davidson SM, Duchon MR, Saeb-Parsy K, Shattock MJ, Robinson AJ, Work LM, Frezza C, Krieg T, Murphy MP (2014) Ischaemic accumulation of succinate controls reperfusion injury through mitochondrial ROS. *Nature* 515 (7527):431-435.
  75. Frank J, Lornejad-Schafer MR, Schoffl H, Flaccus A, Lambert C, Biesalski HK (2007) Inhibition of heme oxygenase-1 increases responsiveness of melanoma cells to ALA-based photodynamic therapy. *Int J Oncol* 31 (6):1539-1545.
  76. Nowis D, Legat M, Grzela T, Niderla J, Wilczek E, Wilczynski GM, Glodkowska E, Mrowka P, Issat T, Dulak J, Jozkowicz A, Was H, Adamek M, Wrzosek A, Nazarewski S, Makowski M, Stoklosa T, Jakobisiak M, Golab J (2006) Heme oxygenase-1 protects tumor cells against photodynamic

- therapy-mediated cytotoxicity. *Oncogene* 25 (24):3365-3374.
77. Kim J, Lim H, Kim S, Cho H, Kim Y, Li X, Choi H, Kim O (2016) Effects of HSP27 downregulation on PDT resistance through PDT-induced autophagy in head and neck cancer cells. *Oncol Rep* 35 (4):2237-2245.
  78. Chatr-Aryamontri A, Breitkreutz BJ, Heinicke S, Boucher L, Winter A, Stark C, Nixon J, Ramage L, Kolas N, O'Donnell L, Reguly T, Breitkreutz A, Sellam A, Chen D, Chang C, Rust J, Livstone M, Oughtred R, Dolinski K, Tyers M (2013) The BioGRID interaction database: 2013 update. *Nucleic Acids Res* 41 (Database issue):D816-823.
  79. Hornbeck PV, Kornhauser JM, Tkachev S, Zhang B, Skrzypek E, Murray B, Latham V, Sullivan M (2012) PhosphoSitePlus: a comprehensive resource for investigating the structure and function of experimentally determined post-translational modifications in man and mouse. *Nucleic Acids Res* 40 (Database issue):D261-270.
  80. Kelder T, van Iersel MP, Hanspers K, Kutmon M, Conklin BR, Evelo CT, Pico AR (2012) WikiPathways: building research communities on biological pathways. *Nucleic Acids Res* 40 (Database issue):D1301-1307.

## **SUPPLEMENTAL INFORMATION**

Supplemental information for this chapter is available at <https://doi.org/10.1007/s00018-016-2401-0>



---

**Part III**

**Metabolomics beyond  
cancer**





---

**Part III**

# **Chapter**

**Metabolic regulation of proteasome activity**

Esther A. Zaal<sup>1</sup>, Klaas Vermaas<sup>1</sup>, Celia R. Berkers<sup>1</sup>

<sup>1</sup> Biomolecular Mass Spectrometry and Proteomics, Bijvoet Center for Biomolecular Research, Utrecht University, Utrecht, The Netherlands

## ABSTRACT

Proteasome activating compounds are of interest as potential therapeutics in neurodegenerative diseases. Recently, we identified 11 compounds that increase proteasome activity. However, how these compounds activate proteasome activity remains elusive.

Here, we used mass spectrometry-based metabolomics in combination with proteasome activity assays to elucidate whether metabolism plays a role in the proteasome activating effect of these compounds.

Our findings show that proteasome activation with the p38 MAPK inhibitor PD169316 results in increased levels of adenosine and adenosine monophosphate (AMP). Metabolic flux studies confirmed that higher purine levels after PD169316 treatment are a result of increased *de novo* synthesis. Further analysis indicate that increased adenosine levels enhance proteasome activity, while AMP has a negative effect on proteasome activity via AMPK activation. Therefore, AMPK inhibition with dorsomorphin enhances the effect of PD169316.

In conclusion, we show that the combination of AMPK inhibition with PD169316 can be a novel therapeutic strategy for neurodegenerative diseases. In addition, our study demonstrate that metabolism influences the response to proteasome activating compounds, underscoring the value of metabolomics in drug development studies.

## INTRODUCTION

The proteasome is a large protein complex that is responsible for the degradation of intracellular proteins. Because protein degradation by the proteasome is involved in many cellular processes, modulating its activity can be of interest for therapeutically purposes. For example, the fact that proteasome inhibition leads to apoptosis particularly in malignant cells has led to the successful application of proteasome inhibitors in haematological cancers [1]. Not only proteasome inhibition, but also proteasome activation is of interest for clinical use.

Proteasome activity declines during aging and loss of proteolytic activities is seen as one of the hallmarks of aging, leading to the accumulation of misfolded, damaged and oxidized proteins [2, 3]. In addition, the accumulation of oxidized proteins results in oxidative stress, which plays a central role in several age related diseases, including heart diseases, atherosclerosis and neurodegenerative diseases [4]. Many neurodegenerative diseases, including Alzheimer's disease and Parkinson's disease, are characterized by accumulation of toxic protein aggregates, such as tau and  $\alpha$ -synuclein, respectively [5]. The accumulation of protein aggregates and oxidized proteins in turn can inhibit proteasome activity, resulting in a loop of low proteasome activity [6, 7]. Increasing proteasome activity extends lifetime in yeast and increased clearance of toxic proteins in human cells [8, 9], illustrating the potential of proteasome activation in the treatment of age-related diseases.

In a recent study, we identified 11 compounds that increased proteasome activity [10]. One of the identified compounds, PD169316, is a p38 mitogen-activated protein kinase (MAPK) inhibitor and further experiments confirmed the involvement of the MAPK signaling pathway in proteasome activation. Although phosphorylation of the proteasome by p38 MAPK and upstream kinase ASK1 has been described to inhibit proteasome activity [11, 12], proteasome activation by PD169316 seems to act via a different mechanism [10]. How inhibition of p38 MAPK by PD169316 activates the proteasome remains to be identified. In addition, the mechanism of proteasome activation of the other identified proteasome activators, which have various targets, remains elusive.

Several studies suggest that proteasome activity is influenced by metabolic regulators, such as cyclic adenosine monophosphate (cAMP) dependent protein kinase (PKA) [13, 14] and mammalian target of rapamycin (mTOR) [15, 16]. In addition, posttranslational modification of the proteasome by O-GlcNAc, of which glucose is a precursor, inhibits proteasome activity [17]. Previously, we have shown that metabolic alterations affect the response to the proteasome inhibitor bortezomib

(see chapter 2 and 3 of this thesis, [18]). Hence, we hypothesize that metabolism also plays a role in the mechanism of proteasome activation.

By studying the effects on cellular metabolism after proteasome activator treatment, we here provide novel insights in the mechanism of proteasome regulation by PD169316. We show that proteasome activation by PD169316 is accompanied with increased levels of adenosine monophosphate (AMP) levels, which has a negative effect on proteasome activity, supporting a negative feedback loop via AMPK activation. In addition, we identify the AMPK inhibitor dorsomorphin as a novel proteasome activator, which has a synergistic effect on proteasome activity in combination with PD169316.

## RESULTS

### **P38 MAPK-mediated proteasome activation induces alteration in nucleotide metabolism**

In a previous study, we identified more than 10 small molecules that increased proteasome activity in intact cells. One of these compounds, PD169316, is an inhibitor of p38 $\alpha$  MAPK. Chemical and genetic inhibition of the MAPK pathway via both up- and downstream modulators of p38 MAPK led to an increase in proteasome activity [10]. However, how the p38 MAPK pathway modulates proteasome activity remains elusive, as well as the mechanism of proteasome activation of the other compounds. Here, we hypothesize that proteasome activity is mediated by metabolic alterations.

To study the effect of PD169316 on metabolism, MeJuso cells were treated with 3  $\mu$ M PD169316 for 4 hours and intracellular metabolites were analyzed with LC-MS analysis. At this concentration, proteasome activity is 2.5 fold increased and has not reached its maximum (Fig. 1). Analyzing intracellular metabolites after 4 hours allowed us to capture fast metabolic responses after proteasome activation, while minimizing side effects. We identified 107 metabolites covering several important metabolic pathways such as glycolysis, tricarboxylic acid cycle and amino acid metabolism (Supplemental fig. S1). Surprisingly, only few metabolites were altered after 4 hours of PD169316 treatment as compared to non-treated controls. Glucose, lactate and pyruvate were downregulated, suggesting lower activity of glycolysis after PD169316 treatment. This is expected, since p38 MAPK is involved in activation of the glycolysis [19, 20]. Interestingly, almost all upregulated metabolites were purine nucleotides (adenosine monophosphate (AMP), inosine monophosphate (IMP), guanosine monophosphate (GMP) and nucleosides (adenosine, inosine and guanine). These metabolites are not only important building blocks for RNA and

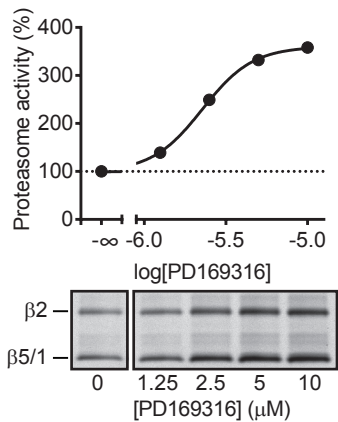


**Figure 1. PD169316 activates the proteasome reaching in a dose dependent manner.**

In gel fluorescent measurements of proteasome activity of Me1JuSo cells after 1-hour incubation with increasing concentrations of PD169316, followed by a 2-hour incubation with Me<sub>4</sub>BodipyFL-Ahx<sub>3</sub>L<sub>3</sub>VS (upper panel). Results represent quantification of in gel fluorescence measurements (lower panel). All signal intensities were normalized to DMSO-treated controls.

DNA, but also play an important role in cell signaling. These results suggest that alterations in nucleotide metabolism might be involved in proteasome activation.

Previously, we have shown that other inhibitors of p38 MAPK were also able to activate the proteasome [10]. We investigated whether the upregulation of nucleotides and nucleosides is a general feature of p38 MAPK inhibition, by incubating cells with losmapimod, a more potent inhibitor of p38 MAPK. The use of the cell-permeable fluorescent proteasome probe Me<sub>4</sub>BodipyFL-Ahx<sub>3</sub>L<sub>3</sub>VS, which covalently binds to catalytically active subunits of the proteasome [21, 22], showed that losmapimod is less potent in activating the proteasome as compared to PD169316 (Fig. 2a). After 3 hours of losmapimod, only 25% proteasome activation occurs at a concentration of 5 μM and a high concentration of 20 μM resulted in a similar effect than 3 μM PD169316 (Fig. 2a). This corresponds with the lower potency of other p38 MAPK inhibitors to activate the proteasome [10] and might suggest that the effect on the proteasome is not directly regulated via p38 MAPK. Mass spectrometry analysis of extracted metabolites indicates that losmapimod treatment results in altered levels of metabolites involved in purine biosynthesis, similar to PD169316 (Fig 2b). Together, these results suggest that p38 MAPK inhibitors mediate alterations in purine nucleotides and nucleosides levels.

To verify whether these findings are limited to p38 MAPK inhibition or are general for proteasome activation, we investigated the metabolic alterations of proteasome activators metergoline, pimoziide, win 62.577 and verapamil [10]. At concentrations of 3 μM, these compounds are able to enhance proteasome activity (win 62.577 >> PD169316 > pimoziide > metergoline > verapamil) (Fig. 2c). Indeed, after 18 hours of incubation with these compounds, levels of metabolites involved in purine synthesis were affected, with adenosine the most upregulated metabolite (Fig. 2d).

These proteasome activators all have different targets than p38 MAPK, suggesting that the increase in purine metabolites is a general feature of proteasome activation and not specific for p38 MAPK inhibitors.

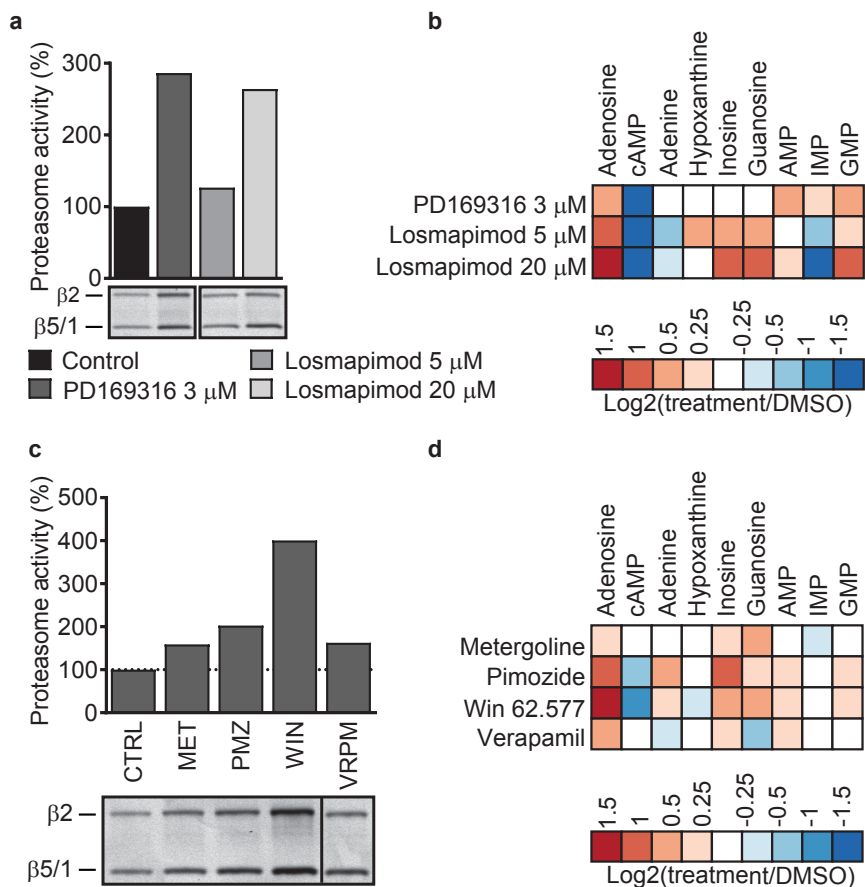


**Figure 2. Proteasome activation increases levels of purine nucleotides.**

**a** Total proteasome activity after a 2-hour incubation with PD169316 or Losmapimod, followed by a 1-hour incubation with Me<sub>4</sub>BodipyFL-Ahx<sub>3</sub>L<sub>3</sub>VS (upper panel). Results represent quantification of in gel fluorescence measurements (lower panel). All signal intensities were normalized to DMSO-treated controls. **b** Heatmap of metabolites involved in purine nucleotide metabolism after 8 hour treatment with PD169316 or Losmapimod at the indicated concentrations. Results are presented as log<sub>2</sub> of the ratio of peak area's between treated and DMSO-treated controls (n=3). **d** Total proteasome activity after 18-hour incubation with different proteasome activators, followed by a 1-hour incubation with Me<sub>4</sub>BodipyFL-Ahx<sub>3</sub>L<sub>3</sub>VS (upper panel). Results represent quantification of in gel fluorescence measurements (lower panel). All signal intensities were normalized to DMSO-treated controls. **e** Heatmap of metabolites involved in purine nucleotide metabolism after 18 hour treatment with different proteasome inhibitors at a concentrations of 3  $\mu$ M. Results are presented as log<sub>2</sub> of the ratio of peak area's between treated and DMSO-treated controls (n=3).

### High adenosine and AMP levels after PD169316 treatment is sustained by increased *de novo* synthesis

Increased levels of purines can be a result of 1) decreased activity of nucleotide catabolic pathways, 2) increased breakdown of DNA and RNA or 3) increased activity of *de novo* synthesis. During purine synthesis, ribose phosphate and glycine are combined to eventually form IMP, which can be further converted to AMP or GMP (Fig. 3a). To investigate the activity of *de novo* purine synthesis, we performed a  $^{13}\text{C}$ -glucose tracer experiment. The heavy carbons of  $^{13}\text{C}$ -glucose are incorporated in purines through multiple pathways, including glycolysis, the pentose phosphate pathway (PPP), serine synthesis pathway (SSP) and one-carbon metabolism (Fig. 3a). To this end, cells were grown in medium containing 25 mM [U- $^{13}\text{C}$ ]-glucose in the presence and absence of 3  $\mu\text{M}$  PD169316 and the incorporation of  $^{13}\text{C}$ -carbon from glucose in the purines was analysed over time with mass spectrometry.

As expected, almost all the ribose-5-phosphate present was  $^{13}\text{C}$ -labeled (M+5), which is synthesized from  $^{13}\text{C}$ -glucose via the PPP. At the same time, glycine levels contained predominantly  $^{12}\text{C}$ -glycine, indicative of low SSP activity. This is expected, since the SSP activity is controlled by the demand for serine, which is present in the cell culture medium [18, 23, 24].  $^{13}\text{C}_2$ -glycine (M+2) levels are increasing over time and lower levels of M+0 and M+2 glycine are present after 24 hours of PD169316 treatment. This could be either a result of lower synthesis, but also a higher usage of glycine.

PD169316 treatment resulted in increased levels of AMP and adenosine as compared to non-treated control, in line with our earlier results. Moreover, higher levels of  $^{13}\text{C}$ -labeled AMP and adenosine were present, especially after 8 and 24 hours, indicative of higher *de novo* synthesis of AMP and adenosine (Fig. 3b). Most of the  $^{13}\text{C}$ -labeled AMP and adenosine levels were  $^{13}\text{C}_5$  (M+5), resulting from incorporation of  $^{13}\text{C}_5$ -ribose-5-phosphate. Glycine incorporation (M+2) and one-carbon metabolism (M+6, M+7) contributed less to the labelling of AMP and adenosine, corresponding to the lower amount of glucose incorporation in these precursors in general (Fig. 3b). Interestingly, no higher levels of total and  $^{13}\text{C}$ -labeled adenine, GMP and inosine were present after PD169316 treatment, suggesting that IMP is preferably converted to AMP and adenosine. Since a decreased nucleotide breakdown will likely result in more unlabeled AMP and adenosine, the high fractions of  $^{13}\text{C}$ -labeled AMP and adenosine suggest that the elevated levels are predominantly a result of *de novo* synthesis. However, whether an increased breakdown of DNA and RNA contributes the enhanced levels is not excluded. Together, these results indicate that proteasome activation with PD169316 is accompanied with increased levels of AMP and adenosine, which is at least partly a result of increased *de novo* synthesis of these purines.

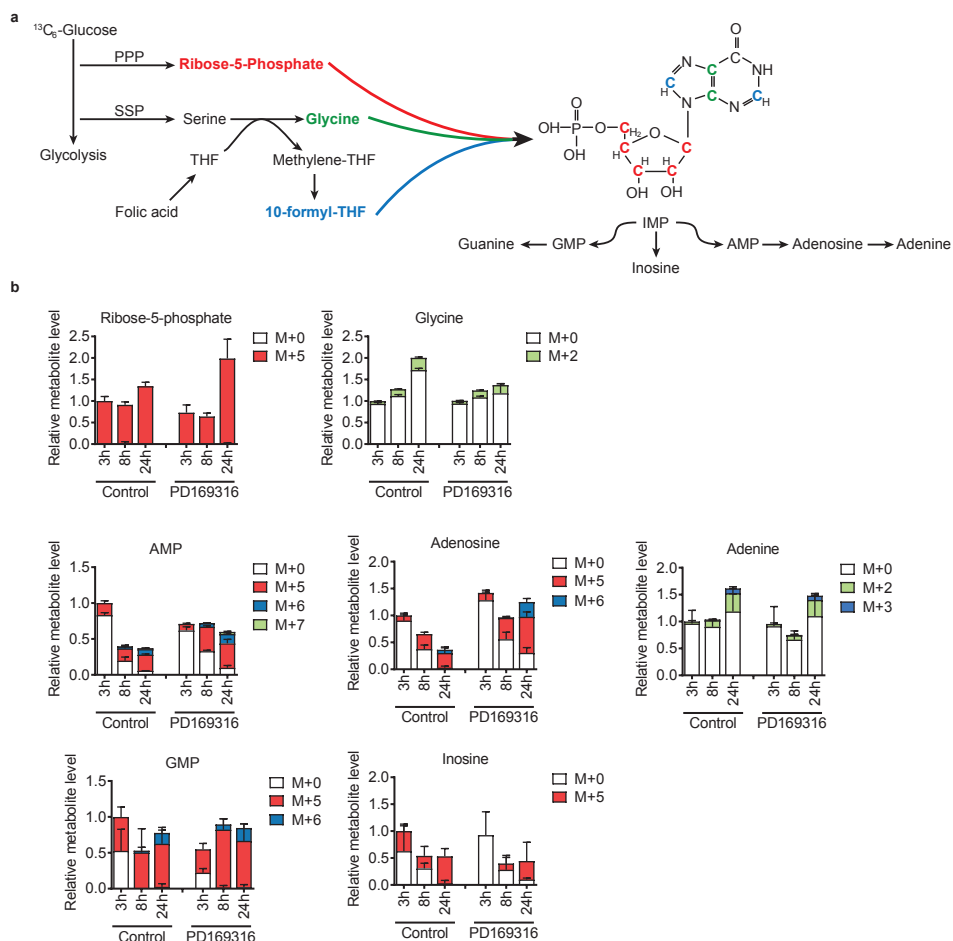


**Figure 3. Proteasome activation by PD169316 is associated with increased purine synthesis.**

**a** Schematic view of *de novo* synthesis of purines with glucose derived carbons from ribose-5-phosphate (in red), glycine (in green) and one-carbon-metabolism (in blue). **b** Intracellular analysis of metabolites involved in purine synthesis after PD169316 treatment. Cells were seeded in DMEM containing 25 mM [ $U$ - $^{13}C$ ] D-glucose and harvested after 3, 8 and 24 hours. Results show relative metabolite levels of normalized peak areas as compared to 3h DMSO-treated controls ( $n=3$ ).

### Induced levels of AMP after PD169316 treatment provides a negative feedback mechanism by AMPK activation

Having found that higher levels of AMP and adenosine were consistent after treatment with PD169316 and other proteasome activating compounds, we further investigated whether these metabolites are involved in modulating proteasome activity. We used specific inhibitors of different enzymes involved in purine synthesis, thereby differentially modulating intracellular purine levels (Fig. 4a). To study the



effects of AMP on proteasome activity, we used the AMP deaminase (AMPD) inhibitor metformin, which inhibits the conversion of AMP to IMP, and thereby increases AMP levels. In addition, metformin also activates AMP-activated protein kinase (AMPK), a direct downstream target of AMP, and thus mimics high intracellular AMP levels [25, 26]. In addition, we used EHNA and tubercidin to elevate intracellular adenosine. EHNA inhibits adenosine deaminase (ADA) and prevents the conversion of adenosine to inosine. Tubercidin inhibits adenosine kinase (ADK), preventing the conversion of adenosine to AMP. By combining EHNA and tubercidin, we expect to increase adenosine, because two important breakdown routes are inhibited (Fig. 4a).

To verify that these inhibitors indeed affect intracellular levels of AMP and adenosine, we analyzed levels of AMP and adenosine by mass spectrometry after 24 hours of treatment, as well as extracellular levels of adenosine (Supplemental Fig. S2a). In addition, we used these combinations in combination with PD169316 and looked at the effect on proteasome activity (Fig 4b).

In line with our earlier results, PD169316 treatment resulted in a 2-fold increase in proteasome activity together higher levels of intracellular AMP and adenosine as compared to non-treated cells (Fig. 4b, Supplemental Fig. S2a). Metformin alone increased levels of AMP, as well as downstream adenosine levels (Supplemental Fig. S2a). Interestingly, metformin treatment resulted in lower proteasome activity (Fig. 4b). The combination of metformin and PD169316 resulted in highly elevated levels of AMP and adenosine and suppressed the effect of PD169316 on the proteasome (Fig. 4b, Supplemental Fig. S2a). Together, these results not only suggest that metformin inhibits proteasome activity, but also that high AMP, likely via AMPK activation, has a negative effect on proteasome activity.

EHNA had only a marginally effect on adenosine levels, alone or in combination with PD169316 (supplemental Fig. S2a). At the same time, EHNA lowered proteasome activity and lowered the effect of PD169316 on the proteasome. We used a combination of tubercidin and EHNA to artificially enhance adenosine levels. The combination of ADK- and ADA inhibition resulted in an extreme rise of both intra- and extracellular levels of adenosine (Supplemental Fig. S2a). The addition of tubercidin, and the rise in adenosine levels, cancelled the inhibition of EHNA on the proteasome alone. Moreover, the combination of EHNA and tubercidin enhances the effect of PD169316 on proteasome activity. These results suggest that high adenosine levels stimulate proteasome activation.

To investigate whether adenosine enhances proteasome activity, we treated cells with adenosine for 24 hours. Indeed, adenosine increased proteasome activity with 50%, suggesting it is involved in proteasome activation (Fig. 4c). However, adenosine

had no effect on the effect of PD169316 on the proteasome, suggesting that high adenosine levels do not mediate proteasome activity followed by PD169316.

Our results indicate that AMP has a negative effect on proteasome activity. High levels of AMP activate AMPK and metformin, which directly activates AMPK, also inhibited proteasome activity [27]. We therefore hypothesized that AMP negatively influences proteasome activity via AMPK activation. Indeed, the AMPK inhibitor dorsomorphin increased proteasome activity in a dose dependent manner, confirming that AMPK inhibits proteasome activity (Supplemental Fig. S2b).

Next, we tested whether AMPK activity affects proteasome activation by PD169316, by using dorsomorphin in combination with PD169316. Interestingly, low concentrations of dorsomorphin greatly enhanced the effect of PD169316 on proteasome activity, while these drugs alone only marginally activated proteasome activity (Fig 4d). Overall, these data suggest that high AMP levels decrease

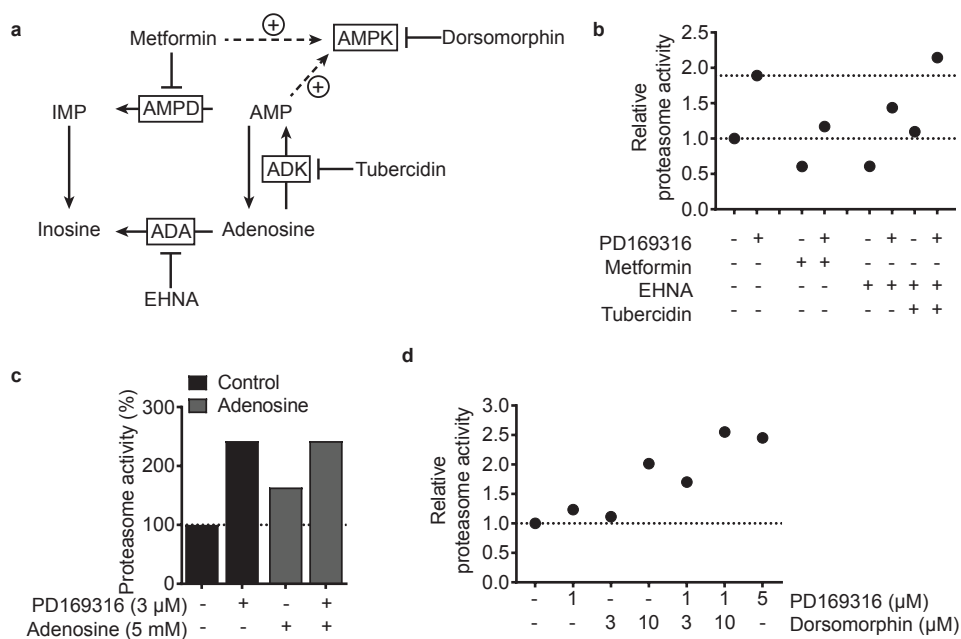


**Figure 4. Inhibitors of adenosine metabolism influence proteasome activity.**

**a** Schematic view of purine nucleotide inhibitors. **b** Total proteasome activity after a 24-hour incubation with different inhibitors, including 1-hour incubation with Me<sub>4</sub>BodipyFL-Ahx<sub>3</sub>L<sub>3</sub>VS. Results represent quantification of in gel fluorescence measurements. **c** Total proteasome activity after a 24 hour incubation with 5 mM adenosine in the presence or absence of 3  $\mu$ M PD169316, including 1-hour incubation with Me<sub>4</sub>BodipyFL-Ahx<sub>3</sub>L<sub>3</sub>VS (upper panel). Results represent quantification of in gel fluorescence measurements (lower panel). **d** Total proteasome activity after incubation of different combinations of PD169316 and dorsomorphin for 24 hours, including 1-hour incubation with Me<sub>4</sub>BodipyFL-Ahx<sub>3</sub>L<sub>3</sub>VS. Results represent quantification of in gel fluorescence measurements, as compared to non-treated control. All signal intensities were normalized to DMSO-treated controls.

proteasome activity by activating AMPK, thereby providing a negative feedback loop after PD169316 treatment. Hence, AMPK inhibition acts synergistically with PD169316 in enhancing proteasome activity.

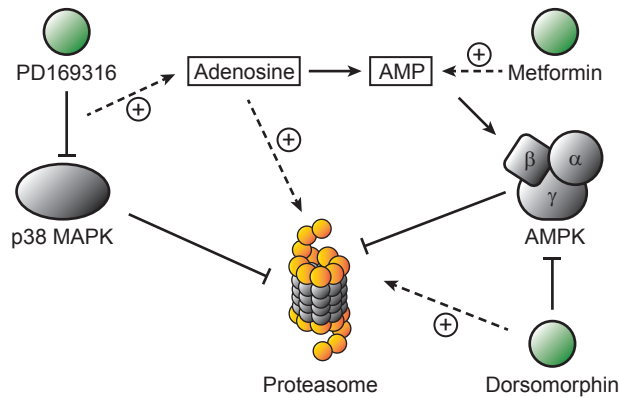


**Figure 5. Proposed model of p38 MAPK mediated proteasome activation.**

PD169316, which is an inhibitor of p38 MAPK, activates proteasome activity. In addition, PD169316 treatment results in increased levels of adenosine and AMP. Adenosine activates proteasome activity via an unknown mechanism, while AMP inhibits proteasome activity via activation of AMPK. Inhibition of AMPK with dorsomorphin activates the proteasome and acts synergistically with PD169316

## DISCUSSION

Proteasome activation is a promising strategy in the treatment for neurodegenerative diseases that are characterized by the accumulation of protein aggregates. Several small molecule proteasome activators have been described [9, 28, 29] and recently, we identified more than 10 novel proteasome activators using activity-based proteasome probes [10]. One of the compounds, PD169316, inhibits p38 MAPK and interfering with the p38 MAPK signaling pathway increases proteasome activity. Although it is known that p38 MAPK inhibits the proteasome by a direct phosphorylation on the proteasome [11], extensive proteomic experiments showed that p38 MAPK inhibitors did not affect phosphorylation status of the proteasome [10].

In this study, we aimed to elucidate the metabolic contributors to proteasome modulation. By using mass spectrometry-based metabolomics, we show that proteasome activation by PD169316 mediates changes in cellular metabolism. In particular, PD169316 treatment increased the activity of purine nucleotide synthesis, resulting in higher levels of adenosine and AMP. We also show that increased levels of AMP and adenosine are not exclusively linked to p38 MAPK inhibition, but are also

present after treatment with other proteasome activating compounds with different targets, indicating that this are general features of proteasome activation.

We demonstrate that proteasome activation by PD169316 results in enhanced purine nucleotide synthesis. In addition, our results suggest that high AMP levels are associated with proteasome inhibition. AMP activates AMPK, which has been shown to be a physiological suppressor of the proteasome [30–32]. We here show that metformin, which activates AMPK [26], lowered proteasome activity, while AMPK inhibition with dorsomorphin enhanced proteasome activity. These findings validate that AMPK is a negative regulator of proteasome activity, but also identify AMP as an important regulator of proteasome activity.

We further show that adenosine enhances proteasome activity, suggesting that high adenosine levels after PD169316 treatment are at least in part responsible for its effect on the proteasome. Interestingly, several studies describe that adenosine can activate p38 MAPK [33, 34], contradicting PD169316 action. However, other studies show that adenosine also is able to mediate inhibition of p38 MAPK and AMPK, which might can explain the proteasome activating action [35].

We propose here that high AMP levels following PD169316 treatment inhibit proteasome activity via activation of AMPK as a feedback mechanism (Fig. 5). In addition, increased adenosine levels seem to enhance proteasome activity, but the exact mechanism how adenosine mediates proteasome activity remains to be identified. Moreover, we here identify dorsomorphin as a novel proteasome activator that acts synergistically with PD169316. As the use of lower doses of synergistically acting drugs result both in lower risk of side effects and higher chances of reaching effective concentrations *in vivo*, the combined use of AMPK and p38 inhibitors could decrease the burden of treatment while increasing its efficacy.

In conclusion, our results show that proteasome activation results in increased purine synthesis, resulting in higher intracellular levels of adenosine and AMP. Whereas adenosine seems to promote proteasome activation, we show that AMP is involved in proteasome inhibition. Moreover, we propose that a combination of AMPK inhibitors and p38 MAPK inhibitors can be a therapeutic strategy for neurodegenerative diseases. In addition, this study underscores that metabolism can influence drug response, highlighting the importance of the metabolomics studies in drug development.

## METHODS

### Reagents

The proteasome activity probe Me<sub>4</sub>BodipyFL-Ahx<sub>3</sub>L<sub>3</sub>VS was a gift from Huib Ovaas (Leiden University Medical Center, The Netherlands). All solvents were obtained from Biosolve. All other chemicals were obtained from Sigma-Aldrich, unless stated otherwise.

### Cell culture

The human melanoma cell line MelJuSo was used for the experiments. Cells were maintained in suspension culture in DMEM (Lonza) medium supplemented with 2 mM L-glutamine (Lonza), 10% fetal bovine serum (FBS) (Gibco) and 100 µg/ml penicillin/streptomycin (Lonza) and were kept at 37°C in humidified 5% CO<sub>2</sub> atmosphere.

### Proteasome activity profiling

Proteasome activity was measured using Me<sub>4</sub>BodipyFL-Ahx<sub>3</sub>L<sub>3</sub>VS as described previously [21]. Cells were seeded in triplicate wells of 6-wells plate at a density of 3-4 x 10<sup>5</sup> cells/well. After 24 hours, media was replaced and incubated with the indicated conditions, followed by a 1-hour incubation with 500 nM Me<sub>4</sub>BodipyFL-Ahx<sub>3</sub>L<sub>3</sub>VS. Cells were washed with PBS, collected by scraping and lysed for 30 min in NP40 lysis buffer (50mM Tris, pH 7.4, 150mM NaCl, 1% NP40) at 4°C, followed by centrifugation at 14.000g to remove membrane fractions, nuclei and cell debris. Protein concentrations were determined using the Bradford assay (Bio-rad) and equal amounts of protein were denatured by boiling in XT Sample buffer (Bio-rad) with 9% β-mercaptoethanol. Proteins were separated on a 4-12% SDS-PAGE gel (Bio-rad) and fluorescence was measured with a Typhoon scanner (GE Healthcare) ( $\lambda_{\text{ex}}/\lambda_{\text{em}} = 488/526\text{nm}$ ). Protein loading was confirmed with a coomassie blue stain.

### Mass Spectrometry based metabolomics

For all experiments, cells seeded in 6-well plates at 3-4 x 10<sup>6</sup> cells/well in DMEM. After 24 hours, media was replaced with fresh DMEM. For <sup>13</sup>C-tracer experiments, media consisted of DMEM containing 25mM [U-<sup>13</sup>C]D-glucose (Cambridge Isotopes). Metabolites were extracted by adding 100 – 200 µl ice-cold MS lysis buffer (methanol/ acetonitrile/uLCMS H<sub>2</sub>O (2:2:1)) to the cell pellets. Samples were shaken for 10 minutes at 4°C, centrifuged at 14.000g for 15 minutes at 4°C and supernatants were collected for LC-MS analysis. LC-MS analysis was performed on an Exactive mass spectrometer (Thermo Scientific) coupled to a Dionex Ultimate 3000 autosampler and pump (Thermo Scientific). The MS operated in polarity-switching mode with

spray voltages of 4.5kV and -3.5kV. Metabolites were separated on a Sequant ZIC-pHILIC column (2.1 x 150mm, 5 $\mu$ m, Merck) with guard column (2.1 x 20mm, 5 $\mu$ m, Merck) using a linear gradient of acetonitrile and a buffer containing 20mM (NH<sub>4</sub>)<sub>2</sub>CO<sub>3</sub>, 0.1% NH<sub>4</sub>OH in ULC/MS grade water. Flow rate was set at 150  $\mu$ L/min. Metabolites were identified based on exact mass within 5 ppm and further validated by concordance with retention times of standards. Metabolites were quantified using LCquan software (Thermo Scientific). Peak intensities were normalized based on median peak intensity. Peak areas of identified metabolites were in their respective linear range of detection.

### **Acknowledgements**

CRB was supported by VENI grant (project 722.013.009) from the Netherlands Organization for Scientific Research (NWO). The authors would like to thank Huib Ovaa for providing Me<sub>4</sub>BodipyFLAhx<sub>3</sub>L<sub>3</sub>VS.

### **Author contributions**

CRB and EAZ developed this study, designed the experiments and wrote the manuscript. EAZ and KV performed the experiments. EAZ and CRB performed data analysis and interpretation.

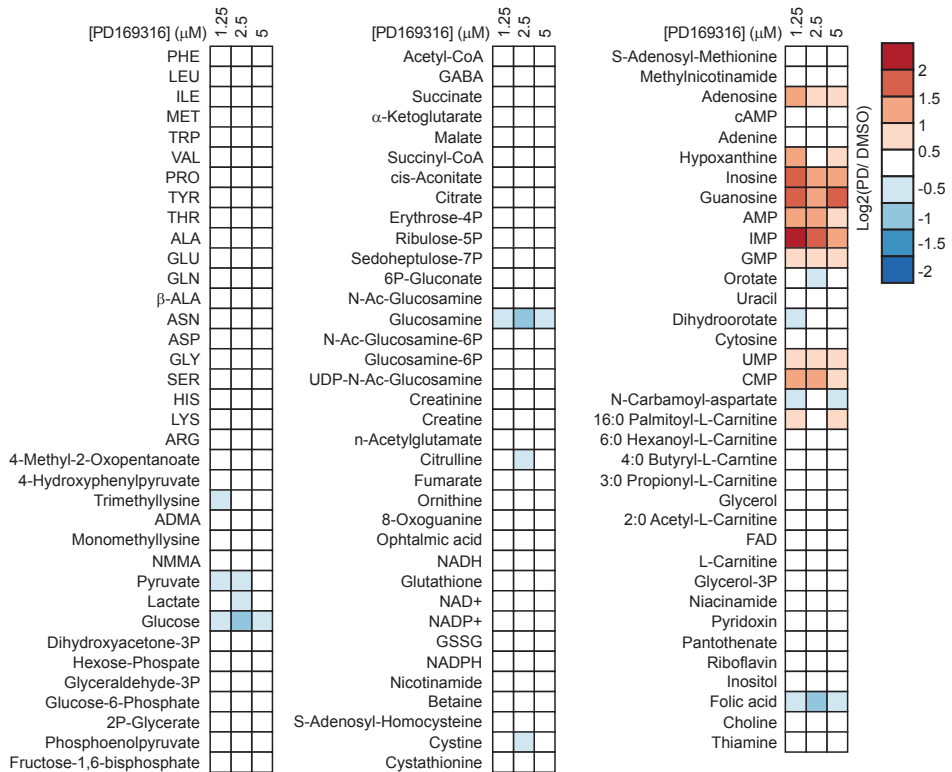
## REFERENCES

1. Anderson KC. The 39th David A. Karnofsky Lecture: bench-to-bedside translation of targeted therapies in multiple myeloma. *J Clin Oncol.* 2012;30:445–52.
2. López-Otín C, Blasco MA, Partridge L, Serrano M, Kroemer G. The hallmarks of aging. *Cell.* 2013;153:1194–217.
3. Tomaru U, Takahashi S, Ishizu A, Miyatake Y, Gohda A, Suzuki S, et al. Decreased Proteasomal Activity Causes Age-Related Phenotypes and Promotes the Development of Metabolic Abnormalities. *Am J Pathol.* 2012;180:963–72.
4. Raynes R, Pomatto LCD, Davies KJA. Degradation of oxidized proteins by the proteasome: Distinguishing between the 20S, 26S, and immunoproteasome proteolytic pathways. *Mol Aspects Med.* 2016;50:41–55.
5. Rubinsztein DC. The roles of intracellular protein-degradation pathways in neurodegeneration. *Nature.* 2006;443:780–6.
6. Saez I, Vilchez D. The Mechanistic Links Between Proteasome Activity, Aging and Age-related Diseases. *Curr Genomics.* 2014;15:38–51.
7. Chondrogianni N, Gonos ES. Proteasome dysfunction in mammalian aging: Steps and factors involved. *Exp Gerontol.* 2005;40:931–8.
8. Kruegel U, Robison B, Dange T, Kahlert G, Delaney JR, Kotireddy S, et al. Elevated proteasome capacity extends replicative lifespan in *Saccharomyces cerevisiae*. *PLoS Genet.* 2011;7:e1002253.
9. Lee B-H, Lee MJ, Park S, Oh D-C, Elsasser S, Chen P-C, et al. Enhancement of proteasome activity by a small-molecule inhibitor of USP14. *Nature.* 2010;467:179–84.
10. Leestemaker Y, de Jong A, Witting KF, Penning R, Schuurman K, Rodenko B, et al. Proteasome Activation by Small Molecules. *Cell Chem Biol.* 2017;24:725–736.e7.
11. Lee S-H, Park Y, Yoon SK, Yoon J-B. Osmotic stress inhibits proteasome by p38 MAPK-dependent phosphorylation. *J Biol Chem.* 2010;285:41280–9.
12. Um JW, Im E, Park J, Oh Y, Min B, Lee HJ, et al. ASK1 negatively regulates the 26 S proteasome. *J Biol Chem.* 2010;285:36434–46.
13. Zhang F, Hu Y, Huang P, Toleman CA, Paterson AJ, Kudlow JE. Proteasome function is regulated by cyclic AMP-dependent protein kinase through phosphorylation of Rpt6. *J Biol Chem.* 2007;282:22460–71.
14. Asai M, Tsukamoto O, Minamino T, Asanuma H, Fujita M, Asano Y, et al. PKA rapidly enhances proteasome assembly and activity in in vivo canine hearts. *J Mol Cell Cardiol.* 2009;46:452–62.
15. Zhang Y, Nicholatos J, Dreier JR, Ricoult SJH, Widenmaier SB, Hotamisligil GS, et al. Coordinated regulation of protein synthesis and degradation by mTORC1. *Nature.* 2014;513:440–3.
16. Zhao J, Zhai B, Gygi SP, Goldberg AL. mTOR inhibition activates overall protein degradation by the ubiquitin proteasome system as well as by autophagy. *Proc Natl Acad Sci.* 2015;112:15790–7.
17. Zhang F, Su K, Yang X, Bowe DB, Paterson AJ, Kudlow JE. O-GlcNAc modification is an endogenous inhibitor of the proteasome. *Cell.* 2003;115:715–25.
18. Zaal EA, Wu W, Jansen G, Zweegman S, Cloos J, Berkens CR. Bortezomib resistance in multiple myeloma is associated with increased serine synthesis. *Cancer Metab.* 2017;5:7.
19. Marsin AS, Bertrand L, Rider MH, Deprez J, Beauloye C, Vincent MF, et al. Phosphorylation and activation of heart PFK-2 by AMPK has a role in the stimulation of glycolysis during ischaemia. *Curr Biol.* 2000;10:1247–55.
20. Liu J, Wen D, Fang X, Wang X, Liu T, Zhu J. p38MAPK Signaling Enhances Glycolysis Through the Up-Regulation of the Glucose Transporter GLUT-4 in Gastric Cancer Cells. *Cell Physiol Biochem.* 2015;36:155–65.
21. Berkens CR, van Leeuwen FWB, Groothuis T a, Peperzak V, van Tilburg EW, Borst J, et al. Profiling proteasome activity in tissue with fluorescent probes. *Mol Pharm.* 2007;4:739–48.
22. de Jong A, Schuurman KG, Rodenko B, Ova H, Berkens CR. Fluorescence-based proteasome activity profiling. *Methods Mol Biol.* 2012;803 January:183–204.
23. Labuschagne CF, van den Broek NJF, Mackay GM, Vousden KH, Maddocks ODK. Serine, but not glycine, supports one-carbon

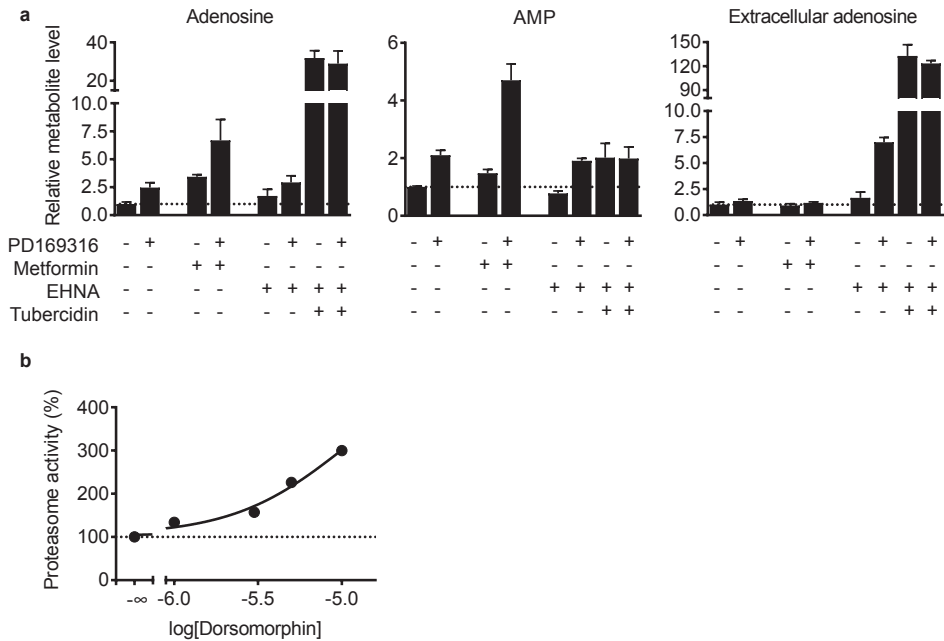
- metabolism and proliferation of cancer cells. *Cell Rep.* 2014;7:1248–58.
24. Maddocks ODK, Berkers CR, Mason SM, Zheng L, Blyth K, Gottlieb E, et al. Serine starvation induces stress and p53-dependent metabolic remodelling in cancer cells. *Nature.* 2013;493:542–6.
  25. Hawley S a, Gadalla AE, Olsen GS, Hardie DG. The Antidiabetic Drug Metformin Activates the AMPK. *Diabetes.* 2002;51 August:2420–5.
  26. Ouyang J, Parakhia RA, Ochs RS. Metformin activates AMP kinase through inhibition of AMP deaminase. *J Biol Chem.* 2011;286:1–11.
  27. Herzig S, Shaw RJ. AMPK: guardian of metabolism and mitochondrial homeostasis. *Nat Rev Mol Cell Biol.* 2017.
  28. Liu Y, Hettinger CL, Zhang D, Rezvani K, Wang X, Wang H. Sulforaphane enhances proteasomal and autophagic activities in mice and is a potential therapeutic reagent for Huntington's disease. *J Neurochem.* 2014;129:539–47.
  29. Myeku N, Clelland CL, Emrani S, Kukushkin N V, Yu WH, Goldberg AL, et al. Tau-driven 26S proteasome impairment and cognitive dysfunction can be prevented early in disease by activating cAMP-PKA signaling. *Nat Med.* 2016;22:46–53.
  30. Viana R, Aguado C, Esteban I, Moreno D, Viollet B, Knecht E, et al. Role of AMP-activated protein kinase in autophagy and proteasome function. *Biochem Biophys Res Commun.* 2008;369:964–8.
  31. Xu J, Wang S, Viollet B, Zou MH. Regulation of the proteasome by AMPK in endothelial cells: The role of O-GlcNAc transferase (OGT). *PLoS One.* 2012;7.
  32. Ronnebaum SM, Patterson C, Schisler JC. Minireview: hey U(PS): metabolic and proteolytic homeostasis linked via AMPK and the ubiquitin proteasome system. *Mol Endocrinol.* 2014;28:1602–15.
  33. Schulte G, Fredholm BB. Signalling from adenosine receptors to mitogen-activated protein kinases. *Cell Signal.* 2003;15:813–27.
  34. Németh ZH, Leibovich SJ, Deitch EA, Sperlágħ B, Virág L, Vizi ES, et al. Adenosine stimulates CREB activation in macrophages via a p38 MAPK-mediated mechanism. *Biochem Biophys Res Commun.* 2003;312:883–8.
  35. Omar MA, Verma S, Clanachan AS. Adenosine-mediated inhibition of 5'-AMP-activated protein kinase and p38 mitogen-activated protein kinase during reperfusion enhances recovery of left ventricular mechanical function. *J Mol Cell Cardiol.* 2012;52:1308–18.



## SUPPLEMENTAL INFORMATION

**Supplemental figure S1. PD169316 treatment affects cellular metabolism.**

Heatmap of identified metabolites after 4 hour treatment with different concentrations of PD169316. Results are presented as log<sub>2</sub> of the ratio of peak area's between treated and control samples (n=3).



**Supplemental figure S2. Inhibitors of adenosine metabolism affect AMP and adenosine levels.**

**a** Intra- and extracellular analysis of adenosine and AMP levels after 24 hours inhibitor treatment. Normalized to DMSO-treated controls. **b** Total proteasome activity after a 1-hour incubation with increasing concentrations of dorsomorphin, followed by a 2-hour incubation with Me<sub>4</sub>BodipyFL-Ahx<sub>3</sub>L<sub>3</sub>VS. Results represent quantification of in gel fluorescence measurements, normalized to DMSO-treated controls.





---

**Part IV**

**Synopsis and  
Perspective**



---

**Part IV**

# **Chapter**

**Summarizing discussion**

## INTRODUCTION

Over the last decades the combination of expanding interest in the role of metabolism in cancer and advances in analytical tools has resulted in increased understanding of metabolic reprogramming of cancer cells. The unique metabolism of cancer holds promise to find novel targets for cancer therapy, as proven by the successful application of existing chemotherapeutic agents that target metabolism, such as methotrexate and 5-fluorouracil. Lately, the identification of metabolic vulnerabilities in cancer cells has also led to the development of several new drugs that target cancer metabolism. In addition, metabolic alterations have been shown to play a role in the sensitivity of cancer cells to anticancer therapies, as reviewed in **chapter 1** and further demonstrated in this thesis. Hence, agents that target metabolism are also appealing for combinational therapy with current drugs to improve cancer therapy.

## IDENTIFICATION OF METABOLIC VULNERABILITIES IN PROTEASOME INHIBITOR RESISTANCE

In the first part of this thesis, I studied the metabolic differences between bortezomib-resistant and bortezomib-sensitive cell lines and showed that bortezomib-resistance is accompanied by several metabolic alterations. In **chapter 2**, I showed that bortezomib-resistant cells have increased glucose flux towards the serine synthesis pathway and pentose phosphate pathway, which contributes to an enhanced antioxidant capacity. In addition, 3-phosphoglycerate dehydrogenase (PHGDH) was identified as one of the most upregulated enzymes in bortezomib-resistant cells as compared to sensitive cells. In **chapter 3**, I further analyzed the metabolic alterations in these cells and showed that bortezomib-resistant cells also have higher activity of the tricarboxylic acid (TCA) cycle and the electron transport chain (ETC). I demonstrated that bortezomib-resistant cells are more sensitive to ETC inhibition, suggesting that ETC inhibitors could be of interest to overcome bortezomib resistance.

While other studies have linked bortezomib resistance to metabolic alterations [1–3], the combination of targeted metabolomics, metabolic flux analysis and proteomics described in this thesis provides novel mechanistic insights into the role of metabolism in mediating bortezomib resistance. This multimodal investigation has resulted in several promising new strategies to improve bortezomib therapy.

Firstly, the overexpression of PHGDH – the rate limiting step in the serine synthesis pathway – indicates that interfering with serine metabolism could be of



interest in bortezomib-resistant cells. PHGDH is often upregulated in cancers and increased expression of PHGDH is also associated with poor prognosis [4–6]. Therefore, PHGDH is seen as an important drug target in cancer metabolism, and PHGDH inhibitors have great potential and it is certainly of interest to test these in bortezomib-resistant cancers [7–9].

Secondly, the results from **chapter 2** indicate that PHGDH expression deserves further evaluation as a prognostic biomarker for bortezomib resistance. I showed that PHGDH overexpression is associated with bortezomib resistance, not only in multiple cell lines, but also in a small cohort of patient samples. Easily obtainable prognostic biomarkers that predict patients' response to bortezomib treatment are currently scarce for multiple myeloma, resulting in ineffective treatments, unnecessary side effects and higher costs [10, 11]. Identifying such biomarkers can greatly increase therapeutic efficacy and efficiency at the individual patient level. Large-scale analyses between PHGDH expression levels and bortezomib response are required to determine its usefulness as a predictor of bortezomib response in a clinical setting.

Thirdly, the results from **chapter 2** raise the possibility that bortezomib efficacy in patients can be increased by removing serine from the diet. Serine starvation has been shown to decrease tumor growth in mouse models without an effect on other amino acids and glucose [12, 13]. Amino acid restriction is already successfully used in the treatment of several inborn errors of metabolism [14], but has not yet been implemented in cancer therapy. At the same time, there is a high interest in the influence of our diet on the development of cancer. Adjuvant treatment of cancer with dietary alterations is thus an interesting option for future therapy. Our results indicate that the combination of nutritional serine restriction with bortezomib is promising because it specifically targets bortezomib-sensitive cells, making the initial drug treatment more effective and thereby preventing the development of resistance. Preventing cells to become resistant may prove a more advantageous strategy than targeting bortezomib resistance, given the fact that almost all patients ultimately develop drug resistance and the lack of clinical options for its treatment. Our results on multiple myeloma's 'serine addiction' therefore warrant further preclinical and clinical evaluation. Studying and possibly implementing a dietary restriction could be more cost-effective than the development of new drugs.

Finally, I showed that bortezomib-resistant cells can be specifically targeted with ETC inhibitors, such as the biguanide phenformin and simvastatin. In **chapter 3**, our extensive analysis of the proteome and metabolome suggests that phenformin and simvastatin act via inhibition of oxidative phosphorylation, which is also upregulated in bortezomib-resistant cells. Although further experiments are needed to confirm

the mechanism of action of these compounds in overcoming bortezomib resistance, a genome-wide gene expression analysis showed that relapsed and bortezomib-resistant patients had higher expression of genes associated with oxidative phosphorylation, supporting that our findings can be expanded to patients. These results are significant from a mechanistic perspective, but, importantly, also from a clinical perspective, as biguanides and simvastatin are widely used for the treatment of type 2 diabetes and hypercholesterolemia, respectively. Our findings are particularly interesting because they are corroborated by the hitherto unexplained clinical observation that biguanide use is associated with a better prognosis in multiple myeloma patients (although these results have not been linked to responses to proteasome inhibitor therapy) [15–17]. Biguanides and simvastatin have been shown to have anti-cancer effects and are currently tested in clinical trials to treat cancer [18]. This makes the approval of these drugs for use in combination therapy with bortezomib easier than for newly developed compounds.

Several challenges lie ahead before therapies targeting metabolism in drug resistant cancers find their way to the patient.

The results from **chapters 2 and 3** indicate that the rewired metabolism in bortezomib-resistant cells forms a complex network of many upregulated anaplerotic pathways resulting in a redundancy of sources for energy- and redox metabolism. This redundancy becomes evident, for example, during starvation assays where bortezomib-resistant, but not bortezomib-sensitive cells, maintain sufficient levels of glutathione after being starved for serine and glycine (the latter being an essential building block for *de novo* glutathione synthesis). Another example can be found in **chapter 3**, where bortezomib-resistant cells survive glutamine starvation, even though glutamine is the main source for TCA cycle metabolites and amino acids that are synthesized from TCA cycle intermediates. Unperturbed by this starvation, resistant cells switch to other sources that fuel the TCA cycle, most likely fatty acids and branched-chain amino acids. The resulting metabolic flexibility makes bortezomib-resistant cells highly adaptable to changing environmental conditions, including limited nutrient availability and (metabolic) drug treatment, as also seen in other cancer cells [19].

Together, the findings in the first part of this thesis underscore the importance of understanding the metabolic network as an interdependent system with many redundancies and specific vulnerabilities. This highlights the value of metabolomics as an important tool for finding metabolic targets. However, a more complete understanding of the metabolic network may be achieved by a combination of -omics methods from other domains. High throughput genetic expression

data (transcriptomics or proteomics) can be combined with metabolite levels (metabolomics) to model and map changes in metabolic pathways in relation to their underlying genetic, epigenetic and regulatory domains [20]. These genome-scale metabolic models are very promising to increase our knowledge about the mechanisms of metabolic alterations in drug resistance.

## **METABOLOMICS IN MULTI-OMICS APPROACHES TO STUDY RESPONSES TO ANTICANCER THERAPY**

The development of advanced analytical techniques allows for the simultaneous quantification of a large variety of molecules to study the genome, transcriptome, proteome and metabolome in an approach called systems biology. These different –omics techniques provide data at different levels of the cell, leading to a better understanding of the pathophysiology of cancer. In the second part of this thesis, I described studies in which metabolomics is combined with other –omics techniques, such as proteomics and transcriptomics, to study the response of cancer cells to different therapies.

The studies described in chapters 4 and 5 were initially focussed on alterations of protein (**chapter 4**) or RNA levels (**chapter 5**). However, the results eventually pointed to altered metabolic states, reiterating the importance of the metabolome. Although many mutations and alterations in protein levels influencing cellular metabolism have been described, recent studies show that genetic factors alone do not determine the metabolic state. Environmental factors appear to influence metabolism to a greater extent than previously thought [21–23]. Many studies also show that specific metabolites themselves can affect proteins and transcription factors and thereby promote tumor growth (so-called oncometabolites) [24–26]. This means that inferences about the metabolic state of the cell based on genetic factors alone are not complete. Therefore, the addition of metabolomics to other -omics data results in a more complete understanding of the metabolic state in these systems and may eventually lead to novel targets.

For example, phosphoproteomic analyses of lapatinib-resistant breast cancer cells in **chapter 4** showed a re-activation of PI3K/AKT/MTOR pathway, which stimulates glycolysis, together with alterations in phosphosites in enzymes involved in glycolysis. The metabolomics analysis showed that lapatinib-resistant cells have higher uptake of extracellular glucose, together with higher secretion of lactate and higher levels of glycolytic intermediates, confirming high glycolytic activity. Many metabolites involved in other pathways were also altered in lapatinib resistance,

illustrating the complexity of metabolic alterations in drug resistance. Moreover, analyses of extracellular metabolites revealed that lapatinib-resistant cells have a higher secretion of acidic metabolites, including glutamate. This might influence drug action by lowering extracellular pH [27], but glutamate secretion can also promote cell growth and invasion in cancer [28, 29], illustrating the possibility to interfere with glutamate secretion in lapatinib resistance.

In **chapter 5**, the transcriptomic data showed an upregulation of HIF-1, a known regulator of metabolism, after photodynamic therapy (PDT). The higher levels of glucose and lactate after PDT treatment suggest higher glycolytic activity, supporting the transcriptomic upregulation of HIF-1. In addition, the alterations in redox state, as shown by differences in reduced and oxidized glutathione and the pentose phosphate pathway, can sustain upregulation of HIF-1. More importantly, the metabolomics analysis showed increased levels of succinate, which can activate HIF-1 and thereby promote cell survival. This suggests that limiting succinate production could be a novel strategy to increase PDT efficacy. Overall, these examples not only illustrate that metabolomics is able to validate alterations on RNA/protein levels, but also demonstrate that novel targets can be discovered when data are analysed from a metabolic viewpoint.

As can be appreciated from both **chapter 4 and 5**, multi-omics experiments result in enormous datasets, with more than 20.000 measurements per experiment. While these experiments show many alterations on different cellular levels, interpreting the biology behind these complex networks remains difficult. First, different sample preparations are needed for the different techniques and experiments are often performed with different sample sets, contributing to poor resemblance of the different -omics data. Therefore, the development of methods to prepare samples from the same starting material is essential for correctly integrating different -omics experiments. Second, alterations on the different -omics domains might occur at different stages after drug treatment. For example, alterations in RNA levels need time to translate to different protein levels, resulting in little similarity between RNA and protein levels when measurements are not performed in steady states. More importantly, the integration of information obtained at different cellular levels is very challenging, since the different domains influence each other and constitute a complex and dynamic network. It is likely that many alterations are present in the different cellular levels, making it difficult to determine the important factors.

In all, I believe that the true strength of using multi-omics lies not in the capability to analyse as much as possible (even though it is impressive that we can), but in the ability to perform in-depth analysis of pathways of interest through all cellular domains in a targeted approach. As illustrated in the first part of my thesis,

combining metabolomics with targeted proteomics aimed at metabolic enzymes not only confirmed the metabolomics data, but allowed me to generate hypotheses that are difficult to derive from either technology alone.

## LIMITATIONS AND OPPORTUNITIES FOR CELL CULTURE-BASED CANCER RESEARCH

An essential limitation of the work presented in this thesis – and of most studies in cancer metabolism – is that the results are mainly based on *in vitro* cell culture experiments. Cell culture-based experiments are fast, relatively cheap, and suitable for highly controlled experiments in terms of nutrient and oxygen availability, as well as the use of isotopic labeling for metabolic flux studies. However, recent work from several groups indicate that the translation of these results to tumors *in vivo* may prove difficult for several reasons [21, 22, 30, 31]. Commonly used cell culture media do not reflect physiological conditions and the use of these media results in altered metabolism and differences in sensitivity towards drugs [30]. This is particularly evident for glutamine metabolism: while glutamine is a main source for cancer cells in culture, recent studies show that it is less important in cancer cells *in vivo* [21, 22]. *In vitro* cultures also lack environmental factors that influence metabolism. These factors include the (limited) availability of oxygen and nutrients and the proximity of other cells such as stromal cells and immune cells [31]. Finally, a tumor shows metabolic heterogeneity due to its three-dimensional structure, resulting in variable oxygen and nutrient availability within the tumour [21, 22].

Moving towards more physiological conditions in cell culture-based assays is therefore important to promote the translation of *in vitro* experiments to treatment improvement in patients. For example, 3D cultures that simulate the metabolic heterogeneity of tumours will likely generate more clinically relevant results and are of great potential in cancer research [32]. In addition, co-culturing tumor cells with other tissues allows for the study of interactions between cancer cells and their microenvironment. For example, co-culture of tumor cells with stromal cells affect the sensitivity to anticancer drugs [33]. In the context of multiple myeloma, the presence of bone marrow stromal cells is also likely to influence metabolism. Hence, it would be interesting to find out whether the presence of stromal cells influences the sensitivity of multiple myeloma cells to bortezomib.

However, despite its fundamental limitations, cell-culture based experiments remain an essential instrument in the understanding of cancer and drug resistance. The results presented in this thesis are the product of an iterative process made

possible by the speed with which cell-culture based experiments can be done. Chapters 2 and 3 of this thesis are based on no less than 250 experiments, mostly yielding negative or unexpected answers. But the sum of these experiments eventually led us to results that were significant, internally consistent and reproducible. We then used clinical material to validate whether our experimental results were in principle consistent with actual patient tumor samples. This final step is essential to prevent the wasting of resources on results that are significant in cell-culture but clinically irrelevant.

## METABOLOMICS BEYOND CANCER

Finally, in **chapter 6**, I demonstrated that metabolism also influences the effect of drugs that are not related to cancer. Here, I showed that the effect of the proteasome activator PD169316 is influenced by the presence of adenosine and adenosine mononucleotide phosphate (AMP), highlighting the importance of the metabolome in drug response. By applying a metabolomics approach, I also showed that proteasome activation by PD169316 activates AMPK, providing a negative feedback loop for proteasome activation. Therefore, inhibition of AMPK with dorsomorphin not only activates the proteasome, but also acts synergistically with PD169316. The upregulation of adenosine was also present after treatment with other proteasome activating compounds such as verapamil, Win 62.577 and pimozide [34]. While the primary targets of these drugs are known, it remains elusive how they activate the proteasome and whether they act via a shared mechanism. Our findings suggest that purine metabolism might be a common feature of proteasome activation. In addition, it has been described that some of these proteasome activators activate cyclic-AMP (cAMP). cAMP, related to adenosine metabolism, has been linked to proteasome activation [35, 36], suggesting that the influence of adenosine nucleotides is not limited to PD169316 but also plays a role in proteasome activation by other compounds. Further studying the role of adenosine signaling could provide novel insights in the regulation of proteasome activation and aid in the development of proteasome activators for clinical use. Overall, this chapter not only shows the potential of metabolomics in screening for new drug targets, but also underscores that it is imperative to be aware of the influence of metabolism on the effect of the drug.

## CONCLUSION

In conclusion, the work described in this thesis illustrates that metabolism plays an important role in the effectiveness of anticancer drugs. I have shown that a combination of metabolomics with other -omics techniques results in a multidimensional picture of cellular responses to drugs. In addition, I have argued that testing the agreement between cell-culture based results and actual patient tumor samples strengthens the validity of preclinical work and helps to prevent false-positive lab-bench results. The metabolic vulnerabilities described in this thesis may be exploited to improve the efficacy of specific anticancer drugs, which warrants further preclinical and clinical investigation. In a broader perspective, I have shown that metabolism also influences the efficacy of non-cancer related drugs. In all, I have demonstrated that altered metabolism is at the center of the cellular drug response and that, consequently, metabolomics needs to be a core instrument in the understanding of drug resistance in cancer.

## REFERENCES

- Maiso P, Huynh D, Moschetta M, Sacco A, Aljawai Y, Mishima Y, et al. Metabolic signature identifies novel targets for drug resistance in multiple myeloma. *Cancer Res.* 2015;75:2071–82.
- Soriano GP, Besse L, Li N, Kraus M, Besse A, Meeuwenoord N, et al. Proteasome inhibitor-adapted myeloma cells are largely independent from proteasome activity and show complex proteomic changes, in particular in redox and energy metabolism. *Leukemia.* 2016;30:2198–207.
- Thompson RM, Dytfeld D, Reyes L, Robinson RM, Smith B, Manevich Y, et al. Glutaminase inhibitor CB-839 synergizes with carfilzomib in resistant multiple myeloma cells. 2017;8:35863–76.
- Locasale JW, Grassian AR, Melman T, Lyssiotis CA, Mattaini KR, Bass AJ, et al. Phosphoglycerate dehydrogenase diverts glycolytic flux and contributes to oncogenesis. *Nat Genet.* 2011;43:869–74.
- Zhang B, Zheng A, Hydbring P, Ambrose G, Ouchida AT, Goiny M, et al. PHGDH Defines a Metabolic Subtype in Lung Adenocarcinomas with Poor Prognosis. *Cell Rep.* 2017;19:2289–303.
- Possemato R, Marks KM, Shaul YD, Pacold ME, Kim D, Birsoy K, et al. Functional genomics reveal that the serine synthesis pathway is essential in breast cancer. *Nature.* 2011;476:346–50.
- Mullarky E, Lucki NC, Beheshti Zavareh R, Anglin JL, Gomes AP, Nicolay BN, et al. Identification of a small molecule inhibitor of 3-phosphoglycerate dehydrogenase to target serine biosynthesis in cancers. *Proc Natl Acad Sci U S A.* 2016;113:1778–83.
- Pacold ME, Brimacombe KR, Chan SH, Rohde JM, Lewis CA, Swier LJYM, et al. A PHGDH inhibitor reveals coordination of serine synthesis and one-carbon unit fate. *Nat Chem Biol.* 2016;12:452–8.
- Wang Q, Liberti M V., Liu P, Deng X, Liu Y, Locasale JW, et al. Rational Design of Selective Allosteric Inhibitors of PHGDH and Serine Synthesis with Anti-tumor Activity. *Cell Chem Biol.* 2017;24:55–65.
- Mulligan G, Mitsiades C, Bryant B, Zhan F, Chng WJ, Roels S, et al. Gene expression profiling and correlation with outcome in clinical trials of the proteasome inhibitor bortezomib. *Blood.* 2007;109:3177–88.
- Ting KR, Henry M, Meiller J, Larkin A, Clynes M, Meleady P, et al. Novel panel of protein biomarkers to predict response to bortezomib-containing induction regimens in multiple myeloma patients. *BBA Clin.* 2017;8 May:28–34.
- Maddocks ODK, Athineos D, Cheung EC, Lee P, Zhang T, van den Broek NJF, et al. Modulating the therapeutic response of tumours to dietary serine and glycine starvation. *Nature.* 2017;544:372–6.
- Maddocks ODK, Berkers CR, Mason SM, Zheng L, Blyth K, Gottlieb E, et al. Serine starvation induces stress and p53-dependent metabolic remodelling in cancer cells. *Nature.* 2013;493:542–6.
- van Vliet D, Derks TGJ, van Rijn M, de Groot MJ, MacDonald A, Heiner-Fokkema MR, et al. Single amino acid supplementation in aminoacidopathies: a systematic review. *Orphanet J Rare Dis.* 2014;9:7.
- Wu W, Merriman K, Nabaah A, Seval N, Seval D, Lin H, et al. The association of diabetes and anti-diabetic medications with clinical outcomes in multiple myeloma. *Br J Cancer.* 2014;111:628–36.
- Chang S-H, Luo S, O'Brian KK, Thomas TS, Colditz GA, Carlsson NP, et al. Association between metformin use and progression of monoclonal gammopathy of undetermined significance to multiple myeloma in US veterans with diabetes mellitus: a population-based retrospective cohort study. *Lancet Haematol.* 2015;2:e30-6.
- Boursi B, Mamtani R, Yang Y-X, Weiss BM. Impact of metformin on the progression of MGUS to multiple myeloma. *Leuk Lymphoma.* 2017;58:1265–7.
- Martinez-Outschoorn UE, Peiris-Pagés M, Pestell RG, Sotgia F, Lisanti MP. Cancer metabolism: a therapeutic perspective. *Nat Rev Clin Oncol.* 2017;14:11–31.
- Keibler MA, Wasylenko TM, Kelleher JK, Iliopoulos O, Vander Heiden MG, Stephanopoulos G. Metabolic requirements for cancer cell proliferation. *Cancer Metab.* 2016;4:16.
- Nilsson A, Nielsen J. Genome scale metabolic modeling of cancer. *Metab Eng.* 2017;43 Pt B:103–12.




21. Davidson SM, Papagiannakopoulos T, Olenchok BA, Heyman JE, Keibler MA, Luengo A, et al. Environment Impacts the Metabolic Dependencies of Ras-Driven Non-Small Cell Lung Cancer. *Cell Metab.* 2016;23:517–28.
22. Hensley CT, Faubert B, Yuan Q, Lev-Cohain N, Jin E, Kim J, et al. Metabolic Heterogeneity in Human Lung Tumors. *Cell.* 2016;164:681–94.
23. Cairns RA, Harris IS, Mak TW. Regulation of cancer cell metabolism. *Nat Rev Cancer.* 2011;11:85–95.
24. Sciacovelli M, Frezza C. Oncometabolites: Unconventional triggers of oncogenic signalling cascades. *Free Radic Biol Med.* 2016;100:175–81.
25. Selak MA, Armour SM, MacKenzie ED, Boulahbel H, Watson DG, Mansfield KD, et al. Succinate links TCA cycle dysfunction to oncogenesis by inhibiting HIF- $\alpha$  prolyl hydroxylase. *Cancer Cell.* 2005;7:77–85.
26. Fan J, Teng X, Liu L, Mattaini KR, Looper RE, Vander Heiden MG, et al. Human phosphoglycerate dehydrogenase produces the oncometabolite D-2-hydroxyglutarate. *ACS Chem Biol.* 2015;10:510–6.
27. Wojtkowiak JW, Verduzco D, Schramm KJ, Gillies RJ. Drug resistance and cellular adaptation to tumor acidic pH microenvironment. *Mol Pharm.* 2011;8:2032–8.
28. Fazzari J, Lin H, Murphy C, Ungard R, Singh G. Inhibitors of glutamate release from breast cancer cells; new targets for cancer-induced bone-pain. *Sci Rep.* 2015;5:8380.
29. Dornier E, Rabas N, Mitchell L, Novo D, Dhayade S, Marco S, et al. Glutaminolysis drives membrane trafficking to promote invasiveness of breast cancer cells. *Nat Commun.* 2017;8:2255.
30. Cantor JR, Abu-Remaileh M, Kanarek N, Freinkman E, Gao X, Louissaint A, et al. Physiologic Medium Rewires Cellular Metabolism and Reveals Uric Acid as an Endogenous Inhibitor of UMP Synthase. *Cell.* 2017;169:258–272.e17.
31. Schug ZT, Vande Voorde J, Gottlieb E. The nurture of tumors can drive their metabolic phenotype. *Cell Metab.* 2016;23:391–2.
32. Pampaloni F, Reynaud EG, Stelzer EHK. The third dimension bridges the gap between cell culture and live tissue. *Nat Rev Mol Cell Biol.* 2007;8:839–45.
33. Straussman R, Morikawa T, Shee K, Barzily-Rokni M, Qian ZR, Du J, et al. Tumour micro-environment elicits innate resistance to RAF inhibitors through HGF secretion. *Nature.* 2012;487:500–4.
34. Leestemaker Y, de Jong A, Witting KF, Penning R, Schuurman K, Rodenko B, et al. Proteasome Activation by Small Molecules. *Cell Chem Biol.* 2017;24:725–736.e7.
35. Zhang F, Hu Y, Huang P, Toleman CA, Paterson AJ, Kudlow JE. Proteasome function is regulated by cyclic AMP-dependent protein kinase through phosphorylation of Rpt6. *J Biol Chem.* 2007;282:22460–71.
36. Asai M, Tsukamoto O, Minamino T, Asanuma H, Fujita M, Asano Y, et al. PKA rapidly enhances proteasome assembly and activity in in vivo canine hearts. *J Mol Cell Cardiol.* 2009;46:452–62.



---

**Part IV**

**Nederlandse  
samenvatting**



---

Kankercellen hebben altijd honger. Voor hun snelle en ongecontroleerde groei hebben zij niet alleen veel energie nodig, maar ook de juiste bouwstenen om zich te vermenigvuldigen. Denk hierbij aan aminozuren (voor de aanmaak van eiwitten), vetzuren (voor de membranen) en nucleotides (voor DNA). Deze kleine moleculen – metabolieten – worden veelal in ons lichaam uit voedingsstoffen gemaakt in een complex netwerk van biochemische reacties: het metabolisme.

Kankercellen hebben niet alleen meer voedsel nodig dan normale cellen, maar ook de manier waarop ze hun voedingsstoffen gebruiken is anders. Al in de jaren '20 werd ontdekt dat kankercellen meer glucose opnemen dan gezonde cellen en dit ook anders gebruiken. Glucose wordt in verschillende stappen omgezet in pyruvaat (of pyrodruivenzuur), een proces genaamd glycolyse. Normaal wordt pyruvaat verder verbrand in de citroenzuurcyclus om energie te verkrijgen, een proces dat zuurstof vereist. Wanneer er onvoldoende zuurstof aanwezig is wordt er energie verkregen door pyruvaat om te zetten in melkzuur, het welbekende 'verzuren' tijdens het sporten. Kankercellen worden echter gekenmerkt door het feit dat ze ook in de aanwezigheid van zuurstof een voorkeur hebben om melkzuur te produceren – een schijnbaar inefficiënte keuze. Maar gelet op de ingenieuze weerbaarheid van kankercellen moet het haast wel zo zijn dat deze inefficiëntie op een andere manier voordelen biedt voor de overleving van de cel.

De afgelopen jaren is er steeds meer onderzoek gedaan naar het veranderde metabolisme in kankercellen. Niet alleen zijn er meer afwijkende metabole routes gevonden in kankercellen, ook is het duidelijk geworden dat dit aangepaste metabolisme een belangrijke rol speelt bij de maligne ontaarding van gezonde cellen.

Kankercellen zijn gewend om te overleven onder variabele en uitdagende omstandigheden in het lichaam. Zij kunnen zich snel aanpassen aan stressvolle situaties, waaronder ook geneesmiddelen gericht tegen kanker. Dit resulteert dan in geneesmiddelresistentie; de kankercellen passen zich aan om de blootstelling aan geneesmiddelen te overleven.

Het onderzoek gepresenteerd in dit proefschrift richt zich op de rol van het metabolisme in geneesmiddelresistente kankercellen. Door te onderzoeken welke metabole routes veranderen wanneer kankercellen resistent raken voor therapie, kunnen er nieuwe manieren gevonden worden om resistente tumoren te bestrijden. Doordat kankercellen als het ware verslaafd raken aan hun nieuwe metabolisme kan hun groei mogelijk geremd worden door in te grijpen op dit unieke metabolisme.


Door de variërende eigenschappen van metabolieten vereist de studie naar het metaboloom – *metabolomics* – zeer specifieke en gevoelige analytische technieken. Massaspectrometrie, waarmee metabolieten gemeten worden op basis van hun massa en lading, is een van de centrale instrumenten in de metabolomics. Een glucosemolecuul weegt minder dan een duizend-miljoen-miljoen-miljoenste gram, maar wordt door dit instrument op precies het juiste gewicht geschat. De massaspectrometer weegt op deze manier duizenden verschillende metabolieten tegelijkertijd. Hierdoor is het mogelijk om in de cel te bepalen welke metabolieten aanwezig zijn en hoeveel daarvan aanwezig zijn.

Wanneer we deze kwantitatieve informatie over metabolieten combineren met reeds bekende intracellulaire chemische reacties kunnen we tot op zekere hoogte afleiden welke routes in de cel worden afgelegd om van grondstof naar eindproduct te komen. Hierbij ontstaat een virtuele kaart van verschillende wegen (*pathways*) die de cel benut om in zijn metabole behoeften te voorzien.

Door de extreme complexiteit van de metabole routekaart is het vaak lastig om definitieve conclusies over de richtingen van reacties te trekken alleen op basis van de relatieve concentraties van metabolieten. Om dit probleem te ondervangen wordt er gebruik gemaakt van nutriënten met stabiel gelabelde atomen. Doordat deze 'zware' atomen ingebouwd worden in metabolieten en gemeten kunnen worden via massaspectrometrie, kan het gebruik van voedingsstoffen gevolgd worden in het complexe netwerk van metabole routes. Hierdoor ontstaat een steeds gedetailleerdere routekaart van de metabole *pathways* in de cel.

Het onderzoeken van de wegen in deze metabole routekaart is een hoeksteen van dit proefschrift. Door te meten welke intracellulaire wegen extra actief zijn (of juist extra rustig) bij geneesmiddelresistente kankercellen ontstaat een beter begrip van het mechanisme van resistentie. Hierdoor kunnen mogelijk nieuwe manieren gevonden worden om de huidige kankertherapie te verbeteren en resistentie tegen te gaan.

In het eerste deel van dit proefschrift beschrijf ik de zoektocht naar metabole veranderingen in bortezomib-resistente kankercellen. Bortezomib is een remmer van het proteasoom, een belangrijke cellulaire machine verantwoordelijk voor de afbraak van eiwitten. Bortezomib wordt ingezet bij de behandeling van multiple myeloom (plasmacelkanker), maar resistentie treedt vaak snel op. Mijn onderzoek laat zien dat bortezomib-resistente cellen hun glucose niet in eerste instantie gebruiken voor energie, maar om hun afweer tegen oxidatieve stress te verhogen via verschillende routes. Daarnaast hebben deze cellen een verhoogde activiteit van de citroenzuurcyclus voor hun energieproductie. Deze mechanismen zijn zelfs zo belangrijk voor deze cellen dat zij meerdere routes hebben geactiveerd om hun



energie en anti-oxidante spiegels op peil te houden. Het remmen van deze pathways zou dus een succesvolle strategie kunnen zijn om bortezomib-resistente kanker te behandelen.

Het tweede deel van dit proefschrift beschrijft verschillende projecten waarin metabolomics gecombineerd wordt met andere -omics technologieën in de zoektocht naar de cellulaire respons van tumorcellen op verschillende geneesmiddelen. De aansturing van een cel gebeurt op meerdere niveaus, zoals DNA, RNA, eiwitten en metabolieten. Veranderingen in een van deze niveaus zal altijd samengaan met veranderingen op de andere niveaus. Door de veranderingen in het metabooloom te vergelijken met veranderingen in deze verschillende lagen, wordt een completer beeld gekregen van de metabole status van een cel.

In het laatste deel van dit proefschrift laat ik zien dat het metabolisme ook invloed heeft op het effect van geneesmiddelen buiten de oncologie. Dit illustreert dat metabolomics van waarde is in het begrijpen van de werking van geneesmiddelen en een belangrijke rol kan spelen in de ontwikkeling van nieuwe geneesmiddelen.








---

# Acknowledgements



Congratulations, you have made it to the end of a difficult read (you have actually read this thesis, right?). Time for me to acknowledge the people who supported me over the last years.

Celia, how lucky I am with you as my supervisor. You are my role model in science: Ambitious, knowledgeable, and appropriately critical about our own data and conclusions. Your door is always open for advice. No matter in what state I entered your office, you always managed to let me walk away with my chin up. Your support and unconditional faith in me helped me to become more proud as a scientist and person. Thank you for everything.

Albert, I very much appreciated your advice and support during my track. You have brought together an incredibly diverse and intelligent group of people – of which I'm very proud to be a part. I am very grateful that you and Celia gave me the opportunity to stay a little longer. I still remember that during one of our first talks, you told me: wait for it, at the end of your PhD you will also do proteomics. Indeed, you were right, but let's admit, is metabolomics not also a bit interesting?

In such a big research group, it is impossible for me to name everybody personally without writing another thesis. I would like to thank all the current and former members of the Hecklab. Without *all y'all*, life at the lab wouldn't be the same and I look back on 4 years of good times with borrels, sinterkerstfeestjes, labuitjes, retreats and lunches.

Clément, from the moment we started our PhD I immediately knew we were going to be friends. I am very sorry you had to work so hard before I could admit that we were not just colleagues. Thank you for persisting and breaking through the wall; your friendship has made the last years amazing, both in- and outside the lab. Kyle, you are one of the kindest and funniest persons I know. Seeing you makes me smile. Although your Texan courtesy can be a bit annoying (please leave the elevator first...), your warm personality made you one of the cornerstones of the lab. Thank you for your support during my many nervous breakdowns. Clément & Kyle, knowing that you will stand beside me on this day makes me happy.

Anna, you made me feel less alone among the protein experts and brought some organization in the metabolomics group. I am sure that things will work out for you this year; take it step by step and believe in yourself! Thanks to all the students that were part of the metabolomics group in the last years. Klaas, Pieter and Haley,


thanks for following my pipet courses, which resulted in valuable contributions in this thesis.

Thanks to my office mates. Celine, thank you for the moments you let me be and for the moments we could talk and laugh about everything. Good luck with the final months, you can do it! Nadine, I loved your calmness, good advice, knowledge about the location of cookies and homemade schnapps. You left a big empty space in our office when you left. Luckily, we soon got company from Elmo – you always enter the office with a smile on your face and this smile is often still present when I leave the office; please be this happy forever!

A big hug for my Bijvoet Boys. Michiel and Philip, how I missed you in the past months! Both of you believed in me from the beginning and I am very thankful for that. Your office door was always open (and closed behind me) so I could safely have a fit in there. I feel lucky that you were around to guide me along the way. Jonas, thanks for all your energy, for all the fun and laughs during our Bijvoet activities. I hope we can schedule a Christmas pub-crawl this year.

Domenico, your support and biological knowledge has helped me a lot. Most importantly though, you have been a great friend and your wedding was one of the highlights of 2017. I'm very happy that you are here to also support me as a post-doc. Please don't move to Vleuten! Wei, you were the first person who dared to start a metabolomics experiment with me! Thank you for all your help and tips, it really improved my skills on different levels. Your biological knowledge is unsurpassed in the lab. Simone, thank you for all the (emotional) support over the last years. It was nice to have someone around who enjoys a broodje saté as much as I do. Renske, I will always think of our SEC experiment on Sinterklaas evening. I am happy that we could work together on different projects (while listening to nice music). Thierry, we shared a big and stressful moment in the meeting room last December and it was very nice to walk side by side in the last months. Matina, I still remember our first culture lab cleaning, all insecure and spraying ethanol all over the place. To you, but also to all the other PhD's in the lab, good luck!

Corine, thank you for the invaluable administrative support you provide for the whole lab. Soenita, thank you for your efforts in the culture lab and, more importantly, for your delicious cakes and desserts. Mirjam, thank you for being always available for my questions, for keeping an eye on me in times of stress and for the stash of candies in your office. Arjan, without you we would have never have a fully productive



mass spec. Thanks for all your patience and positive attitude during my technical questions and all the nitrogen problems. Thanks for all the fun (karaoke) moments.

I would also like to thank all the co-authors from inside and outside the University. A special thanks to Sonja, Gerrit and Jacqueline. Your clinical input was very useful for my project. Michal and Ruud, thanks for your enthusiastic approach towards metabolomics. Thanks to all the people I collaborated with on a variety of projects over the last years.

Hoe mooi het leven in het lab ook is, soms is het heerlijk om te ontsnappen, werk los te laten en tijd door te brengen met vrienden en familie. Deze momenten met fantastische mensen waren voor mij nodig om de energie en inspiratie te behouden voor het onderzoek.

Nerds, ik ben zo blij dat we na onze fantastische tijd in Groningen elkaar nog steeds volop steunen, enorm lachen en mooie avonden beleven. Ik ben trots op wat wij hebben met z'n drieën en wat jullie de afgelopen jaren bereikt hebben. Joost, het is bijzonder hoe onze vriendschap de afgelopen jaren is geëvolueerd. Door jouw positieve kijk op het leven en onvoorwaardelijke steun en vertrouwen in mij weet jij mij altijd weer te motiveren om door te gaan. Bij jou voel ik me veilig. Mirjam, mijn allereerste vriendschap in Groningen, en wat voor een! Ik ben blij dat we, zowel tijdens onze opleiding als ook de afgelopen jaren, dezelfde dingen op een geheel andere manier hebben aangepakt, maar onze vriendschap er altijd als een rode draad doorheen heeft gelopen.

Luxers, bedankt voor alle mooie avonden, borrels, weekenden en vakanties (ja, ook ik was al volop in dit traject toen we in Jordanië waren). De momenten dat we samenkomen bewijst altijd maar weer hoe bijzonder onze connectie is. Leo, wat was het heerlijk om jou zo dichtbij in Utrecht te hebben, zodat ik je altijd kon opzoeken wanneer nodig en andersom. Je bent een toppertje en ik ben blij met jou als vriendin. Eef, wat was ik blij toen jij de move van NYC naar Utrecht maakte! Bedankt voor alle gezelligheid en support. Laten we er in juli een topdag van maken. Jorien en Mathijs, wat een onvergetelijke reis hebben we gemaakt! Bedankt voor de hulp bij het vormgeven van dit boekje; ik ben er zo blij mee!

Thomas en Kees, bedankt voor alle gezelligheid, flügelbingo's en natuurlijk alle lekkere etentjes met Harry Haring, de Zure Bom, intieme amuses en gevallen botertjes. Wie weet komen we er ooit nog achter wat ons perfecte aperitief is!

Merel, Lisette en Antine, wat bijzonder dat we al zo lang vriendinnetjes zijn en dat we elkaar nog steeds geregeld zien. Door onze rijke geschiedenis vol avonturen, pieken en dalen, voelt het altijd vertrouwd. We zien elkaar niet veel, maar ik weet dat ik altijd op jullie kan bouwen.

Deuss, jij hebt me de afgelopen jaren meegenomen naar jouw wereld, waarin ik me thuis voel en alles even achter me kan laten. Bedankt voor alle mooie party's, maar ook voor je luisterend oor wanneer dat nodig was. Ik ben trots dat ik familie van je ben.

Lieve oma, wat is het bijzonder dat je hier bij kan zijn. Nog volop genietend van het leven en van alle mensen om je heen.

Harry, Pauline, Hannah, Joost, Sarah en Anna, het is ongelooflijk bijzonder hoe jullie mij in jullie hart hebben gesloten en ik ben ontzettend dankbaar voor de warmte, liefde en steun die ik van jullie krijg. Ik kijk uit naar nog veel gezamenlijke buitenlandse avonturen.

Lieve papa en mama; zonder jullie had ik hier natuurlijk nooit gestaan. Jullie hebben mij altijd gesteund in mijn keuzes en ervoor gezorgd dat ik kon doen wat ik wilde – ook toen ik zelf nog niet wist wat ik wilde. Lieve Rianne, Irene en Marco, wat ben ik trots om jullie zusje te zijn! Nog altijd zijn jullie voor mij een grote inspiratiebron en het is fijn te weten dat wij altijd voor elkaar klaar staan. Jonas, Anne en Jeroen, jullie zorgen voor de balans binnen de familie Zaal en zijn daardoor onmisbaar geworden. Daarnaast hebben jullie mij de beste rol ter wereld gegeven: Trotse Tante. Lieve Youp, Jesse, Tieme, Ole en Pip: jullie knuffels en lachende gezichtjes zorgen altijd voor een geluksgevoel. Tante Tuc loves you!

HJ, zonder twijfel de belangrijkste persoon. Jij hebt mij geleerd om te oordelen op basis van mijn eigen inzichten en het leven te vormen naar mijn eigen voorwaarden. Jij zorgt ervoor dat ik boven mezelf uitstijg en dingen doe die ik zelf nooit bedacht had. Dankzij jouw eigenwijsheid ben ik afgestudeerd op een project zonder farmaceutische relevantie en heb ik durven solliciteren bij een lab van wereldniveau. Zonder jou had ik nooit aan dit traject durven beginnen en had ik het zeker nooit af kunnen ronden. Bovenal heb jij mij geleerd te genieten van het leven. Laat ze maar kijken naar ons raar gedoe.

Houdoe & Bedankt,

Esther



---

# About the author



---

## LIST OF PUBLICATIONS

### Publications in this thesis

**Zaal EA**, Wu W, Jansen G, Zweegman S, Cloos J, Berkers CR. Bortezomib resistance in multiple myeloma is associated with increased serine synthesis. *Cancer & Metabolism*; 2017;5:7.

Ruprecht B, **Zaal EA**, Zecha J, Wu W, Berkers CR, Kuster B, Lemeer S. Lapatinib Resistance in Breast Cancer Cells Is Accompanied by Phosphorylation-Mediated Reprogramming of Glycolysis. *Cancer Res.* 2017;77:1842–53.

Weijer R, Clavier S<sup>#</sup>, **Zaal EA**<sup>#</sup>, Pijls MME<sup>#</sup>, van Kooten RT<sup>\*</sup>, Vermaas K, Leen R, Jongejan A, Moerland PD, van Kampen AHC, van Kuilenburg ABP, Berkers CR, Lemeer S, Heger M. Multi-OMIC profiling of survival and metabolic signaling networks in cells subjected to photodynamic therapy. *Cell Mol Life Sci.* 2017;74:1133–51.

### Other Publications

Wisse LE<sup>#</sup>, Penning R<sup>#</sup>, **Zaal EA**, van Berkel CGM, ter Braak TJ, Polder E, Kenney JW, Proud CG, Berkers CR, Altelaar AFM, Speijer D, van der Knaap MS, Abbink TEM. Proteomic and metabolic analysis of VWM mouse astrocytes reveal deregulation of ER functions. *Front. Cell. Neurosci.* 2017;11:411

Leestemaker Y<sup>#</sup>, de Jong A<sup>#</sup>, Witting KF, Penning R, Schuurman K, Rodenko B, **Zaal EA**, van de Kooij B, Laufer S, Heck AJR, Borst J, Scheper W, Berkers CR, Ovaa H. Proteasome Activation by Small Molecules. *Cell Chem Biol.*; 2017;24:725–736.e7.

Loayza-Puch F<sup>#</sup>, Rooijers K<sup>#</sup>, Zijlstra J, Moumbeini B, **Zaal EA**, Oude Vrielink JF, Oude Vrielink JF, Lopes R, Pineiro Ulalde A, Berkers CR, Agami R. TGFβ1-induced leucine limitation uncovered by differential ribosome codon reading. *EMBO Rep.* 2017;18:549–57.

Becher I, Werner T, Doce C, **Zaal EA**, Tögel I, Khan CA, Rueger A, Muelbaier M, Salzer E, Berkers CR, Fitzpatrick PF, Bantscheff M, Savitski MM. Thermal profiling reveals phenylalanine hydroxylase as an off-target of panobinostat. *Nat Chem Biol.* Nature Publishing Group; 2016;12:908–10.



Liu Y, Rodrigues JPGLM, Bonvin AMJJ, **Zaal EA**, Berkers CR, Heger M, Gawarecka K, Swiezewska E, Breukink E, Egmond MR. New Insight into the Catalytic Mechanism of Bacterial MraY from Enzyme Kinetics and Docking Studies. *J Biol Chem.* 2016;291:15057–68.

Wu W, **Zaal EA**, Berkers CR, Lemeer S, Heck AJR. CTGF/VEGFA-activated fibroblasts promote tumor migration through micro-environmental detoxification. *Accepted for publication*

Gautier V, Raaijmakers LM, Maddalo G, Kemper K, Rontogianni S, Schmidlin T, Hoekman L, Bleijerveld OB, **Zaal EA**, Berkers CR, Vargas Diaz D, Fitzpatrick MA, Krijgsman O, Heck AJR, Peeper DS, Altelaar AFM. Integrative-omics reveal a molecular network sustaining BRAF mutant melanoma and harbouring Cl-P2a, CDK4.6 and ASCT2 as targetable vulnerabilities. *In revision*

Authors marked with # contributed equally to the respective publications



## **CURRICULUM VITAE**

On June 11th 1988 I was born in Made, Noord-Brabant. After graduating from Sint-Oelbert Gymnasium in Oosterhout in 2006, I studied Pharmacy at the University of Groningen.

During my studies I became interested in the fascinating possibilities of mass spectrometry. For both my Bachelor's and Master's theses, I was lucky enough to be allowed to play with these supremely sensitive (and expensive) instruments. Prof. F.A.J. Muskiet and especially dr. M.R. Heiner-Fokkema introduced me to the intriguing world of cellular metabolism as I developed a method for the analysis of advanced glycation endproducts using liquid chromatography tandem-mass spectrometry.

In December 2013 I started my PhD career in prof. dr. A.J.R. Heck's Biomolecular Mass Spectrometry & Proteomics group at the University of Utrecht. Under the supervision of prof. dr. C.R. Berkers I had the opportunity to combine my fascination for mass spectrometry with my interest in metabolomics, of which the work is presented in this thesis.

